NATIONAL TECHNICAL UNIVERSITY OF ATHENS

SCHOOL OF ELECTRICAL AND COMPUTER ENGINEERING

DIVISION OF INFORMATION TRANSMISSION AND MATERIAL TECHNOLOGY

Design and implementation of digital signal processing algorithms and optical circuits in 5G optical networks

PhD Thesis

by

Konstantina C. Kanta

Αθήνα, Ιούνιος 2024

NATIONAL TECHNICAL UNIVERSITY OF ATHENS
SCHOOL OF ELECTRICAL AND COMPUTER ENGINEERING
DIVISION OF INFORMATION TRANSMISSION AND MATERIAL TECHNOLOGY

Design and implementation of digital signal processing algorithms and optical circuits in 5G optical networks

Doctoral dissertation

by

Konstantina C. Kanta

Συμβουλευτική Επιτροπή : Ηρακλής Αβραμόπουλος
Θεοδώρα Βαρβαρίγου
Νικόλαος Ουζούνογλου

Εγκρίθηκε από την επταμελή εξεταστική επίτροπη την 12/06/24

.....	.....	.....
Ηρακλής Αβραμόπουλος	Θεοδώρα Βαρβαρίγου	Νικόλαος Ουζούνογλου
Καθηγητής Ε.Μ.Π.	Καθηγήτρια Ε.Μ.Π.	Ομότιμος Καθηγητής Ε.Μ.Π.
.....	.....	.....
Νικόλαος Πλέρος	Ιωάννης Παπαδόπουλος	Νεκτάριος Κοζύρης
Καθηγητής Α.Π.Θ.	Αναπληρωτής Καθηγητής Ε.Μ.Π.	Καθηγητής Ε.Μ.Π.

.....
Γεώργιος Κανέλλος
Επίκουρος Καθηγητής Ε.Κ.Π.Α.

Αθήνα, Ιούνιος 2024

.....

Κωνσταντίνα Χ. Καντά

Διδάκτωρ Ηλεκτρολόγος Μηχανικός και Μηχανικός Υπολογιστών Ε.Μ.Π.

Abstract

In the context of this doctoral thesis, the design and implementation of digital signal processing algorithms and optical circuits in 5G optical networks is being investigated. More specifically, the development of an end-to-end transceiver signal processing toolbox, that is tailor made for the generation, demodulation, and treatment of multicarrier signals, that are appropriate for converged analog fiber-wireless transmission schemes is presented. The validation of the functionality of this toolbox, as well as the performance evaluation of CP-OFDM signals propagated over different optical and optical-wireless layouts is showcased within the current document, through the presentation of small-scale laboratory setups and field-trials. In all cases, the bandwidth efficient Analog IFoF transmission scheme, along with mmWave radio equipment have been employed. The DSP-assisted deployed testbeds emulate transport alternatives, aiming to provide efficient solutions towards efficient future mobile X-Haul infrastructures by focusing on the integrability of the investigated transport link into actual Mobile Network Operators' fiber deployments and mobile equipment.

Chapter 1 is an introductory chapter that lays the groundwork for understanding the historical trajectory and transformative milestones that have shaped the mobile communication ecosystem. Moving forward, the pivotal role of optical access network Interfaces in the era of 5G and beyond is illustrated. The exploration deepens with a dedicated focus on Future mobile networks' applications and use cases providing insights into the anticipated applications and performance metrics that will define the landscape of mobile networks in the foreseeable future and pave the path towards future RAN evolution strategies. Chapter 2 investigates analog fiber-wireless links as a crucial element for efficient RAN extensions in 5G networks. This chapter covers various aspects, including the transition to C-RAN architectures, optical transport for MFH, and DSP-assisted analog Fronthaul. Analog RoF-based mobile Fronthaul, mmWave wireless technologies, and proof-of-concept experimental evaluations are also explored. Moving forward, Chapter 3 delves into modulation and signal processing techniques, elucidating the role of these techniques in supporting analog fiber and fiber-wireless transport transmission. It encompasses an in-depth examination of digital modulation schemes, OFDM modulation, multi-carrier candidates for 5G, and the integration of DSP algorithms for processing CP-OFDM waveforms. Chapter 4 shifts the focus to analog fiber-wireless downlink transmission of IFoF/mmWave over in-field deployed legacy PON infrastructure, presenting a detailed analysis of converged PON/mmWave topology through experimental evaluation. The dissertation culminates in Chapter 5, where a live demonstration of an SDN-reconfigurable, FPGA-based TxRx for Analog-IFoF/mmWave RAN is showcased. This chapter provides insights into the envisioned Fronthaul architecture, RFSoC-based A-IFoF transceivers, SDN-powered Management & Control Plane, and the experimental evaluation of the real-time analog Fronthaul topology. In the final chapter, Chapter 6, the dissertation concludes by summarizing key findings and insights gained throughout the exploration of analog fiber and fiber-wireless transport in the realm of 5G networks, while also discussing future research extensions related to the presented work.

Keywords
5G, A-IFoF, DSP, analog optical transceivers, mmWaves, X-Haul, RAN

Περίληψη

Στο πλαίσιο της παρούσας διδακτορικής διατριβής, ερευνάται ο σχεδιασμός και η υλοποίηση αλγορίθμων ψηφιακής επεξεργασίας σήματος και οπτικών κυκλωμάτων σε οπτικά δίκτυα 5G. Συγκεκριμένα, παρουσιάζεται η ανάπτυξη εργαλείων επεξεργασίας σήματος που προορίζονται για χρήση σε αναλογικούς πομποδέκτες, για τη διαμόρφωση, την επεξεργασία και αποδιαμόρφωση κυματομορφών πολλαπλών φερουσών. Οι πομποδέκτες αυτοί είναι αναγκαίοι για την υποστήριξη μετάδοσης πληροφορίας σε αναλογικές οπτικές ή οπτικές-ασύρματες ζεύξεις. Η παρούσα εργασία εστιάζει στην παρουσίαση και επικύρωση της λειτουργικότητας αυτών των αλγορίθμων, καθώς και την αξιολόγηση της ποιότητας σημάτων πολλαπλών φερουσών (CP-OFDM) επείτα από διάδοση σε οπτικές και οπτικές-ασύρματες διατάξεις. Για το σκοπό αυτό παρουσιάζεται μια σειρά πειραματικών δραστηριοτήτων που έλαβαν χώρα είτε σε εργαστηριακό περιβάλλον, είτε σε μεγαλύερης κλίμακας πειραματικών επιδείξεων σε πραγματικές τηλεπικοινωνιακές εγκαταστάσεις. Σε όλες τις περιπτώσεις, χρησιμοποιήθηκε το σχήμα αναλογικής μετάδοσης ηλεκτρικά διαμορφωμένων κυματομορφών σε υψίσυχνο φέρον για το κομμάτι της οπτικής ζεύξης, σε συνδυασμό με ασύρματο εξοπλισμό χιλιοστομετρικού κύματος για τη μετάδοση στον αέρα. Οι δοκιμές που έγιναν είχαν σα στόχο την επίδειξη εναλλακτικών υλοποιήσεων δικτύων μεταφορές, με εφαρμογή σε μελλοντικές υποδομές κινητών δικτύων πρόσβασης κινητής X-Haul, ενώ έμφαση δόθηκε και την επιτυχή ενσωμάτωση των υπό μελέτη αναλογικών δικτύων μεταφοράς είτε σε πραγματικές υποδομές οπτικών ινών είτε σε διασυνδέσης που υποστηρίζονται από εμπορικά διαθέσιμο εξοπλισμό κινητών τηλεπικοινωνιών σε συνεργασία με φορείς κινητής τηλεφωνίας.

Το Κεφάλαιο 1 είναι ένα εισαγωγικό κεφάλαιο που θέτει τις βάσεις για την κατανόηση της ιστορικής πορείας του οικοσυστήματος των κινητών επικοινωνιών. Ταυτόχρονα, επισημαίνεται ο ρόλος των διεπαφών δικτύου πρόσβασης οπτικών συνδέσεων, τόσο στην εποχή του 5G όσο και σε μελλοντικές αναβαθμίσεις των δικτύων κινητών. Το Κεφάλαιο 2 επικεντρώνεται στη χρήση απρόσκοπτης οπτικής-αύρματης μετάδοσης, ως μια πολλά υποσχόμενη εναλλακτική για την κατασκευή αποδοτικών δικτύων πρόσβασης 5G. Αυτό το κεφάλαιο καλύπτει διάφορες πτυχές που αφορούν στα οπτικά-ασύρματα δίκτυα μεταφοράς, συμπεριλαμβανομένης της ενσωμάτωσής τους σε κεντρικοποιημένες αρχιτεκτονικές δικτύων ασύρματης πρόσβασης, της περιγραφής του κοβικού ρόλου του σχήματος αναλογικής οπτικής μετάδοσης ηλεκτρικά διαμορφωμένων κυματομορφών σε υψίσυχνο φέρον στις τοπολογίες αυτές, καθώς και στη χρήση ασύρματου εξοπλισμού χιλιοστομετρικού κύματος. Έπειτα, το Κεφάλαιο 3 αναλύει τις τεχνικές διαμόρφωσης και επεξεργασίας σημάτων που είναι απαραίτητες για την επιτυχή μετάδοση πληροφορίας σε αναλογικές τοπολογίες οπτικής-ασύρματης ζεύξης. Στα πλαίσια αυτά, περιλαμβάνει λεπτομερή εξέταση των διαφορετικών ψηφιακών σχημάτων διαμόρφωσης, της διαμόρφωσης πολλαπλών φερουσών, καθώς και της ανάπτυξης και αξιολόγησης αλγορίθμων ψηφιακής επεξεργασίας σήματος προορισμένων για την περίπτωση σημάτων πολλαπλών φερουσών. Το Κεφάλαιο 4 παρουσιάζει την πρώτη περιαματική αξιολόγηση του σχήματος μεταφοράς που περιγράφεται παραπάνω σε συνθήκες πραγματικών οπτικών εγκαταστάσεων και συγκεκριμένα στο Παθητικό Οπτικό Δίκτυο του Τορίνο. Στη συνέχεια, στο Κεφάλαιο 5 περιγράφεται η επίδειξη ενός ολοκληρωμένου ψηφιακού πομποδέκτη κυματομορφών πολλαπλών φερόντων, ο οποίος μετά από σύνδεση με τυπικά ηλεκτρο-οπτικά στοιχεία (διαμορφωμένο λέιζερ ηλεκτροαπορόφησης και

φωτοδέκτης), χρησιμοποιήθηκε ως αναλογική οπτική διεπαφή, συμβατή με κίνηση Ethernet την ενσωμάτωση ενός αναλογικού καναλιού μεταφοράς, στην υποδομή ενός υπαρκτού δικτύου κινητής τηλεφωνίας στην Αθήνα. Τέλος στο Κεφάλαιο 6, συνοψίζονται τα κύρια αποτελέσματα της παρούσας διδακτορικής διατραβής, ενώ επίσης συζητούνται πιθανές μελλοντικές ερευνητκές δραστηριότητες που σχείζονται με το παρουσιαζόμενο έργο.

Λέξεις Κλειδιά

5G, αναλογική μετάδοση ηλεκτρκά διαμορφωμένου σήματος σε υψίσυχνο φέρον μέσω ίνας, ψηφιακή επεξεργασία σήματος, αναλογικοί οπτικοί πομποδέκτες, χιλιοστομετρικά μήκη κύματος, X-Haul, κινητά δίκτυα πρόσβασης

Ευχαριστίες αντί προλόγου

Η συγγραφή του κεφαλαίου των ευχαριστιών ήταν ένα από τα πιο δύσκολα κομμάτια της παρούσας διδακτορικής διατριβής. Η συλλογή των δεδομένων και της δουλειάς που συντελέστηκε κατά τη διάρκεια των τελευταίων 6,5 χρόνων σε μια συνεκτική εργασία είναι σίγουρα απαιτητική. Ακόμα πιο δύσκολη υπόθεση είναι όμως να χωρέσει κάποιος σε μερικές παραγράφους το χρόνο, τις κοινές εμπειρίες και τις σχέσεις που δημιουργήθηκαν μέσα σ΄αυτά τα χρόνια σε ένα εργαστήριο όπως το PCRL. Ένα χώρο που πολλοί μέχρι σήμερα και με διάφορες ευκαιρίες παρομοίασαν και όχι αδίκως με οικογένεια ή με μια ομάδα που αν κάποια στιγμή γίνεις μέλος της, δεν παύεις να είσαι ποτέ.

Πρώτα απ΄όλα λοιπόν θα ευχαριστήσω το PCRL αυτό καθ΄αυτό. Είναι ένα εργαστήριο με τρομερή δυναμική στο πόσα μπορεί να κάνει, με πόσα διαφορετικά αντικείμενα μπορεί να καταπιαστεί αποτελεσματικά και να προσαρμοστεί τόσο στις επιταγές της εποχής που συνέχεια αλλάζουν και που έχουν μια δυναμική σχέση με τα ενδιαφέροντα των ανθρώπων που το απαρτίζουν. Η δυναμική αυτή από την εικόνα που σχημάτισα στα χρόνια μου στο PCRL οφείλεται σε 3 παράγοντες. Πρώτο και βασικό συστατικό της επιτυχίας: πάντα το PCRL εγκόλπωνε πολύ αξιόλογους ερευνητές με όρεξη και δυνατότητες. Δεύτερο και ίσως ακόμα βασικότερο: πάντα το PCRL εγκόλπωνε πραγματικά αξιόλογους ανθρώπους. Όλοι μας είχαμε τις δικές μας ιδιαίτερες δυνατότητες και αδυναμίες, είχαμε όμως και το ενδιαφέρον να βλέπουμε και τις ιδιαιτερότητες των άλλων και να λειτουργούμε ομαδικά. Να ζητάμε και να δίνουμε με κάθε ευκαιρία βοήθεια σε όποιον τη χρειαζόταν, με στόχο ένα καλό αποτέλεσμα αλλά και το να γνωριστούμε να έρθουμε πιο κοντά και να ομορφύνουμε τη ζωή μας εντός και εκτός εργαστηρίου.

Περνώντας στο τρίτο συστατικό της επιτυχίας, θα αρχίσω πρακτικά το κομμάτι και των πιο προσωπικών ευχαριστιών. Το PCRL δεν είναι αυθύπαρκτο και δεν θα ήταν σίγουρα αυτό που είναι 30 χρόνια τώρα χωρίς τον ιδρυτή του, τον κ. Ηρακλή Αβραμόπουλο. Πρόκειται για έναν άνθρωπο που εκτιμώ βαθύτατα. Τον εκτιμώ γιατί κατάφερε και έφτιαξε το PCRL, εργαστήριο πρότυπο στα μάτια μου για τους λόγους που προανέφερα αλλά και ένα εργαστήριο που σε εμένα προσωπικά έδωσε την ευκαιρία να κάνω τη διπλωματική μου εργασία τελειώνοντας τη σχολή, να εκπονήσω το διδακτορικό μου, να μάθω ένα σωρό πράγματα και να καταπιαστώ με μια σειρά από δραστηριότητες, αλλά και να ταξιδέψω και να γνωρίσω μερικούς από τους πιο καλούς μου φίλους. Τον εκτιμώ όμως και για τη στάση του απέναντι μου και απέναντι στα υπόλοιπα μέλη του εργαστηρίου έναν-προς-έναν. Πρόκειται για έναν άνθρωπο ευγενικό και άμεσο με μεγάλες ευαισθησίες, που ήταν πάντα εκεί για ότι χρειάστηκα και εγώ και όλοι μας.

Θέλω επίσης να ευχαριστήσω τον Δημήτρη Αποστολόπουλο. Ήταν ο supervisor μου για την εκπόνηση του διδακτορικού αλλά και ο πρώτος άνθρωπος με τον οποίο μίλησα για την ένταξή μου στο εργαστήριο. Αυτή η πρώτη συζήτηση με σιγουριά και αμεσότητα με προιδέασε από την πρώτη στιγμή ότι το να κάνω το διδακτορικό μου σε αυτό το εργστήριο θα είναι μια σωστή επιλογή και πράγματι μπορώ εκ των υστέρων να πω ότι ήταν μια αναντικατάστατη εμπειρία ζωής. Ο Δημήτρης πάντα μου ενέπνεε εμπιστοσύνη και ήταν εκεί για να επισημαίνει

τις δυνατότητες και τις αδυναμίες μου, με παρακινούσε και ήταν πολύ υποστηρικτικός σε κάθε επόμενο βήμα που έπρεπε να κάνω σε όλα αυτά τα χρόνια.

Πριν και από αυτό όμως ο πρώτος άνθρωπος με τον οποίο συνεργάστηκα ήταν ο Νίκος Αργύρης. Με τη βοήθεια του ολοκλήρωσα την διπλωματική μου εργασία στο προπτυχιακό μέρος των σπουδών και η συνεργασία αυτή με έκανε να σκέφτομαι ότι ίσως θα ταίριαζα κι εγώ στην ομάδα του PCRL. Είναι ένας άνθρωπος ιδιαίτερα ικανός και έξυπνος και που τα εργαλεία που μου έδωσε φάνηκαν χρήσιμα για χρόνια μετά.

Ο Γιάννης Γιαννούλης ήταν και αυτός από τα πρώτα άτομα με τα οποία συνεργάστηκα στο εργαστήριο. Δεν μπορεί παρά να ξεχωρίσει κανείς το πάθος, το μεράκι και την αγάπη του γι΄ αυτό που κάνει. Πρόκειται για έναν άνθρωπο που εκτιμώ πολύ για το ήθος του, φύσει αισιόδοξο και που ο χώρος του πανεπιστημίου ίσως είναι ιδανικός χώρος γι΄αυτόν. Με μεγάλη όρεξη και ενδιαφέρον για γνώση, τον Γιάννη τον έχω στο μυαλό μου σαν μια αστείρευτη πηγή ιδεών που μπορεί να γεννήσει υλικό για παρότρυνση σε μια σειρά από δραστηριότητες που μπορούν να γεμίσουν πολλά διδακτορικά.

Τον επόμενο σκεφτόμουν αρχικά να τον αφήσω για το τέλος, αλλά αναφέροντας με χρονολογική κάπως σειρά τα μέλη του εργαστηρίου με τα οποία συνεργάστηκα, ήρθε κάπου εδώ η στιγμή για την ιδιαίτερη αυτή μνεία. Τι να πρωτοπώ για τον Παναγιώτη Τουμάση. Θα του άξιζαν σελίδες ολόκληρες για τον πολύ ιδιαίτερο ρόλο του σε όλες τις πτυχές τις ζωής μου μέσα και έξω από το PCRL όλα αυτά τα χρόνια. Με τον Παναγιώτη συνεργαστήκαμε για την εκτέλεση του μεγαλύτερου μέρους των εργασιών που περιγράφονται στη συνέχεια της παρούσας διατριβής, η επίτυχια των οποίων οφείλεται σε μεγάλο βαθμό στην πολύ καλή χημεία και άριστη συνεργασία που είχαμε είτε μέσα στο εργαστήριο είτε μετά όταν έπρεπε να επεξεργαστούμε και να καταγράψουμε τι έχουμε κάνει αλλά και να σκεφτούμε το επόμενο βήμα. Με τον Παναγιώτη ένιωθα ότι μπορούμε να καταφέρουμε οτιδήποτε χρειαστεί και ήταν ένας καλός λόγος να πηγαίνω με χαρά και αισιοδοξία στο εργαστήριο ακόμα και όταν οι δυσκολίες που έπρεπε να αντιμετωπίσουμε ήταν μεγάλες. Κάνοντας έτσι πιο όμορφη την καθημερινότητα μου τόσο στο εργαστήριο όσο και εκτός, από τα πειράματα, τα ταξίδια αλλά και τις συζητήσεις και τις μπύρες μετά, ο Παναγιώτης είναι ένας από τους πιο καλούς μου φίλους και έχει μια πολύ ξεχωριστή θέση στη καρδιά μου, ενώ επηρέασε όχι μόνο την έκβαση του διδακτορικού μου αλλά και το ποιος άνθρωπος είμαι σήμερα. Θα κλείσω αυτή την παράγραφο λέγοντας ότι ο Παναγιώτης πέρα από καταπληκτικός φίλος, ικανός να υπερβεί κάθε δυσκολία με την αμεσότητα και το χιούμορ του, είναι ένας πολυμήχανος και ευρηματικός άνθρωπος που επάξια αποτελεί την καρδιά του εργαστηρίου.

Για ένα μεγάλο χρονικό διάστημα, μέρος της καθημερινότητας μου στο εργαστήριο αποτέλεσε και ο Κώστας Τόκας, που μαζί με τον Παναγιώτη ήμασταν ένα πολύ καλό τρίδυμο για μια σειρά από δραστηριότητες. Πρόκειται για έναν άνθρωπο πολύ ευθύ και οργανωτικό που έπαιξε μεγάλο ρόλο στο να μάθω το πώς να οργανώσω ένα πείραμα αλλά και πώς να επικοινωνήσω τις δυσκολίες μου στους άλλους. Πέρα από αυτό όμως, από την πρώτη μου μέρα στο διδακτορικό, με βοήθησε πολύ στο να εγκλιματιστώ και να αρχίσω να δένομαι με τον κόσμο του PCRL, κέρδισε γρήγορα την εμπιστοσύνη μου και παραμένει ένας πολύ καλός φίλος.

Ο Γιάννης Κανάκης ήταν ο άνθρωπος που καθόταν για χρόνια στο δίπλα γραφείο και όμως τον γνώρισα καλύτερα μόλις τον τελευταίο χρόνο. Πάντα ευγενικός, καλοσυνάτος και

καλοπροαίρετος πρόκειται για έναν άνθρωπο που σε κερδίζει αμέσως με την αύρα του, ενώ από τις πρώτες μου μέρες με βοήθησε στο να νιώθω άνετα στο εργαστήριο. Γνωρίζοντας τον με τα χρόνια διαπίστωσα όμως και το πόσο έξυπνος και ικανός είναι, με ενδιαφέρον για τους γύρω του σε όλα τα επίπεδα. Είναι ένας ακόμα από τους ανθρώπους που εμπιστεύομαι βαθιά, ενώ απ΄τη στιγμή που τον γνώρισα λίγο καλύτερα δε μπορούσε παρά να κερδίσει κι αυτός μια θέση στη καρδιά μου και να γίνει κι αυτός ένας από τους πιο καλούς μου φίλους.

Στο πρώτο μεγάλης κλίμακας πείραμα που έκανα συμμετείχε κι ο Γιάννης Πουλόπουλος. Ένας πολύ ιδιαίτερος και έξυπνος άνθρωπος με πολλή φαντασία και πρωτότυπες ιδέες που με έκανε να διαπιστώσω ότι τα πειράματα που τραβούν μέχρι τις 12 το βράδυ θα είναι από τις όμορφες εμπειρίες που θα έχω να θυμάμαι από την εκπόνηση του διδακτορικού. Είναι ένας άθρωπος που δίνει ζωή στο εργαστηρίο, ενώ σε συνδυασμό με τον Νίκο Ηλιάδη στο πρώτο έτος του διδακτορικού μου αποτέλεσαν πρότυπο πειραματικό δίδυμο στα μάτια μου. Ο Νίκος Ηλιάδης είναι ένας ακόμη ικανός ερευνητής που με βοήθησε πολύ στα πρώτα μου βήματα στο εργαστήριο.

Η Ευρυδίκη Κυριαζή και ο Γιώργος Μπρέστας μου έδωσαν την ευκαιρία να δοκιμαστώ με την καθοδήγηση προπτυχιακών φοιτητών για την εκπόνηση διπλωματικών εργασιών. Μέσα όμως από τη διαδικασία αυτή αναγνώρισα γρήγορα τις δυνατότητές τους και χάρηκα πολύ όταν ήρθαν, μετά το τέλος της διπλωματικής τους, στην ομάδα του PCRL. Ιδιαίτερα ικανοί ερευνητές και οι δύο, με όρεξη και μεράκι για αυτό που κάνουν έφεραν νέο αέρα με τον ερχομό τους στο εργαστήριο. Η Ευριδίκη με το μεράκι και το ενδιαφέρον της για νέες γνώσεις και για την απόκτηση μιας σειράς δεξιοτήτων αλλά και την ενσυναίσθηση που διαθέτει από τη μία, και ο Γιώργος με την επιμονή του και την βαθιά αφοσίωσή του σε ότι καταπιάνεται, αλλά και με τη διάθεσή του να βλέπει με χιούμορ και τα δυσκολότερα προβλήματα, ήταν και οι δύο πολύ δυνατές προσθήκες στην ομάδα. Με την αμοιβαία όρεξη και τις δεξιότητές τους πλαισιώνουν δημιουργικά μια σειρά από δραστηριότητες, ενώ ταυτόχρονα έπαιξαν πολύ κομβικό ρόλο στο να δεθούμε τα τελευταία χρόνια σαν παρέα, να γίνουμε φίλοι και να έχουμε μια πολύ όμορφη καθημερινότητα τα πρωινά στο εργαστήριο και τα βράδια έξω από αυτό.

Ο Γιώργος Συριόπουλος και ο Αργύρης Ντάνος ήταν δύο ακόμα από τις νεότερες αλλά και πολύ καλές ταυτόχρονα προσθήκες της γενιάς αυτής. Ο Γιώργος είναι ακόμη ένας πολύ αξιόλογος ερευνητής με ενφδιαφέρον και μεράκι, με τον οποίο μη έχοντας συνεργστεί άμεσα, μπορώ κυρίως να επισημάνω το πόσο συμβάλει με τον ξεχωριστό αέρα του στην εργασιακή μας και όχι μόνο καθημερινότητα εντός και εκτός εργαστηρίου, ενώ ήταν πάντα πρόθυμος για βοήθεια σε οτιδήποτε χρειάστηκε. Ο Αργύρης πέρα από φαντασία και αποφασιστηκότητα έχει ένα ιδιαίτερο μεράκι και ενδιαφέρον για ότι καταπιάνεται και για εμένα είναι από τα πρώτα άτομα που σκέφτομαι όταν ακούω τη λέξη εργαστήριο. Μαζί με τον Άρη Στάθη, ένα ακόμα πολύ αξιόλογο και επίμονο ερευνητή κάνουν ένα φοβερό δίδυμο ικανό να φέρει εις πέρας οποιαδήποτε, πειραματική και μη, δραστηριότητα τους ανατεθεί.

Η Μαριλύ Σπυροπούλου είναι νομίζω η ήρεμη δύναμη του PCRL. Επίμονη, λεπτομερής και συστηματική έχει χαράξει μια ιδιαίτερη πορεία και έχει αφήσει σημαντική παρακαταθήκη στο εργαστήριο, ενώ σαν δίδυμο με τον Γιάννη Κανάκη απότελουν μια ακόμα από τις ομάδες πρότυπο, επιδεικνύοντας αποτελεσματικότητα μέσα από τις ικανότητές τους αλλά και τη συνεργαστικότητα και τον αμοιβαίο σεβασμό. Ο Χάρης Ζερβός με τον ερχομό του στο

εργαστήριο έφερε και αυτός νέο άερα, με πολλές ιδέες και δυναμική να καταπιαστεί με μια σειρά από νέα αντικείμενα και δραστηριότητες.

Θέλω να ευχαριστήσω ακόμα το Γιάννη Λαζάρου, που παρά το γεγονός ότι συνυπήρξαμε για μικρό χρονικό διάστημα στο εργαστήριο, τον εκτιμώ πολύ για την αμεσότητά του και την προθυμία του να μου προσφέρει απλόχερα τη βοήθεια του. Η Θένια Προυσαλίδη από την άλλη είναι η νεότερη προσθήκη στο εργαστήριο, αλλά γνωρίζοντάς την εδώ και πολλά χρόνια είμαι σίγουρη για την πολύ καλή πορεία που θα ακολουθήσει και θέλω να της ευχηθώ καλή αρχή και καλή σταδιοδρομία.

Επιπλέον θέλω να ευχαριστήσω την Βάσια Λαμπροπούλου, την Πόλυ Βλάση, τη Μαρία Κορμπίλα και την Έλενα Μαριανίδου, για την πολύτιμη βοήθεια και στήριξη σε καθημερινά ζητήματα όλα αυτά τα χρόνια. Ιδιάιτερα η Έλενα είναι μια από τις νεότερες προσθήκες στην ομάδα του PCRL και πολύ γρήγορα έγινε κομμάτι όχι μόνο της ομάδας, αλλά και της παρέας που όπως προείπα δίνει αυτή την ιδιαίτερη, ευχάριστη πινελιά που έκανε ακόμα πιο όμορφη την καθημερινότητά μας.

Πριν κλείσω αυτό τον ιδιότυπο πρόλογο, θέλω να ευχαριστήσω μια σειρά από ανθρώπους που αν και οι ασχολίες μας δεν συνέπεσαν ή συνεργαστήκαμε άμεσα σε μικρό βαθμό, έχουν συμβάλει σημαντικά στην πορεία του PCRL. Πρόκειται για τον Κωστή Χριστογιάννη, τον Χρήστο Κουλουμέντα, τον Πάνο Γκρούμα, τον Λευτέρη Γουναρίδη, την Μαρία Μασαούτη, τον Χρήστο Τσώκο, τον Αδαμ Ραπτάκη, τον Νίκο Λύρα, τον Στάθη Ανδριανόπουλο, την Αδαμαντία Γραμματικάκη και τον Γιώργο Μέγα. Οι άνθρωποι αυτοί συνδιαμορφώνουν και οι ίδιοι την πορεία του PCRL και έτσι μοιραστήκαμε μια κοινή καθημερινότητα, όμορφες συζητήσεις και σε κάποιες περιπτώσεις δεθήκαμε σε κοινά ταξίδια, όπως με το Νίκο και το Στάθη.

Φεύγοντας από τον στενό πυρήνα του ΕΦΕ, θα ήθελα να ευχαριστήσω πολύ τους φίλους μου που καθ'όλη τη διάρκεια του διδακτορικού ήταν εκεί για να μοιραστώ τις καλύτερες στιγμές μου αλλά και για να με στηρίξουν στις πιο δύσκολες. Θέλω να ευχαριστήσω έτσι τη Δέσποινα, την Άννα, το Δημήτρη, την Ευαγγελία και την Ηρώ αλλά και πολλά άλλα άτομα που ομορφαίνοντας την καθημερινότητά μου, μου δίναν κουράγιο να προσπεράσω τις δύσκολες μέρες και να καλοδεχτώ με αισιοδοξία τις επόμενες. Ιδιαίτερες ευχαριστίες θέλω να δώσω στην Μαρία Μαστροκώστα. Πρόκειται για την καλύτερή μου φίλη και πλέον είναι για εμένα η αδερφή που ποτέ δεν είχα. Την αγαπώ πολύ και είναι ένα από τα μεγαλύτερα μου στηρίγματα, όντας πάντα εκεί για να ακούσει και να καθυσηχάσει τις ανησυχίες μου, να μου δώσει πολύτιμες συμβουλές, και πολλές φορές να χαρεί και να συγκινηθεί πριν από εμένα για εμένα στις καλύτερες στιγμές μου. Θέλω ακόμα να ευχαριστήσω τον Γιάννη Μηλαθιανάκη, ο οποίος με συντρόφευσε στο μεγαλύτερο κομμάτι της πορείας μου στο PCRL. Πρόκειται για ένα άνθρωπο με ξεχωριστή θέση στην καρδιά μου. Με την καλοσύνη του και την υπομονή του έπαιξε κι αυτός μεγάλο ρόλο στο να αντέξω τις δυσκολίες, να εξελιχθώ και να γίνω ο άνθρωπος που είμαι σήμερα.

Τέλος θέλω να ευχαριστήσω την οικογένειά μου. Την μητέρα μου Αλεξάνδρα, τον πατέρα μου Χαράλαμπο και την γιαγιά μου Αθανασία. Αρκεί να αναφέρω ότι τους οφείλω σε μεγάλο βαθμό την πορεία μου. Με άφθονη αγάπη με στήριξαν και με βοήθησαν σε καθετί από την πρώτη στιγμή της ζωής μου.

Υ.Γ. Αν έχω ξεχάσει κάποιους απολογούμαι γι’αυτό και εύχομαι να μην μου κρατήσουν κακία γιατί δεν ήταν εκούσιο!

Table of Contents

List of abbreviations

A-IFoF	Analog Intermediate Frequency over Fiber
A-RoF	Analog Radio over Fiber
ADC	Analog-to-Digital Conversion
AMS	Analog Mixed Signal
AOC	Active Optical Cable
APD	Avalanche Photodiode
AR/VR	Augmented Reality/Virtual Reality
ASE	Amplified Spontaneous Emission
ASK	Amplitude-Shift Keying
AWG	Arbitrary Waveform Generator
AWGN	Arbitrary White Gaussian Noise
AWGR	Arrayed Waveguide Grating Router
BBU	Baseband Unit
BH	Backhaul
btb	back-to-back
BS	Base Station
C-RAN	Centralized – Radio Access Network
CEX	Coexistence Filter
CD	Chromatic Dispersion
CFO	Carrier Frequency Offset
CMA	Constant Modulus Algorithm
CO	Central Office
CP	Cyclic Prefix
CP-OFDM	Cyclic Prefix – Orthogonal Frequency Division Modulation
CPRI	Common Public Radio Interface
CPU	Central Processing Unit
CSI	Channel State Information
CU	Central Unit
CW	Continuous Wave
D-RoF	Digital – Radio over Fiber
DAC	Digital-to-Analog Conversion
DAS	Distributed Antenna System
DC	Direct Current
DEMUX	Demultiplexer

DFB	Distributed-feedback laser
DFT	Digital Fourier Transform
DL	Downlink
DML	Directly Modulated Laser
DR	Dynamic Range
DSP	Digital Signal Processing
DU	Digital Unit
DWDM	Dense Wavelength Division Multiplexing
E/O	Electro-optical
EAM	Electro-absorption Modulator
eCPRI	evolved Common Public Radio Interface
EDFA	Erbium-Doped Fiber Amplifier
eMBB	Enhanced Mobile Broadband
EMI	Electromagnetic Interference
EML	Electro-absorption Modulated Laser
eMTC	enhanced Machine-Type Communication
EPC	Ethernet Packet Core
ER	Extinction Ratio
EVM	Error Vector Magnitude
f-OFDM	filtered-Orthogonal Frequency Division Multiplexing
FBMC	Filter Bank Multi-Carrier
FCC	Federal Communications Commission
FDD	Frequency Division Duplexing
FDM	Frequency Division Multiplexing
FEC	Forward Error Correction
FF	Flipflop
FFT	Fast Fourier Transform
FH	Fronthaul
FIR	Finite Impulse Response
FiWi	Fiber-Wireless
FiWiFi	Fiber-Wireless-Fiber
FMC	Fixed Mobile Convergence
FPGA	Field Programable Gateway Array
FSK	Frequency-Shift Keying
FSO	Free Space Optics
FTTA	Fiber-to-the-Antenna
FTTC	Fiber-to-the-Cabinet

FTTH	Fiber-to-the-Home
GFDM	Generalized Frequency Division Multiplexing
GPRS	General Packet Radio Service
GSM	Global System for Mobile
GTY	Gigabit Transceivers
HW	Hardware
IDFT	Inverse Digital Fourier Transform
IF	Intermediate frequency
IFFT	Inverse Fast Fourier Transform
IMD	Inter-Modulation Distortion
IMDD	Intensity Modulation – Direct Detection
IoT	Internet of Things
IQ	In-phase and Quadrature
KPI	Key Performance Indicator
LD	Laser Diode
LO	Local Oscillator
LoS	Line of Sight
LS	Least Squares
LTE	Long Term Evolution
LTE-A	Long Term Evolution – Advanced
LUT	Lookup Tables
M-QAM	Mary Quadrature Amplitude modulation
M-PSK	Mary Phase Shift Keying
MAC	Media Access Control
MC	Multi-Carrier
MFH	Mobile Fronthaul
MIMO	Multiple Input – Multiple Output
mMIMO	massive Multiple Input – Multiple Output
MMS	Multimedia Messaging Service
MMSE	Minimum Mean Squared Error
mmWave	millimeter Wave
MNO	Mobile Network Operator
MSA	Multi-Service Access
MU	Mobile Unit
MUE	Mobile User Equipment
MUX	Multiplexer
MVNO	Mobile Virtual Network Operator

MZM	Mach-Zehnder Modulator
NGFI	Next Generation Fronthaul Interface
NLOS	Non-Line of Sight
NMT	Nordic Mobile Telephone
NOC	Network Operation Centre
NPO	Network, Planning and Orchestration
NR	New radio
NRZ	Non-Return-to-Zero
O/E	Opto-electrical
OBSAI	Open Base Station Architecture Initiation
OCS	Optical Carrier Suppression
ODN	Optical Distribution Network
OFDM	Orthogonal Frequency Division Multiplexing
OFDMA	Orthogonal Frequency Division Multiple Access
OFLL	Optical Frequency Locked-Loops
OLT	Optical Line Terminal
OPLL	Optical Phase Locked-Loops
ORI	Open Radio Equipment Interface
OS	Operating System
OSA	Optical Spectrum Analyzer
OSSB	Optical Single Sideband
OTDR	Optical Time-Domain Reflectometer
OTT	Over The Top
OVS	Open Virtual Switch
PA	Power Amplifier
PAM-4	4-level Pulse Amplitude Modulation
PAPR	Peak-to-Average Power Ratio
PCB	Printed Circuit Board
PCS	Physical Coding Sublayer
PD	Photodiode
PHY	Physical Layer
PIC	Photonic Integrated Circuit
PLS	Physical Layer Split
PM	Phase Modulator
PON	Passive Optical Network
PoF	Power over Fiber
PSD	Power Spectral Density

PSK	Phase-Shift Keying
PtMP	Point-to-Multipoint
PtP	Point-to-Point
QoE	Quality of Experience
QoS	Quality of Service
QPSK	Quadrature Phase Shift Keying
RAM	Random Access Memory
RAMB	RAM block
RAN	Radio Access Network
RAP	Radio Access Point
RAT	Radio Access Technology
RAU	Radio Access Unit
RF	Radio Frequency
RFSoC	RF System on Chip
RIN	Relative Intensity Noise
RoE	Radio over Ethernet
RTT	Round-Trip Time
RRC	Root-Raised Cosine
RRH	Remote Radio Head
RRU	Remote Radio Unit
RS	Remote Station
RTL	Register-Transfer Level
RTO	Real-Time Oscilloscope
RU	Radio Unit
SAP	Service Access Point
SC	Single Carrier
SCM	Sub-Carrier Multiplexing
SDN	Software Defined Network
SDM	Space Division Multiplexing
SDoF	Sigma-Delta over Fiber
SFDR	Spur-Free Dynamic Range
SFO	Sampling Frequency Offset
SFP	Small Form Factor
SFPC	Smart Fiber Passive Component
SMF	Single Mode Fiber
SMS	Short Messaging Service
SNIR	Signal-to-Noise-and-Interference-Ratio

SNR	Signal-to-Noise Ratio
SOA	Semiconductor Optical Amplifier
SSMF	Standard Single Mode Fiber
SW	Software
TCP	Transmission Control Protocol
TDM	Time Division Multiplexing
TEC	Temperature Control
TIA	Transimpedance Amplifier
TIM	Telecom Italia
TDWDM	Time- and Wavelength- Division Multiplexing
TxRx	Transceiver
UC	Use Case
UDP	User Datagram Protocol
UFMC	Universal Filtered Multi-Carrier Modulation
UHD	Ultra-High Definition
UL	Uplink
UMTS	Universal Mobile Telecommunications System
URLLC	Ultra-Reliable Low Latency Communications
V2V	Vehicle-to-Vehicle
VHDL	VHSIC Hardware Description Language
VHSIC	Very High-Speed Integrated Circuits
VLAN	Virtual Local Area Network
VNF	Virtual Network Functions
VOA	Variable Optical Attenuator
VoIP	Voise over Internet Protocol
VoLTE	Voise over Long Term Evolution
VSA	Vector Signal Analyzer
WDM	Wavelength Division Multiplexing
WiFi	Wireless-Fiber
WLAN	Wireless Local-Area Network
XGS	10-gigabit-capable Symmetric
XMD	Cross-Modulation Distortion
ZF	Zero-Forcing

Εκτενής Περίληψη

Οι ασύρματες επικοινωνίες έκαναν την εμφάνισή τους γύρω στο 1895 με τη μετάδοση του κώδικα Μορς μέσω της Ραδιοτηλεγραφίας, χρησιμοποιώντας ηλεκτρομαγνητικά κύματα. Οι σύγχρονες ασύρματες επικοινωνίες χρησιμοποιούν μια παρόμοια μέθοδο μετάδοσης της πληροφορίας που στηρίζεται στη μετάδοση και λήψη ηλεκτρομαγνητικών κυμάτων. Ωστόσο, η εξέλιξη των συστημάτων ασυρμάτων επικοινωνιών έχει προχωρήσει σημαντικά με την πάροδο του χρόνου. Η εξέλιξη αυτή σηματοδοτείται από την εμφάνιση των σύγχρωνων κυψελωτών δικτύων κινητών επικοινωνιών. Η τεχνολογία κυψελωτών δικτύων κινητής έκανε την εμφάνησή της γύρω στο 1980, με τα δίκτυα 1ης γενιάς. Ωστόσο, η ραδγαία αύξηση της τηλεπικοινωνιακής κίνησησης κατά τις τελευταίες δεκατιές, αυξάνει συνεχώς τις απαιτίες από τα δίκτυα ασυρμάτων επικοινωνιών, τα οποία εξελίχθηκαν με πολύ γρήγορους ρυθμούς, φτάνοντας πλέον στην εμφάνιση των δικτύων 5ης γενιάς, ενώ σε ερευνητικό επίπεδο ήδη μελετάται και προετοιμάζεται η επικείμενη μετάβαση στην επόμενη γενιά (6G).

Η συνεχώς επιταχυνόμενη ανάπτυξη των δικτύων 5G σε παγκόσμιο επίπεδο, η οποία καλείται να δόσει λύση στις όλο και πιο αυστηρές απαιτήσεις των χρηστών των δικτύων κινητής, συμπεριλαμβανομένης της υποστήριξης πολύ μεγάλων ταχυτήτων μετάδοσης δεδομένων, χαμηλές τιμές καθυστέρησης, ευριά κάλυψη, υψηλή αξιοπιστία και χαμηλού κόστους προσβάσιμες υπηρεσίες υψηλής ποιότητας. Τα παραπάνω κατηγοροποιούνται στις εξής τρεις περιπτώσεις υπηρεσιών:

- Ευρυζωνική συνδεσιμότητα (eMBB): Στηρίζεται σε μη-αυτόνομες αρχιτεκτονικές δικτύου για την παροχή υψηλής ταχύτητας σύνδεσης στο Διαδίκτυο, μέτρια καθυστέρηση και αντιστοιχεί σε υπηρεσίες όπως ζωντανή μετάδοση βίντεο UltraHD και εφαρμογές εικονικής πραγματικότητας και επαυξημένης πραγματικότητας (AR/VR).
- Διασύνδεση μεγάλου αριθμού συσκευών (eMTC): Πρόκειται για μεγάλης εμβέλειας ευρυζωνική επικοινωνία τύπου συσκευή-με-συσκευή, που στηρίζεται σε τεχνολογίες που προσφέρουν χαμηλό κόστος και χαμηλή κατανάλωση ενέργειας. Το κύριο χαρακτηριστικό αυτού του τύπου συνδεσιμότητας είναι η εξασφάλιση υψηλού ρυθμού δεδομένων, η χαμηλή κατανάλωση ενέργειας και η εκτεταμένη κάλυψη με μειωμένη πολυπλοκότητα συσκευών. Ως εκ τούτου είναι ιδιαίτερα επωφελής για εφαρμογές Διαδικτύου των πραγμάτων (IoT).
- Συνδεσιμότητα υωηλής αξιοπιστίας με πολύ χαμηλές τιμές καθυστέρησης (URLLC): Η περίπτωση αυτή σκοπεύει στην παροχή χαμηλής καθυστέρησης και εξαιρετικά υψηλής αξιοπιστίας, διασφαλίζοντας έτσι υψηλή ποιότητα παροχής υπηρεσιών (QoS), κάτι που δεν μπορεί να επιτευχθεί με τις παραδοσιακές αρχιτεκτονικές δικτύου κινητής τηλεφωνίας. Σκοπεύει στην εξυπηρέτηση εφαρμογών όπως η απομακρυσμένη χειρουργική, η επικοινωνία από όχημα-με-όχημα (V2V), η βιομηχανία 4.0, τα έξυπνα δίκτυα και τα έξυπνα συστήματα μεταφορών.

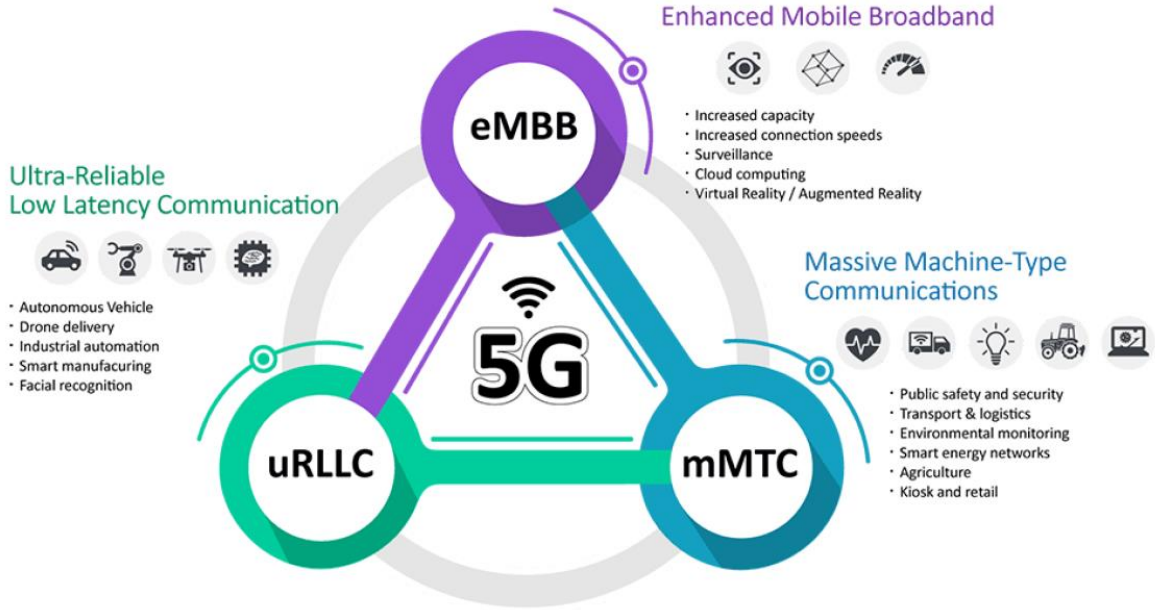

Figure 1. Βασικές υπηρεσίες και εφαρμογές που υποστηρίζονται από τα δίκτυα επόμενης γενιάς.

Τα τελευταία χρόνια, ο μετασχηματισμός των δικτύων πρόσβασης κιντών επικοινωνιών, προκειμένου να προσαρμοστούν στις απαιτήσεις των σύγχρονων υπηρεσιών και εφαρμογών, είναι στο επίκεντρο των ενεργειών που λαμβάνουν χώρα για την εγκαθίδρυση των 5G δικτύων. Σε αυτή την κατεύθυνση, η υιοθέτηση νέων καινοτόμων αρχιτεκτονικών και η ανάπτυξη κατάλληλων τεχνολογιών είναι απαραίτητη. Η υιοθέτηση μιας σειράς λειτουργικών διαιρέσων στα δίκτυα πρόσβασης είναι μια από τις μεθόδους που αξιοποιούνται με σκοπό των μετασηματισμό των δικτύων αυτών. Επιπλέον, καινοτόμες αρχιτεκτονικές που στηρίζονται στη χρήση νέων τύπων ζεύξεων που ορίζονται ως Fronthaul, Midhaul και Backhaul για τη διασύνδεση του δικτύου κορμού με τις απομακρυσμένες κεραίες. Το υψηλό κόστος και η πολυπλοκότητα που συνδέονται με την πλήρη αναβάθμιση του εξοπλισμού των δικτύων πρόσβασης με χρήση νέων τεχνολογιών, οδήγησε στην υιοθέτηση κεντρικοποιημένων διατάξεων δικτύων πρόσβασης (C-RAN). Ταυτόχρονα, η αξιοποίηση νέων οπτικών διεπαφών στο κομμάτι της μεταφοράς πληροφορίας από και προς τις απομακρυσμένες κεραίες, συμπεριλαμβανομένων των αναβαθμίσεων των ήδη υπαρχουσών διεπαφών (CPRI), αλλά και της χρήσης εντελώς νέων τεχνολογιών μεταφοράς δεδομένων, αποτελεί μια πολλά υποσχόμενη λύση για την υπέρβαση των περιορισμών που φέρουν οι υπάρχουσες υποδομές δικτύων κινητής τηλεφωνίας. Στην κατεύθυνση αυτή, η τεχνική μετάδοσης αναλογικών, ηλεκτικά διαμορφωμένων σημάτων σε υψίσυχνα φέροντα, μέσω οπτικής ίνας είναι μια από τις κυριότερες εναλλακτικές υλοποιήσεις δικτύων μεταφοράς δεδομένων που μελετάται τα τελευταία χρόνια στη βιβλιογραφία.

Στοχεύοντας στην μείωση του κόστους εγκατάστασης νέων υποδομών για την υποστήριξη των δικτύων πρόσβασης 5G, η επαναχρησιμοποίηση των ήδη υπαρχουσών οπτκών υποδομών είναι μια ακόμα παράμετρος που παίζει σημαντικό ρόλο στο σχεδιασμό των δικτύων κινητών επικοινωνιών επόμενης γενιάς. Η επαναχρησιμοποίηση των υποδομών των Παθητικών

Οπτικών Δικτύων στις μητροπολιτικές αποτελεί μια πιθανή λύση προς αυτή την κατεύθυνση, χάρη στην προσφορά μεγάλης πυνότητας εγκαταστάσεων οπτικών ινών και μεγάλου πλήθους οπτικών πομποδεκτών. Η πολυπλεξία μήκους κύματος και η πολυπλεξία χρόνου είναι οι δύο βασικές τεχνικές που μπορούν να χρησιμοποιηθούν για την ταυτόχρονη μετάδοση σημάτων 5G μέσω των παθητικών οπτικών δικτύων.

Το όρομα της μετάβασης στην επόμενη γενιά δικτύων και υπηρεσιών επικοινωνίας που θα παρέχουν ευρεία, εξαιρετικά γρήγορη και απρόσκοπτη συνδεσιμότητα, οδηγεί στην ανάγκη σχεδιασμού και υλοποίησης υποδομών δικτύων πρόσβασης, υψηλής χωρητικότητας και υψηλής ευελιξίας. Οι υποδομές νέας γενιάς θα πρέπει να μπορούν να προσαρμόζονται σε μια σειρά από υπηρεσίες που έχουν εντελώς διαφορετικές απαιτήσεις προκειμένου να μπορούν να λειτουργήσουν απρόσκοπτα. Για το σκοπό αυτό, η χρήση δυναμικά επαναπρογραμματιζόμενων πομποδεκτών που βασίζονται σε πλατφόρμες που περιλαμβάνουν συστοιχία-πυλών προγραμματιζόμενη στο πεδίο είναι μια πολλά υποσχόμενη λύση, μιας και επιτρέπει την ευέλικτη ανακατανομή των διαθέσιμων πόρων για τη μεταφορά, δρομνολόγηση και αποθήκευση δεδομένων, αλλά και για την επιτέλεση των ψηφιακών διεργασιών που υποστηρίζουν τις παραπάνω λειτουργίες.

Ταυτόχρονα, οι πολύ αυστηρές απαιτήσεις χωρητικότητας και καθυστέρησης που επιβάλλονται από τους δείκτες απόδοσης των υπηρεσιών που καλούνται να εξυπηρετήσουν τα δίκτυα 5G, επιβάλλουν ουσιαστικά την εισαγωγή του φάσματος χιλιοστομετρικών κυμάτων (mmWave) στα δίκτυα πρόσβασης κινητών επικοινωνιών. Ωστόσο, η τοποθέτηση κυψελών πρόσβασης σε τόσο υψηλές συχνότητες, απαιτούν την εγκατάσταση εξοπλισμού κεραιών σε πολύ κοντινή απόσταση μεταξύ τους αλλά και από τον τελικό χρήστη προκειμένου να υπάρχουν κενά στην κάλυψη. Το πραρπάνω αναμένεται να επηρεάσει σοβαρά το κόστος των μελλοντικών δικτύων πρόσβασης, κατά συνέπεια αναμένεται να οδηγήσει στα εξής τρία μεγάλα προβλήματα:

- Η διαύνδεση των κεντρικών σταθμών βάσης με τις απομακρυσμένες κεραίες δεν μπορεί να στηρίζεται μόνο σε οπτικές ζεύξεις, όπως συμβαίνει μέχρι σήμερα, καθώς αυτό θα απαιτούσε την εγκατάση υπερβολικά μεγάλου αριθμού επιπλεόν οπτκών ζεύξεων.
- Οι χιλιοστομετρικές κεραίες πρόσβασης θα πρέπει να γίνουν πολύ απλές όσον αφορά τη λειτουργικότητα, το υλικό και την ενεργειακή απόδοση για να διατηρηθεί εφικτό το κόστος εγκατάστασης και λειτουργίας.
- Οι χιλιοστομετρικές κεραίες πρόσβασης υποστηρίζουν την μετάδοση μέγαλων ταχυτήτων δεδομένων (τάξεως Gbps), χάρη στην ευρυζωνικότητά τους. Το προτέρημα αυτό της τεχνολογίας αυτής, ωστόσο επιφέρει μια σημαντική πρόκληση. Οι παραδοσιακές διεπαφές που χτηριμοποιούνται για τη διασύνδεση των κεραιών με τους σταθμούς βάσης αδυνατούν να υποστηρίξουν τόσο μεγάλο όγκο δεδομένων και ως εκ τούτου καινοτόμες λύσεις οπτικής μεταφοράς πληροφορίας θα πρέπει να αντικαταστήσουν ή να ενσωματωθούν παράλληλα με τις παραδοσιακές μεθόδους στα δίκτυα πρόσβασης.

Όπως αναφέρθηκε και πιο πάνω, για την υποστήριξη χαμηλής καθυστέρησης, υψηλής χωρητικότητας, οικονομικής απόδοσης και χαμηλής κατανάλωσης ενέργειας, ολόκληρα τα δίκτυα πρόσβασης, από άκρο σε άκρο, θα πρέπει να επανασχεδιαστούν. Ακολουθώντας αυτό το σκεπτικό, η ιδέα της συγκεντροποίησης των πόρων του δικτύου εμφανίστηκε εκ νέου στην εποχή των δικτύων 5G, καθώς παρουσιάζει σημαντικά προτερήματα σε σύγκριση με τις παραδοσιακές τοπολογίες, στις οποίες οι σταθμοί βάσης είναι κατανεμημένοι σε διάφορα σημεία του πεδίου. Η προσέγγιση αυτή της συγκεντρικοποίησης των επεξεργαστικών πόρων του δικτύου, ευνοεί τον διαχωρισμό των ραδιοστοιχείων του σταθμού βάσης (που ονομάζονται Remote Radio Heads, RRH) και των στοιχείων που επεξεργάζονται το σήμα (που ονομάζονται Baseband Units, BBUs). Όπως φαίνεται και στο Figure 2, τα στοιχεία που αναλαμβάνουν την επεξεργασία του σήματος μπορεί να βρίσκονται κεντρικά σε μία τοποθεσία ή ακόμη και εικονικά στο cloud.

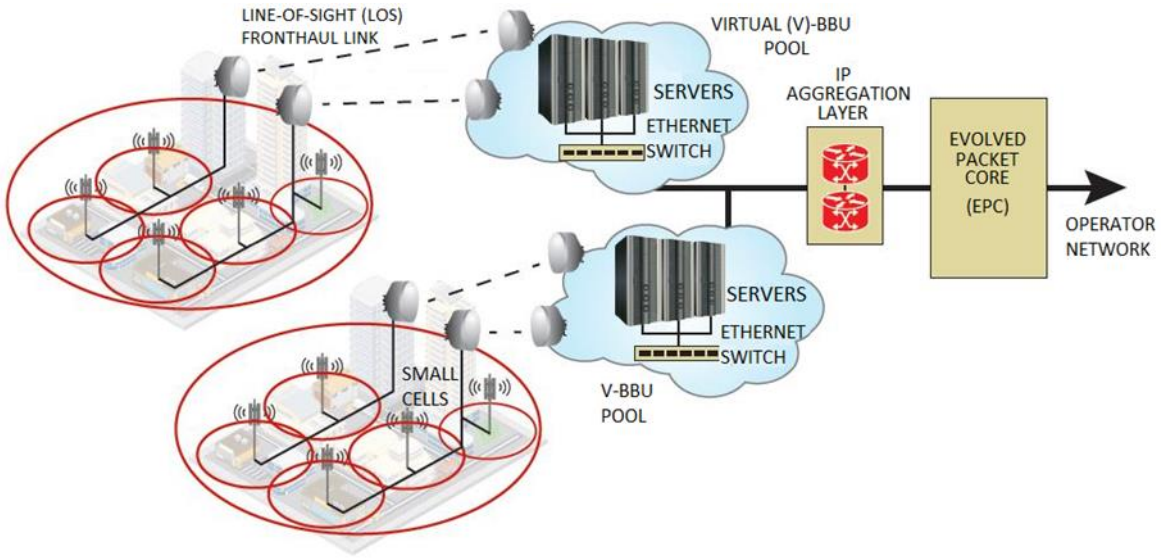

Figure 2. Ενδεικτική κεντρικοποιημένη αρχιτεκτονική που προορίζεται για δίκτυα πρόσβασης κινητών επικοινωνιών και έχει προταθεί από τη Fujitsu για πυκνοκατοικημένες αστικές περιοχές.

Η μεταφορά της τηλεπικοινωνιακής κίνησης μεταξύ των σταθμών βάσης και των κεραιών φαίνεται να επιφέρει σημαντικές πρόκλησεις στις τοπολογίες 5G, που σχετίζονται με την αντιμετώπιση διαφόρων ζητημάτων που αφορούν στην διεπαφή των οπτικών καναλιών με διαφορετικού τύπου πολύπλοκες ραδιοδιεπαφές. Λύση σε αυτά τα προβλήματα καλείται να δόσει η μέθοδος οπτικής μετάδοσης αναλογικών σημάτων, ηλεκτρικά διαμορφωμένα σε υψίσυχνα φέροντα. Με την ενσωμάτωση αυτής της τεχνικής στα οπτικά δίκτυα μεταφοράς, επιτυγχάνεται η οπτική μετάδοση κυματομορφών που είναι κατάλληλες για ασύρματη μετάδοση χωρίς την περαιτέρω επεξεργαία τους στην πλευρά των κεραιών (Figure 3). Η τεχνική αυτή επιτρέπει ταυτόχρονα τη μετάδοση μεγάλου ρυθμού πληροφορίας χρησιμοποιόντας απλούς και οικονομικούς οπτικούς πομποδέκτες. Ένα επιπλέον προτέρημα των αναλογικών αυτών υλοποιήσεων είναι ότι προσφέρουν τη δυνατότητα αρμονικής συνύπαρξης της 5G κίνησης με άλλου τύπου δεδομένα, στην ήδη εγκατεστημένη υποδομή οπτικών ινών που υποστηρίζουν οι τοπολογίες Παθητικών Οπτικών Δικτύων της σταθερής

ενσύρματης γραμμής στις μητροπολιτικές περιοχές. Ωστόσο τα πλεονεκτήματα που αναφέρθηκαν παραπάνω επιφέρον το κόστος της αυξημένης πολυπλοκότητας υλικού στην πλευρά των σταθμών βάσης, οι οποίοι φιλοξενούν το σύνολο των λειτουργιών ψηφιακής επεξεργασίας σήματος που είναι αναγκαίες για τη διαμόρφωση και σωστή λήψη των αναλογικών κυματομορφών. Επιπλέον, η οπτική μετάδοση αναλογικών σημάτων είναι ευαίσθητη σε μια σειρά από φαινόμενα υποβάθμισης της ποιότητας μετάδοσης, οι οποίες με είναι υπεύθυνες για την προσθήκη θορύβου και τη γραμμική ή μη γραμμική παραμόρφωση των ληφθέντων κυματομορφών.

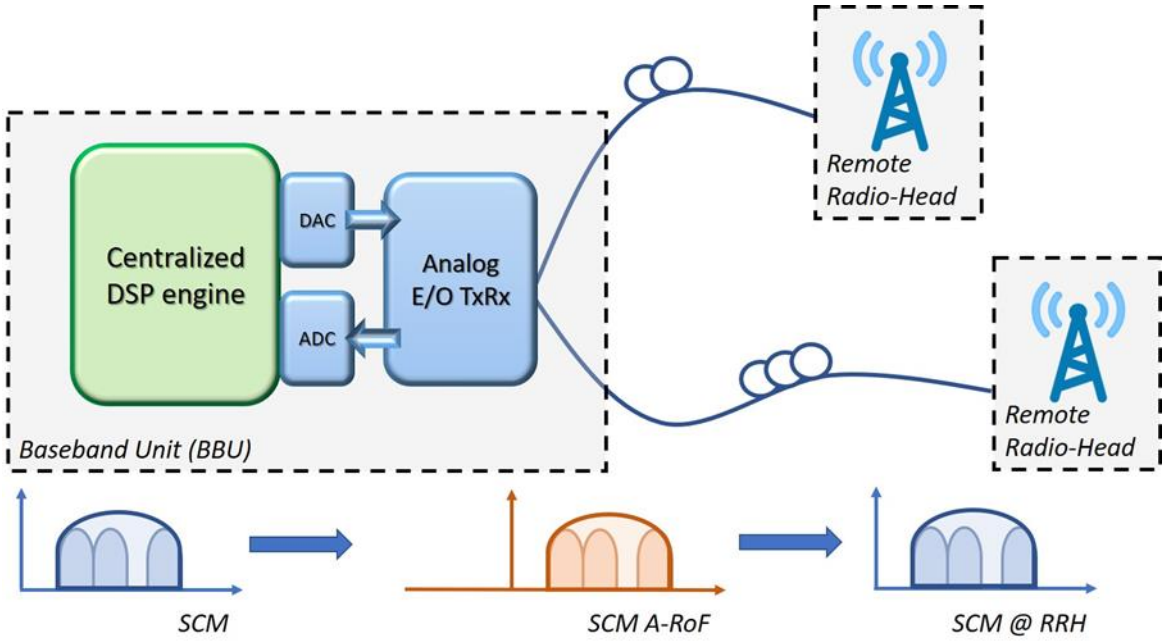

Figure 3. Ενδεικτική τοπολογία που περιλαμβάνει τη μετάδοση αναλογικών κυματομορφών σε οπτική ίνα και στηρίζεται στη χρήση τεχνικών ψηφιακής επεξεργασίας σήματος.

Τα βασικά προτερηματα της τεχνικής μετάδοσης αναλογικών κυματομορφών μέσω οπτικής ίνας είναι τα παρακάτω:

- Χαμηλές τιμές απωλειών
- Χαμηλή πολυπλοκότητα συστήματος
- Χαμηλό κόστος υλοποίησης
- Διαχρονικότητα
- Εύκολη εγκατάσταση και συντήρηση
- Ευρυζωνικότητα
- Ανθεκτικότητα σε παρεμβολές ραδιοσυχνοτήτων
- Χαμηλή κατανάλωση ενέργειας

Ωστόσο, όπως αναφέρθηκε πιο πάνω, η ποιότητα μετάδοσης υποβαθμίζεται από μια σειρά από παράγοντες, οι κυριότεροι εκ των οποίων είναι οι δύο παρακάτω:

- Χρωματική διασπορά, κατά τη μετάδοση στην ίνα

- Μη γραμμική παραμόρφωση που οφείλεται στα ενεργά ηλεκτρονικά και ηλεκτρο-οπτικά στοιχεία της ζεύξης

Ένας τρόπος να υπερβούν τα δίκτυα πρόσβασης επόμενης γενιάς το τεράστιο κόστος εγκατάστασης μεγάλου αριθμού νέων οπτικών ζεύξεων, είναι η χρήση ασυρμάτων κατευθυντικών καναλιών για την διασύνδεση ήδη υπαρχόντων οπτικών τερματικών μεταξύ τους. Οι νέες αυτές ζεύξεις που στηρίζονται στην σειριακή τοποθέτηση κατεθυτντικών σημείο-σε-σημείο οπτικών και ασυρμάτων καναλιών μπορούν να διασυνδέσουν τους σταθμούς βάσεις με τις απομακρυσμένες κεραίες με οικονοκό και ευέλικτο τρόπο. Η μετάδοση αναλογικών κυματοματομορφών πρώτα σε ίνα και έπειτα στον αέρα είναι μια πολύ αποδοτική μέθοδος υλοποίησης τέτοιων διασυνδέσεων. Ανάλογα με το εύρος συχνοτήτων του υποστηρίζει ο ασύρματος χιλιοστομετρικός εξοπλισμός σε αυτού του τύπου τις ζεύξεις, τα συστήματα οπτικής-ασύρματης μετάδοσης χωρίζονται σε δύο κατηγορίες. Στην πρώτη περίπτωση, μεταδίδονται στην ίνα σήματα τα οποία είναι από πριν διαμορφωμένα στην συχνότητα λειτουργίας των ασυρμάτων κεριαών (RoF). Στην δεύτερη περίπτωση αξιοποιείται μια ενδιάμεση φέρουσα συχνότητα για την μετάδοση στην ίνα και πριν την ασύρματη διάδοση του σήματος προστίθεται ένα επιπλέον στάδιο αναλογικής διαμόρφωσης σε ακόμα υψηλότερη φέρουσα συχνότητα (αυτή που υποστηρίζεται από τις τον ασύρματο εξοπλισμό), (IFoF).

Στα πλαίσια της παρούσας διατριβής, υλοποιήθηκαν κάποιες πρώτες δοκιμές που σκοπό είχαν την πειραματική επίδειξη της παραπάνω ιδές. Για το σκοπό αυτό, υλοποιήθηκε μια τοπολογία αναλογικής μετάδοσης διαμορφωμένου σήματος σε ίνα και στη συνέχεια σε χιλιοστομετρική ασύρματη ζεύξη με συχνότητα λειτουργίας στα 60GHz. Η λειτουργία της ζεύξης αυτής στηρίχθηκε στη χρήση αλγορίθμων ψηφιακής επεξεργασίας σήματος τόσο στην πλευρά του πομπού όσο και στου δέκτη. Τα σχήματα διαμόρφωσης που χρησιμοποιήθηκαν ήταν της μορφής: κωδικοποίησης αλλαγής φάσης (PSK) και διαμόρφωσης πλάτους και φάσης (QAM), ενώ ταυτόχρονα δοκιμάτηκε η ψηφιακή πολυπλεξίας πολλαπλών διαμορφωμένων σημάτων σε διαφορετικές φέρουσες συχνότητες, στοχεύοντας στην βέλτιστη αξιοποίηση του διαθέσιμου ευρους ζώνης και στην αύξηση του ρυθμού μετάδοσης δεδομένων. Οι οπτικές αποστάσεις που επιτεύψθηκαν σε αυτή την πειραματική φάση ήταν μεχρι 25km και ο μέγιστος ρυθμός μετάδοσης δεδομένων που επιτεύψθηκε ήταν 24Gbps.

Οι επόμενες παράγραφοι επιχειρούν να εμβαθύνουν στο κομμάτι των τεχνικών διαμόρφωσης και ψηφιακής επεξεργασίας των σημάτων που είναι κατάλληλα για μετάδοση σε αναλογικές οπτικές-ασύρματες ζεύξεις. Έτσι, για την υποστήριξη των τρεχουσών κινητών επικοινωνιών, υπάρχουν δύο κύριοι τύποι τεχνικών διαμόρφωσης της πληροφορίας: διαμορφώσεις ενός φέροντος και διαμορφώσεις πολλαπλών φερόντων. Η διαφορά των δύο αυτών μεθόδων έγκειται στο ότι τα συστήματα διαμόρφωσης ενός φέροντος χρησιμοποιούν μια και μόνο φέρουσα συχνότητα σήματος για τη μετάδοση όλης της πληροφορίας, ενώ τα συστήματα διαμόρφωσης πολλαπλών φερόντων διαιρούν το διαθέσιμο εύρος ζώνης σε πολλά υπο-φέροντα. Στη συνέχεια, η ροή δεδομένων υψηλής ταχύτητας χωρίζεται σε πολλαπλές ροές χαμηλής ταχύτητας, οι οποίες μεταδίδονται παράλληλα πολυπλεγμένες στο πέδιο της συχνότητας, μέσω της διαμόρφωσή τους με χρήση των διαφορετικών υπο-φερόντων. Οι τεχνικές διαμόρφωσης ενός φέροντος έχουν χρησιμοποιηθεί ευρέως σε πολλά συστήματα

ασύρματης επικοινωνίας, συμπεριλαμβανομένων των συμβατικών 1G, 2G, 3G και της ανερχόμενης ζεύξης των δικτύων 4G. Ο λόγος που η χρήση αυτής της τεχνικής ήταν τόσο διαδεδομένη στα ασύρματα συστήματα μετάδοσης των προηγούμενων ειδικά δεκατιών είναι ότι έχουν μια σειρά από προτερήματα. Πρώτα απ 'όλα, έχουν πολύ χαμηλό λόγο ισχύος κορυφής προς μέσο όρο ισχύος (PAPR), ο οποίος είναι ευνοεί τη σταθερότητα των συστημάτων και την υιοθέτηση συσκευών χαμηλού κόστους στο σχεδιασμό συστημάτων ασύρματης επικοινωνίας. Επιπλέον, τα συστήματα διαμόρφωσης ενός φορέα είναι λιγότερο ευαίσθητα στη μετατόπιση συχνότητας και στο θόρυβο φάσης, καθιστώντας ευκολότερο τον συγχρονισμό χρόνου και συχνότητας, ειδικά για συστήματα επικοινωνίας σημείου-προς-σημείο.

Ωστόσο, σε σύγκριση με τις τεχνικές διαμόρφωσης πολλαπλών φερόντων, οι διαμορφώσεις ενός φέροντος παρουσιάζουν σημαντιά μικρότερη αποτελεσματικότητα στην αντιμετώπιση του φαινομένου εξασθένησης του σήματος λόγω πολλαπλών διαδρομών που προκύπτουν από ανακλαστικές επιφάνειες κατά την ασύρματη μετάδοση, οδηγώντας τελικά σε μειωμένη φασματική απόδοση. Η μειωμένη αυτή φασματική απόδοση οφείλεται στην ανάγκη χρήσης μεγάλων κενών διαστημάτων ανάμεσα στα σειριακά μεταδιδόμενα σύμβολα, προκειμένου να αποφευχθεί η παραμόρφωση του σήματος στην πλευρά του δέκτη. Έτσι τα συστήματα διαμόρφωσης πολλαπλών φερόντων φαίνεται να είναι μια πολύ ελκυστική λύση για μελλοντικές υλοποιήσεις των δικτύων πρόσβασης κινητών επικοινωνιών, λόγω της ικανότητάς τους να ξεπερνούν τις προκλήσεις που τίθενται από τα ασύρματα κανάλια που εμφανίζουν εξασθένιση λόγω πολλαπλών διαδρομών. Μεταξύ αυτών των συστημάτων, η τεχική ορθογώνιας πολυπλεξίας διαιρεμένης συχνότητας (OFDM) είναι η πιο γνωστή και καθιερωμένη μέθοδος διαμόρφωσης πολλαπλών φερόντων. Από τη φύση τους, τα συστήματα διαμόρφωσης πολλαπλών φερόντων παρουσιάζουν υψηλή ανθεκτικότητα έναντι της παραμόρφωσης του σήματος λόγω παρεμβολής μεταξύ διαδοχικά διαδιδόμενων συμβόλων (ISI) σε σύγκριση με συστήματα διαμόρφωσης ενός φορέα. Επιπλέον, ειδικά η χρήση της ορθογώνιας πολυπλεξίας διαιρεμένης συχνότητας απλοποιεί σημαντικά το σχεδιασμό του δέκτη και μειώνει το κόστος υλοποίησης του. Αυτό οφείλεται στο γεγονός ότι απλές μέθοδοι επεξεργασίας του ληφθέντος σήματος, οι οποίες στηρίζονται στη χρήση απλών ισοσταθμιστών που επεξεργάζονται το σήμα στο πεδίο των συχνοτήτων, αλλά και στην προσθήκη ενός κυκλικού προθέματος ανάμεσα στα μεταδιδόμενα σύμβολα, ειναι αρκετές για την επιτυχημένη ανάκτηση του σήματος.

Σαν επόμενο βήμα, μια σειρά από εναλλακτικές κυματομορφές πολλαπλών φερόντων, πέρα από την κλασιική τεχνική ορθογώνιας πολυπλεξίας, έχουν εμφανιστεί τα τελευταία χρόνια, ως πιθανές διεπαφές για την οπτική διαύνδεση των απομακρυσμένων κεραιών με τους σταθμούς βάσης, τόσο στα πλαίδια της 5G εποχής αλλά κοιτόντας και προς τις επόμενες γενιές δικτύων κινητών επικοινωνιών. Κομμάτι της παρούσας διατριβής ήταν και η μελέτη των πιο διαδεδομένων κυματομορφών πολλαπλών φερόντων καθώς και η σύγκρισή τους, προκειμένου να προσδιοριστεί η κυματομορφή η οποία τελικά υιοθετήθηκε για περαιτέρω ανάπτυξη και πειραματικές μελέτες. Οι πιο αξιοσημείωτες εναλλακτικές προσεγγίσεις πολλαπλών φερόντων, οι οποίες προσπαθούν με διάφορες τεχνικές να ξεπεράσουν τους περιορισμούς της κλασσικής ορθογώνιας πολυπλεξίας διαιρεμένης συχνότητας χρησιμοποιούν συνήθως ζωνοπερατά φίλτρα ή φίλτρα διαμόρφωσης παλμών και είναι οι

ακόλουθες: η πολυπλεξία φερόντων με χρήση συστοιχίας φίλτρων (FBMC), η τεχνική πολλαπλών φερόντων με μοναδικό φίλτρο, και η γενικευμένη πολυπλεξία διαίρεσης συχνότητας (GFDM).

Μεταξύ των διαφόρων κυματομορφών πολλαπλών φερόντων που προτείνονται για εφαρμογές 5G που μελετήθηκαν στα πλαίσια της παρούσας διατριβής, στο επίκεντρο για τον σχεδιασμό αλγορίθμων ψηφιακής επεξεργασίας σήματος με σκοπό την υλοποίηση ενός αναλογικού πομποδέκτη τέθηκε η κλασσική περίπτωση ορθογώνιας πολυπλεξίας διαίρεσης συχνότητας. Η επιλογή αυτής της κυματομορφής βασίστηκε στη συμβατότητά της με τις τωρινές 4G υλοποιήσεις, καθιστώντας τη ένα πιθανό ενδιάμεσο βήμα για το σταδιακό μετασχηματισμό των δικτύων πρόσβασης κινητών επικοινωνιών, καθώς και στη χαμηλή πολυπλοκότητα υλοποίησης της και άρα στην καταλληλότητά της για χρήση σε πομποδέκτες που στηρίζονται σε επαναπρογραμματιζόμενες πλατφόρμες. Όπως θα εξηγηθεί και στις επόμενες παραγράφους, οι πλατφόρμες αυτές αποτέλεσαν σημαντικό εργαλείο για την πειραματική αξιολόγηση της λύσης αυτής. Οι αλγόριθμοι ψηφιακής επεξεργασίας σήματος που υλοποιήθηκαν για τη δημιουργία ενός αναλογικού πομποδέκτη ικανού να υποστηρίξει τη μετάδοση κυματομορφών ορθογώνιας πολυπλεξίας διαίρεσης συχνότητας σε οπτικές-ασύρματες ζεύξεις απεικονίζονται στο Figure 4.

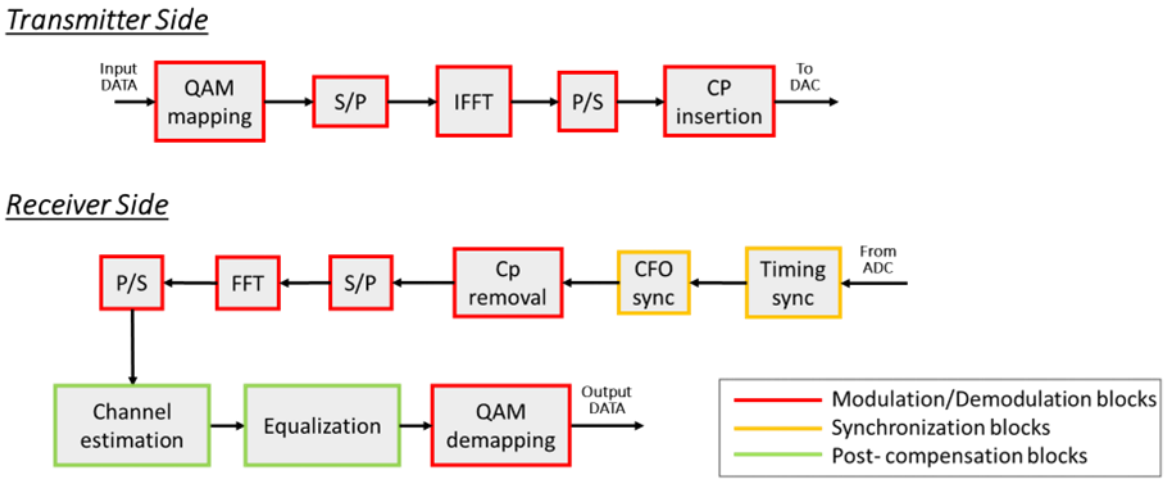

Figure 4. Αλγόριθμοι ψηφιακής επεξεργασίας σήματος για τη δημιουργία ενός αναλογικού πομποδέκτη ικανού να υποστηρίξει τη μετάδοση κυματομορφών ορθογώνιας πολυπλεξίας διαίρεσης συχνότητας

Όπως φαίνεται και στο σχήμα, πρακτικά μελετήθηκαν τριών ειδών αλγόριθμοι: οι αλγόριθμοι που στοχεύουν στη διαμόρφωση και αποδιαμόρφωση των σημάτων, οι αλγόριθμοι που στοχεύουν στο συγχρονισμό και τέλος οι αλγόριθμοι που που χρησιμεύουν στην ισοστάθμιση των ληφθέντων σημάτων. Συγκεκριμένα, οι λειτουργίες που αφορούν στη δημιουργία των συμβόλων πολλαπλών φερουσών, είναι η διαμόρφωση των συμβόλων αρχικά με διαμόργωση πλάτους/φάσης, η αντιστοίχιση των συμβόων αυτών στα ορθογώνια υπο-φέροντα με χρήση μετασχηματισμού Fourier και η εισαγωγή του κυκλικού προθέματος στην πλευρά του πομπού, κάθως και οι αντίστοιχες λειτουργίες στην πλευρά του δέκτη. Σε ότι αφορά το συγχρονισμό, χωρίζεται σε συγχρινισμό χρόνου και συγχρονισμό συχνότητας. Στην πρώτη περίπτωση, οι χρήση ψηφιακών αλγορίθμων στοχεύει στην απαλειφή των αποτυχιών

συγχρονισμού χρονισμού αναφέρονται, λόγω ατελούς ανίχνευσης των πρώτων δειγμάτων εκάθε συμβόλου, που οδηγεί στην εφαρμογή του μετασχηματισμού Fourier σε ελαφρώς μετατοπισμένα χρονικά παράθυρα, που λανθασμένα περιλαμβάνουν δείγματα πό προηγούμενα ή επόμενα σύμβολα. Στην δεύτερη περίπτωση, στόχος είναι η αντιμετώπιση της μετατοπίσης της κεντρικής συχνότητας των υπο-φερόντων που προκαλούνται από κακή ευθυγράμμιση μεταξύ των συχνοτήτων των τοπικών ταλαντωτών της κεραίας πομπού και της κεραίας δέκτη. Τέλος, για το κομμάτι της ισοστάθμισης του σήματος, χρησιμοποιήθηκε η ευρέως διαδεδομένη τεχνική ελαχίστων τετραγώνων, η οποία παρουσιάζει ιδιαίτερα χαμηλή πολυπλοκότητα υλοποίησης.

Για την πειραματική αξιολόγηση των παραπάνω, χρησιμοποιήθηκε μια επαναπρογραμματιζόμενη πλατφόρμα στην πλευρά του πομπού για τη δημιουργία των συμβόλων πολλαπλών φερόντων και εμπορικα διαθέσιμα, χαμηλού κόστους οπτο-ηλεκτρικά και ηλεκτρο-οπτικά στοιχεία που λειτουργούσαν σε ταχύτητες έως 10Gbps. Για την οπτική διαμόρφωση χρησιμοποιήθηκέ ένα λέιζερ διαμόρφωσης μέσω ηλεκτροαπορρόφησης και μια φωτοδίοδος χιονοστοιβάδας. Η ανάκτηση των σημάτων έγινε μετά από λήψη με χρήση παλμογράφου και εφαρμογή αλγορίθμων επεξεργασίας μέσω της πλατφόρμας MATLAB. Η επιτυχής λειτουργία της συνολικής ζεύξης που περιλάμβανε το οπτικό κανάλι και έπειτα μια κατευθυντική ασυρματη ζεύξη με λειτουργία στα 60GHz, επαληθεύτηκε για σήματα εύρους ζώνης 200MHz και 400MHz. Η μέγιστη ταχύτητα μετάδοσης δεδομένω που δείχθηκε ήταν 1.6Gbps. Τόσο η πειραματική διάταξη που χρησιμοποιήθηκε όσο και κάποια ενδεικτικά αποτελέσματα φαίνονται στα επόμενα σχήματα (Figure 5, Figure 6).

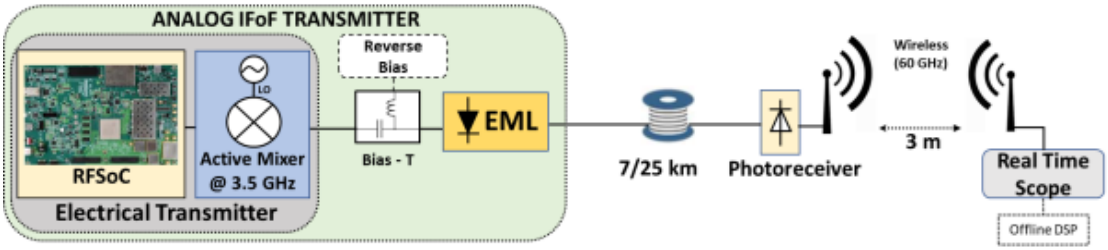

Figure 5. Πειραματική διάταξη για τη μετάδοση σημάτων από οπτική-ασύρματη ζεύξη.

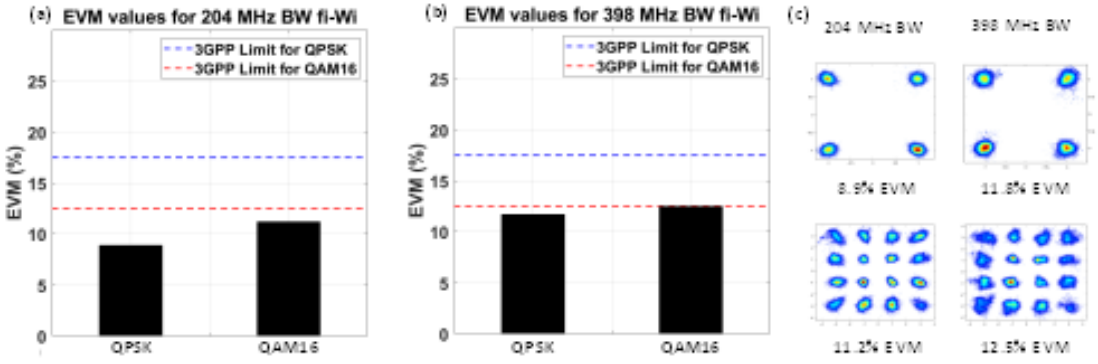

Figure 6. Παρουσίαση αποτελεσμάτων οπτικής-ασύρματης μετάδοσης, με χρήση διαγραμμάτων αστερισμού και τιμών διανυσματικού μεγέθους σφάλματος.

Μετά από την πειραματική αξιολόγηση της παραπάνω αναλογικής οπτικής-ασύρματης ζεύξης, το επόμενο βήμα ήταν η δοκιμή ενσωμάτωσής της σε ένα πραγματικό δίκτυο οπτικών επικοινωνιών. Για το σκοπό αυτό αξιοποιήθηκε το Παθητικό Οπτικό Δίκτυο της TIM, το οποίο διασυνδέοι τους σταθερούς χρήστες στην πόλη του Τορίνο. Η τοπολογία που δείχθηκε προορίζεται για την υποστήριξη οπτικής-ασύρματης διασύνδεσης σταθμών βάσης με απομακρυσμένες κεραίες και συγκεκριμένα αντιστοιχεί στο καθοδικό κομμάτι της ζεύξης που μεταφέρει την πληροφορία προς τις κεραίες. Τα αναλογικά οπτικά σήματα, αρχικά μεταδόθηκαν στο οπτικό δίκτυο του Τορίνο, ταυτόχρονα με την κίνηση των σταθερών χρηστών της πόλης κι έπειτα στάλθηκαν στον αέρα με χρήση ασύρματου εξοπλισμού στα 60GHz. Η πολυπλεξία και αποπολυπλεξία της κίνησης 5G έγινε με χρήση του εξοπλισμού οπτικής πολυπλεξία/αποπολυπλεξίας του Παθητικού Οπτικού Δικτύου, μέσω της τεχνικής πολυπλεξίας μήκους κύματος. Στα επόμενα σχήματα απεικονίζεται η πειραματική διάταξη καθώς και ενδεικτικά αποτελέσματα. Τα αποτελέσματα αυτά δείχνουν επιτυχή λήψη των μεταδιδόμενων σημάτων μετά από οπτική-ασύρματη διάδοση μέσα από τις οπτικές εγκαταστάσεις της TIM, που επιβεβαιώνεται από τις χαμηλές τιμές του διανυσματικού μεγέθους σφάλματος των ληφθέντων συμβόλων.

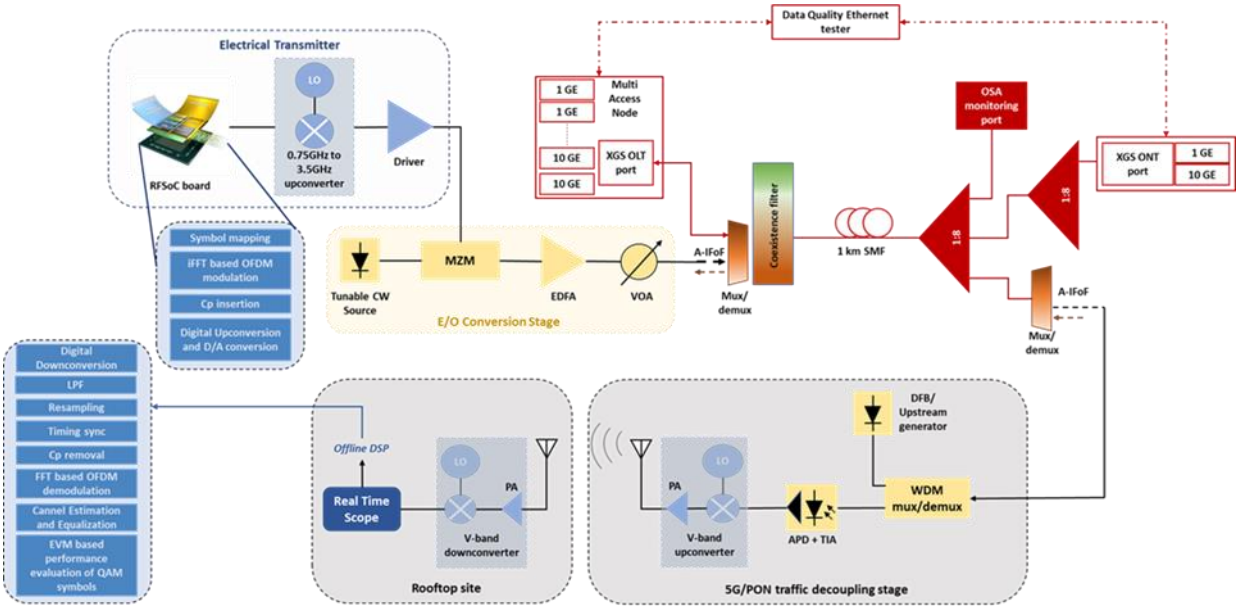

Figure 7. Πειραματική διάταξη της αναλογικής οπτικής-ασύρματης ζεύξης, συμπελιλαμβανομένης της οπτικής υποδομής του Παθητικού Οπτικού Δικτύου στο Τορίνο.

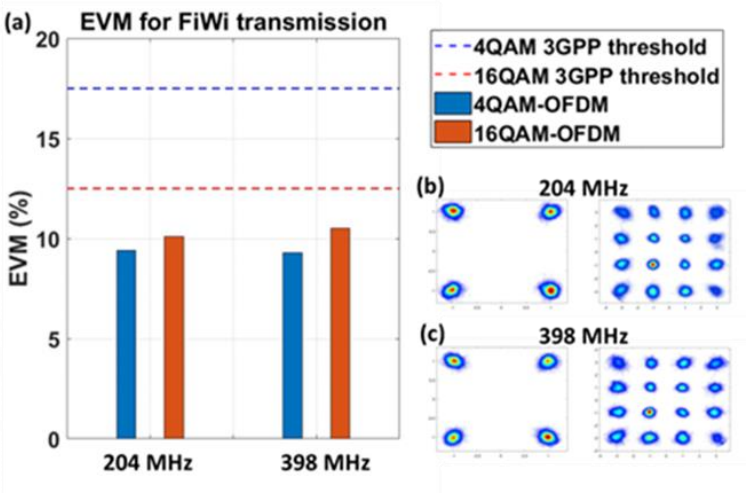

Figure 8. Παρουσίαση αποτελεσμάτων οπτικής-ασύρματης μετάδοσης, με χρήση διαγραμμάτων αστερισμού και τιμών διανυσματικού μεγέθους σφάλματος.

Η πρώτη αυτή μεγάλης κλίμακας πειραματική επίδειξη της μελετηθείσας αναλογικής οπτικής-ασύρματης υλοποίησης ενός δικτύου μεταφοράς για δίκτυα πρόσβασης κινητών επικοινωνιών σε συνεργασία με ένα εγκατεστημένο δίκτυο οπτικών ινών ήταν το πρώτο βήμα για την εξέταση της δυνατότητας ενσωμάτωσης τέτοιων φουτουριστικών λύσεων σε πραγματικές υποδομές δικτύου. Ακολουθώντας αυτή την κατεύθυνση, το επόμενο βήμα ήταν η επίδειξη της ενσαμάτωης του υπό μελέτη αναλογικού πομποδέκτη σε μια πραγματική υποδομή κινητών επικοινωνιών, εγκατεστημένη στην Αθήνα. Η επίδειξη αυτή έγινε στα πλαίσια του ευρωπαϊκού έργου 5GPHOS και η υποδομή που αξιοποιήθηκε πρόσφερε πρόσβαση σε παραγματικό εξοπλισμό πρόσβασης τεχνολογίας 4G. Η ενσωμάτωση του αναλογικού πομποδέκτη στην προαναφερθείσα εγκατάσταση έγινε με χρήση μιας επαναπρογραμματιζόμενης πλατφόρμας, ικανή να εκτελέσει σε πραγματικό χρόνιο λειτουργίες ψηφιακής επεξεργασίας και συμβατής επιπλέον με κίνηση Ethernet για την επεξεργασία πραγμαικών δεδομένων χρηστών. Η παραπάννω πλατφόρμα, σε συνεργασία με ένας ελεγκτή δικτύου, άλλαζε δυναμικά το ρυθμό μετάδοσης δεδομένο, προφέροντας έτσι προσαρμογή του πομποδέκτη στις απαιτήσεις των υπηρεσιών που εξυπηρετούσα ανά πάσα στιγμή. Η πειραματική διάταξη που υλοποιήθηκε καθώς και ενδεικτικά αποτελέσματα φαίνονται στα επόμενα δύο σχήματα (Figure 9, Figure 10).

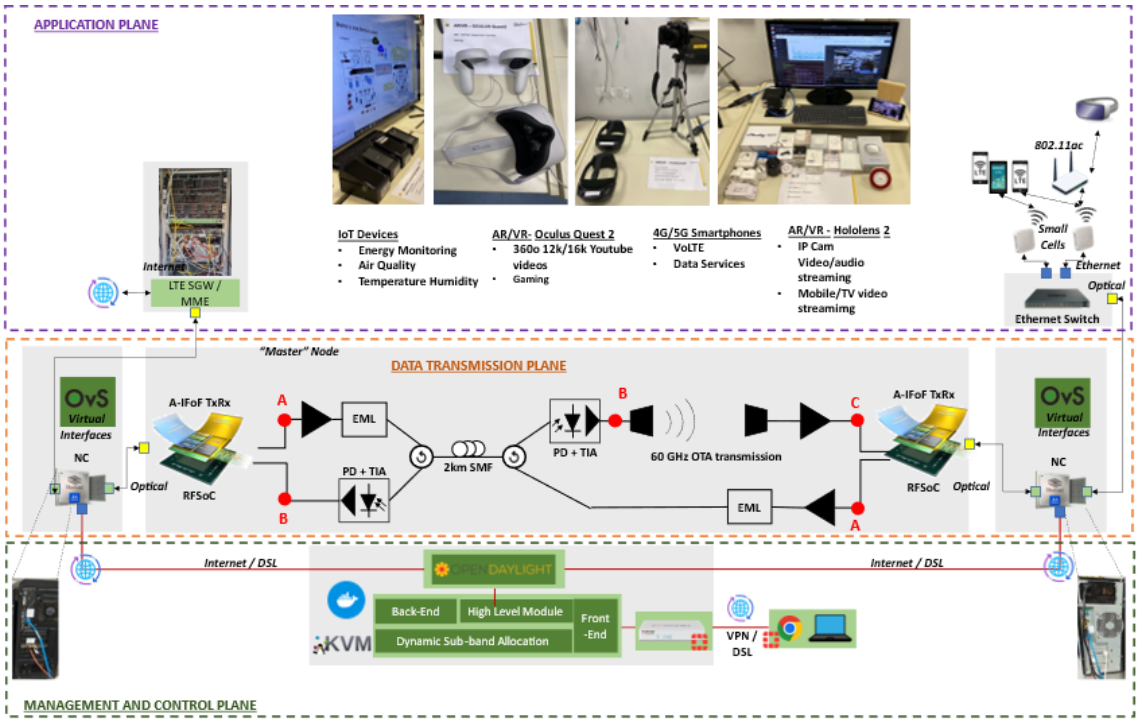

Figure 9. Υλοποιημένη διάταξη της πειραματικής επίδειξης.

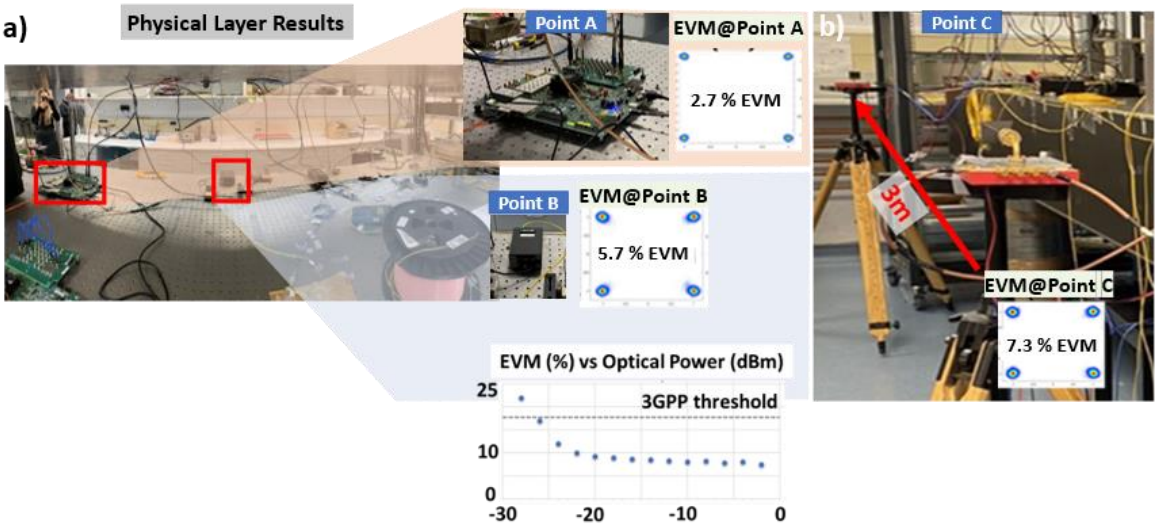

Figure 10. Παρουσίαση ενδεικτικών αποτελεσμάτων της πειραματικής επίδειξης, με χρήση διαγραμμάτων αστερισμού και τιμών διανυσματικού μεγέθους σφάλματος.

Με λίγα λόγια, η πρώτη επιβεβαίωση της σωστής λειτουργίας της υποδομής έγινε με μετρήσεις σε επίπεδο φυσικού στρώματος, μέσω διαγραμμάτων αστερισμού και τιμών διανυσματικού μεγέθους σφάλματος. Η αδιάλειπτη λειτουργία της διάταξης επικυρώθηκε επιπλέον σε επίπεδο εφαρμογών, μέσω της αξιολόγησης της απόδοσης διαφόρων υπηρεσιών, όπως οι εφαρμογές επαυξημένης πραγματικότητας/εικονικής πραγματικότητας που εκτελέστηκαν μέσω της υλοποιημένης υποδομής, καθώς και με μετρήσεις απόδοσης,

χρησιμοποιώντας εργαλεία παρακολούθησης κυκλοφορίας, παρουσιάζοντας μέγιστο ρυθμό δεδομένων ανά χρήστη έως 474 Mbps.

Συμπερασματιικά, η δυνατότητα χρήσης καινοτόμων πομποδεκτών για την υποστήριξη μετάδοσης αναλογικών κυματομορφών σε οπτικές και οπτικές-ασύρματες ζεύξεις εντός της εποχής 5G και πέρα, εξετάστηκε λεπτομερώς στην τρέχουσα διατριβή. Στα πλαίσια αυτά η παρούσα διατριβή επιχείρησε να περιγράψει μια αρχιτεκτονική προσέγγιση για την πραγματική ανάπτυξη και ενσωμάτωση της φωτουριστικής αυτής λύσης σε κλασσικές υποδομές δικτύου και να επικυρώσει την ιδέα αυτή με μια σειρά από πειραματικές δραστηριότητες σε εργαστηριακό περιβάλον αλλά και σε μεγάλης κλίμακας επιδείξεις. Ωστόσο, η συνύπαρξη ψηφιακών και αναλογικών ροών δεδομένων κινητής τηλεφωνίας σε ενοποιημένες τοπολογίες οπτικού δικτύου παραμένει μια πρόκληση. Στην κατεύθυνση αυτή, η χρήση ενεργών, προγραμματιζόμενων οπτικών κόμβων για την ταυτλοχρονη εξυπηρέτηση ετερογενών τεχνολογιών μετάδοσης δεδομένων κινητών επικοινωνιών είναι μια πολύ ελκυστική προσέγγιση που έχει συζητηθεί εκτενώς τα τελευταία χρόνια στη βιβλιογραφία. Ταυτόχρονα σε μια προσπάθεια περιγραφής μεθόδων που θα ενισχύσουν περαιτέρω την αποδοτικότητα των αναλογικών δικτύων μεταφοράς δεδομένων, η ενσωμάτωσή τους με οπτικές ζεύξεις ελεύθερου χώρου είναι ένα ανοιχτό θέμα συζήτησης εντός της επιστημονικής κοινότητας τα τελευταία χρόνια και αναμένεται να παραμείνει στο επίκεντρο καθώς βαδίζουμε στη μετά 5G εποχή.

CHAPTER 1.
Introduction

This section lays the groundwork for understanding the historical trajectory and transformative milestones that have shaped the mobile communication ecosystem. Moving forward, the pivotal role of Optical Access Network Interfaces in the era of 5G and beyond is illustrated. Here, the nuanced details of Optical Interfaces tailored for 5G X-Haul, shedding light on the technological advancements that facilitate the seamless integration of optical solutions into the evolving mobile network architecture are explored. The exploration deepens with a dedicated focus on Future Mobile Networks' Applications, Use Cases, and Key Performance Indicators (KPIs), providing insights into the anticipated applications and performance metrics that will define the landscape of mobile networks in the foreseeable future and pave the path towards future RAN evolution strategies.

1.1. Evolution of mobile networks

Wireless communication made its debut around 1895 with the transmission of Morse code through Radiotelegraphy, utilizing electromagnetic waves. Contemporary wireless communication employs a comparable phenomenon in transmitting and receiving signals through electromagnetic wave transmission. The evolution of wireless transmission has progressed over time, transitioning from radio telephones to the advent of cellular networks in mobile communication. The field of wireless communication has experienced exponential growth over the years.

The initial phase of mobile cellular technology, known as the first generation (1G), emerged in the 1980s with Nordic Mobile Telephone (NMT), primarily catering to voice services. The subsequent generation, 2G, introduced around the 1990s, transitioned to digital systems exemplified by Global System for Mobile (GSM) communication. 2G expanded service offerings to include voice, Short Messaging Service (SMS), and Multimedia Messaging Service (MMS). Among the 2G variations was General Packet Radio Service (GPRS), facilitating customer access to internet services.

The third generation (3G) of mobile communication systems, introduced around the 2000s, aimed to enhance services by providing faster voice, SMS, MMS, video calling, and internet capabilities. This period witnessed exponential growth in data bandwidth and throughput, resulting in improved customer services. Currently, the fourth generation (4G) system is still present, inaugurated in 2010, showcasing substantial advancements over its predecessors. A key differentiator is 4G's superior bandwidth and data throughput when compared to 3G and other technologies [1.1].

As a step forward, LTE-A is an enhanced iteration of the standard 4G LTE, which leverages MIMO (Multiple Input, Multiple Output) technology to integrate numerous antennas for both transmitting and receiving functions. Through MIMO, LTE-A achieves threefold increased speed compared to standard 4G, as multiple signals and antennas can operate concurrently. This advancement in LTE-A translates to a heightened system limit, reduced latency in the application server, and the ability to access triple traffic (Data, Voice, and Video) wirelessly from any location globally. LTE-A demonstrates speeds surpassing 42 Mbps and reaching up to 90 Mbps.

To sum up, over the past three decades, significant advancements have occurred in wireless communication, in the transition from 1G to 4G, to meet the demands for high bandwidth and extremely low latency. The advent of 5G is driven by the continuous tightening of mobile networks' requirements by offering extremely high data rates, enhanced Quality of Service (QoS), low latency, extensive coverage, high reliability, and economically feasible services [1.2].

Categorized into three main types of services, 5G provides (Figure 11):

- **Extreme Mobile Broadband (eMBB):** This employs a non-standalone architecture to deliver high-speed internet connectivity, increased bandwidth, moderate latency, and services such as UltraHD streaming videos, virtual reality, and augmented reality (AR/VR).
- **Massive Machine Type Communication (eMTC**): Released in the 13th specification by 3GPP, eMTC offers long-range and broadband communication for machines at a cost-effective price with minimal power consumption. It ensures a high data rate, low power usage, and extended coverage with reduced device complexity, especially beneficial for Internet of Things (IoT) applications.
- **Ultra-Reliable Low Latency Communication (URLLC):** Designed to provide low-latency and ultra-high reliability, URLLC ensures a rich Quality of Service (QoS) that traditional mobile network architecture cannot achieve. It is tailored for real-time interactions on demand, including applications such as remote surgery, vehicle-to-vehicle (V2V) communication, Industry 4.0, smart grids, and intelligent transport systems.

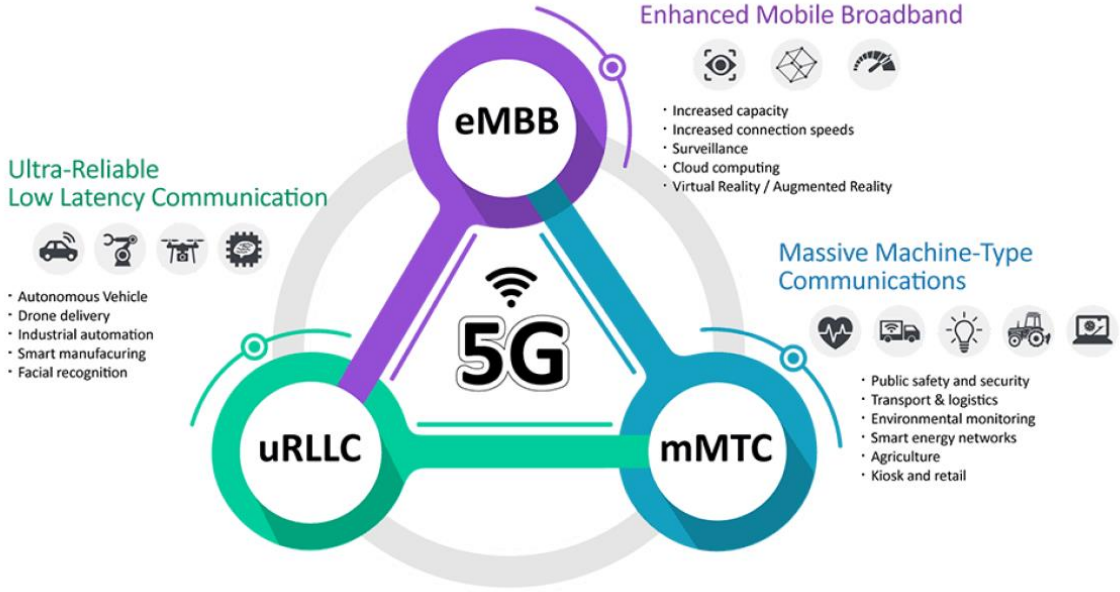

Figure 11. Key 5G advancements.

The next paragraphs focus on the evolution of the optical RAN infrastructures, as well the available optical interfaces and technologies that can support the migration to future mobile networking. Moreover, indicative applications and use case that drive the need for transformation of current deployments are being elaborated on.

1.2. Optical access network interfaces in the 5G and beyond era

Examining the targeted mobile networks' advancements outlined in the previous paragraph, particularly focusing on latency, bandwidth, and reliability, imposes stringent requirements on the architectures and specifications of the radio access network (RAN) [1.3], [1.4]. The RAN equipment has adopted innovative designs to address these challenges. To alleviate the demands on these specifications, diverse functional splits of the RAN machine have been established [1.5], [1.6]. Additionally, novel network segments, namely fronthaul, midhaul, and backhaul, are now defined as X-Haul links connecting the radio equipment to the core network.

The 3GPP 5GRAN architecture outlines the structure of 5G radio base stations (gNBs), comprising three primary functional modules: the Central Unit (CU), the Distributed Unit (DU), and the Radio Unit (RU). The deployment of these modules can vary based on the intended network topology, the specific services, and their constraints, as well as the configuration and location of antenna sites. Two contrasting architectures, Distributed RAN (D-RAN) and Centralized RAN (C-RAN), are proposed to accommodate these variations.

DRAN represents the most traditional and widely adopted configuration, wherein the functions of the CU, DU, and RU remain at the antenna site. A straightforward backhaul link connects this configuration to the 5G core network (5GC). On the other hand, C-RAN offers the potential to reduce the footprint of antenna sites by centralizing and pooling the CU and possibly the DU at a remote location (central office or main office). The adoption of local C-RAN fronthaul is often driven by considerations such as the high cost or complexity of hosting fully updated RAN equipment at the antenna site (due to factors like limited space, energy constraints, or complicated facility access). However, depending on the selected functional split [1.6], transport networks will feature various interfaces designed to carry different traffic types, such as Common Public Radio Interface (CPRI), Open Base Station Architecture Initiative (OBSAI), Open Radio Equipment Interface (ORI), Radio over Ethernet (RoE), or Ethernet-based eCPRI, along with Open-RAN 7.2, each with its specific transport requirements.

In any of the X-Haul segments, it is anticipated that the throughput will range from 10 Gbits/s to 100 Gbits/s. This expectation arises due to the quantization of mobile signal samples in the time/frequency domain, the application of aggregation rates in various RAN equipment, and the choice between high or low layer split implementations [1.6]. Taking the example of the RU, the CPRI/eCPRI throughput is contingent on the radio settings, including factors like frequency range, bandwidth, number of frequency carriers, and MIMO configurations. CPRI traffic encompasses synchronization features crucial for RAN fronthaul, and the latest option, "CPRI10," has been defined with a line bit rate of 24.3 Gbits/s. In comparison to CPRI interfaces, eCPRI employs an Ethernet protocol for data fronthaul with interfaces at 10G/25G/40G/100G base [1.7]. This Ethernet encapsulation enables a reduction in the data rate requirements for fronthaul through flexible functional decomposition while keeping the complexity of the RU in check. For instance, with a high layer split, a majority of functionalities reside in the DU, simplifying and reducing the footprint on the tower or within the building of antenna sites.

The broad spectrum of constraints associated with various X-haul interfaces is not the sole factor driving operators to extend their optical networks beyond simple high-capacity pipes. Within the optical domain, different service classes can already be implemented using legacy equipment to cater to diverse requirements such as bit rates, latency/packet jitter, and service availabilities across various 5G verticals. However, the introduction of network abstraction through Software Defined Networking (SDN) has the potential to be a game-changer, facilitating slicing and fixed access network sharing. SDN could significantly streamline equipment configuration automation by providing vendor-agnostic solutions from the outset. Over time, software-based network abstraction and orchestration could enable practical implementations for scenarios involving multitenancy and multi-operator use cases. This approach aligns with the ongoing trend of virtualization in the mobile domain, supporting intelligent and cooperative fixed-mobile convergence. Ultimately, an intelligent and generic-hardware-based optical node could address the stringent latency requirements of diverse 5G services. This could be achieved by hosting, for example, virtualized RAN functionalities, content platforms, or multiaccess edge computing [1.8],[1.9].

Furthermore, it is essential to address congestion in optical aggregation equipment to ensure the appropriate quality of service for proprietary flows. Indicatively, In France in 2020, over 88% of Orange's antenna sites were linked through Point-to-Point (PtP) optical fiber for fiber to the antenna (FTTA) connections between a central office (CO) and the antenna site. The remaining sites utilized microwave wireless links. With the deployment of 5G's new mobile technology, there is an increased demand for fiber resources, prompting discussions on utilizing fibers deployed for fiber to the home (FTTH)[1.10].

1.2.1 Optical interfaces for 5G X-Haul

PtP networks, which are the prominent interconnecting method between CU/DU/RU equipment, are exclusive links that connect the terminations of two networks and serve as the primary optical connectivity in mobile networks. These networks depend on optical transceivers integrated into the host RAN equipment. Between the DUs and RUs, the majority of fronthaul links are localized, typically situated at the antenna site. Consequently, DUs and RUs are furnished with transceivers featuring limited fiber reach (2 or 10 km) to accommodate this standard FTTA implementation. In the near future, these fronthaul links are expected to support capacities up to CPRI10 (25G) or eCPRI, depending on the RU technologies and radio configurations deployed. This adaptation is essential to address the significant bandwidth expansion required by 5G to realize its full potential. However, it's worth noting that no CPRI interface has been defined beyond 25 Gbit/s to date, and transceivers operating within the outdoor industrial temperature (I-Temp) range (-40°C to 85°C) are imperative at the antenna site.

PtP interfaces are currently experiencing deployment across numerous network segments, with a substantial and expanding presence in the DATACOM sector, constituting over 40% of the optical component volume in 2020 [1.11]. The forecast indicates significant growth in 25G interfaces, particularly for fronthaul applications (CPRI or eCPRI). These interfaces are expected to emerge as the predominant market for fronthaul optical interfaces in the upcoming years.

In line with the prevailing trend and the overall expansion in bandwidth and bit rates, the IEEE and ITU-T are introducing new standards for single-fiber transceivers operating above 10 Gbit/s. There are ongoing efforts for standard convergence aimed at proposing harmonized physical layer parameters. Specifications for 25 Gbits/s have been outlined, with these technologies relying on the same wavelength pair assigned for both upstream and downstream transmissions (1270 nm and 1330 nm ±10 nm). Two primary optical budget classes have been defined to meet the requirements for 5G X-Haul: BR20 or Class S (0–15 dB) for a reach of 20 km, and BR40C or Class B- (10–23 dB) for a reach of 40 km. For transceivers operating at speeds up to 25 Gbit/s, the non-return-to-zero (NRZ) modulation format has been selected. Conversely, the four-level pulse amplitude modulation format (PAM4) has been chosen for 50 Gbits/s by both IEEE and ITU-T. The adoption of PAM4 modulation facilitates the use of

lower bandwidth optical components, allowing the reuse of 25G electrical interfaces and optics.

C-RAN architecture employed D-RoF techniques within the Fronthaul network to eliminate much of the electronic processing in the RRHs, including tasks like MIMO processing and up-conversion. Subsequently, the 5G RAN adopted the functional split concept, redistributing certain electronic functions such as modulation to the RRH to alleviate the bandwidth requirements imposed on the fiber-link fronthaul. The employed Fronthaul standard is eCPRI. The evolution of the RAN has been largely influenced by its bandwidth requirements, particularly in the context of massive-MIMO and mmWave communications. A-RoF, with its considerably lower bandwidth requirements and reduced power consumption compared to D-RoF based Fronthauls, presents itself as a promising RAN solution. Within the A-RoF framework, there is no need for analog-to-digital conversion (ADC) and digital-to-analog conversion (DAC). In the A-RoF's CU, data bits undergo modulation and undergo MIMO processing, followed by up-conversion. The resulting signal is then converted from electronic to optical (E/O) [1.12]. A more comprehensive explanation of this alternative transport scheme, which forms the foundation of the Fronthaul architecture envisioned in the present thesis, will be provided in the subsequent chapters.

Affordable optical components such as directly modulated lasers (DMLs) and PIN receivers enable reaching distances of up to 10 km without the need for digital signal processing or amplification. However, for extended reach requirements, external modulated lasers (EMLs) and/or avalanche photodiode (APD) receivers become necessary, albeit with additional costs. EMLs, known for lower chirp compared to DMLs, contribute to reducing transmission penalties caused by chromatic dispersion in the fiber. The development of APD receivers has resulted in enhanced achievable bandwidth, typically reaching up to 17 GHz, and superior sensitivities compared to PINs, thereby providing greater optical budgets for longer fiber distances.

Having gained a comprehensive understanding of PtP transceiver technologies and the market, there exists a multitude of optical solutions to cater to the requirements of 5G RAN optical transport. In scenarios where operators face high costs associated with renting or deploying new fibers, alternative optical transport solutions become viable options. Aiming to explore RAN optical transport solutions that optimize fiber sharing, the utilization of WDM and TDM interfaces is of vital significance.

Over the past few decades, Wavelength Division Multiplexing (WDM) has undergone development for access networks but has not achieved widespread adoption in the mass market [1.11]. This limited popularity can be attributed to the cost of colorless modules, which have not been competitive with alternative fiber-sharing solutions like Passive Optical Networks (PONs). Additionally, upgrading the technology to high bit rates (>10 G) has posed challenges. In recent times, there has been a development of tunable optics capable of delivering 25 Gbits/s in the C-band, specifically designed for 5G X-Haul and, more notably, for fronthaul applications. The demand for such technology has risen with the deployment of the fifth generation of mobile networks, emphasizing the need to optimize and share optical fiber resources while maintaining PtP logical connectivity with N-to-N terminations. WDM is currently in use in metro and core networks, employing passive optical components to

achieve multiplexing. In this setup, N wavelength channels are transmitted in a shared "trunk" fiber by inserting a Multiplexer (MUX) with N fiber inputs to a single fiber output. Subsequently, demultiplexers (DMUXs) restore the N channels, each over a separate output.

On the other hand, TDM-PONs are extensively deployed in the FTTH and FTTE markets. Commercially available PON solutions now offer bit rates compatible with the transport requirements of 5G traffic [1.13]. Figure 8 illustrates a potential implementation of TDM-PON for backhaul. By sharing the optical fiber with passive optical splitters and deploying a single OLT port for typically 64 ONUs, TDM-PONs are also well-suited to handle the increasing cell density anticipated with the deployment of 5G small cells [1.14]. XGS-PON, which provides 10 Gbit/s symmetrical line rates, has been proposed as a significant candidate for 5G backhaul [1.15] and fronthaul [1.16]. However, it's worth noting that XGS-PONs share a maximum of 8.5 Gbit/s Ethernet actual throughput capacity. The OLT PON port can be accommodated in standard OLT shelves or in any RAN transport equipment, thanks to the development of Smart Fiber Passive Component (SFPC) OLTs. The creation of these intelligent transceivers has been facilitated by recent advancements in virtualization, miniaturization, and Software-Defined Networking (SDN) [1.17].

1.3. Future mobile networks' applications, use cases and KPIs

Towards moving from the existing (even in 4G) network-specific definition and provisioning of applications/services to the 5G envisioned application-driven, flexible, dynamic network services instantiation, the technical activities of 5G are interrelated with the activities focusing on the analysis of stakeholders and their service requirements. The existing (5G-ready), under-development, planned, or even predicted 5G services/applications are versatile in terms of functionality, resource and performance requirements as observed from the large number of technical and market reports by application developers, vendors, consultation services, standardisation organisations and various stakeholders' forums.

To this end, in order to address 5G applications in a coherent manner, 5G-related activities are converging to mapping applications to specific major verticals ([19], [20]), and more specifically to:

- Automotive, especially focusing on services provided in high mobility scenarios, IoT applications/services etc., such as Automated driving, Road safety and traffic efficiency services, Digitalization of transport and logistics, Intelligent navigation, Information society on the road, and Nomadic nodes;
- eHealth, especially focusing on remotely provided health services with high latency and reliability requirements, such as Assets and interventions management in hospitals, Robotics (remote surgery, cloud service robotics for assisted living), Remote monitoring of health or wellness data, and Smarter medication;

- Energy, especially focusing on IoT-based energy monitoring, management, and network control scenarios, such as Grid access, Grid backhaul, and Grid backbone;
- Media and Entertainment, especially focusing on next generation applications/services provisioning such as UHD media, Cooperative media production, highly interactive services, On-site live event experience (Augmented/Virtual Reality video content), Immersive and integrated media etc., as well as,
- Factories of the future, referring to Industry 4.0 setups and applications/services such as Time-critical and Non time-critical process optimization inside factory, Remote maintenance and control, Seamless intra-/inter-enterprise communication, allowing the monitoring of assets distributed in larger areas, and Connected goods.

It becomes obvious that the two categorisations of 5G services based on (1) performance and (2) verticals' requirements, respectively, comprise the two sides of the same coin, and shall be considered in any 5G system specification, development and deployment processes.

Moreover, the current section aims to address some main and indicative 5G Use Cases (UC) for which the 5G and beyond-oriented RAN transformation shall provide suitable network solutions capable of efficiently supporting the telecom demands of all potential stakeholders (subscribers/individuals, fans, tenants/verticals, infrastructure owners, etc.) under (ultra) high traffic demands e.g., when specific crowded events (e.g., football match, concert) are taking place in a specific and usually limited geographical area, while meeting the strict performance QoS requirements (bitrates, latency, reliability, etc.) of the 5G services that are concurrently utilized. Advancing in this direction, the fiber and fiber-wireless transport segments based on A-RoF can present appealing solutions for the practical deployment of Fronthaul, specifically tailored to the scrutinized use cases, as will be detailed in the subsequent sections. To this end, three (3) use cases will be discussed: (a) dense area UC, (b) ultra-dense area UC and (c) hotspot area UC, along with representative usage scenarios.

- Dense areas, which could be served via PON optical access networks, through identifying PON-overlaid and compatible 5G network deployment as the closest to realization. Adapting to the rapidly emerging trends for 25Gb/s and 4x25Gb/s PON access [1.18], 25Gb/s transceiver and interface technologies could support such implementations.
- Ultra-dense areas can be deployed in environments like main city squares, sightseeing sites etc., via dedicated Local FiWi C-RAN infrastructures. Here the high-capacity traffic provision can rely on SDM optical technologies as the intermediate step prior the transition to WDM, in order to enable the rapid adoption of the simplified and mature SDM solutions by equipment vendors and by third-parties willing to install their own small-cell network, like municipalities, universities, etc. This approach can also rely on the modular, flexible and broadband characteristics of MIMO antennas,

targeting Gbps scale wireless data rates through the usage of evolving 5G key technology enablers.

- For Hot-Spot areas, private FiWi C-RAN infrastructures owned by third-parties are probably the business model to be followed, as for example in stadiums, airports, museums, shopping malls etc. To support such densified traffic demand, the ultra-dense deployments need to go one step further, and scale to higher capacity setups by adding wavelengths, benefiting from the potential of A-RoF scheme to be implemented via low-cost, energy-efficient, high analog bandwidth transceiver units, the investigation and implementation of which is main focus of the current thesis.

The rest of this document is organized as follows:

Chapter 2 investigates analog fiber-wireless links as a crucial element for efficient Radio Access Network (RAN) extensions in 5G networks. This chapter covers various aspects, including the transition to Centralized RAN (C-RAN) architectures, optical transport for Mobile Fronthaul (MFH), and Digital Signal Processor (DSP)-assisted analog Fronthaul. Analog RoF-based mobile Fronthaul, mmWave wireless technologies, and proof-of-concept experimental evaluations are also explored. Moving forward, Chapter 3 delves into modulation and signal processing techniques, elucidating the role of these techniques in supporting analog fiber and fiber-wireless transport transmission. It encompasses an in-depth examination of digital modulation schemes, OFDM modulation, multi-carrier candidates for 5G, and the integration of DSP algorithms for processing CP-OFDM waveforms. Chapter 4 shifts the focus to analog fiber-wireless downlink transmission of IFoF/mmWave over in-field deployed legacy PON infrastructure, presenting a detailed analysis of converged PON/mmWave topology through experimental evaluation. The dissertation culminates in Chapter 5, where a live demonstration of an SDN-reconfigurable, FPGA-based TxRx for Analog-IFoF/mmWave RAN is showcased. This chapter provides insights into the envisioned Fronthaul architecture, RFSoC-based A-IFoF transceivers, SDN-powered Management & Control Plane, and the experimental evaluation of the real-time analog Fronthaul topology. In the final chapter, Chapter 6, the dissertation concludes by summarizing key findings and insights gained throughout the exploration of analog fiber and fiber-wireless transport in the realm of 5G networks, while also discussing future research extensions related to the presented work.

References

[1.1] Q. K. Ud Din Arshad, A. U. Kashif and I. M. Quershi, "A Review on the Evolution of Cellular Technologies," 2019 16th International Bhurban Conference on Applied Sciences and Technology (IBCAST), Islamabad, Pakistan, 2019, pp. 989-993, doi: 10.1109/IBCAST.2019.8667173.

[1.2] Dangi, R., Lalwani, P., Choudhary, G., You, I., & Pau, G. (2022). Study and investigation on 5g technology: A systematic review. Sensors, 22(1), [26]. https://doi.org/10.3390/s22010026.

[1.3] P. Chanclou, L. A. Neto, G. Simon, F. Saliou, N. Neyret, E. Thily, D. Abgrall, and D. Minodier, "Choice of optical access innovations to meet today's needs and support the challenges of tomorrow," in Optical Fiber Communication Conference (OFC) (2020), paper W4E.5.

[1.4] P. Chanclou, L. A. Neto, K. Grzybowski, Z. Tayq, F. Saliou, and N. Genay, "Mobile fronthaul architecture and technologies: a RAN equipment assessment [Invited]," J. Opt. Commun. Netw. 10, A1–A7 (2018).

[1.5] P. Sehier, P. Chanclou, N. Benzaoui, D. Chen, K. Kettunen, M. Lemke, Y. Pointurier, and P. Dom, "Transport evolution for the RAN of the future [Invited]," J. Opt. Commun. Netw. 11, B97–B108 (2019).

[1.6] L. M. P. Larsen, A. Checko, and H. L. Christiansen, "A survey of the functional splits proposed for 5G mobile crosshaul networks," IEEE Commun. Surv. Tutorials 21, 146–172 (2019).

[1.7] "Common Public Radio Interface: eCPRI Interface Specification," eCPRI Specification V2.0 2019, http://www.cpri.info/downloads/eCPRI_v_2.0_2019_05_10c.pdf.

[1.8] A. El Ankouri, S. R. Rincón, G. Simon, L. A. Neto, I. Amigo, A. Gravey, and P. Chanclou, "Real-time assessment of PtP/PtMP fixed access serving RAN with MEC capabilities," in Optical Fiber Communication Conference (OFC) (2020), paper M2H.1.

[1.9] S. Das and M. Ruffini, "PON virtualisation with EAST-WEST communications for low-latency converged multi-access edge computing (MEC)," in Optical Fiber Communication Conference (OFC) (2020), paper M2H.3.

[1.10] F. Saliou et al., "Optical access network interfaces for 5G and beyond [Invited]," in Journal of Optical Communications and Networking, vol. 13, no. 8, pp. D32-D42, August 2021, doi: 10.1364/JOCN.425039.

[1.11] OMDIA, "Total optical components forecast 2019–25," 2020, https://omdia.tech.informa.com/OM013799/Total-Optical-Components-Forecast-201925.

[1.12] Li, Yichuan & Xie, Qijie & El-Hajjar, Mohammed & Hanzo, L.. (2021). Analogue Radio Over Fiber for Next-Generation RAN: Challenges and Opportunities.

[1.13] "10-gigabit-capable symmetric passive optical network (XGS-PON)," ITU-T Recommendation G.9807.1, 2016.

[1.14] N. Bhushan, J. Li, D. Malladi, R. Gilmore, D. Brenner, A. Damnjanovic, R. T. Sukhavasi, C. Patel, and S. Geirhofer, “Network densification: the dominant theme for wireless evolution into 5G,” IEEE Commun. Mag. 52(2), 82–89 (2014).

[1.15] A. El Ankouri, L. A. Neto, G. Simon, H. Le Bras, A. Sanhaji, and P. Chanclou, "High-speed train cell-less network enabled by XGSPON and impacts on vRAN split interface transmission,” in Optical Fiber Communication Conference (OFC) (2019), paper W4J.5.

[1.16] S. Bidkar, J. Galaro, and T. Pfeiffer, “First demonstration of an ultra-low-latency fronthaul transport over a commercial TDMPON platform,” in Optical Fiber Communication Conference (OFC) (2018), paper Tu2K.3.

[1.17] G. Simon, A. E. Ankouri, L. A. Neto, P. Chanclou, and D. Kurz, “FTTH and optical LAN synergy enabled by virtual OLT for home, office and campus,” in 45th European Conference on Optical Communication (ECOC), Dublin, Ireland (2019).

[1.18] Pleros, Nikos & Papaioannou, Sotirios & Kalfas, George & Vagionas, Christos & Maniotis, Pavlos & Mitsolidou, Charoula & Miliou, Amalia. (2018). 5G small-cell networks leveraging optical technologies with mm-wave massive MIMO and MT-MAC protocols. 10. 10.1117/12.2297276.

CHAPTER 2.
Analog Fiber-Wireless links in support of efficient RAN extensions in 5G networks

The 5G-PPP vision towards the next generation of communication networks and services that will provide ubiquitous super-fast connectivity and seamless service delivery in all circumstances requires a very high-capacity mobile infrastructure, with ubiquitous capabilities for both last-mile fixed and mobile access. The envisioned network shall be based on general purpose, (field) programmable high-performance hardware that will dynamically offer a range of resources for transport, routing, storage and execution while the network entities will be computing elements gathering programmable resources, interfaces and functions based on virtualization technologies.

The 5G KPIs are highly ambitious and generally sum up to the following:

- Providing 1000 times higher wireless area capacity and more varied service capabilities compared to Fourth Generation (4G).
- Saving up to 90% of energy per service provided. The main focus will be in mobile communication networks where the dominating energy consumption comes from the Radio Access Network (RAN).
- Facilitating very dense deployments of wireless communication links to connect over 7 trillion wireless devices serving over 7 billion people.

The very strict capacity and latency requirements imposed by 5G's KPIs stated above are essentially enforcing the introduction of the millimeter wave (mmWave) spectrum in the access part of the network. Placing, however, mmWave access cells in very close proximity to the end-user is expected to severely impact deployment costs, since it demands the antennas' densification by several orders of magnitude and consequently translates to three major fronthaul (FH) problems:

- The Next Generation Fronthaul Interface (NGFI) deployments cannot rely exclusively on fiber connections reaching every mmWave Service Access Point (SAP) in urban areas, since this would require expensive brown-field fiber deployment.
- The mmWave access antennas must become very simple in terms of functionality, hardware and energy efficiency to maintain feasible investment and operational costs.
- Fronthauling multi-Gbps mmWave data links makes digitized Common Public Radio Interface (CPRI)-based communications infeasible; yielding intolerable FH requirements as mmWave mMIMO (massive Multiple-Input Multiple-Output) is entering the field.

Incentivized to optimally address the above issues, the investigation of an analog optical/wireless fronthaul/backhaul (FH/BH) solution that targets to meet the ambitious 5G requirements, has been the pillar of this phD thesis. The targeted solution is based on a low Physical Layer (PHY) split (split-PHY), placing most of the hardware on the centralized unit, while at the same time employing Digital Signal Processing (DSP) assisted Analog-Radio-over-Fiber (A-RoF) transmission that allows for high-order advanced modulation formats that can support ultra-high bandwidth data transfer. Native Ethernet-packet transport over the proposed FH/BH is a crucial parameter towards holistic cross-medium administration of the optical/wireless/time resources.

The above architecture has been extensively investigated within the European H2020 project 5G-PHOS [2.1]. 5G-PHOS aimed to architect and evaluate 5G broadband wireless networks for dense, ultra-dense and Hot-Spot area use cases drawing from recent results in the area of optical technologies towards producing and exploiting a powerful photonic integrated circuit technology toolkit. It aimed to streamline advances in multi-format and multi-bitrate optical communications, in InP transceiver, in Triplex optical beamformers and in integrated optical add/drop multiplexers in order to migrate from CPRI-based towards integrated Fiber-Wireless (FiWi) packetized C-RAN fronthaul supporting massive mmWave MIMO communications. It pursuesd: a) a set of SDN-programmable units, called FlexBox and FlexBox-Pro, compatible with the emerging 25Gb/s PON access networks and can deliver FiWi traffic ranging between 25-400Gb/s, b) a set of three different 64x64 MIMO Remote Radio Head configurations exploiting analog optical beamforming and producing 25Gb/s,100Gb/s and 400Gb/s wireless data-rates, c) an integrated FiWi packetized fronthaul for supporting Medium-Transparent Dynamic Bandwidth Allocation mechanisms and cooperative radio-optical beamforming, d) a converged FiWi SDN control plane for optimally orchestrating both the optical and the wireless resources.

The envisioned architecture exploits integrated optical technologies towards enhancing FiWi convergence to realize cost-effective and energy-efficient 5G network solutions for high-density use cases. More specifically it benefits from existing scientific results in the area of photonics in order to architect 5G networks for dense, ultra-dense and hotspot areas incorporating Photonic Integrated Circuits (PICs) in optical mmWave signal generation, and DSP-assisted optical transmission, in view of a seamless, interoperable, Radio Access Technology (RAT)-agnostic and Software Defined Networking (SDN)-programmable FiWi 5G network. The innovation potential of FH/BH implementation approach can be summarized in the following bullets:

- **Advancing 5G system, functional, logical and physical architectures**. One of the most valuable innovations introduced by the envisioned architecture relies on the design and evaluation of a RAT-agnostic PON-overlaid integrated FiWi fronthaul. The proposed architecture promotes the network sharing paradigm by combining wavelength/frequency/time/space domains and supporting Over The Top (OTT) and Mobile Virtual Network Operator (MVNO) services.

- **Involving technology enablers for 5G RAN Platforms (HW & SW)**:
    - novel PICs for 5G RANs, and

- advanced antenna systems employing MIMO arrangements at mmWave frequencies.

- **Advancing 5G integrated FH/BH transport network systems** by defining and implementing intelligent and co-operative integrated FiWi fronthaul.

Targeting to support the described architectural approach for future mobile networks, the presented research work focuses on the concept of Digital Signal Processing (DSP)-assisted optical transmission capable to support analog mobile fronthauling (MFH). This RoF concept aims to alleviate the bandwidth limitations of the 5G MFH through the use of analog optics, which can carry native wireless data signals via installed fibers. This ambitious analog concept within the 5G landscape is introduced, emphasizing the structural changes and challenges that analog MFH attempts to address. In the next paragraphs, the architectural shift towards Centralized Radio Access Network (C-RAN) topologies, which put the traditional digital MFH transport on the question, is thoroughly discussed. The DSP-enabled Analog architecture supporting the MFH is then presented, focusing on the digital functions undertaken from a powerful centralized DSP engine. Preliminary experiments that provide a proof-of-concept validation of this A-RoF concept are also discussed.

2.1. Mobile Network Expansion and Centralized Topologies

2.1.1 The transition towards C-RAN architectures

The exponential growth of the number of femto-cells to meet the demands of mobile traffic is one of the prominent features of 5G architectures that are still under investigation. To support low latency, high capacity, cost-effectiveness and low energy consumption, the entire end-to-end network should be overhauled. In 4G mobile networks, many Mobile Network Operators (MNOs) operate using a Distributed Radio Access Network (D-RAN), in which the 4G radio at the macro site tower consists of a collocated Baseband Unit (BBU) at the base of the tower [2.2]. The main advantage of D-RAN is the efficient use of backhaul bandwidth which can be achieved through various well-established technologies (Ethernet, Passive Optical Network (PON), etc.) [2.3]. However, dense 5G cellular topologies apply significant pressure on the static nature of D-RAN where BBUs are assigned statically to a number of cells. The spatial and temporal volatility of mobile traffic makes the static D-RAN topologies suboptimal and new flexible topologies are needed to obtain energy and cost savings for the MNOs [2.4].

Following this rational, the idea of centralization has been re-invented in the era of 5G networks, since it presents significant offerings compared to traditional D-RAN topologies [2.5]. The C-RAN approach favors the separation of radio elements of the base station (called Remote Radio Heads, RRH) and the elements processing the base band signal (called BBUs),

which are centralized in a single location or even virtualized into the cloud. This approach, which has become a hot research topic in both academia and industry [2.6], benefits from simpler radio equipment at the network edge, easier to operate and cheaper to maintain, while the main RAN intelligence (BBUs) is centralized in the operator-controlled premises. The centralization is further enhanced with cloud computing [2.4], providing elasticity, and virtualization with possibility for multitenancy among MNOs. Several main 5G use cases, such as Virtual Reality (VR) applications, which require the real-time processing of massive amount of data, can push much of the processing from a local server to the cloud [2.7]. This practically means that the computational resources can be pooled and dynamically allocated to a virtual BS, which brings cost-effective hardware and software design [2.8]. Figure 12 provides a practical implementation of the above architecture showing a small-cell based C-RAN approach proposed from Fujitsu in a dense urban environment [2.2]. Beyond the software-centric solutions, the C-RAN approach needs also a paradigm shift on the hardware side to meet the challenges for the centralized baseband processing that serves a large number of RRHs. At the heart of this change, powerful Field Programmable Gate Array (FPGA) boards can offer the capability to implement high-throughput 5G transceivers for the data plane while they can also realize the Software Defined Network (SDN) functions described above for the software-centric architecture [2.9]. It should be noted that since the D-RAN remains the dominant deployed architecture of the antenna sites, research efforts should be considered that target a smooth transition towards 5G RAN ecosystem, supporting the coexistence of D-RAN and future C-RAN topologies [2.10].

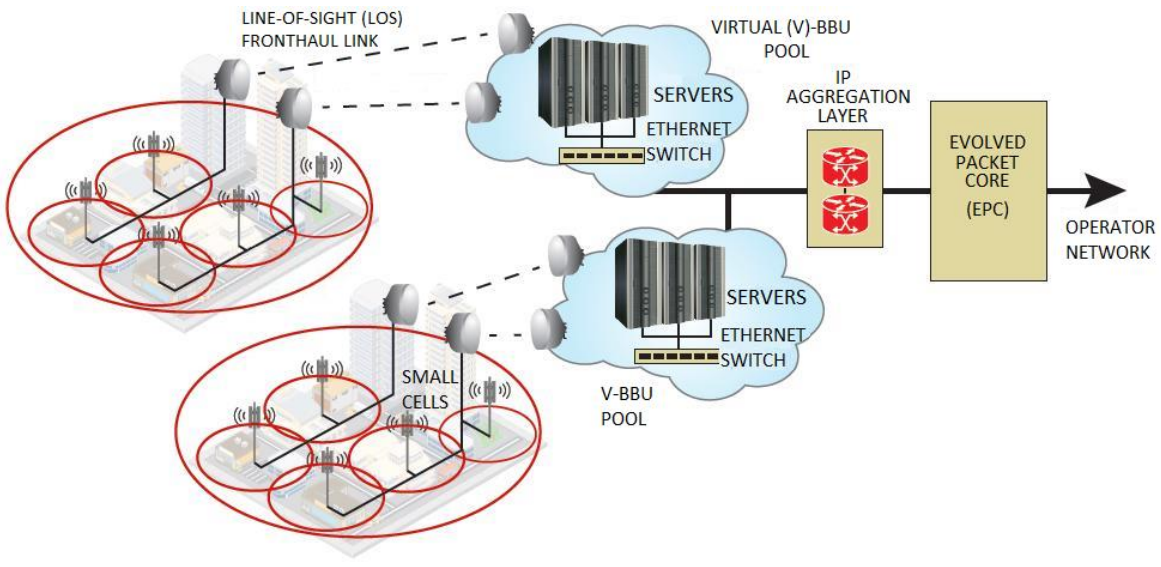

Figure 12. C-RAN architecture that has been proposed from Fujitsu for mobile scenarios within dense urban environment [2.2].

2.1.2 Optical transport for MFH

The fronthaul mobile traffic transport between the BBUs and RRHs seems to be a significant challenge for 5G topologies, since it needs to address several issues related to the convergence of optical channels with complex radio interfaces. In the C-RAN architecture designed for the Long-Term Evolution-Advanced (LTE-A) mobile network, the fronthaul interface is based on Common Public Radio Interface (CPRI). This Digitized-RoF (D-RoF) interface which relies on a link transmitting In-phase and Quadrature (IQ) data of the baseband signal components, suffers from low bandwidth efficiency since it uses the available bandwidth to send IQ data samples, decreasing thereby the effective data rate of the transport [2.11]. In this context, several solutions have been proposed to overcome this bandwidth wall, which mainly focus on compressed CPRI techniques with minimal impact on the optics and fiber network. The emerging need for fronthaul compression has been addressed in the current LTE-A fronthaul links, through a large set of CPRI compression algorithms [2.12]. Compressed CPRI links in a high-speed Pulse-Amplitude-Modulation-4 (PAM-4) are actively investigated, offering a 2x rewards on bandwidth efficiency of the D-RoF approach [2.13].

The CPRI compression techniques offer remarkable bandwidth gains without any structural shift on the current C-RAN architectures. However, the cost of increased complexity at the BBU side needs to be considered, while bandwidth limitations still come from digital electronics and their interfaces at the BBU side [2.14]. To overcome this challenge, Physical (PHY) functional split has been proposed as a possible solution for the MFH by shifting some DSP operations from BBUs to RRHs. This functional split between BBU and RRH relaxes the BBU digital overloading and lowers the fronthaul bandwidth requirements on the optical link. However, it faces great challenges when advanced coordination functionalities are required for a large number of RRHs while the latency budget is also affected through extra processing burden [2.15], [2.16]. An alternative D-RoF concept can be implemented through Open Base Station Architecture Initiation (OBSAI) which is also implemented through a packet-based interface [16]. Since the mapping methods of CPRI are more efficient than OBSAI [2.17], most global vendors and MNOs have chosen CPRI for deployed C-RAN topologies.

A-RoF revolutionizes the MFH landscape by fully releasing the bandwidth capabilities of mmWave bands, requiring only simple functions to exploit the offered bandwidth of the fronthaul part. Moreover, Analog MFH implementations for 5G services can harmonically co-exist over the installed fiber infrastructure supporting PON topologies of fixed wireline services [2.18],[2.19]. These unique benefits come at a cost of increased hardware complexity at the BBU since it hosts the entire set of DSP functions. In addition, the optical distribution of radio signals over Intermediate Frequency/Radio Frequency (IF/RF) carriers is susceptible to a number of generation and transmission impairments, which in turn add noise and distortion due to channel nonlinearities [2.20].

The A-RoF approach described in the current thesis aims to address the above challenges through the use of powerful DSP engines implemented at ultra-high-speed FPGA boards. The proposed DSP-assisted A-RoF solution, proposes a structural shift in the current MFH

deployments since it aims to combine the implementation of DSP-based functions for ultra-broadband radio signals (covering the entire unlicensed 57-64 GHz band) with the electro-optic conversion and transmission through installed fiber infrastructure.

2.1.3 DSP-assisted analog Fronthaul

Several studies explore the advantageous approach of DSP assisted A-RoF fronthaul approach. In the technique presented in [2.21], a number of IQ data channels, each of them corresponding to a single CPRI stream, are multiplexed and transmitted through the fronthaul link in an Intermediate Frequency-over-Fiber (IFoF) scheme. Such implementations combine commodity optical transceiver modules, carrying low bandwidth components (~10 GHz), with high-speed Digital to Analog Converters (DACs) and Analog to Digital Converters (ADCs) [2.22]. Build upon this concept, an A-RoF architecture with DSP functionalities is presented in Figure 13.

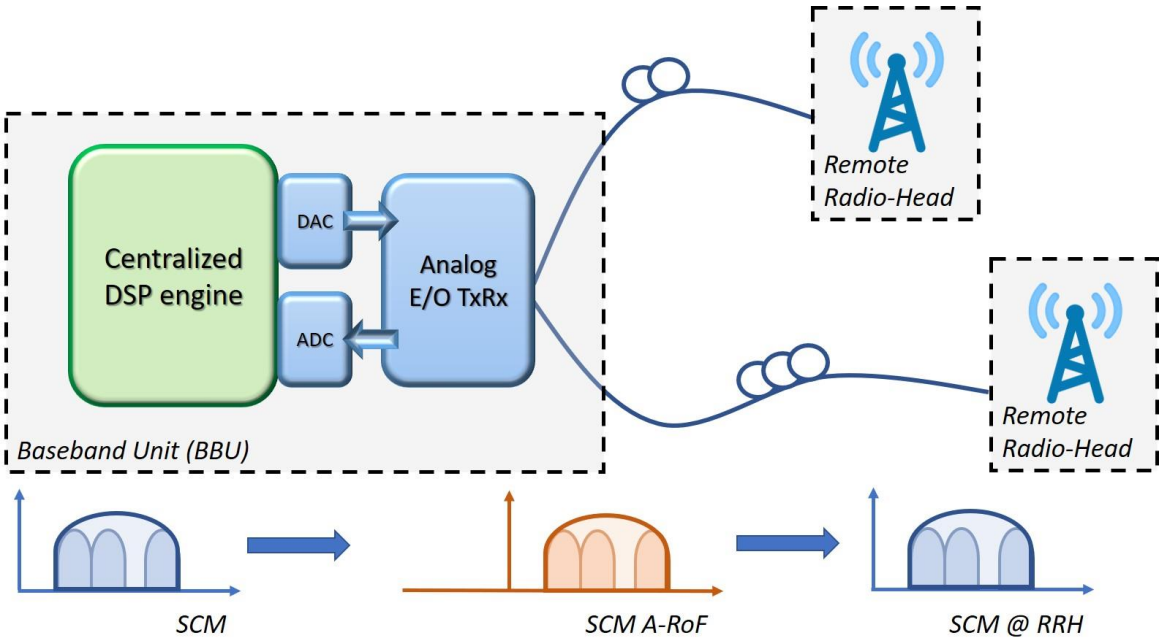

Figure 13. DSP-enabled Analog-RoF concept.

The core of the proposed BBU architecture is a centralized DSP engine, which is responsible for implementing the physical layer functionalities for the fronthaul link. The set of these functions covers all the necessary coding/decoding, modulation and MIMO processing of the wireless channel signals. These radio signals are generated by high-performing DACs, first transmitted through the installed fiber and eventually over the air interface at the mmWave frequency band. Such an A-RoF/mmWave Fronthaul approach realizes actual centralized-RAN, since the complete set of baseband operations are digitally performed in the BBU, removing thereby any processing stage from the RRHs. A first advantage of this approach is

the advanced implementation of inter-cell coordination. As the baseband processing for the radio signals to/from different RRHs is done at the same engine, tighter coordination of neighboring antennas becomes more feasible. As an example of advanced inter-cell cooperation, it is possible that two (or more than two) radiowave signals are jointly received and processed in the BBU pool so that so-called network MIMO can be achieved. Moreover, it ensures scalability since many RRHs can be placed when the capacity demands are increased in a plug-and-play manner. Besides, advanced inter-cell coordination enables better management of interference between adjacent cells, a critical point for 5G ultra-dense cellular networks [2.23]. Finally, the centralization of DSP engine in the BBU pool can also offer significant energy and cost savings using coordination schemes among them [2.24], while the hardware resources at the RRH side are practically minimized.

2.2. A-RoF-based mobile Fronthaul, using a centralized DSP engine

Looking into more detail on the core blocks of the centralized DSP engine, the one that lies closer to the RRH is the Modulation and Channel Mapping block. In this stage, the digital sequences are mapped into the appropriate waveforms that will be transmitted over the Fiber/Wireless link. Digital modulation techniques support the generation of any Single-Carrier (SC) or Multi-Carrier (MC) scheme (e.g. Orthogonal Frequency-Division Multiplexing (OFDM)-like waveforms), thus allowing for compatibility with the current LTE standards, future upgrade to 5G candidate waveforms (eg. Universal-Filtered Multi-Carrier (UFMC), Filter Bank Multi-Carrier (FBMC), General Frequency-Division Multiplexing (GFDM) [30]) as well as more forward-looking approaches thanks to the arbitrary waveform generation capabilities of the engine. A higher bandwidth efficiency is achieved compared to D-RoF approaches of CPRI and Physical Layer Split (PLS) where the bandwidth is utilized for serial transmission of digitized IQ waveforms. In the A-RoF scheme low Intermediate Frequencies (~5 GHz) are employed to carry the modulated radio signals, resulting in bandwidths which are accommodated by typical low-cost transceivers.

Moreover, the use of Digital Sub-Carrier Multiplexing (SCM) techniques can also be adopted to further increase the bandwidth efficiency. For the SCM generation, digital upconversion schemes are employed to obtain the appropriate IF frequencies for A-RoF transmission, eliminating the need of external analog mixers and local oscillators. An additional advantage of employing SCM schemes, we fully utilize the bandwidth offered by the A-RoF components.

As the “DSP-free” RRH units are not capable of baseband signal processing, the centralized DSP engine serves on a two-fold dimension. For the downlink direction, digital pre-distortion based on the fiber/wireless channel response is performed. Channel estimation methods based on training sequences determine the magnitude and phase response of the FiWi link. Thus, the response of electrical and optical components such as DACs, RF drivers, modulators,

filters and photoreceivers of the optical part and RF mixers, up/down converters of the antenna subsystem is reversed using linear equalizers implemented with Finite Impulse Response (FIR) filters. Figure 14 illustrates a channel response extracted by a real experimental testbed with both optical and RF frontends. In the uplink, equalization stages are enhancing the demodulation and detection of the received radio signals after Wireless/Fiber transmission.

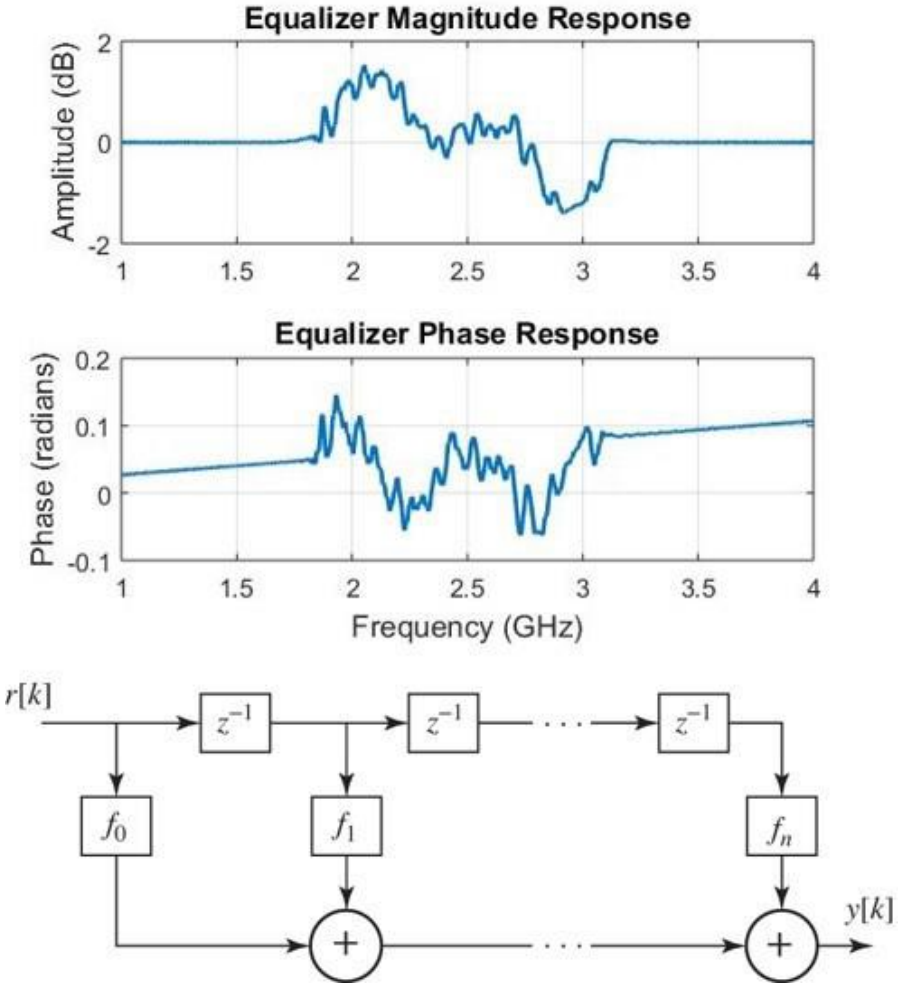

Figure 14. FIR equalizer is implemented by the Frequency Response of the A-RoF link.

Since the A-RoF based MFH scheme appears to be significantly more efficient compared to D-RoF approaches, accommodation of multiple RRHs' traffic can be achieved. In the special case where two or more RRHs serve the same small cell or coverage area, the DSP engine can be employed to perform equalization utilizing the spatial channel characteristics and antenna diversity, thus realizing a DSP MIMO system. Such MIMO processing capabilities along with robust coding schemes offer significant reduction in operational margins in terms of required Signal-to-Noise-and-Interference-Ratio (SNIR) and received power levels [2.25].

The implementation of the above rich digital portfolio within the centralized BBU will be undertaken by powerful FPGA boards. The use of these powerful FPGAs is to accelerate the

critical functions of the baseband chain and sustain the necessary throughput to meet the bitrate and latency requirements within 5G. Since the FPGA boards becomes the essential part of the envisaged digital engines, the design, implementation and validation of real-time testbeds has become a significant point of interest for the 5G hardware research community [2.26], [2.27]. Through the literature, several works have been conducted setting key specifications for FPGA implementation and proposing efficient implementations to meet the 5G network goals [2.28], [2.29].

2.3. Analog RoF-based Optical Transport links

Radio over fiber represents an analog optical connection employed for transmitting information through optical fiber. It accomplishes this by sending modulated RF signals between a central station and a base station. This modulation can occur either directly with the radio signal or at an intermediate frequency. RoF systems are favored primarily due to their minimal signal loss, exceptionally broad bandwidth, and robustness. Additionally, radio over fiber can harness millimeter waves to function as a high-speed wireless network, either locally or within a personal area. Within buildings, RoF systems are increasingly employed to enhance cellular coverage. RoF serves to reduce the costs of radio systems by streamlining remote antenna sites and facilitating the efficient sharing of costly radio equipment situated at central stations. The radio signals distributed by RoF systems span a wide frequency range, typically within the GHz) region, depending on the specific applications.

In contemporary times, the expansion of wireless communication data capacity has been dramatic, driven by the diverse demands of system users. This expansion has evolved from handling basic voices and simple messages to accommodating multimedia and future services with advanced capabilities. Radio over Fiber (RoF) systems offer a promising solution to address numerous pressing needs within telecommunication networks. These systems have the potential to deliver the required bandwidth for efficiently transmitting broadband data to end-users. Additionally, RoF systems offer advantages such as low attenuation loss and immunity to radio frequency interference [2.30], [2.32]. In a RoF system, the majority of signal processing tasks, including coding, multiplexing, RF generation, and modulation, are centralized within the Central Office (CO). This centralized processing approach contributes to cost-effectiveness for Base Stations (BS). Consequently, RoF technology is poised to play a pivotal role in the upcoming generation of mobile communication systems [2.33].

RoF technology is employed in various fields, including optical signal processing, as well as applications such as broadband wireless access networks, electronic warfare, imaging, spectroscopy, and radio astronomy. In these scenarios, an optical fiber is utilized to transmit a radio signal, usually in the millimeter-wave band, using laser sources and electro-optical devices [2.34]. In a nutshell, RoF is a crucial innovation that seamlessly merges wireless and fiber optic networks. It plays a vital role in providing wireless broadband connectivity across various applications, including last-mile solutions, expanding existing radio coverage and capacity, and facilitating backhaul solutions [2.35].

2.3.1 Concept and Architecture of RoF

Radio-over-Fiber technology leverages optical fiber connections to transmit modulated RF signals from the Base Station (BS) to the Remote Antenna Unit (RAU). In the context of narrowband communication systems, tasks such as frequency up-conversion, carrier modulation, and multiplexing of the RF signal are traditionally handled at the BS before being transmitted to the antenna. However, RoF introduces the capability to centralize these RF signal processing functions at a single shared location known as the headend. Subsequently, it employs optical fiber for distribution, benefiting from its minimal signal loss characteristics, which include 0.3 dB/km for 1550 nm wavelengths and 0.5 dB/km for 1310 nm wavelengths, to transmit the RF signals to the RAUs [2.36].

Through this approach, RAUs undergo substantial simplification since they are tasked primarily with optoelectronic conversion and amplification functions. The consolidation of RF signal processing functions allows for shared equipment usage, dynamic resource allocation, and a streamlined system operation and maintenance process. These advantages can lead to significant cost savings in both the installation and ongoing operation of the system, particularly in the case of wide-coverage broadband wireless communication systems, where a dense network of Base Stations (BS) or Remote Access Points (RAPs) is essential, as previously mentioned.

Typically, RoF transmission systems can be categorized into two primary groups based on the frequency range of the radio signal they are designed to transport:

- RF-over-Fiber (Radio Frequency over Fiber)
- IF-over-Fiber (Intermediate Frequency over Fiber)

In the RF-over-fiber architecture, a high-frequency RF (radio frequency) signal, typically exceeding 10 GHz, is superimposed onto a lightwave signal prior to its transmission through the optical link. Consequently, wireless signals are directly distributed optically to base stations at these high frequencies. At the base stations, they are subsequently converted from optical to electrical signals, amplified, and then transmitted via an antenna. This approach eliminates the need for frequency up and down conversion at the individual base stations, simplifying the implementation and resulting in a cost-effective solution [2.37].

In the IF-over-fiber architecture, an intermediate frequency (IF) radio signal with a lower frequency, typically below 10 GHz, is employed to modulate light before it is carried over the optical link. Consequently, prior to being transmitted through the air, the signal needs to undergo up-conversion to reach the RF (radio frequency) range at the base station [2.38].

The architectural layout of a bidirectional A-RoF-based transport network, enabling the interconnection of CUs/BBUs to the remotely located RRUs, is depicted in Figure 15.

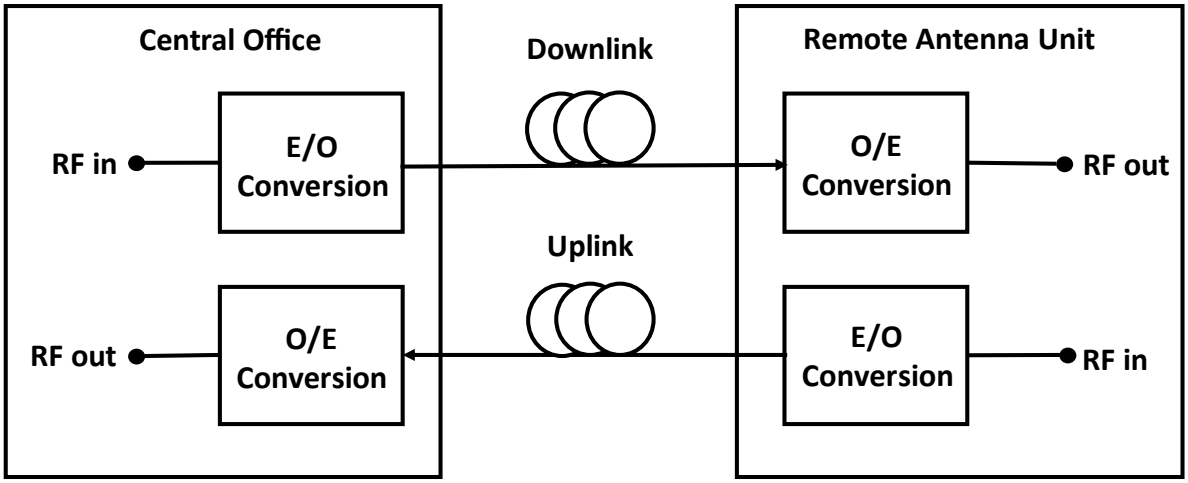

Figure 15. The Radio over Fiber System Architecture [2.30]

The primary benefits of RoF technology can be summarized as follows:

- **Low attenuation**

It is widely recognized that signals transmitted via optical fiber experience significantly lower attenuation compared to other transmission media, especially when contrasted with wireless mediums. Employing optical fiber enables signals to traverse greater distances, thereby reducing the requirement for signal repeaters.

- **Low complexity**

RoF technology incorporates the concept of a remote station (RS), which comprises solely of an optical-to-electrical (O/E) converter (with an optional frequency up or down converter), amplifiers, and an antenna [2.39]. This approach allows for the relocation of resource management and signal generation components from the base station to a centralized site, facilitating shared usage among multiple remote stations and resulting in a streamlined architectural design.

- **Lower cost**

A more straightforward configuration for the remote base station translates to reduced infrastructure expenses, decreased power consumption by devices, and simplified maintenance, all of which collectively contribute to lowering the overall installation and upkeep costs. Additional cost savings can also be achieved through the adoption of budget-friendly graded index polymer optical fiber [2.39].

- **Future-proof**

Fiber optics are engineered to accommodate gigabits per second speeds, ensuring their capacity to support the speeds anticipated in future network generations for an extended

period. Additionally, RoF technology is both protocol and bit-rate agnostic, making it adaptable to utilize existing as well as forthcoming technologies.

- **Easy Installation and Maintenance**

"In RoF systems, the headend hosts sophisticated and costly equipment, simplifying the Remote Antenna Units (RAUs). The modulation and switching equipment is centralized at the headend and is shared among multiple RAUs. This configuration results in more compact and lighter RAUs, ultimately reducing the costs associated with system installation and maintenance [2.40].

- **Multi-Operator and Multi-Service Operation**

RoF provides operational flexibility for the system. Depending on the microwave generation method employed, the RoF distribution system can be designed to maintain signal-format neutrality. For example, utilizing the Intensity Modulation and Direct Detection (IM-DD) technique can be configured to function as a linear system, thus achieving transparency [2.40].

- **Large Bandwidth**

Optical fibers provide a vast bandwidth, with three primary transmission windows exhibiting minimal attenuation: 850 nm, 1310 nm, and 1550 nm wavelengths. In a single-mode optical fiber (SMF), the cumulative bandwidth across these three windows exceeds 50 THz. The extensive optical bandwidth of optical fibers offers numerous advantages beyond their capacity for efficiently transmitting microwave signals. This substantial optical bandwidth empowers high-speed signal processing, which could be challenging or even unfeasible to achieve using electronic systems.

- **Immunity to Radio Frequency Interference**

The resistance to Electromagnetic Interference (EMI) is an exceptionally appealing characteristic of optical fiber communication, particularly in the context of microwave transmission. This advantage stems from the fact that signals are conveyed as light within the fiber. Due to this EMI immunity, fiber cables are the preferred choice, even for short connections operating in the millimeter wave spectrum.

- **Reduced Power Consumption**

The use of uncomplicated Radio Stations results in lower power consumption. The bulk of complex equipment is situated at the central station. In certain scenarios, the antenna sites can operate in an inactive mode. For instance, in some 5 GHz Fiber-Radio systems with pico-cells (small radio cells), the Base Stations can be set to an inactive mode [2.41].

Incorporating analog RoF schemes into the optical transport infrastructure of mobile networks, offers significant advantages, but it also presents certain challenges. RoF, due to its analog modulation and light detection nature, is fundamentally an analog transmission system. Consequently, signal impairments like noise and distortion, which are crucial in analog communication systems, also play a significant role in RoF systems [2.42]. These impairments tend to constrain the Noise Figure (NF) and Dynamic Range (DR) of RoF links. DR holds particular importance in mobile (cellular) communication systems like GSM, as the power received at the Base Station (BS) from Mobile Units (MUs) can vary widely. For example, the RF power received from an MU in close proximity to the BS can be much higher than the RF power received from an MU several kilometers away within the same cell. Analog optical fiber links introduce noise from various sources, including the laser's Relative Intensity Noise (RIN), the laser's phase noise, the photodiode's shot noise, the amplifier's thermal noise, and the fiber's dispersion. In Single Mode Fiber (SMF)-based RoF systems, chromatic dispersion may limit fiber link lengths and result in phase de-correlation, leading to increased RF carrier phase noise [2.35]. Multi-Mode Fiber-based RoF systems face limitations due to modal dispersion, severely constraining available link bandwidth and distance. It's important to note that while the RoF transmission system itself is analog, the distributed radio system need not be analog; it can be digital and employ comprehensive multi-level signal modulation formats like QAM or Orthogonal Frequency Division Multiplexing (OFDM).

2.3.2 Transmission techniques for RoF technology

Various optical methods are available for generating and transmitting radio signals through fiber. This section provides a brief overview of some of these techniques.

- **Direct modulation technique**

  In this approach, the RF signal is directly imposed on the light source's intensity, and then direct detection is employed with a photodetector (PD) to retrieve the RF signal. This method, known as Intensity Modulation Direct Detection (IMDD), is the simplest and most cost-effective means of optically distributing RF signals. Prior to transmission, the RF signal requires appropriate pre-modulation. After traveling through the fiber and undergoing direct detection by a PD, the resulting photocurrent accurately reproduces the RF signal that was originally applied at the head end [2.43]. At the remote antenna site, the PD and band-pass amplifier work together to convert the received optical signal back into an RF signal for transmission via the antenna (Figure 16, Figure 17).

  This method offers several key advantages: simplicity, robustness, and cost-effectiveness. Additionally, when low dispersion fiber is paired with an external modulator, the system can achieve linearity. The transmitter configuration is exceptionally straightforward and budget-friendly, though its performance is notably constrained by laser modulation-related issues. Commercially available RoF systems employing direct microwave

intensity modulation of a laser diode are suitable for limited RF frequencies, typically up to approximately 2 GHz. These systems are employed in wireless services such as Global System for Mobile Communication (GSM) and Universal Mobile Telecommunications System (UMTS). However, the primary drawback of this technique lies in its inability to operate at higher microwave frequencies due to the restricted modulation bandwidth of the laser diode and the effects of fiber dispersion, which lead to fading of the two modulation sidebands. Addressing such high-frequency microwave frequencies necessitates advanced, very-high-frequency optical analog transmitters and receivers, along with meticulous fiber dispersion compensation techniques [2.44], [2.45].

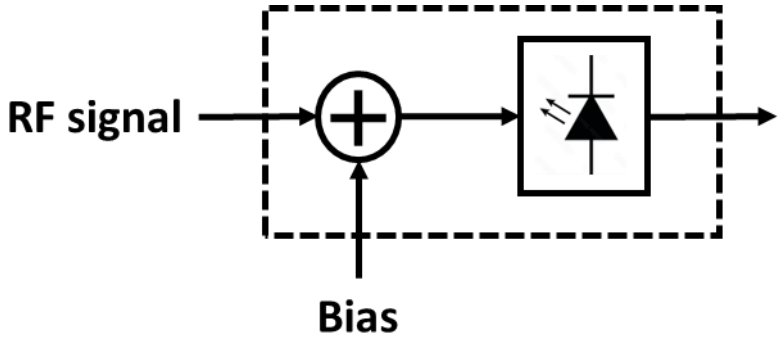

Figure 16. Laser-based direct intensity modulation method.

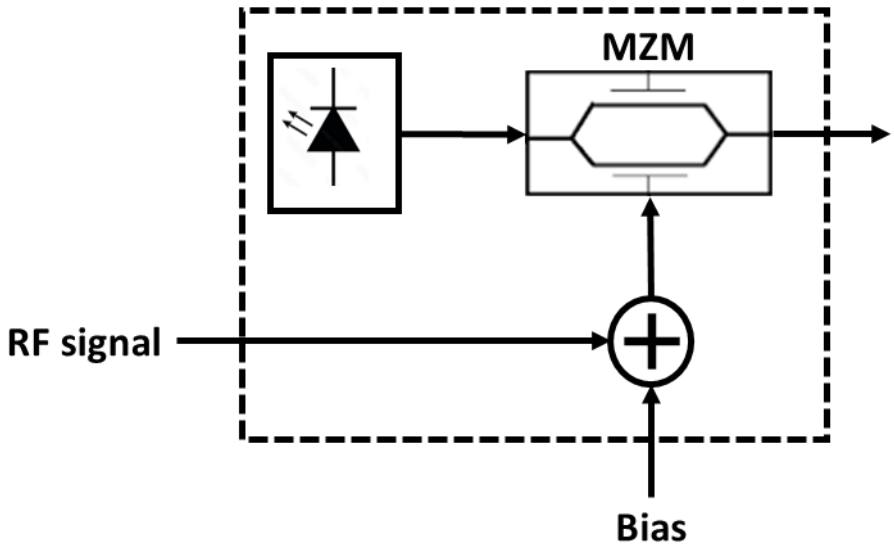

Figure 17. External modulator-based direct intensity modulation method.

- **External modulation technique**

To address the limitations associated with direct modulation, employing external modulation presents a clear and effective solution. Among various approaches, optical external modulation stands out as a strong choice for generating optical millimeter-wave

signals with excellent spectral purity. External modulation is particularly advantageous at high radio frequencies (typically above 10 GHz). A basic implementation involves a continuous wave (CW) laser followed by an external modulator. This modulator introduces modulation to the laser light, typically at an intermediate frequency (IF) or a millimeter-wave tone [2.45]. Operating the laser in CW mode helps mitigate the excessive chirping of pulses during external modulation. In this approach, high-speed external modulators like Mach–Zehnder modulators (MZM), electroabsorption modulators (EAM), or phase modulators (PM) are employed. The output from these modulators is subsequently optically filtered.

The two methods for generating millimeter-wave signals will be briefly outlined. In the intensity modulation-based approach, the system implementation is significantly simplified as it eliminates the need for a tunable optical filter. In this system, an MZM is incorporated and biased at the maximum transmission point of its transfer function to effectively suppress the odd-order optical sidebands. To remove the optical carrier, a fixed-wavelength notch filter is applied. The result is a stable, low-phase noise millimeter-wave signal with a frequency four times that of the RF drive signal [2.45]. It's important to bias the MZM at either the minimum or maximum point of its transfer function to suppress the odd-order or even-order optical sidebands. Bias drift at the wrong point could compromise system robustness, necessitating sophisticated control circuits to minimize bias drift.

The second method utilizes an optical phase modulator (PM), which offers the advantage of not requiring a DC bias, effectively eliminating bias drift issues. This constitutes a key benefit of employing optical PMs, making them a preferable choice. Consequently, in the intensity modulation approach, it is recommended to replace the MZM with an optical PM [2.46]. However, the drawback of the aforementioned approach lies in the necessity of employing an ultra-narrowband optical filter, which can lead to reduced system stability and increased costs. While external modulators are straightforward, they come with certain disadvantages, notably significant insertion loss. Nonetheless, external modulators can accommodate bandwidths of up to 40 GHz and bit rates exceeding 10 Gbps, rendering them highly suitable for long-distance optical communication networks. It's worth noting that the external modulation method is not without its challenges, including distortion caused by the inherent nonlinearity of the modulators, high power consumption, and increased complexity. Consequently, this modulation system tends to be more costly compared to direct modulation [2.45], [2.46].

- **Heterodyne modulation technique**

This technique involves the simultaneous transmission of two or more optical signals, which are then mixed or heterodyned in the receiver. Among the resulting heterodyning products, one or more yield the desired RF signal. The process begins with modulating the optical intensity from a laser diode (LD) using an external modulator. This modulator is biased at the inflection point of its modulation characteristic and driven by a sinusoidal signal operating at half the microwave frequency. Consequently, the modulator's output produces a two-tone optical signal with a tone spacing equal to the microwave frequency.

Heterodyning leads to the creation of the desired amplitude-modulated microwave signal. In some instances, multiple LDs may be used, enabling the realization of a multi-wavelength RoF system. A tunable Wavelength Division Multiplexing (WDM) filter can be employed to select the desired wavelength radio channel at the antenna site [2.46]. Given that phase noise can pose significant challenges in millimeter-wave transmission, meticulous attention must be paid to minimize phase noise introduced by the heterodyning signals. This approach effectively mitigates the impact of chromatic dispersion and offers frequency flexibility, accommodating frequencies ranging from a few megahertz up to the terahertz region [2.45], [2.46].

- **Optical frequency/phase-locked loops**

This method is employed to mitigate sensitivity to phase noise, specifically by tracking small-scale phase perturbations. However, it does not suppress small-scale frequency variations caused by phase noise. The fundamental configuration of Optical Frequency Locked-Loops/Optical Phase Locked-Loops (OFLL/OPLL). It comprises a free-running master laser, a Positive Intrinsic Negative (PIN) photodiode, a slave laser, a frequency or phase detector, an amplifier, a loop filter, and a microwave reference oscillator. The combined outputs of the master and slave lasers are divided into two parts: one is utilized within the OPLL/OFLL at the head end, while the other part is transmitted to the Remote Antenna Unit (RAU). To generate a microwave signal, the optical signal at the head end is heterodyned using a photodetector (PD). The resulting signal is then compared with the reference signal. In the case of OFLL, a frequency error signal (or a phase error signal in the case of OPLL) is fed back to the slave laser [2.46]. Consequently, the slave laser is compelled to track the master laser at a frequency offset corresponding to the frequency of the microwave reference oscillator. The primary advantage of this technique is its capability to generate high-quality RF signals characterized by narrow linewidths and excellent temperature-tracking capabilities. Additionally, OPLLs exhibit a wide locking range [2.47]. Conversely, OFLL techniques offer the advantage of being feasible with standard and reasonably priced Distributed Feedback (DFB) lasers [2.46], [2.47].

- **Dual-mode lasers**

The primary limitation of optical heterodyning-based techniques lies in their sensitivity to phase noise in the two heterodyning signals, as well as their dependence on the polarization state difference between the two heterodyning carriers. One method to achieve correlation of optical modes involves eliminating the phase shift in the Distributed Feedback (DFB) laser, preventing oscillation at the Bragg frequency. This leads to the creation of a device known as the dual-mode laser (DML), which emits two modes, one on each side of the Bragg frequency [2.48]. By adjusting the grating strength coefficient, the desired mode separation can be achieved. The key advantage of this approach is its avoidance of complex feedback circuitry. However, due to its limited locking range, this method has constraints regarding tunability [2.47], [2.48].

2.3.3 Performance degradation factors in A-RoF transmission

As RoF systems rely on the transmission of analog signals through optical fibers, their performance is often constrained by several impairments, including optical fiber chromatic dispersion, phase noise, and nonlinearity [2.49]. The major types of impairments in RoF systems are summarized in the following paragraphs:

- **Fiber Chromatic Dispersion**

One significant challenge in RoF systems, particularly when operating in higher RF bands like the mm-wave range, is the influence of fiber chromatic dispersion [2.50]. Chromatic dispersion in optical fibers refers to the phenomenon wherein the phase velocity of light varies with its frequency. Consequently, different frequency components within the lightwave signal experience varying velocities as they propagate through the fiber. This chromatic dispersion often results in fading effects within RoF systems. When an RF signal is modulated onto an optical carrier for transmission through an optical fiber, as depicted in Figure 18, two sidebands emerge on either side of the optical carrier, with their separation matching the RF signal frequency. As this RF-modulated optical signal travels through the optical fiber, chromatic dispersion causes different phase delays for these two sidebands. Consequently, when the photodetector (PD) performs square-law detection, the generated RF signal is influenced by the distinct phase delays introduced by fiber dispersion. To address this limitation, the OSSB (Optical Single Sideband) and OCS (Optical Carrier Suppression) schemes have been proposed and extensively studied [2.51], [2.52]. In the OSSB scheme, only one RF sideband, along with the optical carrier, is preserved, substantially reducing the impact of fiber chromatic dispersion. Conversely, in the OCS scheme, the optical carrier is suppressed following optical modulation, and two RF sidebands with an RF frequency-based spacing are employed. The interaction between these two RF sidebands generates the RF signal upon detection by the PD, making this scheme more tolerant to fiber chromatic dispersion.

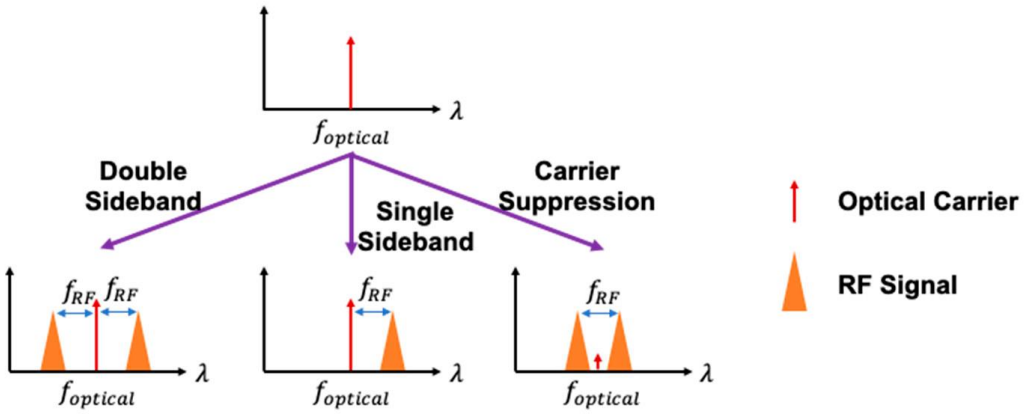

Figure 18. RoF system RF signal modulation schemes [2.49].

- **Nonlinearity**

  Another significant constraint in RoF systems is nonlinearity, encompassing both optical fiber nonlinearity and nonlinearity associated with optical modulators[2.53], [2.54], [2.55]. The nonlinear behavior of optical modulators results in inter-modulation distortion (IMD) and typically imposes limits on the system's dynamic range [2.53], [2.54]. In multiband RoF systems, it can also lead to subcarrier intermodulation and data-dependent cross modulation [2.55]. The optical fiber, used for signal transmission, also exhibits nonlinear characteristics, introducing nonlinear impairments to the RoF signal after fiber transmission. These impairments include self-phase modulation and four-wave mixing. To address nonlinear impairments in RoF systems, various linearization techniques have been extensively explored [2.49]. One well-studied linearization approach is feedforward [2.56], [2.57], which, for instance, achieved up to a 10 dB improvement in spur-free dynamic range (SFDR) across a wide bandwidth from 7 GHz to 18 GHz, as reported in Reference [2.57]. However, the feedforward scheme often entails high complexity and requires precise calibration. To tackle these challenges, alternative optical linearization techniques have been proposed, such as the dual parallel modulation scheme, which reduced IMD by up to 38 dB [2.58]. Other techniques include the mixed-polarization scheme [2.59], [2.60], the dual electro-absorption modulators scheme (e.g., achieving IMD suppression by over 16 dB and SFDR improvement by over 8 dB as reported in Reference) [2.61], the gain modulation scheme, which reduced IMD by over 7 dB and improved the dynamic range by about 11 dB [2.62], and the cascaded modulator and semiconductor optical amplifier (SOA) scheme [2.63]. Additionally, the pre-distortion technique has been proposed and demonstrated [2.64], enabling the compensation of predictable nonlinearities. This approach achieved a 6 dB improvement in IMD along with a 14 dB peak enhancement in dynamic range. These techniques effectively mitigate nonlinear effects in RoF systems, allowing for increased modulation depth of the RF signal and, consequently, an improved system dynamic range.

In addition to the challenges posed by fiber chromatic dispersion and the nonlinearity resulting from optical fibers and optical modulators, RoF systems are also affected by various other impairments. These include amplified spontaneous emission (ASE) noise stemming from optical amplifiers (e.g., EDFA), phase noise due to the laser source's limited linewidth [2.65], and the inherent square-law detection characteristics of optical-to-electrical conversion by the photodetector (PD) [2.55]. These impairments place constraints on the performance of RoF systems, and these limitations become more pronounced as the RF carrier frequency increases, such as in the case of mm-wave frequencies.

To mitigate the effects of these impairments in RoF systems, digital signal processing (DSP) techniques have garnered significant attention and have led to substantial improvements in system performance [2.66]. One notable advantage of employing DSP for impairment compensation lies in its adaptability and flexibility, which can be adjusted as needed. A plethora of DSP algorithms have been proposed and investigated for RoF systems, addressing various impairments, including laser phase noise, the limited dynamic range resulting from

optical modulator nonlinearity [2.54], [2.67], and fiber chromatic dispersion [2.66]. In addition to the application of DSP at the receiver side for signal processing post-transmission, research has also explored the transmitter side using the digital predistortion principle, where the signal is pre-compensated prior to transmission.

2.4. mmWave wireless technologies in mobile RAN

One of the most notable distinctions of 5G from its predecessors in cellular systems lies in the recognition that the traditional sub-6 GHz spectrum falls short in meeting the demands of emerging applications. A solution emerged in the form of the millimeter wave (mmWave) spectrum. Initially deemed unsuitable for mobile operations due to unfavorable propagation characteristics, advancements in device and antenna technologies have now rendered them feasible for commercial wireless applications [2.68]. Consequently, the 5G standards gave rise to the advent of commercial mmWave communication.

Looking ahead, it becomes apparent that we are gradually transitioning towards applications such as virtual and augmented reality, UHD video conferencing, 3D gaming, and the integration of wireless technology into brain-machine interfaces. These applications will impose even more stringent constraints on throughput, reliability, and latency requirements. Following the successful implementation of mmWave communication, researchers naturally turned their attention to previously unexplored radio frequency (RF) bands, particularly the THz band situated above the mmWave spectrum. The vast bandwidth of THz waves makes them suitable for numerous applications demanding ultra-high data rates. By combining the capabilities of sub-6 GHz, mmWave, and THz bands, we can unlock the true potential of many emerging applications. Additionally, the small wavelength of THz waves makes them applicable for micro and nano-scale communication. Historically, THz bands were limited to imaging and sensing due to the lack of feasible and efficient devices operating at these frequencies. However, recent advancements in THz devices suggest that THz communication is poised to play a pivotal role in the forthcoming generations of communication standards [2.69].

Prior to the 4G cellular standard, commercial (cellular) communication was confined to traditional bands up to 6 GHz, now known as sub-6 GHz cellular bands. However, within the 6-300 GHz range, there are numerous bands with substantial bandwidths that were employed for diverse non-cellular purposes, including satellite communications, radio astronomy, remote sensing, and radars, among others. Recent advancements in antenna technology have made it feasible to extend the use of this spectrum to mobile communication. The frequency band ranging from 30 to 300 GHz, with wavelengths between 1 and 10 mm, is termed the mmWave band. It provides hundreds of times more bandwidth compared to the sub-6 GHz bands. Although mmWave communication systems face challenges such as higher penetration and blockage losses, researchers have demonstrated that these effects can be beneficial in mitigating interference in modern cellular systems characterized by dense

deployment of small cells. This naturally leads to more aggressive frequency reuse and enhanced data security due to the higher directionality requirements at mmWave frequencies [2.70]. Frequencies in the mmWave range, approximately from 24 GHz to about 100 GHz, are already being explored as part of the 5G standard. Looking ahead to 6G and beyond systems, researchers are also delving into the 0.1-10 THz band, collectively referred to as the THz band. The lower end of this spectrum is particularly of interest for communication applications.

The expanded bandwidth available in the mmWave spectrum facilitates the viability of multi-gigabit wireless communication, paving the way for numerous innovations [2.70]. For example, mmWave frequencies can support wireless backhaul connections between outdoor base stations (BSs), reducing the costs associated with land acquisition, installation, and maintenance of fiber optic cables, particularly in ultra-dense networks (UDNs). Moreover, this capability enables the transformation of current wired data centers into entirely wireless ones, with data servers communicating via mmWave frequencies through highly directed pencil-beams. Another potential application lies in in-motion vehicle-to-vehicle (V2V) communication in high-mobility scenarios, including bullet trains and airplanes. In these scenarios, mmWave communication systems, coupled with sub-6 GHz systems, have the potential to offer improved data rates [2.71].

Additionally, the THz spectrum comprises bands with available bandwidths of several tens of gigahertz, supporting data rates in the terabits per second (Tbps) range. THz communication benefits from the integration of thousands of sub-millimeter antennas and experiences lower interference due to higher transmission frequencies. Consequently, it can support bandwidth-intensive and low-latency applications like virtual reality gaming and ultra-HD video conferencing. The maturation of THz communications is expected to benefit various applications, including nano-machine communication, on-chip communications, the Internet of Nano Things [2.72], and intra-body communication of nano-machines. It can also be integrated with bio-compatible and energy-efficient bio-nano-machines communicating using chemical signals (molecules), a form of communication known as molecular communication [2.73].

2.4.1 mmWave-based Fiber-Wireless Bridges for mobile transport deployments

As explained in the previous sections, A-RoF technology is anticipated to offer higher spectral efficiency, inherent in analog transmission systems, along with low power consumption and latency [2.74], [2.75]. Given that only optical-to-electrical (O/E) conversion is necessary, the complexity of the Distribution Unit (DU) can be substantially reduced, allowing for remote control of transmitted wireless signals. This becomes especially crucial in scenarios requiring the deployment of a large number of antenna units. Moreover, A-RoF systems have demonstrated compatibility with Power-over-Fiber (PoF) technology, enabling electric power supply through optical fibers [2.76]. However, the non-linearity of the optical link and fiber

chromatic dispersion impose limitations on both the affordable transmission length and the desired performance [2.77]. Despite the evident advantages of both analog and digital RoF technologies, their deployment faces challenges due to operational inflexibility, limited resilience, and cost considerations. These challenges are particularly pronounced in areas where optical links are susceptible to outages from fiber cuts or lack existing fiber infrastructure.

A-RoF-based Fi-Wi systems operating in the mmWave spectrum region offers a promising solution for robust and adaptable communication systems. This technology leverages large bandwidth mmWave links to establish flexible, cost-effective, and energy-efficient broadband wireless access networks. It also serves as a fiber backup, enhancing network resiliency [2.74]. Depending on the frequency range of the radio signal being transported, A-RoF based Fi-Wi systems can be implemented using two main architectures: (i) RF-over-fiber (RFoF) and (ii) intermediate frequency-over-fiber (IFoF).

In the RFoF-based Fi-Wi architecture, optical heterodyning and photonic up-conversion techniques are employed, directly up-converting lower frequency or baseband RF signals to the mmWave band. However, this approach has lower spectral efficiency, and a local oscillator (LO) is still necessary at the remote antenna unit (RAU) for the down-conversion process in full-duplex and relay systems. On the other hand, the IFoF-based Fi-Wi architecture involves sending a lower-frequency LO signal (e.g., <40 GHz) to the RAU in a separate optical channel for mmWave up/down conversion. This enables the use of lower bandwidth optical and RF devices [2.78]. This approach simplifies both the mmWave Tx. and Rx. antennas, making it more appealing for full-duplex systems and fiber-wireless-fiber links, known as a seamless Fi-Wi bridge. This design keeps the RAU configuration as simple as possible. Figure 19 illustrates potential application scenarios of the A-RoF based Fi-Wi system, including disaster-affected areas, dense communication areas, Distributed Antenna Systems (DAS), and mobile fronthaul networks.

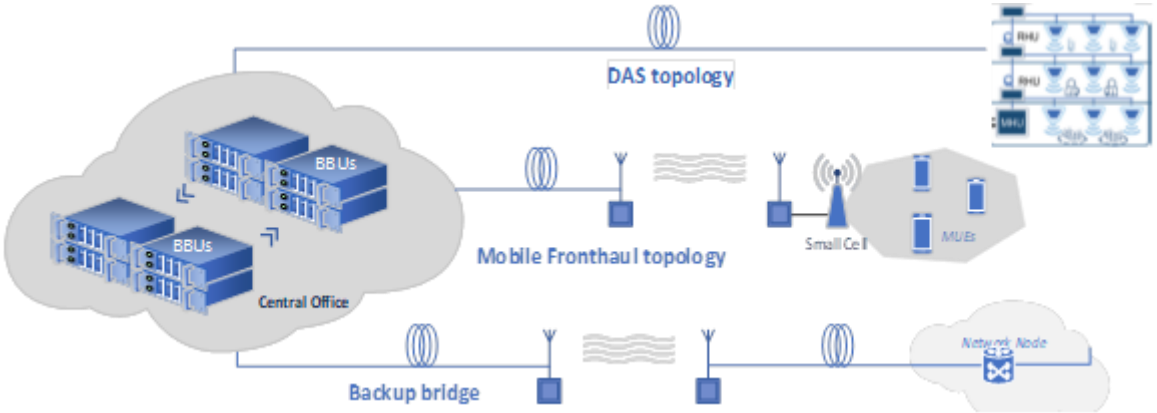

Figure 19. Fiber-mmWave- based topologies for beyond-5G application scenarios and network segments

Numerous research endeavours have explored and showcased the capabilities of A-RoF based Fi-Wi systems in high-capacity wireless transmission systems and mobile fronthaul/backhaul systems [2.79]. These initiatives primarily adopt RFoF configurations. Notably, the RFoF

configuration benefits from the latest advancements in digital signal processing (DSP)-based optical communication technologies, enabling the generation and transmission of higher-order modulation formats using RoF technologies. Utilizing an RFoF-based Fi-Wi system, multi-gigabit-per-second wireless transmission has been demonstrated in the Q-band, W-band, and D-band. Other research endeavors have proposed the use of A-RoF based Fi-Wi configurations as an efficient approach for mobile fronthaul and backhaul systems, addressing the requirements of 5G networks.

Although mmWave and THz bands have a huge potential for their usage in communication, there are significant challenges in their commercial deployments. In particular, communication in these bands suffer from poor propagation characteristics, higher penetration, blockage and scattering losses, shorter coverage range, and a need for strong directionality in transmission. These challenges have obstructed the inclusion of mmWave and THz bands in standards and commercial deployments until now. With the advancements in modern antenna and device technologies, it is now becoming feasible to use these bands for communications. The challenges regarding adoption of mmWave communications in RAN deployments as well the potential gains are discussed in the following paragraphs.

2.4.2 Main Challenges

In spite of the theoretical possibilities of achieving exceptionally high data rates, several critical technical obstacles hinder the utilization of mmWave in mobile networks. These challenges encompass significant path loss, elevated penetration loss, increased power consumption, blockages caused by shadowing, hardware impairments, and more. Subsequent to this statement, we will provide a concise overview of these issues.

- **Pathloss**

  In the transmission through free space, the received signal power (beyond the Kirchhoff area) can be calculated using the Friis transmission formula [2.80]. The wavelength of mmWave signals is considerably shorter than that of conventional microwave communication signals, which operate at carrier frequencies below 6 GHz. As a result, the pathloss of mmWave signals is significantly higher than that of microwave signals, assuming all other conditions, including antenna gains, remain constant. Although the pathloss for mmWave is generally elevated, it remains practical to establish communication over distances typical in urban mobile networks, ranging from a few hundred meters [2.80] to even a few kilometers [2.81]. The use of directive antennas has demonstrated the feasibility of communication ranges up to 10 km under favorable conditions [2.82]. However, in less pristine air conditions, factors such as rain attenuation and atmospheric/molecular absorption contribute to increased pathloss, thereby limiting the communication range [2.82], [2.83]. The impact of these factors varies with the carrier frequency.

- **Penetration loss**

The discussion on pathloss assumes line-of-sight (LoS) communications, but the challenge of high penetration loss becomes more pronounced in non-line-of-sight (NLoS) scenarios. In indoor settings, although the penetration losses for clear glass and dry walls are relatively low for 28 GHz signals (similar to microwave bands), the losses escalate significantly for materials like brick and tinted glass (approximately 28 dB and 40 dB, respectively), which is notably higher than at microwave bands [2.84]. These penetration losses tend to increase at higher frequencies. Consequently, achieving coverage indoors with mmWave nodes deployed outdoors, and vice versa, poses difficulties due to the substantial penetration loss.

- **Hardware impairments and design challenges**

Practical transceiver hardware faces impairments such as Phase Noise (PN), non-linear Power Amplifiers (PAs), I/Q imbalance, and restricted ADC resolution [2.85]. These factors place limitations on channel capacity [2.86], especially when aiming for high spectral efficiency. Conversely, research has demonstrated in [2.87] that MIMO communication links are less susceptible to the impact of hardware impairments compared to single-antenna links.

In mmWave communication systems, mixers play a crucial role in signal up-conversion at the transmitter and down-conversion at the receiver. Local oscillators are employed to generate carrier signals operating at the desired carrier frequency. However, owing to the inherent random deviation of the output signal frequency around the carrier, achieving exact synchronization between the oscillators at the transmitter and receiver becomes impractical. This mismatch can be characterized as phase PN, as the frequency offset introduces a random phase difference for the time domain samples. The sensitivity to PN is heightened in mmWave communication systems compared to conventional ones, primarily due to the elevated carrier frequency.

Another significant hardware challenge in mmWave technology involves non-linear PAs, as providing linear amplification to signals with very wide bandwidth proves to be a complex task. In practical terms, each amplifier exhibits non-linear behavior, including the clipping of input signals with large amplitudes and differential amplification of various frequencies. The widely employed model for describing such non-linear characteristics is the modified Rapp model [2.88].

Finallly, the elevated and broader frequency bands characteristic of mmWave communication systems introduce numerous technical challenges in the design of circuit components and antennas. These challenges span from device-level intricacies to architectural considerations, while particular emphasis is put on the formidable obstacles posed by phase noise and IQ imbalance in realizing mmWave RF circuits [2.89].

2.4.3 Motivation for employing mmWave llinks

After enumerating the primary challenges, it is essential to keep in mind the principal motivations for employing mmWave communications.

- **Extensive and uninterrupted available bandwidth**

In comparison to microwave communications, one significant advantage of mmWave communications is the availability of extensive bandwidth. However, it's important to note that a wider bandwidth doesn't always translate to higher rates in the noise-limited region [2.89]. Currently, the global available bandwidth for mobile networks (2G, 3G, 4G, and LTE-Advanced spectrum) is less than 780 MHz, with each major wireless provider having approximately 200 MHz of spectrum [2.80]. This limited bandwidth is insufficient for delivering Gbps rates to multiple devices, as it would require substantial per-device spectral efficiency.

In contrast, mmWave bands offer substantial bandwidth for future mobile networks. As depicted in Figure 4, the potentially available bandwidth in mmWave bands can exceed 150 GHz [2.90], even after excluding unfavourable bands like the water vapor absorption band (164–200 GHz). With 150 GHz of spectrum, a low spectral efficiency of 1 b/s/Hz is adequate to achieve a rate of 150 Gbps. This low spectral efficiency simplifies implementation and makes the unused frequency bands highly attractive. For instance, in October 2003, the FCC announced that the 71–76 GHz, 81–86 GHz, and 92–95 GHz frequency bands (collectively referred to as the E-band) would be available for ultra-high-speed data communication, including point-to-point WLAN, mobile backhaul, and broadband Internet access. The E-band provides a total bandwidth of 12.9 GHz (60-90 GHz). More recently, in July 2016, the FCC allocated large bandwidths in mmWave bands for cutting-edge wireless communications, specifically the 64-71 GHz unlicensed bands (along with the previous 57-64 GHz) and the 27.5-28.35 and 37-40 GHz licensed bands [2.89].

- **Short wavelength and narrow beamwidth**

In contrast to signals in the sub-6 GHz bands, mmWave signals possess a considerably shorter wavelength, enabling the integration of a large number of antennas into a compact array [2.80]. This characteristic significantly broadens the potential applications for large-scale antenna communications in future mobile networks. Simultaneously, the presence of numerous antenna elements results in a narrow beamwidth [2.91]. The advantageous aspect of this property lies in heightened security against eavesdropping and jamming, as well as increased resilience against co-user interference. This implies that the spectrum can be efficiently reused in space, allowing for the deployment of numerous interfering point-to-point MIMO systems (or multiuser MIMO systems) within a limited spatial region.

- **Massive MIMO implementation potential**

A challenge associated with massive MIMO systems is the expense and intricacy of hardware required to effectively harness a large number of antennas in the mmWave region. Depending on the current mmWave products offered by vendors, the number of antenna elements at the gNB (gNodeB) can range from 128 to over 1,000.

In the mmWave context, it is crucial to have support for beam-sweeping to accurately estimate or identify the direction of interest. However, this process introduces additional overhead in terms of Channel State Information (CSI) acquisition, which increases with the number of antennas. This is due to the fact that as the number of antennas grows, the beams become narrower, necessitating the support for more beams.

The beamforming gain in the mmWave spectrum is notably higher when compared to sub-6GHz. This is attributed to the ability to pack a greater number of antenna elements into the same form factor, resulting in a more focused and sharper beam. Additionally, the sharper beam contributes to enhanced spatial separation between users, consequently boosting the performance of MU-MIMO [2.92].

2.5. Proof-of-concept experimental evaluation of Fiber/mmWave transport layout

In this section, preliminary experiments that provide a proof-of-concept validation and performance evaluation of the discussed analog fiber/mmWave transport concept are presented. More specifically, a DSP assisted A-IFoF concept to efficiently accommodate multiple broadband radio signals using commercial off-the shelf electronic/photonic components is introduced. Within this frame, a centralized BBU which serves a number of RRHs, provides a complete set of digital functionalities allowing for the optical transport of the radio waveforms through the installed fiber infrastructure and their transmission through the air using mmWave carriers. In this centralized approach, the appropriate data signal waveforms are generated in the DSP-enhanced BBU and seamlessly transported through the fiber/wireless link. This centralized approach concentrates the entire digital processing of the link on the BBU side while the served RRHs are responsible only to handle the vast spectral slices with their mmWave radio hardware. These experimental studies have revealed the impact of optical transport channel impairments (fiber loss, chromatic dispersion, nonlinearities due to electro-optic conversion) on complex-modulated IF carriers generated from the BBU. Different types of IQ signals in terms of symbol rate, number of radio bands, modulation type and radio carrier frequencies, have been employed to quantify the A-RoF performance using Error Vector Magnitude (EVM) measurements at the receiver side. The Fi-Wi transmission experiments was evaluated on both DownLink (DL) and UpLink (UL) operation and the additional distortion due to V-band RF electronics considering the effects of a realistic 60 GHz indoor wireless environment. The DL/UL operation was demonstrated for Single Carrier (SC) radio bands, carrying different M-QAM signals.

2.5.1 Analog IFoF link parameters investigation

Figure 20 depicts the experimental setup employed for the evaluation of the IFoF scenarios. An Arbitrary Waveform Generator (AWG) was used to provide the data signals for both single- (Ch1) and multi- (Ch1 to Ch6) band scenarios at modulation rates up to 1.25 Gbd. The programmable data source allowed the necessary Tx-side DSP operations described in the previous section. Pulse shaping (using Root Raised Cosine (RRC) shaping filters with roll-off factor $\alpha = 0.2$) and digital pre-distortion of the optoelectronic components were performed to the following experiments. To this end, channel estimation (using pilot tones) has been performed, prior the actual data transmission, where an amplitude and phase channel response was estimated on the frequency domain. Through the AWG, the pre-distorted data signals were digitally upconverted to the selected IF. A single-drive MZM was used to generate the IFoF signal carrying the radio bands with the intensity modulator biased at the quadrature point ($V\pi/2$). A Continuous Wave (CW) DFB-laser emitting at 1543.73 nm of +10 dBm provided the optical carrier to the IFoF transmitter.

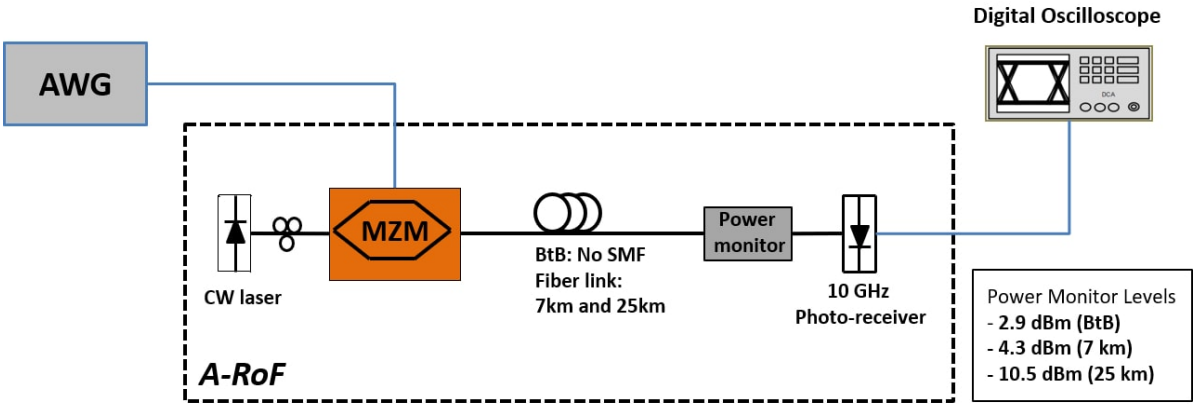

Figure 20. Experimental Setup of the Analog RoF link.

Two fiber links of Standard SMF (SSMF) (7 km & 25 km) were used to investigate the role of fiber length on the optical transmission. The optical power of the IFoF signal was measured by means of an optical power meter set prior to an off-the-shelf 10 GHz linear photo-receiver comprised of a photodiode (0.7 A/W responsivity) and a low-noise amplifier with 20 dB gain.

The Single-Band experiments were carried out by using an IF frequency of 5 GHz. The IFoF transmission at 5 GHz was selected in order to meet the specifications of the mmWave Upconverter at the radio part. Such selection easily accommodates the entire bandwidth (~7GHz) within the targeted unlicensed radio band and provides resilience against the power fading due to CD for fiber lengths up to 25 km [2.93].

Experimental studies on A-RoF MFH link were performed focusing on the symbol rate and the modulation order of the IF signal. The goal of this study was to fully characterize the effect of fiber channel for various radio signal characteristics. Besides, leveraging from the DSP capabilities for generating any complex modulation scheme at the transmitter side, the

feasibility of increased spectrum utilization was also demonstrated. Generating different types of complex waveforms carrying symbols rates of 1 Gbd, EVM values below the limits set by 3GPP specification were achieved [2.94] (with a minimum EVM margin of 5% for 64-QAM signals) for each format investigated, without any additional equalization stage at the receiver side. The successful IFoF transmission of a 128 QAM modulated IF carrier over a 25-km optical link corresponds to a spectral efficiency 5.83 b/s/Hz for the A-RoF link. EVM measurements for set of M-QAM and M-PSK schemes are presented in Table 1 and the respective constellation diagrams after detection and demodulation are also shown in Figure 21. Moreover, the reported results indicate that an identical EVM penalty of less than 2.7% was introduced by the fiber part for all the modulation types. This result implies that the IFoF transmission can be resilient to fiber channel impairments supporting more complex modulation types without any significant quality distortion.

Table 1. EVM measurements for different modulation formats at 1 GBaud

IF: 5GHz	**EVM rms (%)**		**EVM Req. (%) [2.94]**
Modulation format	**Back-to-back**	**25km**	
QPSK	1.68	4.37	17.5
8-PSK	1.78	4.52	N/A
16-QAM	2.16	4.62	12.5
64-QAM	2.19	4.84	8
128-QAM	2.29	4.90	N/A

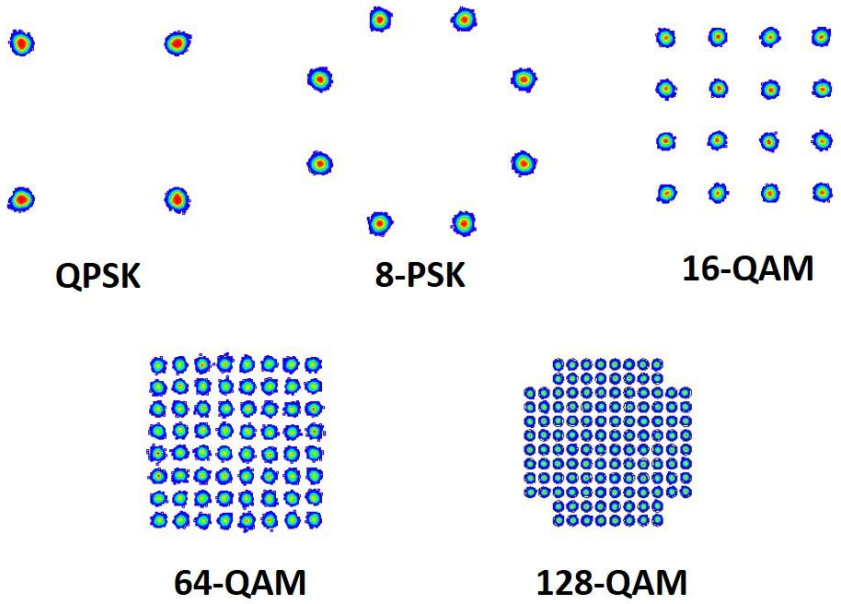

Figure 21. Constellation diagrams of the received signals at different modulation schemes after transmission over 25 km SMF.

Table 2 summarizes the measured EVM values for different symbol rates. It can be observed that for symbol rate variations between 500 Mbd to 1.25 Gbd, the EVM is slightly increasing from 2.66% to 5.50%, after 25 km transmission. Through this result a good agreement between the theory and experiment is appeared since the fiber CD introduces severe distortion for wideband signals [2.93]. Nevertheless, the measured EVM values are well below the EVM threshold for a QPSK modulated signal as specified by 3GPP. The respective constellation diagrams of the received signals at 25 km length are also depicted in Figure 22. This result reveals a strong scalability potential of further increase the transmission rate of a single IF-modulated band.

Table 2. EVM measurements for different symbol rates for a QPSK signal

IF: 5GHz / QPSK	EVM rms (%)		EVM Req. (%) [2.94]
Symbol Rate	Back-to-back	25km	
500 MBd	1.45	2.66	17.5
750 MBd	1.64	3.24	
1 GBd	1.70	4.37	
1.25 GBd	1.74	5.50	

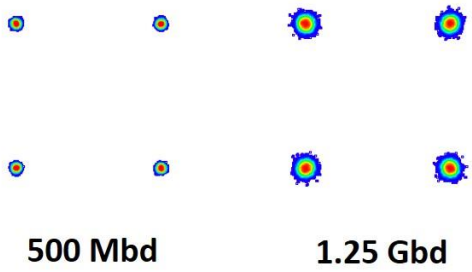

Figure 22. Constellation diagrams of the received signals for different baud rates after transmission over 25 km SMF.

The next evaluation step involves the increase of the overall bandwidth utilization for the proposed A-RoF concept by introducing a digitally generated SCM signal to extend the operating bandwidth of the single carrier approach which was discussed in the previous section.

Exploiting once more the DSP capabilities on generation of complex waveforms, four different subcarriers have been digitally synthesized, before feeding a single DAC channel in order to generate the desired multiband radio signal. The 4 sub-bands were assigned at 0.625 GHz, 1.875 GHz, 3.125 GHz and 4.375 GHz center frequencies (around 2.5 GHz) and each of them was modulated at 1 Gbd symbol rate, pulse-shaped with a root raised cosine filter ($\alpha = 0.2$), utilizing thereby a total 5 GHz bandwidth. Figure 23(a) shows that in the case of back-to-back measurement, all sub-bands have almost the same performance and the modulation type does not affect the measured EVM values. After transmission over the 25 km fiber link, the effect of dispersion-induced power fading is evident, since the higher frequency components suffer from severe distortion compared to lower ones. The use of a higher order modulation format slightly increases the EVM value. With EVM values below 9%, all QPSK, 16 QAM and 64-QAM schemes achieve accepted performance in all the allocated spectrum bands [2.94]. With a 64 QAM scheme an overall capacity of 24 Gb/s is achieved.

To further extend the above SCM approach, a 6 band SCM signal was generated by exploiting the high bandwidth DAC provided by the AWG. A total bandwidth of 7.2 GHz with a center IF carrier at 3.6 GHz was achieved. In this case, the sub-carriers' center frequencies were selected to be 0.6 GHz, 1.8 GHz, 3 GHz, 4.2 GHz, 5.4 GHz and 6.6 GHz while each of them was modulated with a QPSK at 1 Gbd. The performance was evaluated after 7 km and 25 km of fiber transmission and this set of measurements is depicted in the plots of Figure 23(b). As in the case of 4 bands, the first 3 subcarriers exhibit similar performance, while the bands located at higher frequencies result in higher EVM values. Such performance degradation for the 2 higher frequency bands can be explained, considering the RF plan for Subcarrier Multiplexing scheme as described in [2.95] and taking into account the severe distortion due to nonlinear Intermodulation effects [2.96]. The impact of dispersion is evident after 25 km transmission but not in the case of 7 km as it was originally expected. Higher frequency carriers would be needed to observe the effect of dispersion in a shorter fiber link, like this of 7km.

Comparing the EVM performance between the single band and multiple band IFoF transmission, it is evident that the signal distortion is increased for increased number of radio bands as it is expected. Moving towards wide-band, multi carrier approaches, the analog photonic links suffer from cross modulation distortion (XMD) which introduces severe distortion in the modulated in-band of each signal [2.96].

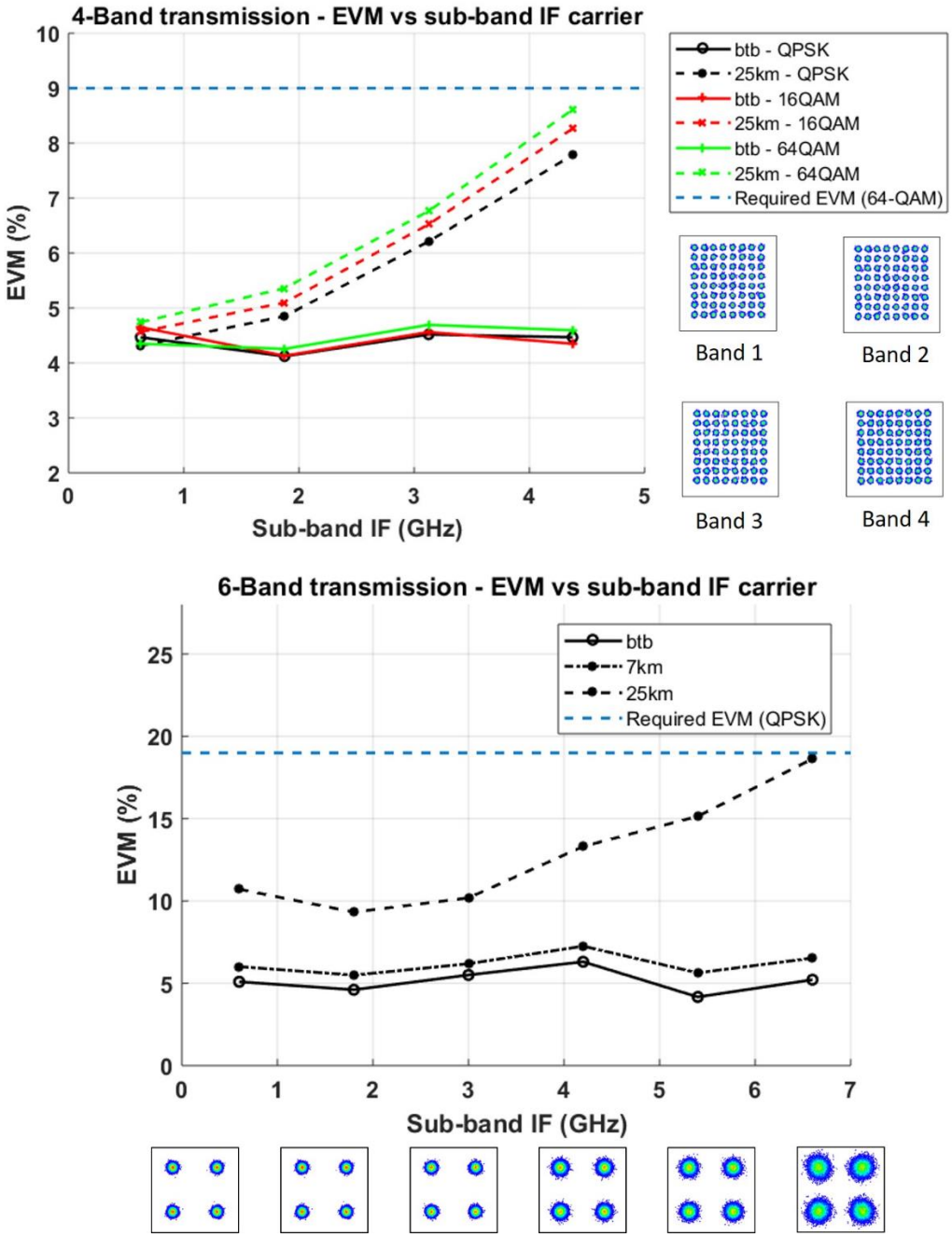

Figure 23. EVM measurements for each sub-band of the SCM A-RoF link (a) 4-bands, Constellation diagrams for 64-QAM after 25km, (b) 6-bands, Constellation diagrams for QPSK after 25km.

Combining the proposed A-RoF IM/DD optical fronthaul topology with commercial V-band radio hardware (operated at 57-64 GHz unlicensed band), indoor wireless measurements using directional antenna elements were performed.

Figure 24 illustrates the experimental setups employed for both UL/DL scenarios. For the DL operation (Figure 24(a)) the signal after the transmission through the A-RoF link was received by a photoreceiver (Avalance Photodiode (APD) Transimpedance Amplifier (TIA)). This IF modulated output is fed into a mmWave upconverter connected to a V band directional antenna (Tx-antenna). The V-band converter had a nominal noise figure of 8 dB at maximum gain. Standard pyramidal gain horn V-band antennas of 23 dBi gain and 10° beamwidth were employed. The signal received by an identical antenna located in a 5 m horizontal distance from the Tx-antenna. The antennas, together with the up- and downconversion units, were mounted on wooden tripods and kept fixed at a height of 1.4 m above the floor. We evaluated the Fiber-Wireless (Fi-Wi) link on the receiver side by capturing the modulated data on a real time oscilloscope. Since none of the antennas perform equalization or any baseband processing, the response of the mmWave components (e.g. local oscillators, mixers, filters, waveguides) was evaluated using the DSP platform at the Rx antenna.

For the UL operation (Figure 24(b)), the IF modulated signal feeds directly the Tx-antenna frontend, while the Rx-antenna is used as the driving signal for the MZM of the A-RoF link. The now reversed Wireless/Fiber link (along with the passive and active electronic components) is evaluated at the output of the A-RoF link where the photoreceiver provides the input to the Digital Oscilloscope for offline processing.

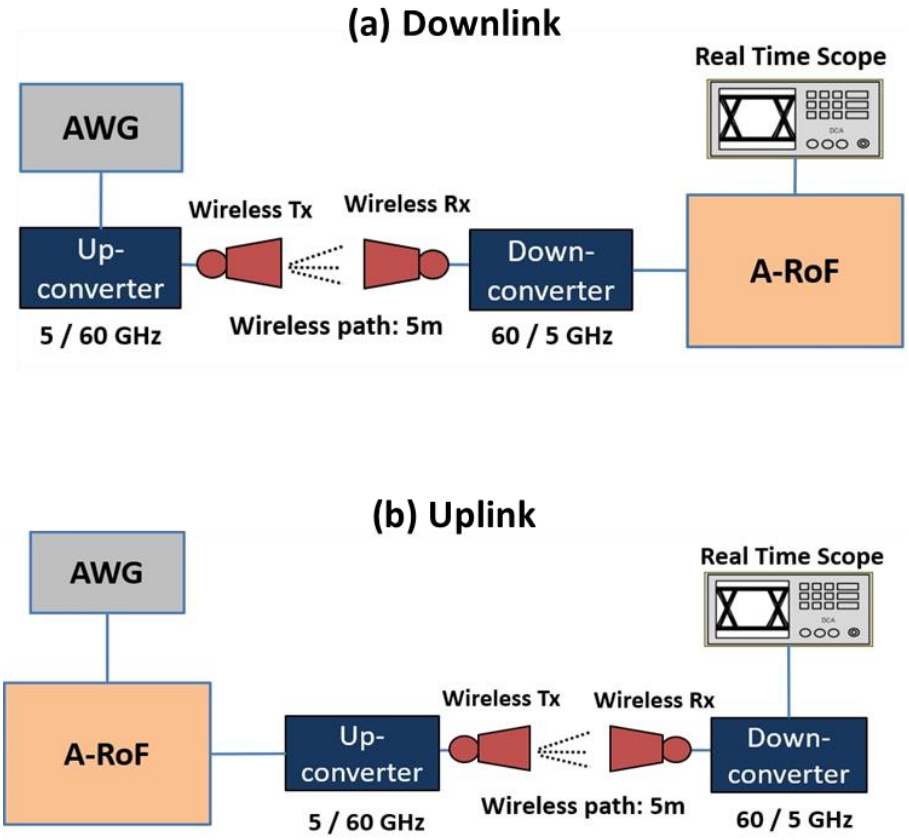

Figure 24. Experimental Setup of the Analog RoF/mmWave link. (a) Downlink direction, (b) Uplink direction.

In both cases, after the digitization of the received signals, digital down-conversion from the IF frequency to baseband was performed. There, matched filtering, resampling and proper timing synchronization were applied in order to extract a single-sample per symbol sequence. For the equalization stage, a static 5-tap Radius Directed Constant Modulus Algorithm (CMA) algorithm was employed for off-line equalization of both fading effects stemming from both fiber-air transmission and to remove the frequency response from mmWave components. Finally, a carrier phase recovery stage compensated for the phase noise due to local oscillators' mismatches. Statistical constellation analysis and error counting was employed for estimating and measuring the transmission quality.

In this experiment Single-Carrier QPSK and 16 QAM at 1 Gbd symbol rate were employed as modulated radio signals. A root-raised-cosine pulse shaping filter with 20% excess bandwidth resulted in a total 1.2 GHz to be transmitted through the fiber/wireless link. In Figure 25 we present an EVM bar diagram for both uplink and downlink operation using the above modulation types. Two different test cases were investigated by introducing the long fiber part of 25 km. The reported results reveal that the combined fiber/wireless link (25 km fiber and 5 m air-transmission) achieve accepted performance in terms of EVM as specified by the 3GPP specification. A fair direct comparison between the UL/DL cases should not, however, be considered from the above results since both cases were investigated by keeping constant the setup parameters (Electro-optic modulator, RF amplifiers, optical and RF power

levels). Under realistic conditions, both cases would be implemented by using dedicated opto-electronic parts for each case (UL/DL) being properly configured at optimum points.

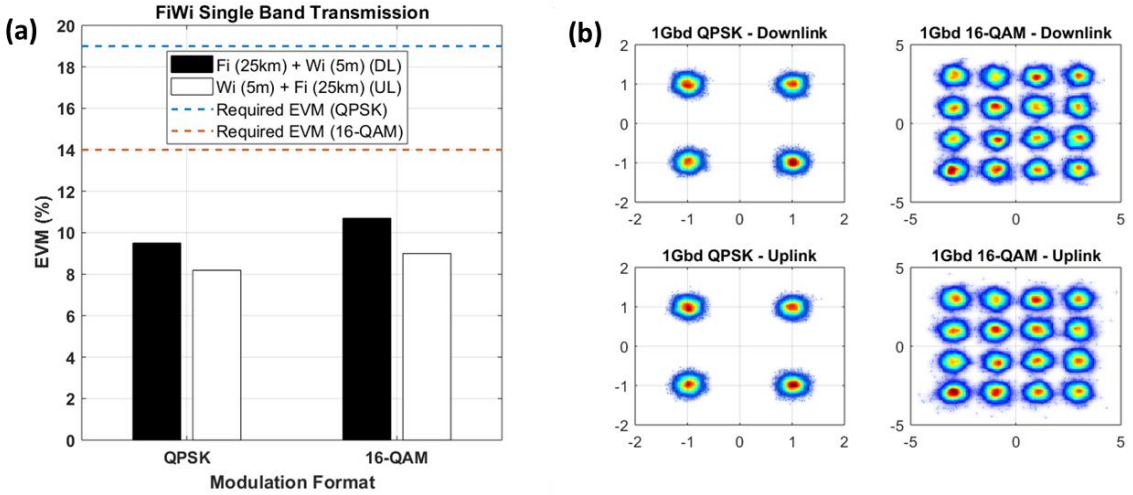

Figure 25. (a) EVM bar-diagram measurements for A-RoF/mmWave transmission in uplink and downlink directions (b) Constellation diagrams for QPSK and 16-QAM after Rx-side DSP.

Concluding, a DSP-assisted A-RoF/V-band topology was experimentally validated and reported in [2.97] and in [2.98], offering the generation and transmission of broadband radio signals capable of supporting the targeted specifications for 5G-era. Single Carrier and Digital Subcarrier multiplexed signals with high order modulation formats (M-PSK and M-QAM) have been examined for increasing the overall capacity of the fronthaul link, exhibiting robust performance for fiber distances up to 25 km. The optical transport of multiband radio signal carrying up to 24 Gb/s (using 64 QAM signals) was experimentally demonstrated showing EVM values below 9%.

Radio devices operating at V-band connected to the A-RoF link and an evaluation of the complete fiber/wireless channel has been performed for both UL/DL cases. Demodulation and detection of the radio signals has been achieved utilizing standard DSP only after the fiber/wireless transmission without any processing units at the antenna subsystems. Single carrier schemes at 1 Gbd using QPSK and 16 QAM formats were detected and demodulating utilizing receiver-side DSP. The fiber-wireless transmission of 4 Gb/s was successfully demonstrated for both UL/DL cases using 16 QAM schemes exhibiting EVM below the 14% requirements for systems operating at the region of the mmWave regime.

References

[2.1] https://cordis.europa.eu/project/id/761989

[2.2] "The Benefits of Cloud-RAN Architecture in Mobile Network Expansion", Application Note from Fujitsu Network Communications Inc. (2014).

[2.3] Agata and K.Tanaka, "NG-EPON for Mobile Access Network", presented in IEEE 802 Plenary Session, March 2014, Beijing, China.

[2.4] A. Checko et al., "Cloud RAN for Mobile Networks – A Technology Overview", IEEE Communications Surveys & Tutorials, Vol.17, Issue 1, pp. 405-426 (2015).

[2.5] China Mobile Research Institute, "C-RAN: The Road Towards Green RAN," White Paper, 2013. Available: http://labs.chinamobile.com/cran/

[2.6] Manli Qian et al, "A super base station based centralized network architecture for 5G mobile communication systems", Digital Communications and Networks (2015).

[2.7] M. Koziol, "Mobile World Congress 2018: Don't Expect 5G Service Anytime Soon", posted in spectrum.ieee.org, 2 March 2018. https://spectrum.ieee.org/tech-talk/telecom/wireless/mobile-world-congress-2018-5g-isnt-for-you

[2.8] D. Wubben et al., "Benefits and impact of cloud computing on 5G signal processing: Flexible centralization through cloud-RAN," IEEE Signal Process. Mag., vol. 31, no. 6, pp. 35–44, Nov. 2014.

[2.9] M. Milosavljevic, "FPGAs for Reconfigurable 5G and Beyond Wireless Communication", presented in NMI FPGA Network: "Safety, Certification and Security", University of Hertfordshire, 19 May 2016, Hatfield, UK.

[2.10] C. Raack, J.M. Garcia, R. Wessaly, "Centralized versus Distributed Radio Access Networks: Wireless intergation into Long Reach Passive Optical Network", in Proc. of CTTE 2015, 9-10 November 2015, Munich, Germany.

[2.11] A. Olivia et al., "An Overview of the CPRI specification and its application to C-RAN based LTE scenarios", IEEE Communications Magazine, Vol. 54, Issue 2, pp. 152-159 (2016).

[2.12] White paper from Altera. "The Emerging Need for Fronthaul Compression", June 2016.

[2.13] F. Lu et al. "Adaptive Digitization and Variable Channel Coding for Enhancement of Compressed Digital Mobile Fronthaul in PAM-4 Optical Links", IEEE Journal of Lightwave Technology, Vol.35, No.21,pp.4714-4720 (2017).

[2.14] N. Carapellese et al, "BBU placement over a WDM aggregation network considering OTN and overlay fronthaul transport,," European Conf. on Optical Com. (ECOC), pp. 1-3, 2015.

[2.15] K. Miyamoto, S. Kuwano, J. Terada, and A. Otaka, "Split-phy processing architecture to realize base station coordination and transmission bandwidth reduction in mobile fronthaul," presented at the Optical Fiber Communications Conf. Exhib., Los Angeles, CA, USA, 2015, Paper M2J.4.

[2.16] J. Armstrong, "OFDM for Optical Communications," Journal of Lightwave Technology, vol. 27, no. 3, pp. 189-204, Feb.1, 2009.

[2.17] M. Nahas, A. Saadani, J. Charles, and Z. El-Bazzal, “Base stations evolution: Toward 4G technology,” in Telecommunications (ICT), 2012 19th International Conference on. IEEE, 2012, pp. 1–6.

[2.18] X. Hu, C.Ye and K.Zhang, “Converged Mobile Fronthaul and Passive Optical Network Based on Hybrid Analog-Digital Transmission Scheme”, in Proc. of Optical Fiber Communications Conf (OFC) 2016, paper No. W3C.5, 20-24 March 2016, Anaheim, CA, USA.

[2.19] G. Kalfas et al., "Non-Saturation Delay Analysis of Medium Transparent MAC Protocol for 60 GHz Fiber-Wireless Towards 5G mmWave Networks," J. Lightwave Technol. 35, 3945-3955 (2017).

[2.20] C. Lim et al., “Mitigation strategy for transmission impairments in millimeter-wave radio-over-fiber networks”, Journal of Optical Networking, Vol.8, No.2, pp.201-214 (2009).

[2.21] X. Liu, H. Zeng, N. Chand and F. Effenberger, "Efficient Mobile Fronthaul via DSP-Based Channel Aggregation," in Journal of Lightwave Technology, vol. 34, no. 6, pp. 1556-1564, March, 15 2016.

[2.22] X. Liu, H. Zeng, N. Chand and F. Effenberger, "CPRI-compatible efficient mobile fronthaul transmission via equalized TDMA achieving 256 Gb/s CPRI-equivalent data rate in a single 10-GHz-bandwidth IM-DD channel," 2016 Optical Fiber Communications Conference and Exhibition (OFC), Anaheim, CA, 2016, pp. 1-3.

[2.23] Nurul Huda Mahmood et al, “A centralized inter-cell rank coordination mechanism for 5G systems”, 13th International Wireless Communications and Mobile Computing Conference (2017).

[2.24] B.J.R. Sahu, S. Dash, N.Saxena, A. Roy, “Energy-Efficient BBU Allocation for Green C-RAN”, IEEE Communications Letters, Vol.21, Issue 7, pp. 1637-1640 (2017).

[2.25] C. Masterson, “Massive MIMO and Beamforming: The Signal Processing Behind the 5G Buzzwords”, Analog Devices White Paper, June 2017.

[2.26] P. Harris, et al. "Performance characterization of a real-time massive MIMO system with LOS mobile channels." IEEE Journal on Selected Areas in Communications 35.6 (2017): 1244-1253.

[2.27] M. Wu, B.Yin, G. Wang, C.Dick, J.R. Cavallaro, and C.Stuper, “Large-Scale MIMO Detection for 3GPP LTE: Algorithms and FPGA Implementations”, IEEE Journal of Selected Topics in Signal Processing, Vol.8, Issue 5, pp. 916-929 (2014).

[2.28] T.H. Pham, S.A. Fahmy, and I.V. McLoughlin. "An End-to-End Multi-Standard OFDM Transceiver Architecture Using FPGA Partial Reconfiguration." IEEE Access 5 (2017): 21002-21015.

[2.29] S. Malkowsky et al., “The World’s First Real-Time Testbed for Massive MIMO: Design, Implementation and Validation”, IEEE Access, Vol.5, pp.9073-9088 (2017).

[2.30] Rajpal, Shivika and Goyal, Rakesh. "A Review on Radio-Over-Fiber Technology-Based Integrated (Optical/Wireless) Networks " Journal of Optical Communications, vol. 38, no. 1, 2017, pp. 19-25. https://doi.org/10.1515/joc-2016-0020

[2.31] Nasoha, H. and Idrus, S.M.. “Modeling and performance analysis of WCDMA radio over fiber system.” Applied Electromagnetics, 2007. APACE 2007. AsiaPacific Conference. 2007. pp.1 to 4.

[2.32] Nirmalathas, A., Gamage, P.A., Lim, C., Novak, D . and Waterhouse, R. Digitized Radio-Over-Fiber Technologies for Converged Optical Wireless Access Network. Journal of Lightwave Technology. 2010. 28(16): pp: 2366 to 2375.

[2.33] Sasai, H., Niiho, T., Tanaka, K., Utsumi, K. and Morikura, S. Radio-overfiber transmission performance of OFDM signal for dual-band wireless LAN systems. Microwave Photonics, 2003. MWP 2003 Proceedings. International Topical Meeting, vol., no., pp. 139- 142, 10-12 Sept. 2003.

[2.34] Seeds, A.J. & Williams, K.J. (2006). Microwave photonics. IEEE Journal of Lightwave Technology, Vol. 24, No. 12, December 2006, ISSN 4628-4641.

[2.35] Anthony Ng'oma, 2005 Radio-over-Fiber Technology for Broadband Wireless Communication Systems, Doctoral Thesis, University of Eindhoven.

[2.36] Christina Lim, Ampalavanapillai Nirmalathas, Masuduzzaman Backul, Prasanna Gamage, Ka Lun Lee, Yizhuo Yang, Dalma Novak and Rod Waterhouse. "Fiber-Wirless Networks and Subsystem Technologies" Journal of Lightwave Technology, Vol. 28, No. 4, Feb. 15, 2010.

[2.37] D.Wake, "Radio over Fiber Systems for Mobile Applications" in Radio over Fiber Technologies for Mobile Communications Networks", H. Al-Raweshidy, and S. Komaki, ed. (Artech House, Inc, USA, 2002).

[2.38] K.Hong, "Radio over Fiber based Network Architecture",der Technischen Universitat Berlin,2005.

[2.39] Y. Watanabe, "Current Status of Perfluorinated GIPOF and 2.5 Gbps Data Transmission over it", in Proceedings of OFC '03, USA, 2003, pp. 12 – 13.

[2.40] D. Wake, and K. Beachman, "A Novel Switched Fibre Distributed AntennaSystem", in Proceedings of European Conference on Optical Communications (ECOC'04), Vol. 5, 2004, pp. 132 – 135.

[2.41] Jianjun Yu et al, "Radio-over-optical-fiber networks: introduction to the feature issue", Journal of Optical Networking, Vol. 8(5) , pp 488-481, 2009.

[2.42] D. K. Mynbaev, L. L. Scheiner, "Fiber Optic Communications Technology",(Prentice Hall, New Jersey, 2001).Communications, Vol. 5, No. 2, 177- 187, (Kluwer, 2003).

[2.43] Goyal R, Randhawa R, Kaler RS. Single tone and multi tone microwave over fiber communication system using direct detection method. Optik 2012; 123:917–23.

[2.44] Singh S, Kapoor A, Kaur G, Kaler RS, Goyal R. Investigation on wavelength re-modulated bi-directional passive optical network for different modulation formats. Optik 2014; 125:5378–82.

[2.45] Vyas AK, Agrawal N. Radio over fiber: future technology of communication. Int J Emerging Trends Technol Comput Sci2012; 1:233–7.

[2.46] Goyal R, Kaler RS. A novel architecture of hybrid (WDM/TDM) passive optical networks with suitable modulation format. Opt Fiber Technol 2012; 18:518–22.

[2.47] Abd El-Naser A, Mohammed MM, El-Halawany E, Zaki Rashed AN, Eid MM. Recent applications of optical parametric amplifiers in hybrid WDM/TDM local area optical networks. Int J Comput Sci Inform Secur 2009;3; 125:14–24.

[2.48] Kosek H, He Y, Gu X, Fernando X. All-optical demultiplexing of WLAN and cellular CDMA radio signals. J Lightwave Technol 2007; 25:1401–9.

[2.49] He, J.; Lee, J.; Kandeepan, S.; Wang, K. Machine Learning Techniques in Radio-over-Fiber Systems and Networks. Photonics 2020, 7, 105. https://doi.org/10.3390/photonics7040105.
[2.50] Lim, C.; Lee, K.-L.; Nirmalathas, A.; Novak, D.;Waterhouse, R. Impact of chromatic dispersion on 60 GHz radio-over-fiber transmission. In Proceedings of the Annual Meeting of the IEEE Lasers and Electro-Optics Society, Acapulco, Mexico, 9–13 November 2008; pp. 89–90.
[2.51] Weiß, M.; Huchard, M.; Stohr, A.; Charbonnier, B.; Fedderwitz, S.; Jager, D.S. 60-GHz photonic millimeter-wave link for short-to-medium range wireless transmission up to 12.5 Gb/s. J. Lightw. Technol. 2008, 26, 2424–2429.
[2.52] Li, X.; Yu, J.; Zhang, J.; Xiao, J.; Zhang, Z.; Xu, Y.; Chen, L. QAM vector signal generation by optical carrier suppression and precoding techniques. IEEE Photon. Technol. Lett. 2015, 27, 1977–1980.
[2.53] Lim, C.; Attygalle, M.; Nirmalathas, A.; Novak, D.;Waterhouse, R. Analysis of optical carrier-to-sideband ratio for improving transmission performance in fiber-radio links. IEEE Trans. Microw. Theory Techn. 2006, 54, 2181–2187.
[2.54] James, J.; Pengbo, S.; Nkansah, A.; Xing, L.; Gomes, N.J. Nonlinearity and noise e ects in multi-level signal millimeter-wave over fiber transmission using single and dual wavelength modulation. IEEE Tran. Microw. Theory Tech. 2010, 58, 3189–3198.
[2.55] Wang, J.; Liu, C.; Zhu, M.; Yi, A.; Cheng, L.; Chang, G.-K. Investigation of data-dependent channel cross-modulation in multiband radio-over-fiber systems. J. Lightw. Technol. 2014, 32, 1861–1871.
[2.56] Zhang, X.; Zhu, R.; Shen, D.; Liu, T. Linearization technologies for broadband radio-over-fiber transmission systems. Photonics 2014, 1, 455–472.
[2.57] Ismail, T.; Liu, C.-P.; Mitchell, J.E.; Seeds, A.J. High-dynamic-range wireless-over-fiber link using feedforward linearization. J. Lightw. Technol. 2007, 25, 3274–3282.
[2.58] Park, S.-H.; Choi, Y.-W. Significant suppression of the third intermodulation distortion in transmission system with optical feedforward linearized transmitter. IEEE Photon. Technol. Lett. 2005, 17, 1280–1282.
[2.59] Korotky, S.K.; Ridder, R.M. Dual parallel modulation schemes for low-distortion analog optical transmission. IEEE J. Sel. Areas Commun. 1990, 8, 1377–1381.
[2.60] Haas, B.M.; Murphy, T.E. A simple, linearized, phase-modulated analog optical transmission system. IEEE Photon. Technol. Lett. 2007, 19, 729–731.
[2.61] Hraimei, B.; Zhang, X.; Jiang, W.; Wu, K.; Liu, T.; Xu, T.; Nie, Q.; Xu, K. Experimental demonstration of mixed-polarization to linearize electro-absorption modulators in radio-over-fiber links. IEEE Photon. Technol. Lett. 2011, 23, 230–232.
[2.62] Shen, Y.; Hraimei, B.; Zhang, X.; Cowan, G.E.R.; Wu, K.; Liu, T. A novel analog broadband RF predistortion circuit to linearize electro-absorption modulators in multiband OFDM radio-over-fiber systems. IEEE Tran. Microw. Theory Tech. 2010, 58, 3327–3335.
[2.63] Lee, S.-H.; Kang, J.-M.; Choi, I.-H.; Han, S.-K. Linearization of DFB laser diode by external light-injected cross-gain modulation for radio-over-fiber link. IEEE Photon. Technol. Lett. 2006, 18, 1545–1547.

[2.64] Hraimel, B.; Zhang, X. Low-cost broadband predistortion-linearized single-drive x-cut Mach-Zehnder modulator for radio-over-fiber systems. IEEE Photon. Technol. Lett. 2012, 24, 1571–1573.
[2.65] Li, L.; Zhang, G.; Zheng, X.; Li, S.; Zhang, H.; Zhou, B. Phase noise suppression for single-sideband, modulation radio-over-fiber systems adopting optical spectrum processing. IEEE Photon. Technol. Lett. 2013, 25, 1024–1026.
[2.66] Kim, B.G.; Bae, S.H.; Kim, H.; Chung, Y.C. DSP-based CSO cancellation technique for RoF transmission system implemented by using directly modulated laser. Opt. Express 2017, 25, 12152–12160.
[2.67] Cui,Y.; Dai,Y.; Yin, F.; Lv, Q.; Li, J.; Xu, K.; Lin, J. Enhanced spurious-free dynamic range in intensity-modulated analog photonic link using digital postprocessing. IEEE Photon. J. 2014, 6, 7900608.
[2.68] T. S. Rappaport, S. Sun, R. Mayzus, H. Zhao, Y. Azar, K. Wang, G. N. Wong, J. K. Schulz, M. Samimi, and F. Gutierrez, "Millimeter wave mobile communications for 5G cellular: It will work!" IEEE access, vol. 1, pp. 335–349, 2013.
[2.69] H. Sarieddeen, N. Saeed, T. Y. Al-Naffouri, and M.-S. Alouini, "Next generation terahertz communications: A rendezvous of sensing, imaging, and localization," IEEE Communication Magzine, vol. 58, no. 5, pp. 69–75, May 2020.
[2.70] Tripathi, S., Sabu, N.V., Gupta, A.K., Dhillon, H.S. (2021). Millimeter-Wave and Terahertz Spectrum for 6G Wireless. In: Wu, Y., et al. 6G Mobile Wireless Networks. Computer Communications and Networks. Springer, Cham. https://doi.org/10.1007/978-3-030-72777-2_6.
[2.71] J. G. Andrews, T. Bai, M. N. Kulkarni, A. Alkhateeb, A. K. Gupta, and R. W. Heath, "Modeling and analyzing millimeter wave cellular systems," IEEE Transactions on Communications, vol. 65, no. 1, pp. 403–430, 2016.
[2.72] I. Akyildiz and J. Jornet, "The internet of nano-things," IEEE Wireless Communication, vol. 17, no. 6, pp. 58–63, Dec. 2010.
[2.73] N. V. Sabu and A. K. Gupta, "Analysis of diffusion based molecular communication with multiple transmitters having individual random information bits," IEEE Transaction on Molecular, Biological and Multi-Scale Communication, vol. 5, no. 3, pp. 176–188, Dec. 2019.
[2.74] M. Tornatore, G.-K. Chang, and G. Ellinas, Eds., Fiber-Wireless Convergence in Next-Generation Communication Networks: Systems, Architectures, and Management. Berlin, Germany: Springer-Verlag, 2017.
[2.75] V. A. Thomas, M. El-Hajjar, and L. Hanzo, "Millimeter-wave radio over fiber optical upconversion techniques relying on link nonlinearity," IEEE Commun. Surv. Tut., vol. 18, no. 1, pp. 29–53, First Quarter 2016.
[2.76] T. Umezawa et al., "100-GHz fiber-fed optical-to-radio converter for radio and power-over-fiber transmission," IEEE J. Sel. Topics Quantum Electron., vol. 23, no. 3, pp. 23–30, May 2017.
[2.77] A. Bekkali et al., "Novel chromatic-dispersion-induced power fading compensation technique for broadband RoF systems based on dual-frequency driving of DP-MZM," in Proc. 43rd Eur. Conf. Opt. Commun., 2017, pp. 1–3.

[2.78] A. Bekkali and K. Nishimura, “Seamless convergence of radio-over-fiber and millimeter-wave links for highly resilient access networks,” in Proc. IEEE Wireless Commun. Netw. Conf., 2016, pp. 1–6.
[2.79] A. Bekkali, T. Kobayashi, K. Nishimura, N. Shibagaki, K. Kashima and Y. Sato, "Millimeter-Wave-Based Fiber-Wireless Bridge System for 8K UHD Video Streaming and Gigabit Ethernet Data Connectivity," in Journal of Lightwave Technology, vol. 36, no. 18, pp. 3988-3998, 15 Sept.15, 2018, doi: 10.1109/JLT.2018.2856115.
[2.80] T. S. Rappaport et al., “Millimeter wave mobile communications for 5G cellular: It will work!” IEEE Access, vol. 1, pp. 335–349, May 2013.
[2.81] G. R. MacCartney, S. Sun, T. S. Rappaport et al., “Millimeter wave wireless communications: New Results for Rural Connectivity,” in Proc. All Things Cellular 16: 5th workshop on All things cellular proceedings, in conjunction with ACM mobiCom, Oct. 2016.
[2.82] C. Kourogiorgas, S. Sagkriotis, and A. D. Panagopoulos, “Coverage and outage capacity evaluation in 5G millimeter wave cellular systems: Impact of rain attenuation,” in Proc. 9th European Conf. Antennas Propagation (EuCAP), Apr. 2015, pp. 1–5.
[2.83] Y. P. Zhang, P. Wang, and A. Goldsmith, “Rainfall effect on the performance of millimeter-wave MIMO systems,” IEEE Trans. Wireless Commun., vol. 14, no. 9, pp. 4857–4866, Sep. 2015.
[2.84] A. Ghosh, “The 5G mmWave radio revolution,” Microwave Journal, vol. 59, no. 9, pp. 22–36, Sep. 2016.
[2.85] C.-S. Choi, Y. Shoji, H. Harada, R. Funada, S. Kato, K. Maruhashi, I. Toyoda, and K. Takahashi, “RF impairment models for 60GHz-band SYS/PHY simulation,” Tech. Rep., IEEE 802.15-06-0477-01-003c, Nov. 2006.
[2.86] E. Björnson, P. Zetterberg, M. Bengtsson, and B. Ottersten, “Capacity limits and multiplexing gains of MIMO channels with transceiver impairments,” IEEE Commun. Lett., vol. 17, no. 1, pp. 91–94, Jan. 2013.
[2.87] E. Björnson, M. Matthaiou, and M. Debbah, “Massive MIMO with nonideal arbitrary arrays: Hardware scaling laws and circuit-aware design,” IEEE Trans. Wireless Commun., vol. 14, no. 8, pp. 4353–4368, Aug. 2015.
[2.88] C. Rapp, “Effects of HPA-nonlinearity on a 4-DPSK/OFDM-signal for a digital sound broadcasting system,” in Proc. of the Second European Conference on Satellite Communications, Liege, Belgium, Oct. 1991.
[2.89] Xiao, Ming & Mumtaz, Shahid & Huang, Yongming & Dai, Linglong & Li, Yonghui & Matthaiou, Michail & Karagiannidis, George & Björnson, Emil & Yang, Kai & I., Chih-Lin & Ghosh, Amitava. (2017). Millimeter Wave Communications for Future Mobile Networks. IEEE Journal on Selected Areas in Communications. PP. 10.1109/JSAC.2017.2719924.
[2.90] Z. Pi and F. Khan, “An introduction to millimeter-wave mobile broadband systems,” IEEE Commun. Mag., vol. 49, no. 6, pp. 101–107, Jun. 2011.
[2.91] H. Huang, C. B. Papadias, S. Venkatesan,“MIMO Communication for Cellular Networks” Springer US, 2012.
[2.92] https://www.5gmmwave.com/5g-mmwave/beamforming-in-5g-mmwave-radios/

[2.93] C. Lim et al., “Mitigation strategy for transmission impairments in millimeter-wave radio-over-fiber networks”, Journal of Optical Networking, Vol.8, No.2, pp.201-214 (2009).
[2.94] 3GPP specification TS 38.201, NR; Physical layer; General description, April 2017.
[2.95] R. Hui et al., “Subcarrier Multiplexing for High-Speed Optical Transmission”, Journal of Lightwave Technology, Vol.20, No.3, pp.417-427 (2002).
[2.96] X. Liang, et al., “Digital suppression of both cross and inter-modulation distortion in multi-carrier RF photonic link with down-conversion”, Optics Express, Vol.22, No.23, pp.28247-28255 (2014).
[2.97] N. Argyris et al., "DSP enabled Fiber-Wireless IFoF/mmWave link for 5G Analog Mobile Fronthaul," 2018 IEEE 5G World Forum (5GWF), Silicon Valley, CA, USA, 2018, pp. 482-487, doi: 10.1109/5GWF.2018.8516964.
[2.98] N. Argyris et al., "A 5G mmWave Fiber-Wireless IFoF Analog Mobile Fronthaul Link With up to 24-Gb/s Multiband Wireless Capacity," in Journal of Lightwave Technology, vol. 37, no. 12, pp. 2883-2891, 15 June15, 2019, doi: 10.1109/JLT.2019.2897109.

CHAPTER 3.

Modulation and signal processing techniques, in support of Analog Fiber/Fiber-Wireless transport transmission

The following paragraphs delve into the realm of modulation and signal processing techniques crucial for supporting Analog Fiber/Fiber-Wireless transport transmission. Within this chapter, a comprehensive exploration of modulation techniques in mobile communication systems is provided. Here, a nuanced understanding of digital modulation schemes and OFDM modulation unfolds, unraveling the fundamental principles that underpin effective signal modulation in mobile communication contexts. Then, the focus shifts to multi-carrier candidates for 5G and beyond in mobile communication, delving into the array of candidates that hold promise for the evolving landscape of mobile communication systems. Moreover, a detailed examination of the description of DSP algorithms' implementation for the processing of CP-OFDM waveforms is provided, shedding light on the sophisticated algorithms integral to the effective processing of CP-OFDM waveforms in the context of analog fiber and fiber-wireless transport transmission. This chapter serves as a pivotal juncture in the dissertation, offering a profound understanding of the modulation and signal processing intricacies essential for advancing analog transport within fiber and fiber-wireless frameworks and concludes with the report of initial experimental testing and results, that validate the functionality and potential of the implemented DSP platform.

3.1. Modulation techniques in mobile communication systems.

To support current mobile communications, there are two main types of communication techniques: single-carrier modulations and multicarrier modulations. Single-carrier modulation systems use a single signal frequency to transmit data symbols, while multicarrier modulation systems divide the frequency channel into numerous subcarriers. The high-rate data stream is then split into multiple low-rate streams, which are transmitted in parallel on the subcarriers.

Single-carrier modulation techniques have been widely used in many wireless communication systems, including conventional 1G, 2G, 3G, and the uplink of 4G deployments. Compared to multicarrier modulation, single-carrier modulations have several advantages. First of all, they have very low peak-to-average power ratio (PAPR), which is beneficial for the stability of systems and the adoption of low-cost devices in the design of wireless communication systems. Moreover, single-carrier modulation systems are less sensitive to frequency shift and phase noise, making it easier for time and frequency synchronizations in wireless communication systems, especially for point-to-point communication systems. Therefore,

single-carrier modulations are still employed in 4G standards, such as SC-FDMA, which is the key technique of the uplink in the long-term evolution (LTE) standard. SC-FDMA uses N-point discrete Fourier transform (DFT) and M-point (N < M) inverse discrete Fourier transform (IDFT) modules at the transmitter, resulting in low PAPR of the transmitted signal. Additionally, the insertion of cyclic prefix (CP) allows for channel equalization in the frequency domain, so that simple single-tap equalizers can be employed for channel equalization [3.1].

However, when compared to multicarrier modulations, single-carrier modulations exhibit less effectiveness in dealing with multipath fading channels, leading to reduced spectral efficiency. As technology progresses, wireless communication systems are evolving towards greater broadband capabilities. For instance, the current LTE operates within a 20 MHz broadband region, while 5G and beyond wireless communication systems occupy 800 MHz or even more [3.2]. The expansion of bandwidths in single-carrier modulation systems causes symbol intervals to decrease, thereby increasing their vulnerability to the effects of multipath fading channels. This susceptibility exposes single-carrier modulation systems to inter-symbol interference (ISI), which can only be addressed through the utilization of intricate multitap equalizers. Consequently, this introduces higher complexity and cost to the system.

Multicarrier modulation systems are gaining increasing interest because of their capability to overcome the challenges posed by multipath fading channels. Among these systems, OFDM stands as the most renowned and established multicarrier modulation system. Although the concept of OFDM was initially introduced in 1966, its commercial implementation was delayed until the 1980s due to hardware limitations. Subsequently, OFDM found extensive applications across various communication systems, including digital audio broadcasting [3.2], digital video broadcasting [3.4], asymmetric digital subscriber line, and wireless local area network systems [3.5],[3.6]. Currently, OFDM stands as the key technique for downlink transmission in the LTE standard [3.7],[3.8].

Multicarrier modulation techniques divide the entire frequency range into multiple subcarriers and transmit a high-rate data stream by distributing it among these subcarriers as several low-rate data streams in parallel. This parallel transmission in multicarrier modulation systems leads to longer symbol intervals compared to single-carrier modulation systems. As a consequence, multicarrier modulation systems exhibit improved resilience against the inter-symbol interference (ISI) effect when compared to single-carrier modulation systems. For example, in OFDM systems, a simple single-tap frequency-domain equalizer can be employed with the assistance of a cyclic prefix, resulting in a cost-effective receiver design. However, multicarrier modulation systems face various technical challenges [3.9], which will be detailly discussed in the following paragraphs, but can be summarized as follows:

- **High PAPR:**

  The issue of high Peak-to-Average Power Ratio (PAPR) poses a challenge for all multicarrier modulation systems, impacting both the implementation of transmitters and the overall performance of the system. In multicarrier modulation, the signal consists of multiple independent subcarrier signals. When these subcarriers exhibit similar phases,

the signal, with its similar initial phase, modulates each subcarrier signal, resulting in a high peak power level at specific instances. However, power amplifiers have a limited linear range, which introduces nonlinear distortion when amplifying signals with high power levels. This distortion significantly degrades the overall system performance. Due to this limitation, multicarrier modulations are employed only in the downlink of LTE, while single-carrier modulations are used for the uplink. This decision is made to mitigate the detrimental effects of high PAPR on system performance and ensure optimal signal transmission.

- **Time and frequency synchronizations:**

Time and frequency synchronization play a crucial role in wireless communication. Multicarrier modulation signals have longer intervals compared to single-carrier signals, which makes them less susceptible to time synchronization errors when compared to single-carrier modulations. However, due to the division of the frequency band into multiple subcarriers in multicarrier modulation systems, each subcarrier occupies a narrow frequency range that is susceptible to frequency deviations. As a result, multicarrier modulation systems are more sensitive to frequency synchronization errors when compared to single-carrier modulations. In the case of OFDM systems, even small frequency shifts can lead to significant frequency synchronization errors and cause intercarrier interference (ICI), which severely degrades the system's performance.

- **Channel estimation and detection:**

Wireless channel conditions have a significant impact on the performance of wireless communication systems, making channel estimation and equalization crucial aspects. Channel estimation techniques can be categorized into two main types: blind and non-blind channel estimations. Blind channel estimations do not rely on training sequences and offer the potential for achieving high spectral efficiency. However, they often suffer from drawbacks such as limited estimation accuracy, high computational complexity, and restricted flexibility. As a result, blind channel estimations are not suitable for real-time systems that require accurate and efficient estimation. On the other hand, non-blind channel estimations employ training sequences to achieve improved estimation accuracy and flexibility. These techniques can be utilized in real-time systems. However, the utilization of training sequences consumes valuable time-frequency resources and leads to a reduction in spectral efficiency. Therefore, it is crucial for wireless communication systems to achieve better performance while minimizing the use of training sequences. This entails finding a balance between accurate estimation and efficient utilization of system resources.

- **MIMO:**

The integration of MIMO (Multiple Input Multiple Output) with multicarrier modulations has garnered recognition as a crucial technique initially in 4G standards due to its remarkable capability to enhance channel capacity. As a result, the combination of MIMO

and multicarrier modulations is widely anticipated to hold substantial potential in the field of wireless communications.

Despite the implementation challenges it presents, multicarrier modulations are regarded as a pivotal technology for future wireless communication systems. In the realm of 4G standards, OFDM has already been adopted as the downlink technique. However, the issue of high spectral sidelobes is becoming increasingly problematic as spectrum resources grow scarce. Spectrum sensing in cognitive radio systems also poses significant challenges. While OFDM is considered a potential candidate for multicarrier-based cognitive radio systems due to its utilization of the fast Fourier transform (FFT) for spectral analysis and modulation/demodulation, it has limitations in this particular context. For instance, mitigating mutual interference between primary and secondary users requires sacrificing transmission bandwidth. Furthermore, the FFT operation fails to meet the dynamic range requirements for detecting spectrum holes. Therefore, exploring alternative methods for multicarrier processing is necessary to overcome the limitations associated with the FFT operation in OFDM. This exploration is essential for advancing the field and finding innovative solutions to enhance the effectiveness of multicarrier modulations in cognitive radio systems. In the following subsections, the generation methods and parameters of both single- and multi- band modulation formats will be discussed.

3.1.1 Digital Modulation schemes

In both single and multi-carrier modulation techniques, an essential step is the digital encoding of the bit-based information to complex symbols. The primary objective of modern modulation techniques is to maximize the utilization of the available spectrum by accommodating a significant amount of data within a limited bandwidth. This objective, commonly referred to as spectral efficiency, quantifies the speed at which data can be transmitted within a given bandwidth. Common digital modulation techniques include amplitude-shift keying (ASK), frequency-shift keying (FSK), phase-shift keying (PSK), and Quadrature Amplitude Modulation (QAM). The above methods rely on the use of the Amplitude, Frequency or/ and Phase characteristics of a sinusoidal for data transmission.

The current section will focus mostly on QAM, which is the digital modulation technique that combines phase and amplitude control. Quadrature amplitude modulation (QAM) involves the utilization of two digital baseband signals that are mutually independent. These signals are then used to modulate two carrier signals that possess identical frequency and are mutually orthogonal. The resulting modulated signals, being orthogonal within the same bandwidth, enable the attainment of parallel transmission of digital signals in both phase and quadrature [3.10]. The general expression of the QAM signal is:

$$S_{MQAM}(t) = \sum_{n} A_n g(t - nT_s)\cos\left(\omega_c t + \theta_n\right)$$

In this formula, A_n is the amplitude of the baseband signal, $g(t - nT_s)$ is the waveform of a single baseband signal, and the width is T_s.

Constellation diagrams serve as visual representations of the quality and distortion of a digital signal. In real-world scenarios, it can be challenging to distinguish and pinpoint individual modulation errors within these diagrams. Hence, it is advisable to assess the measured constellation diagrams utilizing mathematical and statistical techniques to ensure accurate evaluation. Figure 26 shows some indicative examples of QAM constellation diagrams.

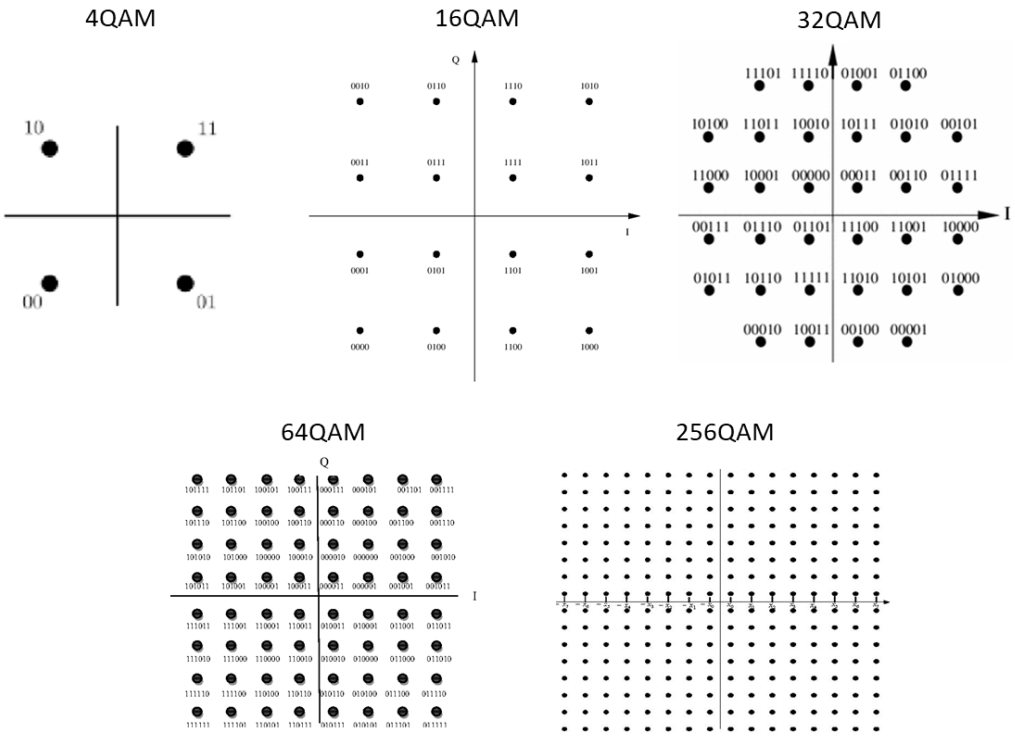

Figure 26. Indicative constellation diagrams for 4/16/32/64/256-QAM modulation formats.

The key parameters for the evaluation of QAM modulated transmission, based on the retrieved constellation diagrams are: (a) peak-to-average power ratio γ, (b) minimum Euclidean distance between constellations d_{min}, and minimum phase offset θmin. The minimum Euclidean distance, denoted as d_{min}, represents the smallest distance between points on the QAM signal constellation. This parameter quantifies the QAM signal's resistance to Gaussian noise, where a larger d_{min} indicates better protection against such noise. Therefore, d_{min} directly influences the performance against anti-Gaussian white noise. The minimum phase shift, denoted as θ_{min}, represents the smallest phase difference between signal points on the standard QAM constellation. This parameter indicates the QAM signal's ability to resist anti-phase jitter and its sensitivity to clock recovery accuracy. A larger θ_{min} implies greater resistance and stronger anti-phase jitter capability.

Finally, for a QAM signal to exhibit satisfactory performance, its constellation diagram must fulfill three requirements:

- The signal should have a small peak-to-average ratio, ensuring a smoother envelope for the modulated signal. This characteristic enhances the signal's resistance to nonlinear distortion.
- The minimum Euclidean distance between signal points should be maximized to achieve optimal performance against additive white Gaussian noise.
- The minimum phase offset between constellation points should be maximized to improve the signal's ability to counteract phase jitter. This includes mitigating effects of clock jitter and anti-channel phase jitter, thereby enhancing timing recovery performance.

In summary, a high-performing QAM signal should possess a low peak-to-average ratio, a large minimum Euclidean distance between points, and a substantial minimum phase offset between constellation points.

3.1.2 OFDM Modulation

With the establishment of modern communication systems, OFDM modulation, which has been around for several decades, has transitioned from being theoretical concepts in textbooks and research labs to practical applications. These techniques are now extensively utilized in data delivery systems across various platforms, including phone lines, digital radio and television, and wireless networking systems. In the current section, OFDM modulation technique will be presented as a special case of FDM multiplexing.

Frequency division multiplexing (FDM) enhances the concept of single carrier modulation by dividing a single channel into multiple subcarriers. The available data rate for transmission in the channel is allocated among these subcarriers. The distribution of data across the subcarriers does not have to be uniform, nor do the data streams need to originate from the same source. This approach offers several advantages, such as the ability to employ dedicated modulation and demodulation techniques tailored to specific types of data. It also facilitates the simultaneous transmission of diverse data sets that may require different modulation schemes for optimal delivery. In FDM systems, it is common to insert a guard band between modulated subcarriers to ensure that the spectrum of one subcarrier does not interfere with another. While this guard band helps maintain signal integrity, it results in a reduced effective information rate compared to a single carrier system employing similar modulation [3.11].

If the aforementioned FDM system had the capability to utilize a set of orthogonal subcarriers, it could have achieved a higher level of spectral efficiency. In this scenario, the need for guard bands, which are essential in enabling individual demodulation of subcarriers in a typical FDM system, would no longer be necessary. By employing orthogonal subcarriers, their spectra could overlap, resulting in an increased spectral efficiency. As long as orthogonality is preserved, it remains possible to recover the signals of individual subcarriers, even when their spectra overlap.

When the dot product of two deterministic signals is zero, it indicates that these signals are orthogonal to each other. Orthogonality can also be understood in the context of stochastic processes. If two random processes are uncorrelated, they are considered orthogonal. Considering the random nature of signals in a communication system, this probabilistic understanding of orthogonality provides an intuitive grasp of its implications in OFDM. In this article, we will explore how OFDM is practically implemented using the Discrete Fourier Transform (DFT). As per signals and systems theory, the sinusoids of the DFT form an orthogonal basis set, allowing a signal in the DFT vector space to be represented as a linear combination of these orthogonal sinusoids. The DFT can be viewed as correlating the input signal with each of the basis sinusoidal functions. When an input signal carries energy at a particular frequency, the correlation with the corresponding basis sinusoid exhibits a peak. At the OFDM transmitter, this transform is employed to map the input signal onto a set of orthogonal subcarriers, which are the orthogonal basis functions derived from the DFT. Similarly, the transform is used at the OFDM receiver to process the received subcarriers, and the signals from these subcarriers are combined to estimate the source signal from the transmitter. The orthogonal and uncorrelated nature of the subcarriers plays a crucial role in OFDM, yielding powerful outcomes. Due to the uncorrelated nature of the DFT basis functions, the correlation performed for a specific subcarrier only captures energy from that corresponding subcarrier. Energy from other subcarriers, being uncorrelated, does not contribute. This segregation of signal energy allows the spectra of OFDM subcarriers to overlap without causing interference.

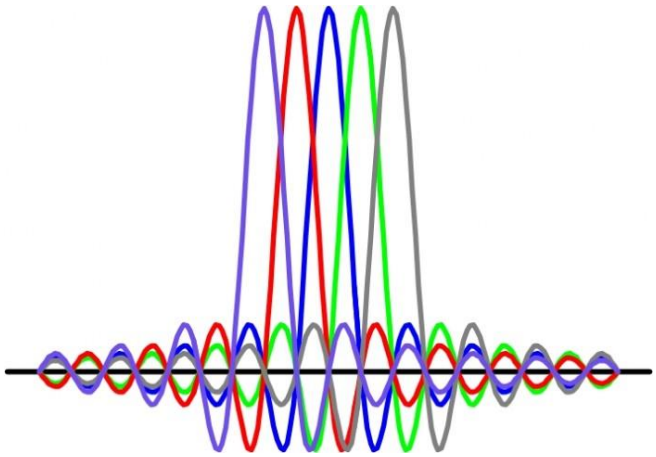

Figure 27. Spectral representation of the orthogonal subcarrier multiplexing in an OFDM signal.

Figure 27 illustrates a simplified spectral representation of the orthogonal subcarrier multiplexing in an OFDM signal. Although such systems have been constructed, their practicality diminishes rapidly as the number of subcarriers increases. Each subcarrier carries one bit of information (N bits in total) based on its presence or absence in the output spectrum. The frequencies of the subcarriers are carefully chosen to create an orthogonal set of signals, and these frequencies are known to the receiver. It is important to note that the output is updated at regular intervals T, which defines the symbol period and serves as the temporal boundary for maintaining orthogonality. In the frequency domain, the side lobes of the

resulting sinusoidal functions produce overlapping spectra. However, the individual peaks of the sub-bands align perfectly with the zero crossings of the other sub-bands. This overlap of spectral energy does not hinder the system's ability to recover the original signal. At the receiver, the incoming signal is multiplied (i.e., correlated) with the known set of sinusoids to regenerate the original set of transmitted bits. The digital implementation of an OFDM system enhances these fundamental principles, and further advancements can be made.

The concept behind analog implementation of OFDM can be extended to the digital realm through the utilization of the DFT and its inverse, the inverse Discrete Fourier Transform (IDFT). These mathematical operations are widely employed to convert data between the time-domain and frequency-domain. In the context of OFDM, these transforms are particularly relevant as they enable data mapping onto orthogonal subcarriers. For instance, IDFT is employed to convert frequency-domain data into time-domain data. To carry out this operation, the IDFT correlates the frequency-domain input data with its orthogonal basis functions, which are sinusoids at specific frequencies. This correlation process can be seen as mapping the input data onto the sinusoidal basis functions.

In practical implementations, OFDM systems utilize a combination of Fast Fourier Transform (FFT) and inverse Fast Fourier Transform (IFFT) blocks, which are mathematically equivalent to the DFT and IDFT, respectively, but more efficient for implementation. In an OFDM system, the source symbols (e.g., QPSK or QAM symbols that would be present in a single carrier system) are treated as if they are in the frequency domain at the transmitter. These symbols serve as inputs to an IFFT block, which brings the signal into the time domain. The IFFT block processes N symbols at a time, where N represents the number of subcarriers in the system. Each of these N input symbols has a symbol period of T seconds. It is important to note that the basis functions for an IFFT are N orthogonal sinusoids, with each sinusoid having a different frequency. The lowest frequency corresponds to DC. Each input symbol acts as a complex weight for the corresponding sinusoidal basis function. As the input symbols are complex, their values determine both the amplitude and phase of the sinusoid for the respective subcarrier. The output of the IFFT is the summation of all N sinusoids, providing a straightforward means to modulate data onto N orthogonal subcarriers. The block of N output samples from the IFFT constitutes a single OFDM symbol. The length of the OFDM symbol is NT, where T refers to the IFFT input symbol period mentioned earlier.

After undergoing additional processing, the time-domain signal resulting from the IFFT is transmitted through the channel. At the receiver, an FFT block is employed to process the received signal and convert it back into the frequency domain. Ideally, the FFT output should represent the original symbols that were initially sent to the IFFT at the transmitter. When these FFT output samples are plotted on the complex plane, they form a constellation, such as a 16-QAM constellation. However, the time-domain signal does not possess a constellation representation. When plotted on the complex plane, the time-domain signal appears as a scatter plot without a defined pattern. Consequently, any receiver processing that relies on the concept of a constellation, such as symbol slicing, must take place in the frequency domain.

In most wireless systems, a significant issue arises from the presence of a multipath channel. In such an environment, the transmitted signal reflects off multiple objects, leading to the reception of several delayed versions of the signal at the receiver. This multipath effect causes

distortion in the received signal. Similar problems can also occur in wired systems due to reflections caused by impedance mismatches in the transmission line.

The presence of a multipath channel poses two challenges for an OFDM system. The first challenge is intersymbol interference, which occurs when the received OFDM symbol is distorted by the previously transmitted symbol. This interference is akin to intersymbol interference observed in single-carrier systems. However, in single-carrier systems, the interference typically results from multiple previous symbols, whereas in OFDM systems, the interference is predominantly caused by the preceding symbol alone. This distinction arises due to the longer symbol period in OFDM systems compared to the time span of the channel. The second challenge, specific to multicarrier systems like OFDM, is referred to as intrasymbol Interference. This interference arises from the interaction among subcarriers within a given OFDM symbol.

- **Intersymbol interference:**

Let's consider the scenario where the time span of the channel is L_C samples in length. In contrast to a single carrier system with a data rate of R symbols per second, an OFDM system employs N subcarriers, each operating at a data rate of R/N symbols per second. This reduction in data rate by a factor of N causes the OFDM symbol period to increase by a factor of N. By appropriately selecting the value of N, the length of the OFDM symbol becomes greater than the time span of the channel. Consequently, the effect of intersymbol interference manifests as distortion in the first L_C samples of the received OFDM symbol. Given that only the initial few samples of the symbol experience distortion, one can consider incorporating a guard interval to mitigate the impact of intersymbol interference. This guard interval can be a segment of all zero samples transmitted preceding each OFDM symbol. Since it does not contain any useful information, the guard interval can be discarded at the receiver. If the length of the guard interval is appropriately chosen to be longer than the time span of the channel, the integrity of the OFDM symbol itself will remain intact. Thus, by eliminating the guard interval, the effects of intersymbol interference can be effectively mitigated.

- **Intrasymbol interference:**

Practical systems do not utilize a guard interval as it does not effectively prevent intrasymbol interference, which is the type of interference where an OFDM symbol interferes with itself. Instead, the solution to mitigating intrasymbol interference involves a discrete-time property. In continuous-time, a convolution in the time domain corresponds to a multiplication in the frequency domain. However, in discrete-time, this property holds true only if the signals are of infinite length or if at least one of the signals is periodic within the range of convolution. Having an infinite-length OFDM symbol is impractical, but it is possible to make the OFDM symbol exhibit a periodic nature. To achieve this periodicity, the guard interval is replaced with a cyclic prefix, which is a replica of the last L_P samples of the OFDM symbol. The length of the cyclic prefix, denoted as L_P, is chosen to be greater than the length of the channel, L_C. The cyclic prefix

is redundant information and is discarded at the receiver. Similar to the guard interval, removing the cyclic prefix eliminates the effects of intersymbol interference. Furthermore, due to the specific construction of the cyclic prefix, the cyclically-extended OFDM symbol appears periodic when convolved with the channel. An important consequence of this approach is that the effect of the channel on the OFDM symbol becomes multiplicative rather than convolutive.

3.2. Multi-carrier candidates for 5G and beyond mobile communication.

OFDM format, which has been extensively discussed in the previous sections, is the most prominent multi-carrier modulation case and has been adopted in the deployed LTE mobile networks, while different flavors of this modulation technique have been adopted or are considered for 5G and beyond deployments. A typical example is the OFDMA (Orthogonal Frequency-Division Multiple Access) technology, which is used in the air interface stage of 5G New Radio (5G NR), allowing mobile connectivity. Specifically, OFDMA is a variant of OFDM designed to accommodate multiple users simultaneously. It efficiently allocates resources in both the time and frequency domains, enabling support for numerous users, including those with diverse usage patterns and data demands. In contrast, traditional OFDM can only allocate resources sequentially, limiting its multi-user capabilities. As a step forward, a series of alternative, beyond-OFDM multicarrier waveforms have emerged during the past years, serving as radio interfaces in the 5G and beyond era. The most prominent of these OFDM-like candidates have been considered within the presented work and a comparative study was performed prior to the identification of the waveform that was adopted for further experimental studies. This study was based on the extraction of system-level specifications from different use cases and network scenarios targeted in the 5G and beyond era. The most remarkable alternative multi-carrier approaches, which attempt to overcome CP-OFDM limitations, are using band-pass or pulse-shaping modulation filters and are the following: Filter Bank Multi-Carrier (FBMC), Universal Filtered Multi-Carrier (UFMC), and Generalized Frequency Division Multiplexing (GFDM).

The main difference between the FBMC and the CP-OFDM is the filtering operation applied for each sub-carrier. The spectrum profile of a single subcarrier for each one of these to formats is shown in Figure 28. Such operation significantly reduces the power of the side-lobes while the tolerance to ICI and ACI is improved. The PAPR is still high, but it appears less effective on the side-lobes. Moreover, the use of filters eliminates the need for cyclic prefix. The weak points of FBMC are the complexity of the required filters (number of taps ~ 4*FFT size), which scales up the implementation complexity and the latency budget. Furthermore, the ramp-up and down of the filters reduces the bandwidth efficiency, since filtered sub-carriers cannot be located as closely as in the case of CP-OFDM sub-carriers. FBMC uses Offset-QAM formats, which makes it sensitive to frequency synchronization errors and makes handling of MIMO difficult, as the synchronization of multiple users can be

damaged both by frequency shifts and by failures in the synchronization of the I and Q components of the Offset-QAM symbols. Finally, FBMC is not recommended for transmission of small packets, which require short transmission time intervals. In contrast to this, the ramps at the edges of the filters are long, increasing also the latency of the system[3.12], [3.13].

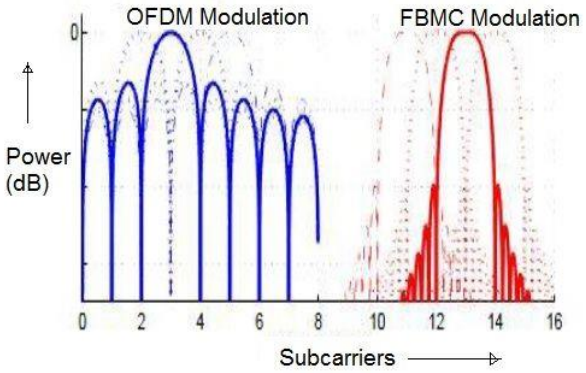

Figure 28. PSD of a single carrier in standard OFDM and FBMC modulation formats.

UFMC seems to be a strong candidate as a multicarrier waveform in 5G implementations. The main difference between FBMC and UFMC is that, for the latter, the filtering is applied on a group of sub-carriers, as shown in Figure 29, which depicts a UFMC modulation example with of 10 sub-bands, each including 20 subcarriers. As a result, it fairly suppresses the side-lobes, without achieving the performance of FBMC, though. The ramp-up and down of non-rectangular windowing in time imposes zero-padding between successive symbols, which is much shorter than the cyclic prefix of CP-OFDM. The structure of the UFMC waveform presents similarities with the structure of CP-OFDM with practically the same implementation complexity. UFMC waveform is conducive to small packets and is recommended for applications where MIMO transmission is required. Nevertheless, UFMC is not as robust as CP-OFDM against ISI and is prone to synchronization failures which may lead to ICI, since the subcarriers may not be perfectly synchronized. The side-lobes of UFMC are also suppressed but without achieving the low power of the side-lobes of the FBMC waveform [3.12][3.14].

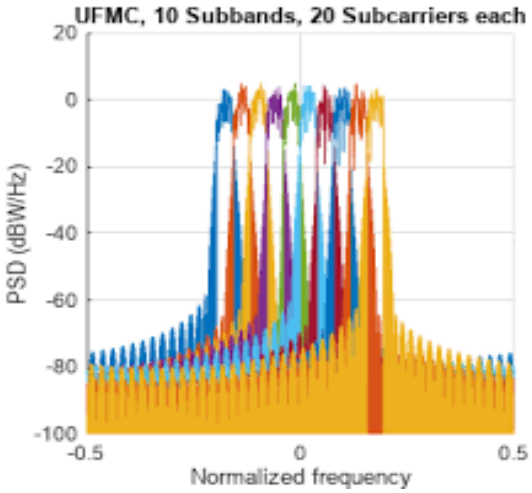

Figure 29. PSD of UFMC format consisting of 10 sub-bands with 20 subcarriers each.

The last post-OFDM waveform that has been investigated in the literature is GFDM, which can be considered as a block-oriented filtered multi-carrier waveform. The transmission block consists of a set of symbols in time which corresponds to a respective set of sub-carriers. A pulse-shaping filter is applied to each subcarrier while the subcarriers do not have to be orthogonal, hence the name of the waveform. The PSD of an indicative GFDM modulation example is presented in Figure 30. A cyclic prefix is added between subsequent blocks. GFDM reduces the power of the side-lobes, just like FBMC and UFMC. The GFDM implementation complexity is very low, and the waveform is quite robust to synchronization failures and can be used to achieve MIMO transmission with relatively low complexity. GFDM has flexible design and is appropriate for small packet transmission. Big block transmission is not recommended though, since the whole block has to be received and in turn demodulated. Although GFDM is robust to ISI and ICI distortion, the non-orthogonal condition within its structure makes this waveform vulnerable to transmission impairments and the ramp-up and down of the filters [3.13],[3.15].

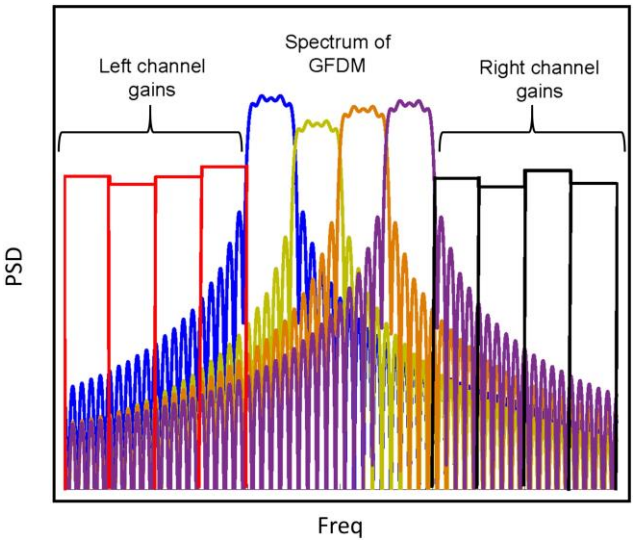

Figure 30. PSD of a GFDM modulation example.

In the table below, the strong and weak points of the discussed multicarrier waveforms are comparatively represented. The network profile corresponding to indicative 5G-related use-case scenarios that are related to the density of the user equipment devices that concurrently access the same RRU is also included so as to investigate the possible matching of the different waveforms -for each case.

Table 3. Post-OFDM candidate waveforms comparison

Features	Waveforms (higher number indicates better performance)				Scenario/Use Case		
	CP-OFDM	FBMC	UFMC	GFDM	Dense Area	Ultra-Dense Area	Hotspot Area
ISI tolerance	***	***	***	**	✓	✓	✓
ICI tolerance	**	***	**	*		✓	✓
OoB side-lobes suppression	*	***	**	**			
PAPR -> OoB side-lobes power increase	*	***	**	**			
frequency synchronization errors tolerance	**	*	**	***		✓	✓
CP/ZP (spectral efficiency decrease)	*	***	**	**			
MIMO	**	*	***	***	✓	✓	✓
implementation complexity	***	*	**	***			✓
flexibility and possibility of small packets transmission	**	*	***	***			✓

The selection of proper multi-carrier waveform/waveforms, corresponding to the demands of the targeted use case is important for achieving high performance. Thus, the correlation between the pros and cons of the forenamed waveforms and the needs of the operation scenarios should be considered. Although a more detailed description of the different use-case parameters would be helpful in this direction, we can come to a few general assumptions,

based on the information provided, till now. The most fundamental operation of all three use-cases is Multiple-Input Multiple-Output (MIMO) transmission. The increase of the density of antennas and users, though, scales up the system requirements. In the ultra-dense and the hotspot area, channel impairments can be much more challenging to handle, leading to an aggravation of ICI. The support of multiple users can be efficiently achieved by adjustment of the transmitted packets to the individual conditions, resulting to the assumption that flexibility and possibility of small packets transmission are crucial for the ultra-dense and hotspot use cases. Especially for the hotspot area, the synchronization of the data received from multiple points will be a challenge and contingent frequency synchronization failures will have to be avoided. Finally, it should be taken into consideration that in cases with heavy demands, like a hotspot area, the complexity of the signal generation should stress the employed analog transceivers as little as possible.

Along with the candidate post-OFDM waveforms proposed for 5G cellular systems, an approach to the features of such a multicarrier waveform is attempted. The duration of the transmitted symbols is a crucial parameter for the system performance in wireless links. Symbols with very small duration can be easily affected by multipath propagation, resulting in ISI. ISI can be alleviated by the choice of symbols, a few times longer than the delay spread (trms) of the channel [3.16]. The symbol duration, finally determines the number of sub-carriers per band, as shown in (1), where Tsymbol refers to the symbol duration and dfc is the spacing between subsequent sub-carriers.

$$T_{symbol} = \frac{1}{df_c} \tag{1}$$

On the other hand, the use of spectrally narrow subcarriers, and thus long OFDM symbols, can lead to phase noise related to frequency mismatches between the radio mixing units for up-/down-conversion of the wirelessly propagated signal, which in high frequencies, included the mmWaves can cause strong CFO to the received signals and severely impair the transmission performance.

In the block diagrams below (Figure 31), indicative structures of a CP-OFDM and UFMC transmitter and receiver are presented.

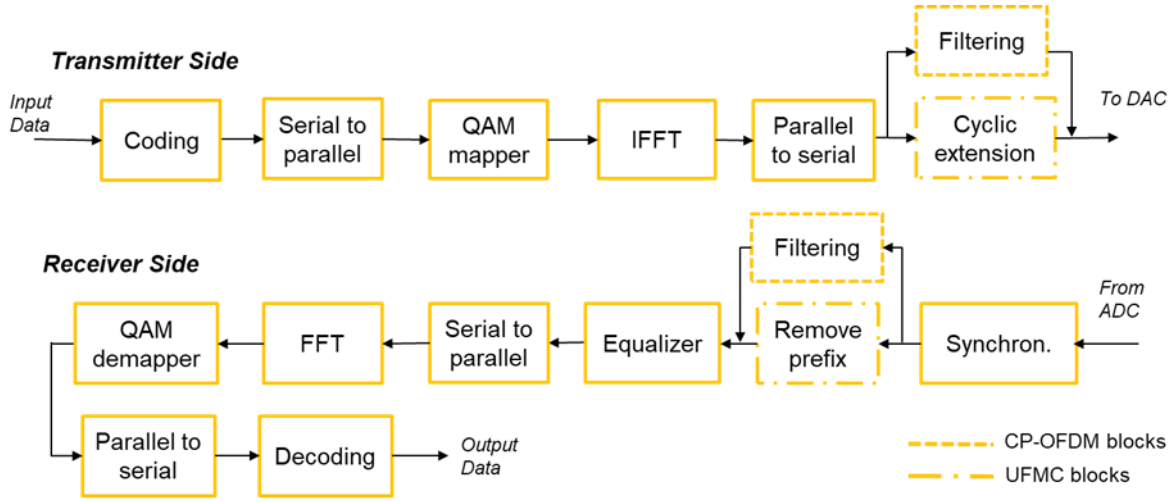

Figure 31. Block diagrams of a CP-OFDM and UFMC transmitter and receiver.

3.3. Description of the DSP algorithms' implementation for the processing of CP-OFDM waveforms.

Among the various multi-carrier waveforms proposed for 5G implementations that have been discussed in the previous paragraphs, the focus for the DSP algorithms' implementation has been put on the CP-OFDM format. The selection of this format was based on its compatibility with LTE, low implementation complexity and suitability for multi-band transmission. The implemented transmitter and receiver side block chains are shown in

Figure 32 and correspond to a complete processing functionalities' portfolio supporting single-band CP-OFDM signals generation and retrieval. An analysis of the main DSP functions is provided in the following paragraphs.

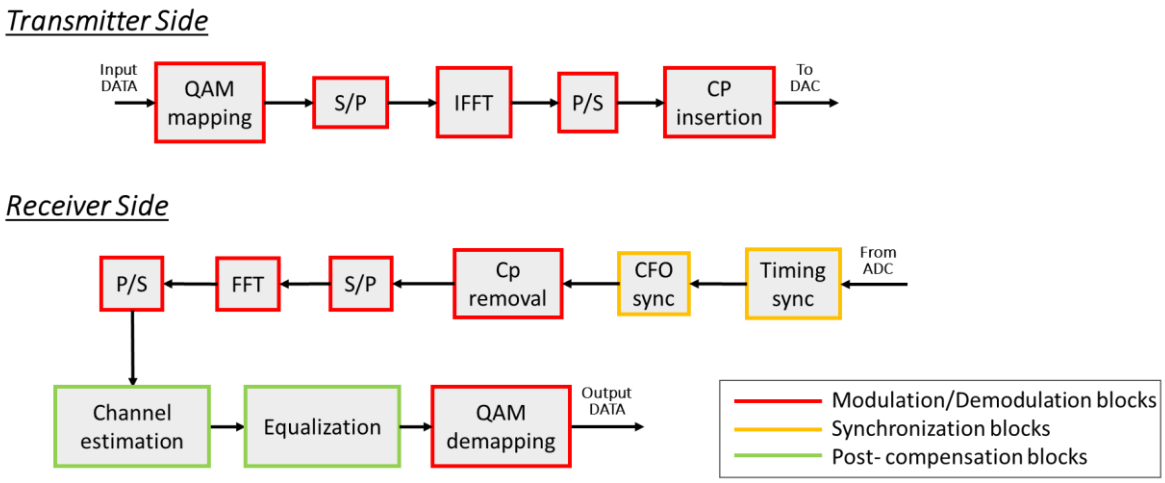

Figure 32. Block diagrams of implemented transmitter and receiver DSP chain.

- **CP-OFDM generation and demodulation**

The DSP blocks represented with red colour in Figure 32, are used for the generation and demodulation of the CP-OFDM signals. Specifically, the operations of these blocks are the modulation of the QAM symbols, their mapping to orthogonal sub-carriers and the CP insertion/removal at the transmitter side and the corresponding operations at the receiver side. The above processing steps can be supported by standard algorithms, thus the critical step for the definition of the signal generation and demodulation DSP blocks is the selection of the waveform dimensions and more specifically the FFT length, the size of the QAM constellation and the CP length. The criteria leading to the definition of the FFT size, the CP length and the M-QAM modulation format, are discussed below, where a methodology of defining the CP-OFDM parameters will be followed. Table 1 summarizes the targeted specifications for CP-OFDM waveforms.

The delay spread of the 5G femtocells is the first parameter to be determined. Some experiments that have been carried out at outdoor, urban environment, at close range (corresponding to femtocells radius), using directional antennas, imply that in case of Line-of-Sight (LOS) propagation the delay spread is less 20 ns. In Non-LOS (NLOS) propagation or adverse channel conditions the delay spread can at most be 50ns [33], [34]. In case of CP-OFDM, to minimize the effect of channel impairments, it is recommended that the length of the cyclic extension be approximately Tcp=4×trms and the symbol duration be Tsymbol = 4,8,16 or 32×Tcp [3.17]. In addition, the size of the QAM constellation deployed, plays a major role for achieving high values of capacity. The main criterion that determines the possibility of detecting and demodulating high order QAM formats (QPSK, 16-QAM or 64-QAM), is the SNR of the received signal.

Table 4. Implemented waveforms' specifications.

	CP-OFDM Waveforms' Specifications
Band-size	200MHz/400MHz
FFT length	256
Cp-length	32
M-QAM format	Up to 16-QAM

To facilitate the DSP engine development, CP-OFDM signals were generated in MATLAB and evaluated under various scenarios. These initials studies focused on the validation of these initial generation/demodulation transceiver's components proper functionality, as well the assessment of their impact to signal quality, in simulation environment. Figure 33 shows the generated CP-OFDM waveform. Figure 33(a) depicts the spectrum of the digitally generated signal, while the constellations exhibited in Figure 33(b), correspond to an indicative carrier

of the receiver-side 16-QAM modulated signal at the output of the FFT block. Through MATLAB, Additive White Gaussian Noise (AWGN) was inserted to the signal to evaluate the BER performance of the received signal versus SNR degradation, hence the possibility for data recovery after the application of a FEC algorithm. Figure 33(b) depicts the effect of the inserted AWGN to the points of the received constellations, for 40dB, 30dB, 20dB and 15dB SNR values. As expected, the SNR reduction results to deterioration of the constellation quality. An important parameter that had to be defined was the minimum SNR value that would allow successful signal demodulation. For this purpose, the EVM of the receiver side constellations were measured, resulting to the EVM-SNR curve, depicted in Figure 33(d). According to this curve, for successful 16-QAM transmission, the EVM limit of 11.5%, set by 3GPP standards corresponds to SNR values of less than 15dB, for the specific CP-OFDM waveform.

Finally, the calculated EVM values can be utilized for an estimation of the received BER, leading to the BER curve depicted in Figure 33(d). For comparison purposes, the same measurements were also performed for an f-OFDM signal with the same specifications as the CP-OFDM signal, as this waveform can also be supported by the DSP toolbox that has been implemented. The only difference between these two muti-carrier waveforms is that for the generation of f-OFDM signals, the application of a low-pass filtering stage, after the insertion of CP is required. There are two main filter categories met in the literature, the soft-truncated sinc filters, including Hann and RRC window, and the equiripple filters based on the Remez exchange algorithm [3.18]. Taking into account that equiripple filtered signals are prone to ISI and the extended use of rrc filters, the latter was the filter of choice in 5GPhos. Since a RRC filter is applied to the signal in the transmitter side, a symmetric RRC filter must also be applied to the receiver side as well before the CP removal. For the current study an 28-tap RRC filter was applied. As it can be seen in Figure 33(c), the insertion of the f-OFDM filter enhances signal robustness. Taking into account the characteristics of the f-OFDM signals and the distortion generated by the RoF and the wireless link, proper selection of algorithms for signal pre-distortion, synchronization and equalization can be performed.

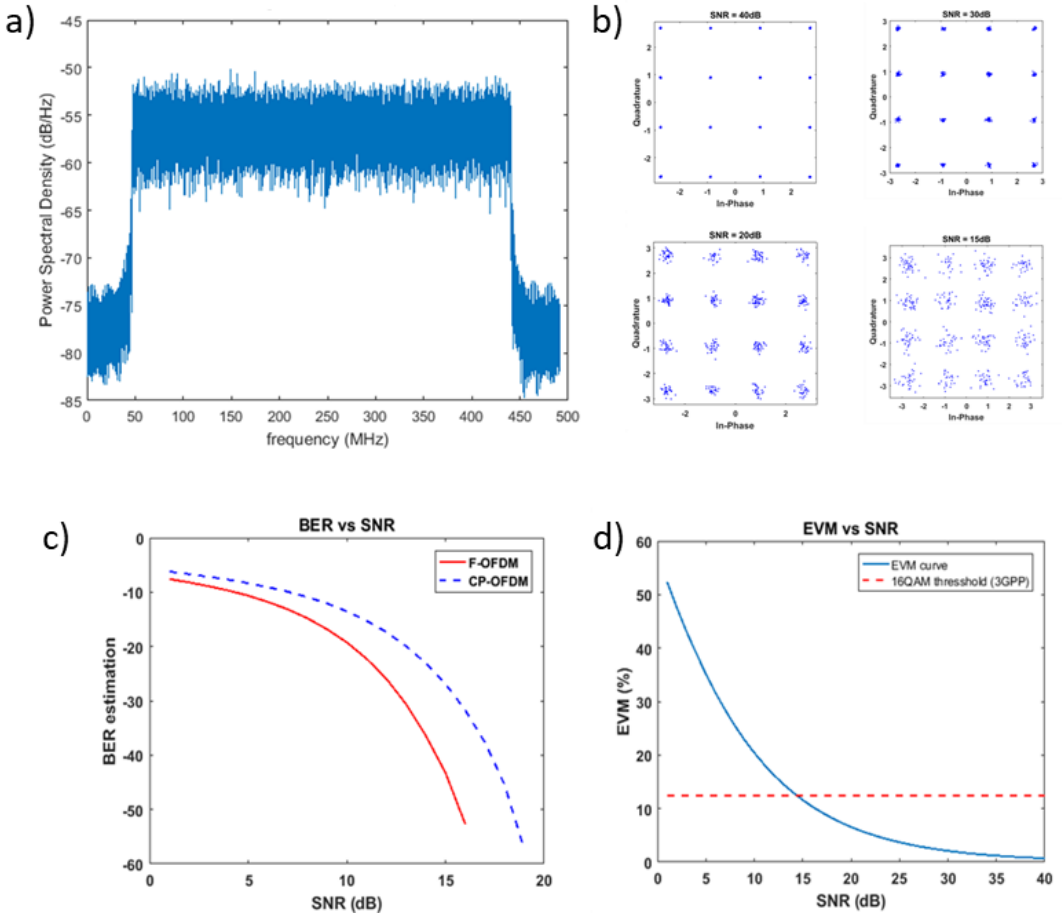

Figure 33. Spectrum of CP-OFDM waveform, (b) respective constellation diagrams for 40dB, 30dB, 20dB and 15dB SNR values, (c) BER curves for f-OFDM and CP-OFDM, and (d) EVM-SNR curve for CP-OFDM signal.

- **<u>Timing and frequency synchronization</u>**

A major drawback of multi-carrier waveforms transmission is their susceptibility to synchronization errors, both in time and frequency domain. Timing synchronization failures refer to imperfect detection of the initial sample of an OFDM symbol, leading to applying the FFT algorithm to a time window slightly shifted, hence including few samples of the previous or the next OFDM symbol while missing few samples of the symbol to be processed. Frequency synchronization failures, correspond to frequency shifts of sub-carriers caused by misalignment between the RF frequencies of the local oscillators, described by the term carrier frequency offsets (CFO), or by errors in the sampling frequencies of the transmitter and receiver converters, called sampling frequency offsets (SFO). In all cases described above, both ISI and ICI are introduced to the signal, resulting to severe, accumulating, signal degradation, making it difficult for the next in chain DSP blocks to process the signal effectively.

The first processing step after signal reception is the time domain FFT window synchronization (see Fig. 1). The operating principle of this block relies on identifying in the received signal an expected time domain sequence or some form of repetition. For this purpose, both a preamble and a Cyclic Prefix (CP) are used. The preamble is utilized by the DSP algorithms dealing with synchronization issues and channel estimation and consists of one or more well known to the receiver symbols. These symbols are transmitted before a sequence of a specific number of data symbols and again before the next data sequence of the same length. Thus, ADC sampling errors may affect only few data symbols, instead of accumulating during the signal transmission and distorting the signal even more over time. Moreover, preamble retransmission provides information about signal characteristics, such as frequency offsets which are useful for frequency synchronization. The selected preamble for the current work consists of 2 symbols, which can also be used for CFO compensation, as described below. These two symbols are retransmitted before every 8 data symbols, forming a frame of 10 symbols, similar to other wireless standards, such as LTE and 802.11.

To achieve timing synchronization, the first step is to track the preamble in the received signal. This is done through a correlation algorithm being executed at the receiver side, which compares the known preamble with successive windows of the received samples of length equal to the preamble. The points, at which the correlation function becomes maximum, correspond to the beginning of a 10 OFDM-symbols length frame, including the preamble. To experimentally test the performance of this algorithm, an AWG was used to generate multi-carrier frames while a Real-Time Scope served as a receiver. Figure 34(a) shows a graphical representation of the obtained results for the correlation function. The fact that the distance between two maximization points is equal to the length of an OFDM frame confirms the algorithm's proper operation.

The algorithm described above correctly indicates the beginning of the OFDM frames, enabling a coarse calculation of the first sample position of each OFDM symbol. Nonetheless, a slight misalignment of the FFT window can occur for few OFDM symbols when this method is applied, leading to undesired ICI. As such, a "second stage" algorithm for detection of each symbol is usually applied. The latter is based on the repetition of the CP, correlating sample sequences of length equal to the CP length and distance equal to the FFT length minus the CP length. The maximization of the correlation function indicates the detection of the initial sample of the OFDM-symbol CP, and by extension the FFT window. Figure 34(b) depicts the CP-based synchronization algorithm experimental results. The correlation function peaks appear at a distance equal to the OFDM-symbols length, as originally expected, validating the algorithm's functionality.

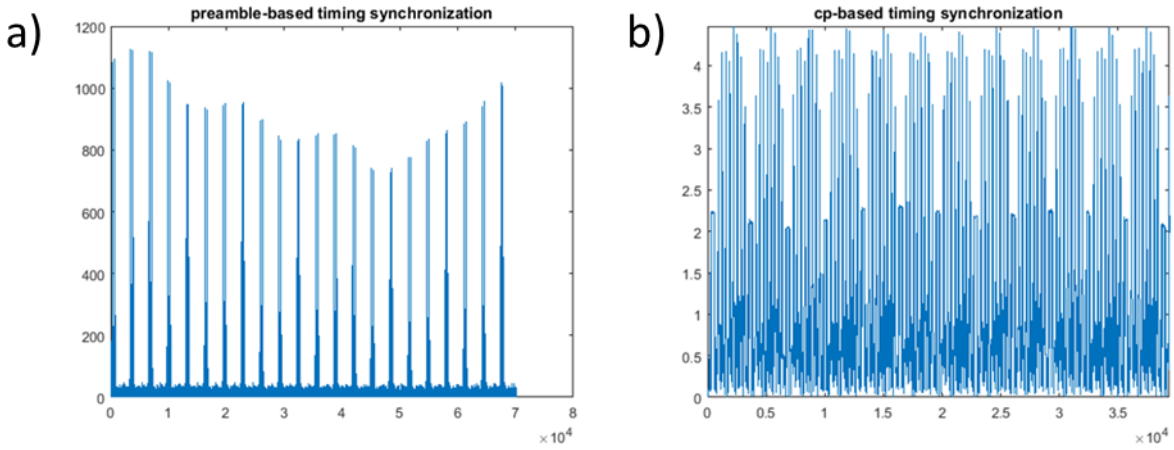

Figure 34. Preamble-based timing algorithm and (b) CP-based synchronization algorithm experimental results.

Following timing synchronization, the correction of frequency shifts is the next step towards OFDM signal synchronization. As previously mentioned, CFO result to severe signal degradation and demand algorithmic treatment. Frequency offsets caused by the up- and down-conversion frequency misalignment may lead to a frequency shift of the signal spectrum and as such, to a misalignment of the receiver FFT taps with the received signal sub-carriers. In addition, the orthogonality between the sub-carriers is lost and ICI occurs. This frequency shift is constant over all the sub-carriers and increases linearly in the time-domain. Thus, most methods aiming at CFO compensation are being applied in the time domain. A widespread technique, which will also be used in the current DSP chain, is based on the calculation of the phase difference between two successively transmitted identical symbols, namely the Preamble symbols. An autocorrelation function is utilized for the measurement of the phase offset between every transmitted sample of the first preamble symbol and the corresponding sample of the second preamble symbol. An average of the measured frequency shifts is calculated and applied to the received samples of the respective OFDM frame. The corrective frequency offset is inserted to the signal, by means of a phase rotation, linearly increasing over time.

For the evaluation of the previously described algorithm, the digitally modulated and up-converted multicarrier waveform was extracted before digital-to-analog conversion by the AWG and digitally down-converted and demodulated with the use of MATLAB. For the down-conversion process, varying IF values, slightly shifted from the up-conversion frequency, were used, leading to CFO. Figure 35 depicts the signal under the impact of CFO, with and without the correction algorithm application, for a 5MHz and 10MHz frequency offset. It can be clearly seen in the figure that the use of the proposed algorithm has significantly improved the received signals quality.

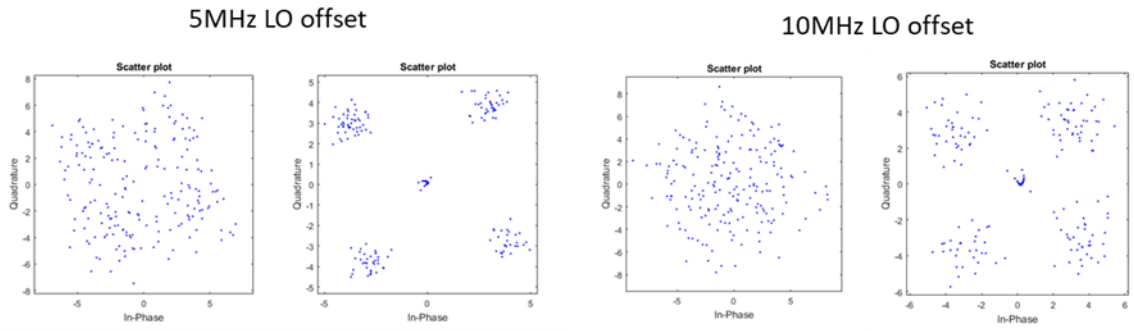

Figure 35. CFO effect and algorithmic correction for a 5MHz and a 10MHz offset.

- **<u>Tx pre-compensation and Rx equalization</u>**

Any transmission means can be considered a combination of two effects: the deterministic response imposed by the channel and the random changes introduced by the noise. To reconstruct the propagated signal, the receiver must be capable of reverting the channel response and ideally minimizing the impacts of channel noise. This procedure, known as equalization, is an essential step towards signal recovery. In this section, a set of methods aiming to the reconstruction of CP-OFDM modulated signals are being discussed. These methods benefit from the OFDM format's structure and more specifically, the parallelization of the data into a set of lower bit-rate channels which are affected by a quasi-flat frequency response [3.19].

To achieve correct demodulation of the received signal, an estimation of the inverted channel response has to be calculated and applied to the signal, minimizing the impact of the channel noise and frequency selectivity. The term "channel" refers to the whole transmission link which may include the length of the SSMF fiber, the radio units, but also any electro/optical conversion and amplification stages, in the case of Fiber-Wireless transmission. The previously mentioned processes can be implemented either at the receiver side, through the means of an equalization filter, or at the transmitter side, deploying a pre-distortion filter.

A significant advantage of multi-carrier waveforms is their robustness to chromatic dispersion and wireless link multipath effects. Moreover, thanks to the cyclic prefix insertion to the transmitted CP-OFDM symbols, the time-domain signal presents periodicity which allows for a much simpler channel estimation in frequency domain. Thus, the receiver side equalization can be performed by a single-tap filter. In RF systems, an estimate of the channel impulse response is usually extracted by the transmission of pilot sub-carriers. The pilot sub-carriers can be whole CP-OFDM symbols like the preamble symbols, part of few symbols of the frame, or specific sub-carriers of every CP-OFDM symbol. The latter method of pilot mapping was adopted for the presented implementation. In general, the number of pilots required depends on the transfer function of the wireless channel and the frequency of fast fading. To properly define the equalization requirements of the developed DSP chain, an experimental investigation relying on converged A-IFoF/mmWave transmission was performed, which resulted on the use of 21 pilot subcarriers evenly distributed among 200 data carriers.

As far as the channel estimation algorithm is concerned, two widespread schemes commonly applied in RF systems are discussed below.

- **Zero Forcing (ZF) method**

This scheme attempts to minimize inter-user interference by comparing the received pilot values with those ideally expected and estimates the channel impulse response for all the transmitted sub-carriers by means of interpolation. The computation complexity of this algorithm is low, resulting in its application in many operating systems, like LTE. However, by focusing on minimizing the interference, the received power at the user suffers, thus leading to an SNR decrease.

- **Minimum Mean Square Error (MMSE) method**

This method offers a balance between increasing SNR on the receiver and reducing interference. This approach is the most complex in terms of signal processing power requirements. It introduces a regularization term to the optimization that allows for a balance point to be found between the noise covariance and the transmitted power. The regularization term arises from an initial modeling of the wireless link, which is in most cases inevitable. The lack of this knowledge is the main reason for which its implementation is more complex than this of a ZF estimator. Sometimes, it is also referred to, in literature, as regularized zero forcing.

3.4. Integration and experimental evaluation of developed DSP toolbox

In this section, a set of initial experimental results, captured after fiber and converged A-IFoF/V-band air transmission, are presented. These experimental studies aimed to evaluate the DSP assisted A-IFoF concept for efficient accommodation of both single and multiple radio signals, using commercial off-the shelf electronic/photonic components, employing the CP-OFDM modulation format. Prior to the description of the experimental layouts that were deployed for analog fiber and FiWi transmission performance evaluation, the key components of these layouts, used for electro-optical conversion and vice-versa, as well the radio boards and antenna units that served the IF-to-RF conversion and wireless propagation will be described.

3.4.1 IM/DD electro-optic units for A-IFoF links

In the deployed analog testbeds, highly linear optoelectronic units were used to realize an IM/DD communication strategy. In more detail, the use of an Electro-absorption Modulated

Laser (EML)-based analog IFoF transmitter was selected as a cost effective, integrated solution that has been extensively proposed for the emerging densified 5G network topologies [3.20], as also discussed in previous sections. Despite the benefits of using EMLs, in terms of cost-/power- efficiency, there are still some challenges related to their electro-absorption performance, which typically degrades under high incoming optical power, due to saturation effects induced by slow sweep-out time of photogenerated carriers.

Here, using a standard Phosphorus-based material process as detailed in [3.21], a linear high-power EML was employed, featuring a 500μm-long DFB laser and a 150μm-long EAM monolithically integrated on InP substrate, as shown in Figure 36. The EML was assembled, and wire bonded on a Temperature Controlled (TEC) Printed Circuit Board (PCB) for testing at chip-characterization probe stations. A detailed characterization of this prototype EML unit, developed by III-V labs, has been reported in [3.22], including the measured output power, power-voltage (P-V) curve and frequency response. The emission wavelength of the EML was 1557.3nm with an output power of 5.8 dBm, when operated at 20oC and 100mA current injection, while featuring a Side Mode Suppression Ratio of 50 dB. The obtained P-V curve for increasing voltage values reveals a linear response with more than 10 dB Extinction Ratio (ER) between the -1V and -2V region, while the S21 frequency response of the EML when biased at around -1.5V reveals a 3dB bandwidth of 17 dB.

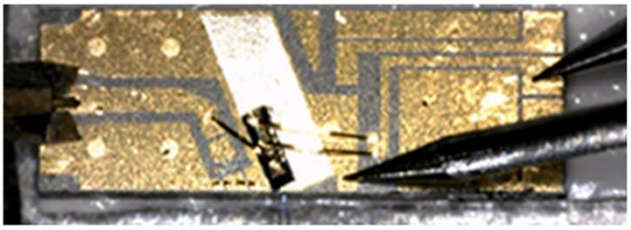

Figure 36. Microscope image of the fabricated EML on a PCB, probed with a GSG tip and DC-needles

At the receiver side, a commercial off-the-shelf photo-receiver was used to detect the analog optical signals, providing thereby the radio waveforms to the mixer stages of the radio boards, that were used for the establishment of wireless connectivity. More specifically, a 10GHz photoreceiver comprising an Avalance Photodiode (APD) and a Transimpedance Amplifier (TIA) was used for optoelectrical conversion of the received A-IFoF signals.

3.4.2 mmWave radio equipment for converged FiWi transmission

For the wireless propagation of the IF complex up-converted waveforms, a set of mmWave IF-to-RF up-/down-converters, connected to V-band directional antenna modules were used. A block diagram of the V-band mixing boards is shown in Figure 37. In order to generate the V-band carriers, numerical controlled oscillators provided a lower frequency carrier which was then quadrupled within the converter's internal circuitry. For the upconverter, after

mixing the input IF with the carrier, a two-stage amplification stage (Driver and Power Amplifier) was used prior feeding the antenna element. On the other side, at the down-converter, a low-noise amplifier after the antenna was providing the input to the mixer. The mixer output was the IF down-converted signal. On each side, the LO, the mixer and the RF amplifiers were integrated on a single Tx/Rx board. As a result, two identical boards were used to establish the link. The IF to RF gain of the boards ranged from 20 dB to 38 dB and both converters had a nominal noise figure of 8 dB at maximum gain. Finally, standard pyramidal gain horn V-band antennas of 23 dBi gain and 10° beamwidth were employed for OTA propagation. The antennas, together with the up- and down-conversion units, were mounted on wooden tripods and kept fixed at a height of 1.4 m above the floor.

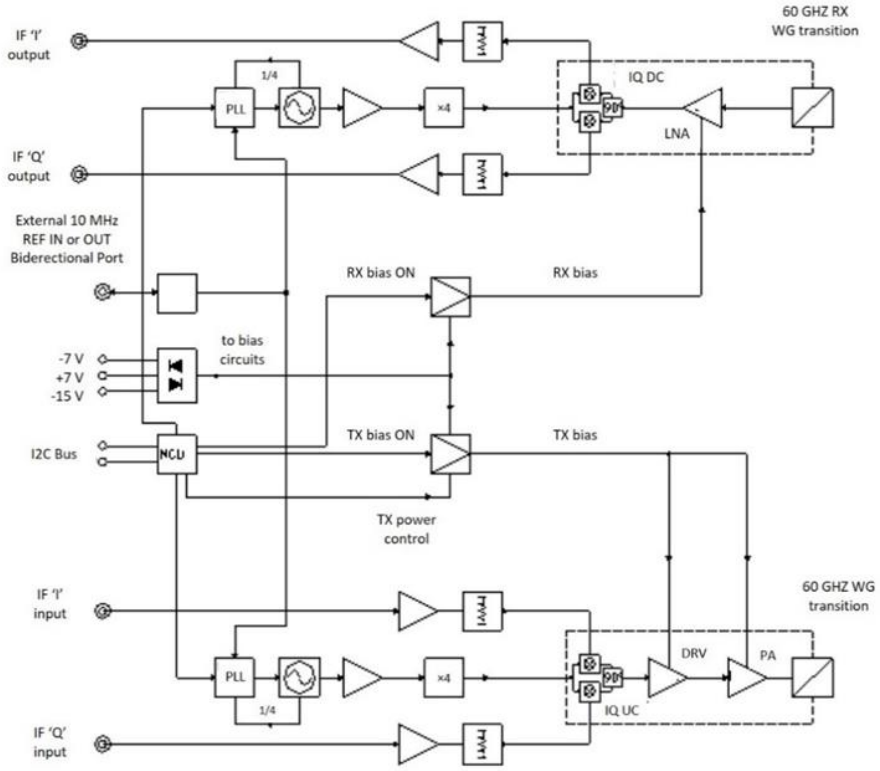

Figure 37. Block diagram of the mmWave up- and down-converter circuit.

3.4.3 Experimental performance of single-/multi-band analog Fi/FiWi transmission

The first evaluation step of the investigated DSP-enabled analog Fi/FiWi topology involves the transmission of multicarrier waveforms, generated, and demodulated by standard commercially available tools. To this extent, we used an AWG to generate CP-OFDM signals for both single- and 4-band transmission scenarios. The signal modulation was performed by the control software of the employed AWG device, which was a Keysight M8195A generator with 30GHz analog bandwidth and sampling rate of up to 64GSa/s. 16QAM modulation

scheme was applied to the sub-carriers multiplexed with a 1024-tap FFT. Each band occupied a bandwidth of 400MHz, while being transmitted at a rate of 500MSa/s after the insertion of zero subcarriers at the edges of the waveform. For baseband-to-IF up-conversion, the IF value employed for single-band transmission was 5 GHz, while for the multi-band transmission, the IF values were set at 2.87 GHz, 3.29 GHz, 3.71 GHz and 4.13 GHz. The data carriers were 833 out of 1024 and no pilot carriers were used at this experimental study since channel estimation and equalization algorithms were not used. The CP added to the signal had a length of 0.0625 times the OFDM-symbol length, corresponding to 64 samples. 2 symbols were repetitively transmitted, one of which was a preamble. At the receiver side, a Keysight DSO X 93304Q, with 33GHz analog bandwidth and up to 80GSa/s sampling rate, was used for signal detection. Demodulation of the received waveform was performed via the RTO embedded data analysis software (VSA software). The DSP functions applied through the software were the minimum, including demodulation and synchronization. The signal synchronization was performed with the aid of the CP.

Figure 38 depicts the set-up deployed for the evaluation of the OFDM transmission over the Fi-Wi link. The analog waveform generated by the employed AWG device was fed to the monolithically integrated high power EML module, which was responsible for electrical-to-optical conversion. After only few meters of SSMF fiber transmission, the optical signal was fed to the 10GHz photoreceiver. Finally, the IF modulated signal at the output of the photodetector was wirelessly propagated at 5m, by means of the V-band radio units described in the previous paragraphs.

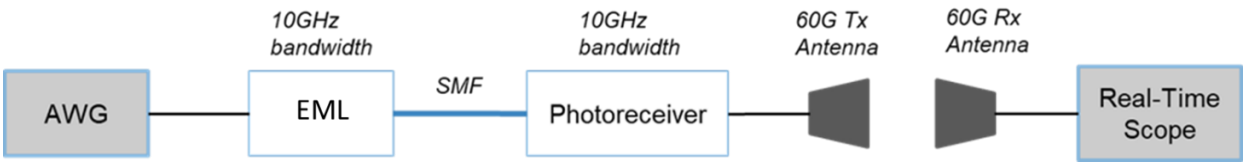

Figure 38. Experimental set-up of the Analog Fi-Wi link for CP-OFDM transmission.

Figure 39 depicts the RF spectrum, constellation diagram and the EVM value per sub-carrier, of the electrical back-to-back signal. For these measurements the AWG device was directly connected to the RTO. The mean EVM value of all data subcarriers of the captured CP-OFDM signal was 1.9%.

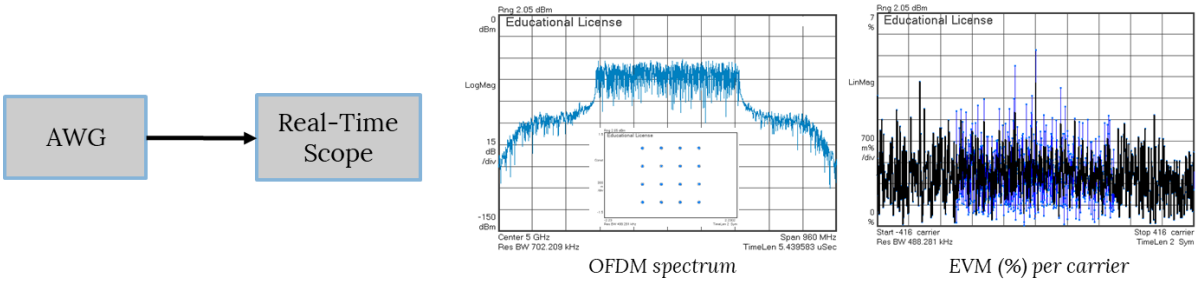

Figure 39. RF spectrum, constellation diagram and EVM measurements per carrier of the electrical signal at the output of the AWG.

Figure 40 shows the results after mere optical transmission. In this initial experimental phase, the possibility of optically transmitting the OFDM waveform even without advanced signal processing tools is indicated, achieving decent signal quality. Moreover, multi-band transmission severely distorts the signal, which presented a mean EVM value of 4.38% in the case of single-band transmission. This value is significantly decreased, compared to the EVM values of 4-band transmission, as shown in Table 5. This observation verifies the theoritically expected high out-of-band spectrum leakage of the CP-OFDM waveform, being one of the reasons why the insertion of a pulse-shaping filter would be necessary in a bandwidth aggregation scenario that rally on multiple transmission bands. In contrast to the optically transmitted waveforms, the data captured after FiWi transmission could not be demodulated, without the use of an equalization stage.

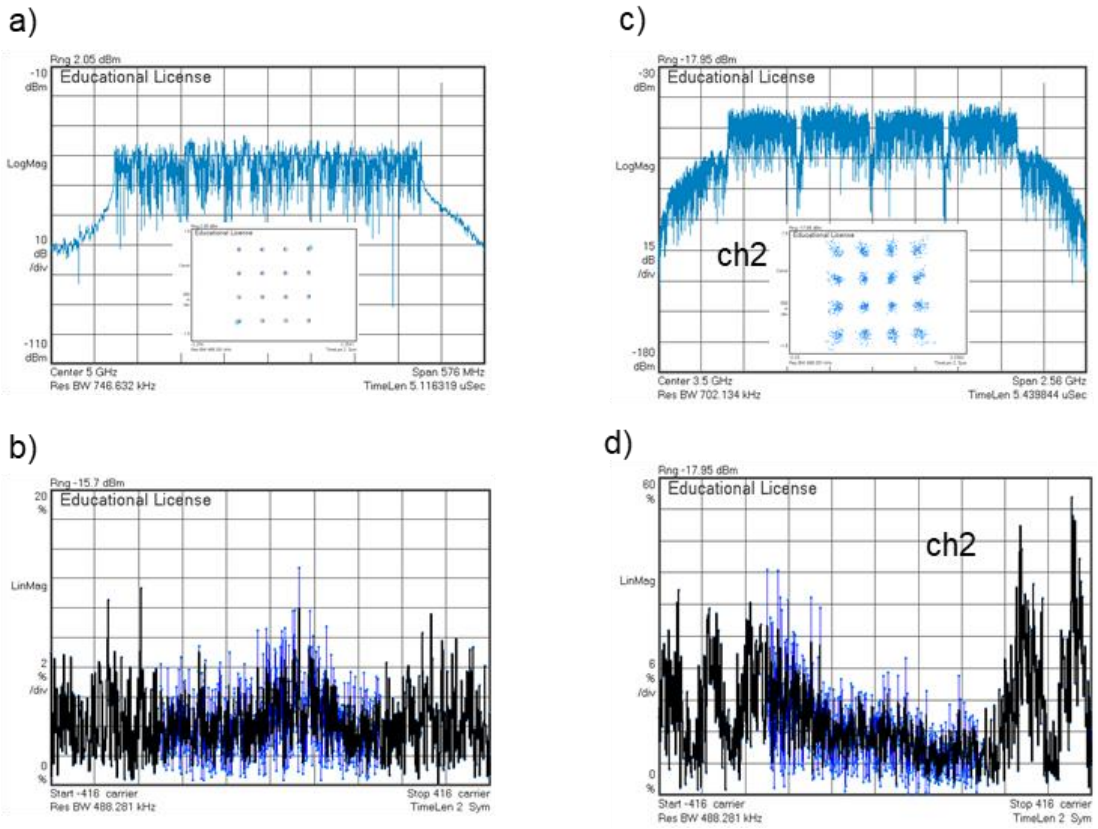

Figure 40. A-IFoF transmission results, including a) single-band transmitted bandwidth, with indicative constellation and b) EVM per sub-carrier, c) 4-band transmitted bandwidth, with indicative constellation for ch2 and d) EVM per sub-carrier for ch2.

Table 5. Mean EVM measurements for all transmitted bands.

Band #	Mean EVM rms (%)
1	14.2
2	14.7
3	17
4	14.1

The next step of these proof-of-concept FiWi experimental activities was the replacement of the AWG device, with a real-time processing engine, which combined with the employed EML modulation unit, served as an analog IFoF transmitter. The experimental evaluation of this analog transmitter in both fiber and FiWi transmission cases was the first step towards the deployment, study and demonstration of real-time analog links operating along deployed operators' infrastructures, as presented in following sections.

The core element of the analog IFoF transmitter was a Xilinx Zynq Ultrascale+ RFSoC device on ZCU111 development board [3.23], which was used to implement the transmitter side DSP in real time. The RFSoC device offers an embedded hardware platform for the deployment of

the FiWi transmitter, significantly alleviating performance and development costs. FPGA circuit design relied heavily on pipelining techniques at multiple levels: task-level pipelining was employed between successive functions in the DSP chain while, at low RTL level, deep-pipelining techniques were applied to increase the operating frequency of the micro-operations in each processing block/function. Additionally, to increase the throughput of each block, the arithmetic operations were parallelized while evaluating its mathematical formulas. At higher-level, a flexible interface was developed to be attached both to the Ethernet core of the FPGA and the embedded CPUs. The employed RFSoC device is depicted in Figure 41.

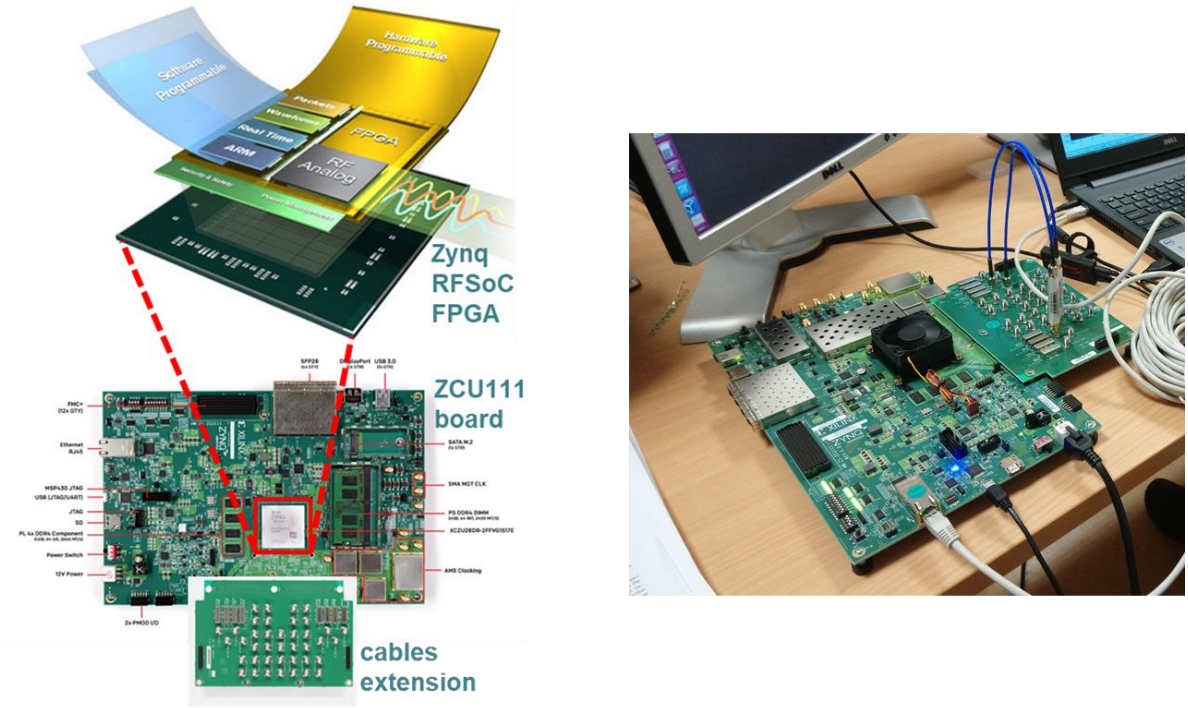

Figure 41. Pictures of the RFSoC platform.

Figure 42 shows the experimental setup that was used to evaluate the FiWi link, consisting of three main blocks: the analog IFoF transmitter, the fiber/wireless downlink transmission segment and the evaluation stage. The transmitted signals are CP-OFDM modulated signals, generated using a fixed 256-tap inverse Frequency Fourier Transform (iFFT) algorithm. The FPGA clock was real time adjusted at 256MHz or 500MHz, corresponding to the transmission of 204 MHz or 394 MHz useful bandwidth, after zero-padding (52 out of 256 sub-carriers). The above band sizes were selected having in mind the 3GPP New Radio (NR) specifications [3.24]. Since the FFT size was kept fixed, minimizing the use of the FPGA resources, the sub-carrier spacing was adapted to the clock frequency, resulting to 1MHz spacing for the 204 MHz Band and 2.1MHz for the 398 MHz band. The modulation format of the sub-carriers was real-time adjusted to QPSK or QAM16. A cyclic prefix of 64 samples length was inserted to the signal before the Digital to Analog Converter (DAC). The RFSoC's DAC (sampling rate up to 4Gsa/s) generated analog IF signals at a central frequency of 750 MHz through a digital up-conversion stage, The output of the RFSoC, was measured to have a voltage swing

of 390mVpp and was further up-converted at 3.5GHz IF, via an analog frequency up-conversion stage, composed of an active mixer and a local oscillator.

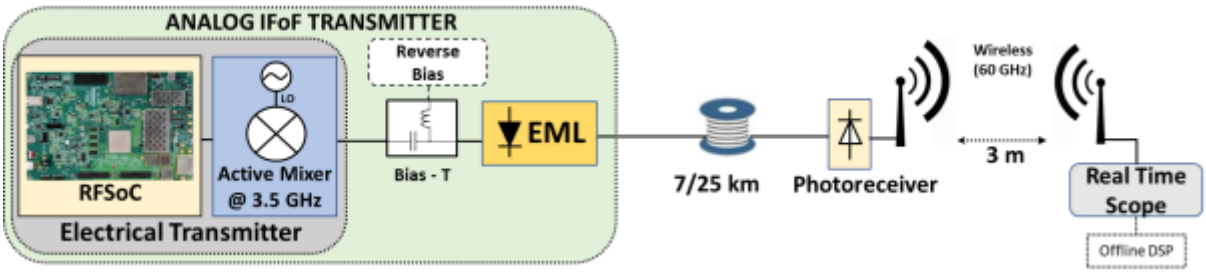

Figure 42. Fi-Wi transmission experimental setup.

The output of the active mixer was then connected to the RF port of a bias tee responsible to drive the Electro Absorption Modulator (EAM) segment of EML. The driving voltage for the EAM section of the chip was set at 560mVpp, whereas the reverse bias voltage of -0.63V was used to ensure linear operation. The laser segment of the EML was injected with 110mA current while operated at 23.6° C, providing +2 dBm of optical power at emission wavelength of 1560.42nm. The optical output was then transmitted over a fiber spool of Standard Single Mode Fiber (SSMF). The IFoF signal of -3.5 dBm was detected by an off-the-shelf 14 GHz linear photoreceiver after its propagation over up to 25-Km SSMF spools. The photoreceiver output was connected to the IF-to-mmWave upconverter radio board operating at 60-GHz and the V-band directional transmitter-side antenna module (Tx-antenna), discussed in the previous paragraphs. The identical Receiver-side antenna module (Rx-antenna) located in a 3 m horizontal distance was used to receive the mmWave radio waveforms and the mmWave-to-IF downconverter was connected to a Real Time Oscilloscope. At the receiver side, off-line DSP was applied to the signal, including demodulation of the received OFDM symbols, as well as a Zero-Forcing (ZF) equalization algorithm. For the channel estimation, 21 pilot sub-carriers multiplexed with the data subcarriers were also transmitted.

Figure 43 depicts the EVM performance of the transmitted OFDM-based IFoF signals after the 7km, 25km fiber link as well a set of obtained constellation diagrams after the post-processing chain. Taking into account that the Error Vector Magnitude (EVM) measured at the electrical Tx output was 3% for the QPSK-OFDM format and 3.9% for the QAM16-OFDM signals, the short reach optical part of the setup, including the EML, the 7km SSMF and the 14GHz photoreceiver, degrades the 204MHz signal performance by 3.8% (for the QPSK-OFDM) and 3.7% (for the QAM16-OFDM) and the 398MHz signal EVM by 4.3% (for the QPSK-OFDM) and 4.5% (for the QAM16-OFDM), indicating the absence of strong limiting effects related to the active electro-optic modules response or to the fiber transmission. By extending the fiber spool link from 7-Km to 25km fiber link, the obtained EVM penalty was slightly increased by less than 2.5%. This added EVM penalty mainly originated from the lower received optical power linked with the fiber loss, since the dispersion-induced power fading can be neglected for this low IF carrier frequency [3.25].

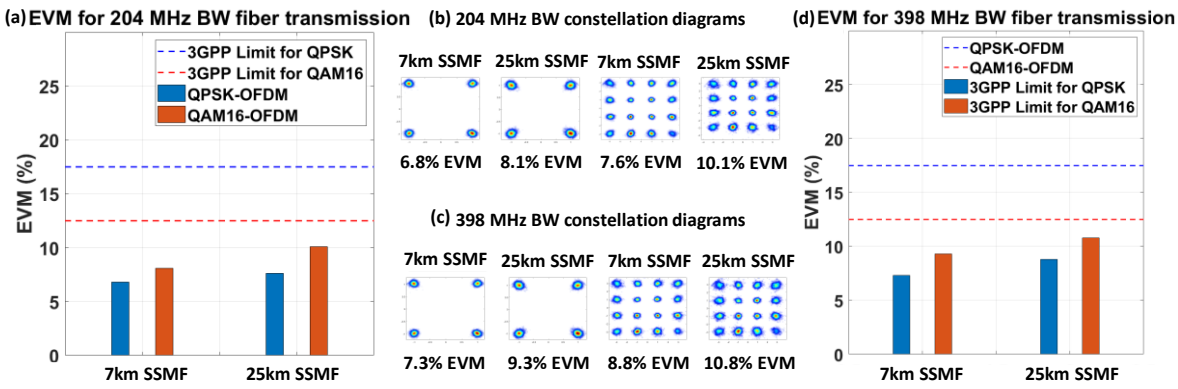

Figure 43. (a) EVM values for 204 MHz BW after 7km and 25 km fiber transmission, (b) Constellation diagrams for 204 MHz BW after 7km and 25 km fiber transmission, , (c) Constellation diagrams for 398 MHz BW after 7km and 25 km fiber transmission and (d) EVM values for 398 MHz BW after 7km and 25 km fiber transmission.

The second part of the present experimental study focused on the performance evaluation of a DL scenario by exploiting the deployed fiber-Wireless topology. Figure 44 illustrates an EVM bar diagram of the QPSK-OFDM and QAM16-OFDM modulated radio for both 204 MHz and 398 MHz bands after 25km fiber transmission and OTA transmission over 3m horizontal distance using V-band radio equipment. The introduction of the active V-band radio part and of the link, caused an increase of the EVM performance of our link by less than 1.1% for the 204 MHz band, whilst the EVM performance was degraded by less than 2.5% for the wider version of radio bands at 398 MHz band. The above EVM penalties are mainly associated with the IF/mmWave radio boards that included Power Amplifiers (PAs) and complex frequency translation stages [3.26]. It should be also mentioned that higher order QAM OFDM waveforms occupying wider bandwidths suffer from severe distortion reflected into their higher EVM values, while the presence of nonlinear distortion was also evident in all 16-QAM constellation diagrams. Nevertheless, the transmission in all cases was successful according to the 3GPP specifications for systems that employ radio transmission at frequencies >28 GHz [3.24].

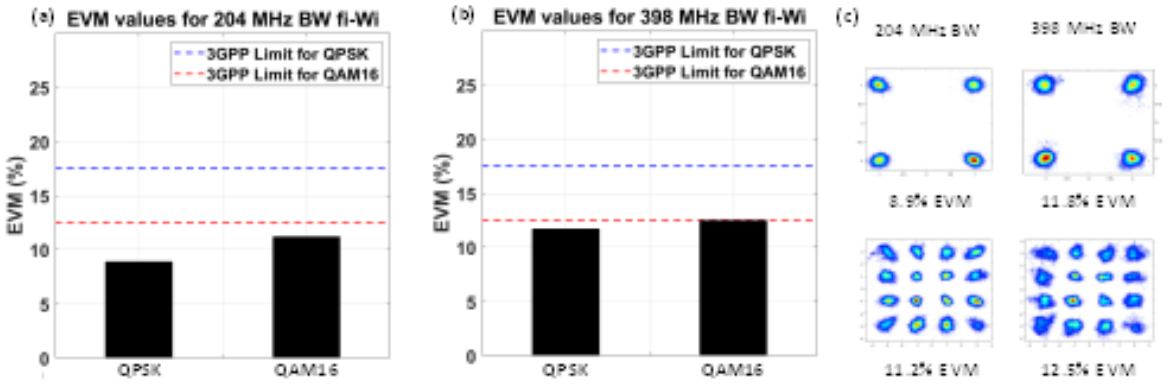

Figure 44. (a) EVM values for 204 MHz BW after 25 km fiber/V-band wireless transmission, (b) EVM values for 398 MHz BW after 25 km fiber/V-band wireless transmission and (c) Constellation diagrams for both cases.

References

[3.1] Myung HG, Junsung J, Goodman D. Single carrier FDMA for uplink wireless transmission. IEEE Veh Technol Mag 2007;1(3):30–8.

[3.2] 3GPP TSG-RAN5 Meeting #94-eR5-220914 Online, 21st Feb 2022 - 4th Mar 2022.

[3.3] ETSI EN 300 401 V1.3.3. Radio broadcasting systems; digital audio broadcasting (DAB) to mobile, portable and fixed receiver; 2001.

[3.4] Nee RV, Prasad R. OFDM for wireless multimedia communications. London, UK: Artech House Publisher; 2000.

[3.5] IEEE 802.11. Draft supplement to standard for telecommunications and information exchange between systems-LAN/MSN specific requirements. Part 11: wireless MAC and PHY specifications: high speed physical layer in the 5 GHz band; 1999.

[3.6] IEEE P802.11-TASK GROUP G. Project IEEE 80211g standard for higher rate (20+Mbps) extensions in the 24 GHz band; 2003.

[3.7] Ghosh A, Ratasuk R, Mondal B, Mangalvedhe N, Thomas T. LTE-advanced: next-generation wireless broadband technology. IEEE Wirel Commun 2010;17(3): 10–22.

[3.8] Deruyck M, Joseph W, Lannoo B, Colle D, Martens L. Designing energy efficient wireless access networks: LTE and LTE-advanced. IEEE Internet Comput 2013;17(5):39–45.

[3.9] Tao Jiang, Da Chen, Chunxing Ni, Daiming Qu, Chapter 1 - Introduction, OQAM/FBMC for Future Wireless Communications, Academic Press, 2018, Pages 1-24, ISBN 9780128135570, https://doi.org/10.1016/B978-0-12-813557-0.00001-2.

[3.10] Bin Zhang et al 2020 IOP Conf. Ser.: Mater. Sci. Eng. 782 042048

[3.11] Ergen, M., Principles of OFDM. In: Mobile Broadband. Springer, Boston, MA. https://doi.org/10.1007/978-0-387-68192-4_4.

[3.12] F. Schaich and T. Wild, "Waveform contenders for 5G — OFDM vs. FBMC vs. UFMC," 2014 6th International Symposium on Communications, Control and Signal Processing (ISCCSP), Athens, Greece, 2014, pp. 457-460, doi: 10.1109/ISCCSP.2014.6877912.

[3.13] Farhang-Boroujeny, Behrouz and Hussein Moradi. “OFDM Inspired Waveforms for 5G.” IEEE Communications Surveys & Tutorials 18 (2016): 2474-2492.

[3.14] Knopp, R. & Kaltenberger, Florian & Vitiello, Carmine & Luise, Marco. (2016). Universal filtered multicarrier for machine type communications in 5G.

[3.15] Hamiti, Enver & Sallahu, Fatlum. (2015). Spectrum Comparison between GFDM, OFDM and GFDM Behavior in a Noise and Fading Channel. The International Journal of Electrical and Computer Engineering Systems. 2. 39-43.

[3.16] A. A. Zaidi et al., "Waveform and Numerology to Support 5G Services and Requirements," in IEEE Communications Magazine, vol. 54, no. 11, pp. 90-98, November 2016, doi: 10.1109/MCOM.2016.1600336CM.

[3.17] Kim, Taekyu & Lee, Seongbong & Park, Sin-Chong. (2006). Hardware Design of CP Length Detector for the WirelessMAN-OFDM System. 10.1109/ISPACS.2006.364700.

[3.18] J. McClellan and T. Parks, "A unified approach to the design of optimum FIR linear-phase digital filters," in IEEE Transactions on Circuit Theory, vol. 20, no. 6, pp. 697-701, November 1973.
[3.19] L. A. Neto, “Étude des potentialites des techniques de modulation multiporteuse pour les futurs reseaux d’ acces optique WDM et TDM PON”, docteur de l’ universite de Limoges, December 2012.
[3.20] https://www.fujitsu.com/us/imagesgig5/FNC-Fujitsu-C-RAN-Mobile-Architecture-Migration-White-Paper.pdf, accessed De-601 cember 2021
[3.21] H. Debregeas, et. al. "Record 6dBm electroabsorption modulated laser for 10Gb/s and 25Gb/s high power budget access networks," Proc. OFC, Th4G.5, Los Angeles, 2017.
[3.22] Vagionas, Christos & Papaioannou, Sotirios & Argyris, Nikos & Kanta, Konstantina & Iliadis, N. & Giannoulis, Giannis & Apostolopoulos, Dimitrios & Avramopoulos, Hercules & Caillaud, C. & Debregeas, H. & Kalfas, George & Pleros, Nikos. (2018). A 6-Band 12Gb/s IFoF/V-Band Fiber-Wireless Fronthaul Link Using an InP Externally Modulated Laser. 1-3. 10.1109/ECOC.2018.8535219.
[3.23] M. Yasan, Xilinx, Zynq UltraScale+™ RFSoC Product Overview.
[3.24] 3GPP, TS 38.104 V15.3.0, Table 9.6.2.3-1, Oct. 2018.
[3.25] N. Argyris et al., “DSP enabled Fiber-Wireless IFoF/mmWave link for 5G Analog Mobile Fronthaul”, in Proc. IEEE 5G World Forum, 9-11 July, 2018, Silicon Valley, CA, USA.
[3.26] N. Argyris et al.,”A 5G mmWave Fiber-Wireless IFoF Analog Mobile Fronthaul Link With up to 24-Gb/s Multiband Wireless Capacity”, J. Lightw. Technol., vol. 37, no. 12, pp. 2883-2891, Jun. 2019.

CHAPTER 4.

Analog fiber-wireless downlink transmission of IFoF/mmWave over in-field deployed legacy PON infrastructure

In order to respond to the numerous, continuously emerging capacity-intensive applications and mobile broadband services [4.1], MNOs are constantly focusing on the adoption of next generation mobile network technologies and infrastructure expansions as means to increase network capacity. These network upgrades, however, will not be enough to meet the rising capacity demand, without the adaptation of fronthaul alternatives, that can surpass the widely discussed capacity and scalability challenges of (Common Public Radio Interface) CPRI-based deployments [4.2]. To make this transition towards new fronthaul interfaces economically viable for the infrastructure owners, the concurrent and even co-operative operation of heterogenous technologies and transport layouts, within the quite mature, standard Radio Access Network (RAN) environment should be pursued and validated in real field-experiments.

4.1. Fiber-Wireless A-RoF/mmWave links overlaid in a legacy PON infrastructure

As presented in the previous sections, Centralized Radio Access Network (C-RAN) topologies are currently considered the most promising means for densification of the access points and the mobile network with reduced deployment costs, by introducing a pooling of enhanced baseband processors at a centralized location capable of serving multiple radio stations at the end points with statistical multiplexing of hardware resources. Following the above rationale, the passive optical network (PON) currently appears to be an appealing optical candidate transport solution, benefitting from wide deployment and inherent support of point-to-multi-point (PtMP) network topologies with efficient use of fiber installations. Consequently, working towards achieving RAN densification with 5G traffic overlaid on PON networks, poses the requirement to overcome the bandwidth-hungry nature of the PtP CPRI standard, as it would induce excessive costs for mobile network operators [4.3].

In general, the development of analog fronthauling schemes allows for more spectrally efficient and cost-effective transportation of mmWave radio links with immense 5G wireless traffic, bearing also promise for developing a unified and truly converged optical network capable of transporting both legacy traffic, coming, e.g., from fixed broadband services, fiber-to-the-home (FTTH), or 4G CPRI-based traffic, as well as traffic stemming from emerging

5G optical transport streams, towards true fixed mobile convergence (FMC) with deployed mmWave radio links. Towards implementing the above FMC vision, two main approaches that have been taken into consideration, based on variable functional splits, e.g., being promoted and standardized by the enhanced CPRI (eCPRI) protocol, are the following. The first approach is associated with 7.x layer splits and Ethernet-based fronthauling solutions that introduce some form of packetized traffic to reduce the capacity requirements. Collaborating with the first one, the second approach includes alternative low layer transport schemes, such as the analog radio over fiber (A-RoF) solution that is being presented in the current thesis.

The reuse of the legacy PON infrastructure in support of 5G fronthauling architectures has been extensively investigated. Fronthaul via 25G WDM-PON, which is an integration of WDM and TDM-PON, is the most prominent solution to address the increased hardware requirements of 5G networks, due to its compatibility to the eCPRI protocol in terms of interfacing, rates and latency, as well as its simple operation and large scalability regarding future deployments [4.4]. For the D-RoF transmission, the PON infrastructure can accommodate both the data transmission and the processing functions required. In such a topology, however, the units that are responsible for the prioritization and time multiplexing of both the PON and the 5G traffic can significantly increase the latency of the 5G streams, in case the PON traffic rises. In such a scenario, an exclusively D-RoF based topology may fail to accommodate 5G services demanding ultra-low latency.

A-IFoF is a promising candidate for the implementation of low-latency 5G networks, enabling centralized processing, hence the removal of processing functions from the fiber-to-wireless (and vice-versa) transition nodes, being the PON terminals in the studied FMC topology. To benefit from the advantages of both A-IFoF and D-RoF implementations, their coexistence over the PON infrastructure has been discussed and experimentally demonstrated in [4.5]. TWDM-PON is a compliant topology with this hybrid RoF scheme, as it can benefit from the allocation of the unused ITU-T channels to the A-IFoF waveforms, expanding also the exploited bandwidth.

Focusing on the analog part of such a hybrid-RoF transmission over PON, a DL/UL solution was investigated, which exploits the legacy infrastructure's deployed fiber links, without requiring support from its processing nodes. In this coexistence solution, the existing Mux/Demux devices enable the establishment of point to point WDM pairs of channels connecting the MSA nodes with the remote sites. This A-IFoF-based investigated solution, requires only analog-processing at the remote site (optical detection and IF-to-V-band conversion for the DL, V-band-to-IF conversion and optical modulation for the UL), relaxing it from any digital processing.

The following paragraphs focus on the demonstration of a seamless analog Fiber-Wireless (FiWi) transport link, employing A-IFoF signals over an FMC topology deployment of Telecom Italia's (TIM's) PON legacy infrastructure, directly connected to a mmWave wireless link, recirculating traffic between Ethernet-compliant analog IF-transmit interfaces of an FPGA at the network nodes. It should be mentioned that the downlink (DL) operation of the presented FMC topology was experimentally demonstrated.

4.1.1 PtP and PtMP Fiber-Wireless Distribution Architectures over PON Infrastructures

The increasing demand for high-speed services to residential customers motivated the introduction of fiber-to-the-cab (FFTC) or FTTH architecture over PONs in the access segment [4.6], where the significant costs of excavation, installation, and supply of new infrastructures impose the maximum reuse of existing investments [4.7]. In urban areas, the passive fiber optic infrastructure for residential FTTH can provide the enabling platform to overlap an optical wavelength-differentiated layer on current traffic systems. In PON standards, this coexistence is facilitated by an appropriate wavelength plan for each system as specified by ITU Telecommunications Standardization Sector (ITU-T) Recommendations [4.8]. Mobile fronthaul or mid-haul are possible beneficiaries of this new layer availability [4.9]. Moreover, resources for these new connectivity segments are to be found not only in the optical but also in the wireless domain according to sites' placement and infrastructural constraints, service penetration, and bandwidth requirements.

Site approvals for locations in dense urban environments are getting increasingly difficult, and requirements for a variety of installation options, enabling fast and invisible deployments and sharing existing infrastructure, are continuously increasing. If small cell deployments and 5G hotspots can exploit existing assets where power already exists, such as public lighting or information kiosks [4.10], it is not necessary for a fiber connection to be available everywhere for their fronthauling. In this direction, a practical solution has recently been presented in [4.11], where an analog converged fiber-wireless scheme is proposed in order to create a spectrally efficient PtMP network capable of wirelessly interconnecting a large number of access points, without the need for expansive fiber deployment, while allowing compatibility with eCPRI traffic and/or mature Ethernet-based low-cost equipment.

As such, mmWave technologies have recently been introduced as x-haul for outdoor urban small cells [4.12], enabling low-latency connectivity over hundreds of meters. Smallcell

layer coverage can be provided in a PtP and/or PtMP architecture from a centralized rooftop towards mmWave access points whose antennas have configurable steerable and shaped beams to minimize energy consumption, limit interference, and focus capacity to where it is needed. The rooftop is fed through an optical link, provided by a dedicated fiber or using a shared PON infrastructure, forming a PtMP fiber-wireless architecture able to provide either fronthaul, mid-haul, or backhaul functionalities in the analog domain, taking advantage of A-RoF's inherent low latency and spectral efficiency while maintaining compatibility with the eCPRI's central unit/digital unit/radio unit architecture [4.11]. To better exploit configurability as a function of coverage, capacity, and cooperation while minimizing at the same time latency in transport and in protocol mapping, an overall integrated solution is advisable, with the same data format on the wireless section and on the wired optical one. Furthermore, a PtMP architecture allows for cooperative sharing of capital expenditure (CAPEX) investment.

The native OFDM radio signals suited for over-the-air (OTA) mmWve propagation in the 60 GHz band, properly down-converted to an IF below 10 GHz, can be transported as in the

optical section as an A-IFoF signal [4.13]. The use of an IFoF transport layer based on 10 GHz electro-optic (EO) bandwidth units has been selected allowing for higher spectral efficiency compared to the optoelectronics needed for generating and detecting A-RoF signals at mmWave frequencies. Despite being a proprietary signal, this architecture allows for PtMP transparent transport from a CRAN distributed unit to a pool of mobile sites, implementing an end-to-end fronthaul, mid-haul, or backhaul according to the functional split chosen by the mobile stack [4.14], while enabling C-RAN-inherent CoMP capabilities, already demonstrated in A-RoF wired [4.15] and fiber-wireless transmissions [4.16], offering multiple input–multiple output (MIMO) processing directly on the radio signal [4.11].

Finally, and perhaps mostly important for the future, promoting the approach of disaggregated nodes with software virtual network functions (VNF) and commercial off–the-shelf components, FiWi and fiber-to-the-cabinet/home (FTTx) services can be provisioned and operated on a common multi-service access (MSA)-node hardware, with specified and dedicated transceivers carrying the optical-to-electrical (and vice versa) functionalities [4.17]. Besides the optical transceivers the proposed FPGA implementation for the Ethernet-to-IFoF conversion can also be integrated with the switching and computing resources devoted to optical line termination (OLT) line cards [4.18], thereby maximizing the gains of shared infrastructure at the MSA node.

4.1.2 Deployed PON Infrastructure

Through this work, the IFoF/V-band transport layer of our proposed architecture is experimentally demonstrated over TIM's PON deployed fiber infrastructure as shown in Figure 45 (a). For the needs of this field demonstration, the passive fiber infrastructure is a WDM layer overlapped over the in-field FTTH architecture of TIM in Turin, while the FiWi equipment has been deployed within the 5G-PHOS H2020 project [4.19]. Considering the 5G networks' low-latency restrictions, up to 20 km IFoF transmission over the deployed infrastructure can be supported [4.20].

The optical legacy PON infrastructure in TIM is part of the deployed optical access network, carrying FTTC and FTTH services to business and residential users (Figure 45(b)). Two levels of optical splitters are included in the optical distribution network (ODN), usually two 1:8 power dividers, that allow for a maximum number of 64 users for each OLT port of the PON tree.

The first level of splitting is deployed in a cabinet in the street (Figure 45(b)), while the second one is provisioned usually inside buildings. Two different splitters are deployed in the cabinet: a 1:4 and a 1:8 splitter (Figure 45(d)). The optical connection has an insertion loss of around 10 dB for a 1:4 splitter and 13 dB for a 1:8 splitter. These values include splitter loss, fiber loss, and points of flexibility loss under the sidewalk and in patch panels inside buildings.

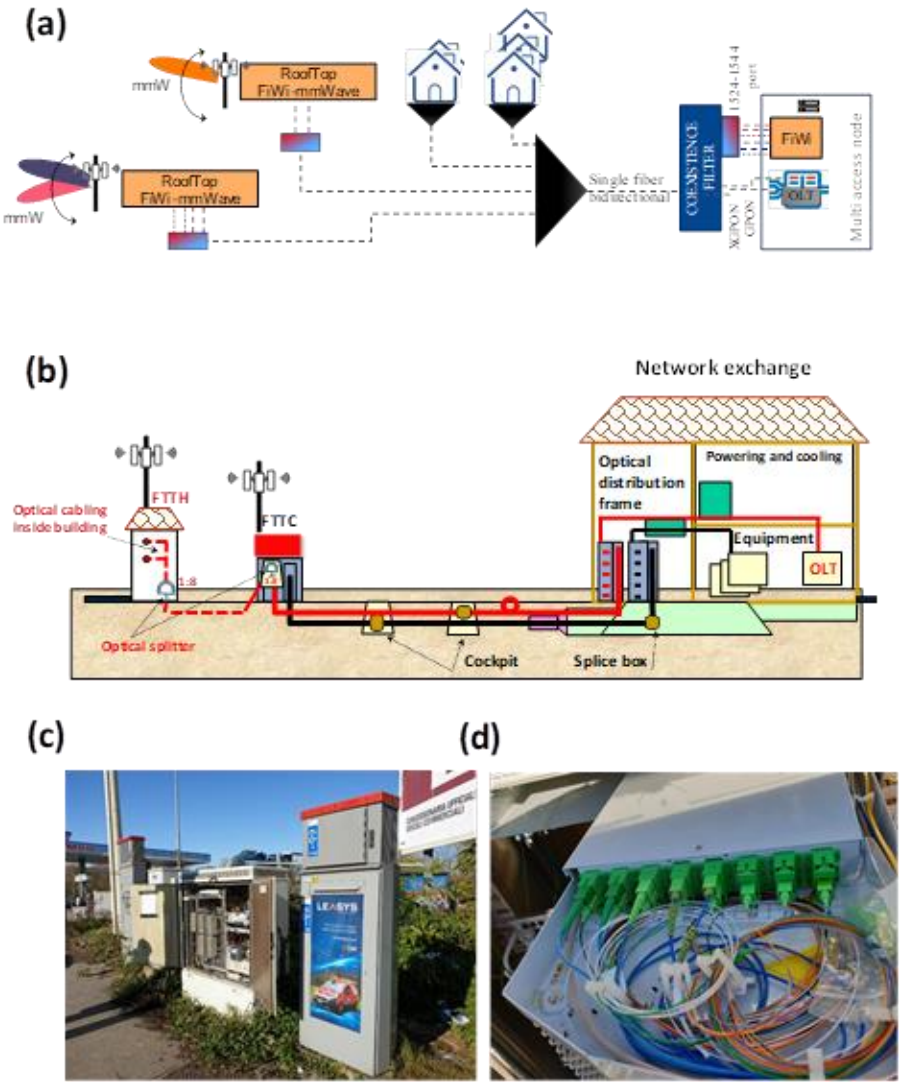

Figure 45. (a) FiWi architecture over legacy PON. (b) Schematic view of the in-field optical infrastructure. (c) Street cabinet installation in Turin. (d) Splitters located in a sub-unit of the cabinet rack.

In the network exchange, residential traffic is running bidirectionally over a single fiber by means of 10-gigabit-capable symmetric passive optical network (XGSPON) (10G symmetrical) interfaces in commercial multi-service access equipment using wavelength allocation in Figure 46(a) for discriminating uplink (UL) and downlink (DL) (1270 nm for the downstream wavelength, 1578 nm for the upstream wavelength). In the optical distribution panel in the main network exchange, a coexistence filter (CEx) allows for wavelength overlapping of different layers of PON systems. As shown in Figure 46(b), the CEx has less than 1 dB of insertion loss/port and more than 60 dB of rejection of other bands.

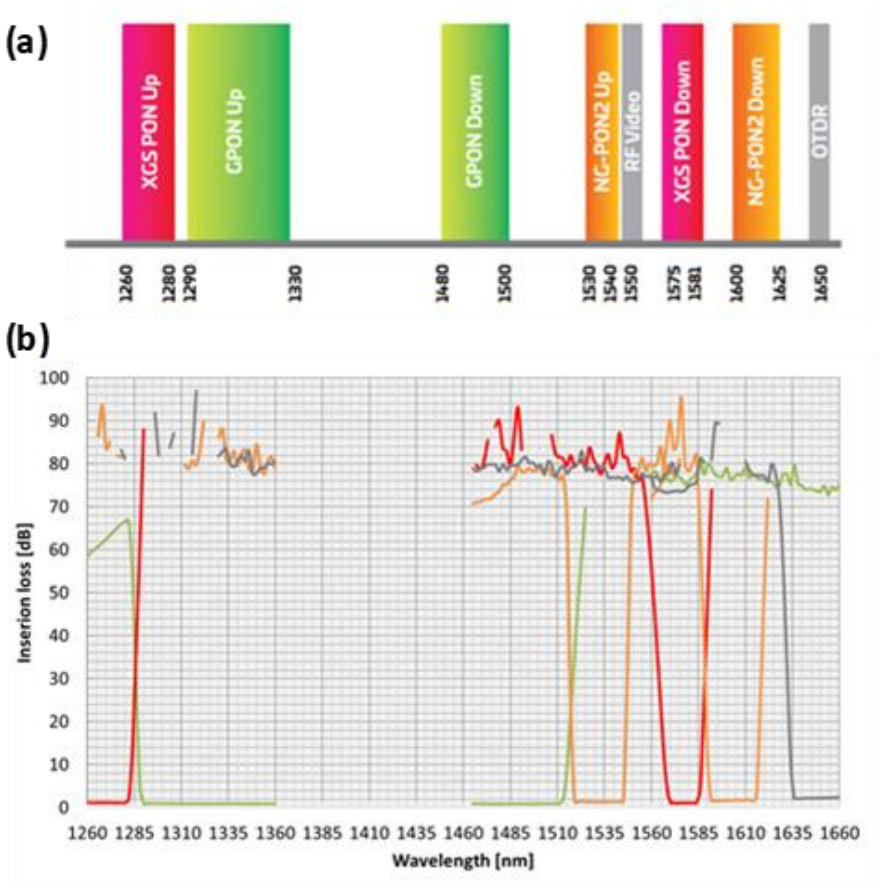

Figure 46. (a) PON wavelength bands according to ITU-T Recommendation G.989.2 and (b) CEx insertion loss as a function of wavelength.

Using a 100 GHz grid over the upstream Next-Generation PON 2 (NGPON2) transmission window, as specified in ITU-T G.989.2 [4.8], more than 10 bidirectional channels can be allocated in the 1530–1544 nm window (196.1 to 194.2 THz, 20 carriers, 10 ULs and 10 DLs). The exploitation of the NGPON2 band for this kind of application is promoted by the fact that NGPON2 time- and wavelength-division multiplexing (TDWDM) systems have not been massively deployed yet, and their introduction is time after time being postponed due to the relative high cost of the solution; the upcoming bandwidth request for dense WDM (DWDM) fronthaul could likewise benefit from the huge market of C-band DWDM transceivers. A further 10 channels are available in the same band by using the downstream window around 1596–1603 nm, but this option has not been considered in this work; it is viewed as a potential future expansion band.

By considering a launch optical power value of +10 dBm-like NGPON2 optics [4.8] and a sensitivity around -13 dBm, an overall span budget of 23 dB can be exploited, including transmission penalties (due to dispersion, in-band and out-of-band crosstalk) and WDM layer insertion losses as shown in Table 6. The link budget can be allocated between splitter losses (D) and fiber attenuation (F) in the ODN, plus the interconnections of splices and panels (E). Both plain and angled connectors are deployed in the patch panels of the ODN. The WDM layer accounts for around 3 dB, leaving a further 2 dB margin for extra losses or for coping with low-performance transmitters and/or detectors.

Table 6. WDM layer insertion losses

Component	[dBm]	[dB]
Tx power	10	
A – WDM MUX and DEMUX loss		2
B – CEx loss		1
C – transmission penalties		2
D – 1:8 splitter loss		9
E – connectors, splices (N x 0.5 dB)		4
F – fiber attenuation (10km)		3
WDM layer IL (A - B)		3
Overall span budget (C - F)		18
Margin		2
Rx power	-13	

To complete the overall description of the legacy infrastructure, a 1 GbE (Gb Ethernet) basket of services is provided to customers, including high-priority video, best effort Internet, and Voice over Internet Protocol (VoIP). Packet loss, throughput, and latency have been continuously measured during the experiment by means of a data quality analyzer feeding test traffic bidirectionally both into the MSA node and in a selected end-user 10-gigabit-capable symmetric (XGS) ONT.

Finally, for the establishment of bidirectional DL/UL links over the proposed converged FiWi link, the received traffic at the rooftop site can be mapped to analog IF signals for wireless-fiber transmission. For the wireless UL stream transmission, frequency-division duplexing (FDD) can be adopted. FDD has been widely used in deployed mobile networks and combined with massive-MIMO, and beamforming techniques have been discussed as a promising method of maximizing throughput for 5G New Radio (NR) [4.21]. After wireless reception and RF-to-IF down-conversion, the upstream can be optically modulated to wavelengths exclusively dedicated to the UL operation, minimizing the interference with the DL and propagated over the PON infrastructure. In both transmission directions, the 5G traffic propagates over individual IF data streams, uncorrelated to the legacy traffic, until their WDM multiplexing through multiplexer (MUX)/demultiplexer (DEMUX) devices, which are used to establish point to point pairs of channels connecting the MSA nodes with the remote sites and vice versa.

4.2. Experimental Evaluation of a converged PON/mmWave topology

In this section, the experimental results on the performance evaluation of the proposed FMC architecture are presented. To this extent, the deployed TIM optical access infrastructure described in the previous paragraphs was used as the optical layer where the analog IFoF/V-band transport scheme was integrated. The first part provides the implementation details of the experimental setup for both optical and mmWave counterparts. The performance evaluation studies are subsequently discussed in the second part of this section.

4.2.1 Experimental Setup

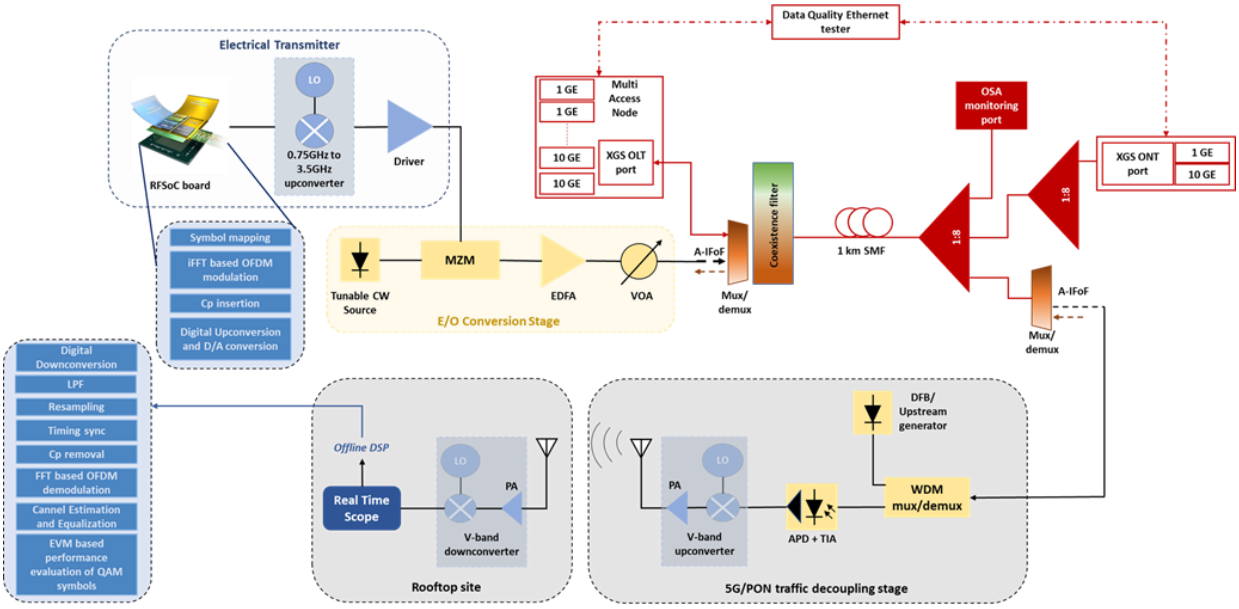

Figure 47. Experimental setup of A-IFoF/mmWave link, including the TIM's optical legacy infrastructure.

Figure 47 shows the experimental setup of the proposed A-IFoF architecture. The core element of the A-IFoF transmitter was a Xilinx Zynq Ultrascale+ RFSoC device on a ZCU111 development board [4.18]. The employed RFSoC board comprises the FPGA chip, which can include any custom very high-speed integrated circuits (VHSIC) hardware description language (VHDL) function for DSP together with the integrated digital-to- analog converter (DAC)/analog-to-digital converter (ADC) units and thus enables not only the generation but also the detection and digital processing of a signal, which is crucial for the operation of a full-duplex link. In this work, the FPGA unit implemented the real-time transmitter side DSP, while its DACs (sampling rate up to 4Gsa/s) generated analog IF signals at a central frequency of 750 MHz through a digital up-conversion stage. More specifically, the employed RFSoC platform includes eight DAC and eight ADC units. Two out of the eight available DACs were used for the processing of the baseband (I/Q) data stream and the generation of the low IF signal. The voltage swing at the output of the RFSoC was 390 mVpp. An analog frequency

up-conversion stage, composed of an active mixer and a local oscillator, was used to upconvert the RFSoC output signal at 3.5 GHz. The use of the external analog mixer provides to the proposed scheme an additional degree of flexibility by enabling the generation of higher IFs and thus surpasses limitations set by the DACs' sampling rate (up to

4GSa/s). As such, the presented electrical transmitter can be easily adjusted to the operation requirements of different radio boards. At the same time, the exploitation of external analog mixers optimizes the use of the RFSoC DACs' resources, allowing the up-conversion of all four streams that can be generated by the RFSoC to higher IF values, supporting a bandwidth efficient subcarrier multiplexing (SCM) scheme [4.22]. The employed mixer could operate at a frequency range from 30 MHz to 7 GHz, with C1 dB conversion gain, resulting in a 450 mVpp signal at its output.

For the electro-optic conversion of the analog IF signals, a single drive 15 GHz Mach–Zehnder modulator (MZM) was used, modulating a 1542.14 nm (194.4 THz) continuous-wave (CW) signal provided by a tunable laser source with +13.5 dBm optical power. The MZM driving voltage had to be 5.6 Vpp to minimize the signal degradation related to the electro-optic conversion, and thus an RF low-noise amplifier with 40 KHz to 38 GHz operation bandwidth and 22 dB gain was used to amplify the output of the active mixer. The optical power of the A-IFoF signal was a crucial parameter for the transmission over the legacy infrastructure. Therefore, in order to partially compensate for the MZM's high insertion loss of 9.6 dB, an optical amplification stage composed of an Erbium-Doped Fiber Amplifier (EDFA) and a Variable Optical Attenuator (VOA) was employed, providing a total gain of +4 dB.

The A-IFoF signal was fed to the optical legacy infrastructure through the CEx filter (and a WDM MUX in case of multicarrier operation) and transmitted over the field deployed fiber link. At the same time, the XGS legacy traffic was running through the link in parallel with the signal generated by the optical A-IFoF transmitter. The overall signal (legacy and A-IFoF) was accessed through one of the ports of the in-field installed PON passive splitter and directed back to the lab. A second port from the same splitter was connected to an optical spectrum analyzer (OSA) for monitoring purposes. To decouple the A-IFoF signal from the legacy traffic, a WDM DEMUX was employed to the setup, and the A-IFoF wavelength was demultiplexed. The same device was also used to insert an upstream carrier, emulating bidirectional transmission. For the generation of the upstream carrier, a Distributed Feedback (DFB) laser source with +4 dBm optical power was used to generate a 1542.94 nm CW (194.3 THz), at a distance of 100 GHz from the downstream, that is, corresponding to the first neighbor channel using the ITU-T 100 GHz grid. The insertion of an upstream tone to the link can provide insight on possible interference between UL and DL streams occupying neighboring ITU-T channels. Given that the DL IF signal has a narrow bandwidth, up to 400 MHz, the effect of the UL direction on the DL signal depends on the transmitted optical power in each direction. Thus, the upstream can be emulated via a CW tone to enable the acquisition of realistic EVM measurements for the DL signal. For the detection of the IFoF signal, a 10 GHz linear photoreceiver composed of an avalanche photodiode (APD) and a low noise transimpedance amplifier (TIA) with 20 dB gain was used. The received optical power was -

14 dBm, implying a transmission power budget of around 22 dB, including both the legacy field infrastructure and the filters for the WDM A-IFoF layer.

For the wireless transmission, the IF signal at the output of the photoreceiver, which had a voltage swing of 140 mVpp, was fed to the IF-to-V-band upconverter, centered at 60 GHz. The employed up-conversion board's IF input could range between 1 and 5 GHz and corresponded to an RF output ranging from 58 to 63 GHz. The output of the 60 GHz mixer was led to a dual-amplification stage consisting of a driver and a power amplifier and then to the directional horn Tx-antenna element, featuring 10 beamwidth and 23 dBi gain. An identical Rx antenna was located at a 2 m horizontal distance from the Tx antenna, forming the 60 GHz wireless link. Both frequency conversion modules had a nominal noise figure of 8 dB at maximum gain. The received RF signal was amplified through a low noise amplifier and downconverted to 3.5 GHz IF by the Rx-side V-band-to-IF downconverter. The two antenna elements, as well as the up/downconversion circuits, were located at a height of 0.5 m from the ground. An external signal generator, providing a 10 MHz tone with -10 dBm power, was used as a reference for both the antenna's internal phase-locked loops (PLLs). These PLL circuits are integrated into the IF-to-V-band boards and are required for the operation of the boards' local oscillators, which generate the reference tone for the IF-to-RF conversion and vice versa. The 3.5 GHz IF output of the downconverter, which had a voltage swing of 300 mVpp to 400 mVpp, was connected to a real-time scope (sampling rate 100 GSa/s, analog 3-dB bandwidth ~33 GHz) sampled at 12.5 GSa/s and stored for offline demodulation and performance evaluation.

Data transmission was supported by the DSP algorithms executed in real time at the transmitter's FPGA board. To this extent, a fixed bit stream was M-ary quadrature amplitude modulated (QAM) and mapped to the iFFT algorithm for the generation of the OFDM symbols. At this development stage of the implemented A-IFoF transceiver, the transmission of a fixed known bit stream was exploited to determine the pilot allocation frequency for the receiver-side channel estimation. The modulation format of the subcarriers was real-time adjusted to 4QAM or 16QAM. The RFSoC clock was also real-time adjusted at 256 MHz or 500 MHz, corresponding to the transmission of 204 MHz or 394 MHz of useful bandwidth, after zero padding (52 out of 256 subcarriers). Since the FFT size was kept fixed, minimizing as such the use of the FPGA resources, the subcarrier spacing was adapted to the clock frequency, resulting in 1 MHz spacing for the 204 MHz band and 1.95 MHz for the 398 MHz band.

To implement the DSP functions in an RFSoC, a parametric and pipelined architecture was implemented with VHDL and Xilinx Vivado 2018.2. The iFFT component was implemented as a fully pipelined Radix-2 engine and performs a 256-point transform. The QAM modulator was designed as a flexible read-only memory (ROM)-based component, where pre-stored pairs of normalized I/Q values reside and can be configured at runtime to switch between modulation formats. The DSP pipeline relies on minimal buffering and handshaking between components to guarantee continuous flow without relying on a multi-rate approach (we use a single clock domain). As a result, the total cost of Tx in terms of FPGA resources, specifically lookup tables (LUTs), flipflops (FFs), random access memory (RAM) blocks (RAMBs), and DSP blocks, was 2007 LUTs, 3459 FFs, 30 DSPs, and 17 RAMB18 (iFFT consumes 1339

LUTs, 2117 FFs, 30 DSPs, and 8 RAMB18; QAM consumes 258 LUTs, 382 FFs, and 4 RAMB18; whereas 410 LUTs, 960 FFs, and 5 RAMB18 are utilized for buffering and control operations). Finally, regarding the latency performance of the real-time Tx implemented on the deployed RFSoC platform, 4.67 us on average was measured for a bit of information to pass through the entire Tx pipeline until conversion to analog (0.08 us for QAM modulation, 2.45 us for iFFT, 2.14 us for buffering and other control operations, such as pilots and zeros insertion). The Tx baseband processing latency added to the 1 km transmission over the PON delay (5 us) and the 2 m wireless propagation delay (less than 0.01 us), corresponding to a latency budget of 9.68 us, neglecting the Rx-side offline DSP.

At the receiver side, the offline DSP toolbox that was presented in Chapter 3, was applied to the digitized sample sequence at the output of the scope to retrieve the baseband data signal. More specifically, the sampling rate of the baseband complex signal was decreased so as to equal the OFDM symbol rate through a resampling algorithm. Through a cp-based timing synchronization algorithm [4.23], the first sample of each time-domain OFDM symbol was tracked. Afterwards, the cp was removed and an FFT algorithm was used to demodulate the OFDM symbols. Finally, a least-squares (LS) equalizer was applied to the frequency-domain signal [4.24]. For the channel estimation, 21 subcarriers were used as pilot subcarriers. The performance of the received signal was evaluated through the EVM measurement of the QAM-modulated received subcarriers.

4.2.2 Results and Discussion

The first step of the performance evaluation of the A-IFoF transmission was to evaluate the performance of the electrical IF transmitter. Figure 48 depicts the EVM performance of the OFDM/4QAM 204 MHz signal at the output of the RFSoC, at the output of the upconverter, and finally at the output of the RF driver. The initial signal generated by the RFSoC had an EVM of 2.7%, while the insertion of the mixer to the setup induced an EVM increase by 1.8% as a result of the additive noise coming from the active components of the up-conversion unit. The RF amplifier further increased the EVM by 2.3% as expected, due to the susceptibility of OFDM waveforms to the nonlinear distortion effects of the high-power amplifier (HPA) [4.25]. Finally, at the output of the electrical transmitter, the signal's 4QAM-OFDM 204 MHz EVM was found to be 6.8%, a value that was considered as the reference electrical EVM for both modulation formats and bandwidths.

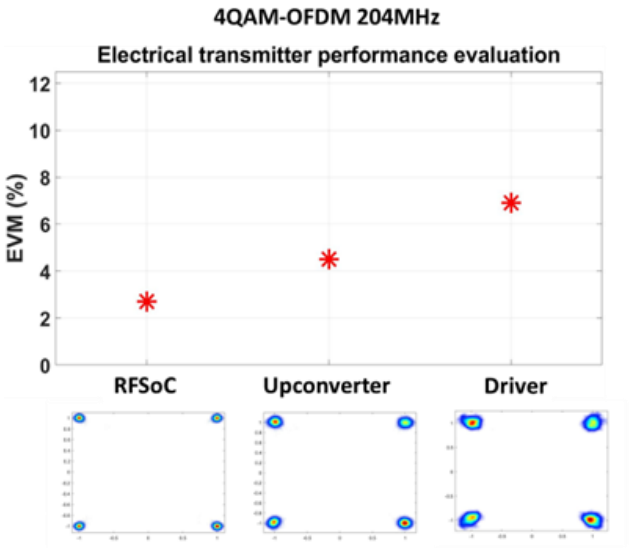

Figure 48. EVM measurements and constellation diagrams of the received 204MHz 4QAM-OFDM signal at the output of the RFSoC board, the analog upconverter and the RF driver.

The second part of the experimental study focused on the performance evaluation of the A-IFoF transmission over the TIM's optical legacy infrastructure. A set of back-to-back (btb) results was captured for all possible data signal combinations generated by the RFSoC, after replacing the fiber PON with a VOA inserting the same amount of optical loss, so as to keep a fixed optical input power value to the photoreceiver. Figure 49 depicts the EVM values and a set of indicative constellation diagrams corresponding to the signals captured after optical transmission. It is obvious that the contribution of the optical transceiver components to the signal degradation is less than 0.6% EVM for all modulation formats and bandwidths, indicating the absence of strong limiting effects related to the active electro-optic modules' response. The insertion of the legacy infrastructure to the setup introduced an extra EVM penalty of less than 0.5%, compared to the optical btb results, thus indicating that there is negligible interference between the A-IFoF signal and the legacy traffic. Finally, the transmission of the upstream tone at a neighbor channel of the ITU-T grid to the optical channel carrying the A-IFoF signal, caused a further EVM increase by 1% per average, as a result of the interference between the two neighboring channels. In all cases however, the A-IFoF transmission was successful, according to the 3GPP specifications for systems that employ radio transmission at frequencies >28 GHz [4.26].

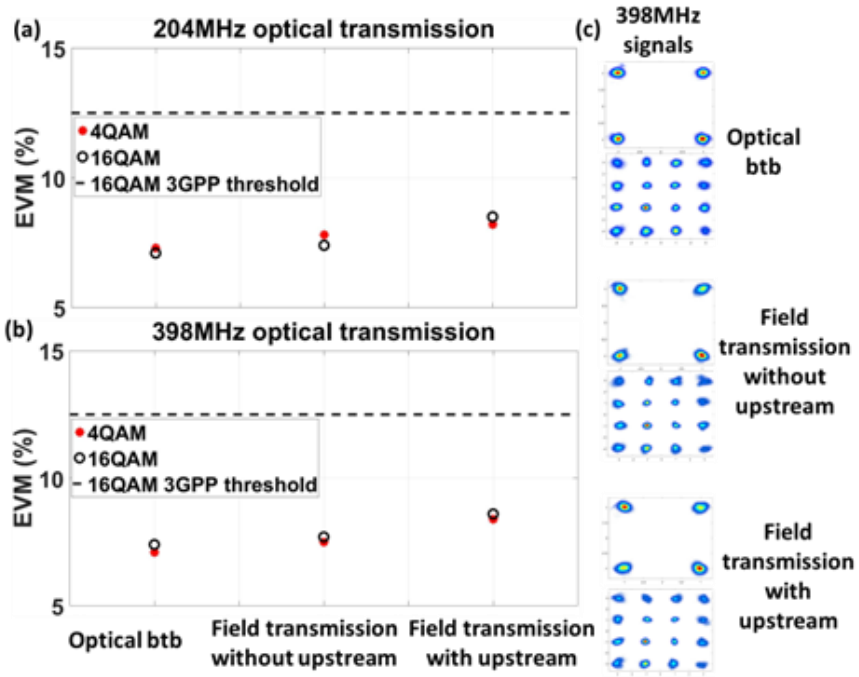

Figure 49. (a) 204 MHz 4QAM/16QAM-OFDM and (b) 398 MHz 4QAM/16QAM-OFDM EVM measurements for the A-IFoF transmission over the optical legacy infrastructure and (c) Constellation diagrams corresponding to the 398 MHz 4QAM-OFDM and 16QAM-OFDM received signals.

Figure 50 represents the EVM values and constellation diagrams that correspond to the retrieved signals after a combined FiWi transmission. For this part of the experimental study, the whole setup depicted in Figure 47 was exploited. As such, the OFDM IFoF signal was transmitted through the legacy optical infrastructure, coexisting with the legacy traffic and the upstream and after optical detection, it was transmitted through the 60GHz wireless link. For this scenario, the constellation diagrams of Figure 50, and especially the 16QAM-OFDM diagrams [4.20], show evidence of nonlinear distortion of the signal caused by the multiple amplification stages used in the link. Nonetheless, the EVM performance of both modulation formats at both 204MHz and 398MHz bandwidth, meet the 3GPP requirements (17.5% for QPSK and 12.5% for 16QAM), indicating successful FiWi transmission.

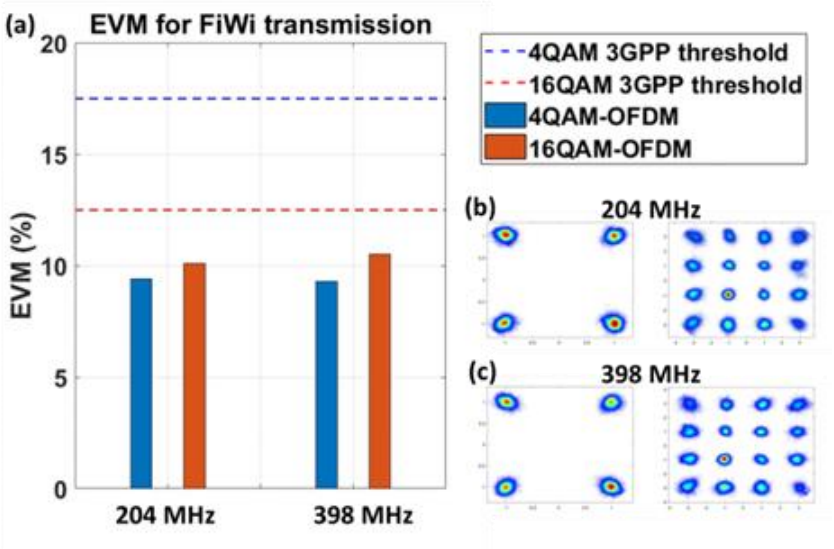

Figure 50. (a) 204 MHz and 398 MHz 4QAM/16QAM-OFDM EVM measurements after transmission through the optical legacy infrastructure/V-band wireless link and constellation diagrams of the (b) 204 MHz and (c) 398 MHz signals.

The last part of the study focused on the potential of increasing the total capacity of the deployed infrastructure by utilizing more than one of the available ITU-T grid channels for transmitting multiple A-IFoF optical streams over the PON. To evaluate this scenario, the performance of the FiWi transmission over different optical channels of the 100GHz ITU grid was examined, coexisting with an upstream tone transmitted firmly at 1542.94 nm. More specifically, the tunable CW source feeding the MZM was tuned per testing case to one of the channels from 194.4 to 193.9 THz, which was then modulated to a 16QAM-OFDM 400MHz signal, corresponding to the maximum possible bandwidth of 1.4GHz, after removing the pilot subcarriers. Figure 51 illustrates the EVM values and constellation diagrams of the received signals. The figure clearly shows that the EVM variations between the different channels do not exceed 1.8%, implying similar performance over all tested wavelengths combinations. The impact of the interference caused by the upstream tone is negligible in the 1542.14 nm to 1544.53 nm region, where small variations exist on the received EVM values. The interference effect is most notable in the case of simultaneous transmission of downstream and the upstream both in the same ITU channel. As the distance between the two streams increases, the performance of the IFoF signal improves as expected. It should also be noted at this point that the 1545.32 nm to 1546.12nm region is beyond the operational range the WDM filter inserted after the legacy field infrastructure, thus leading to low power reception of the transmitted A-IFoF signal and as a result, a small EVM increase. The main scope of this test was to evaluate the performance near the upper wavelength border of the CEX and to investigate if penalties occur due to the filters' concatenation (CEX + MUX/DEMUX). Results demonstrated that at least two more channels in addition to the 10 already planned can be successfully transmitted with negligible penalties.

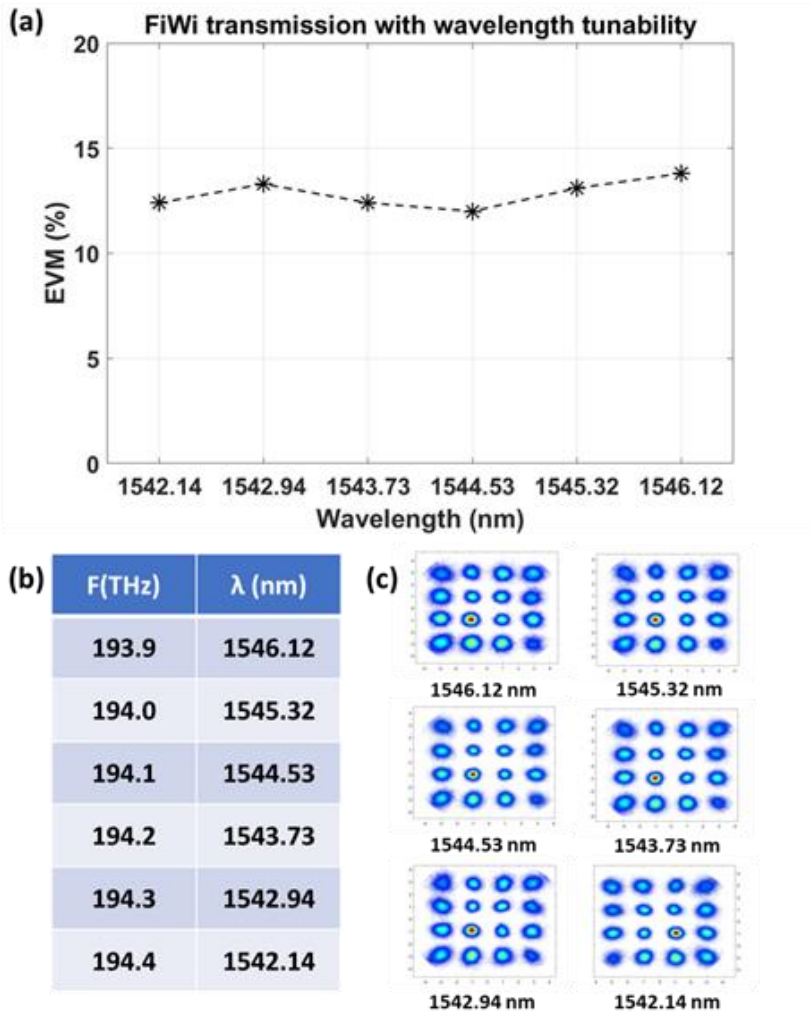

Figure 51. (a) EVM measurements after PON/OTA transmission, after tuning the optical transmission carrier to different ITU-T channels, (b) Matching of the transmission wavelengths to the corresponding 100GHz Grid channels and (c) the corresponding constellation diagrams.

Finally, since, the setup includes field transmission, it should be mentioned that the loss budget is time dependent and can vary by up to 2dB. This variation can be evident to the results in form of small EVM variations, related to the performance of the photoreceiver or the wireless transmission components, which are fed with a different value of optical/RF power.

References

[4.1] Bismi B.S, Saniya Azeem, "A survey on increasing the capacity of 5G Fronthaul systems using RoF", Optical Fiber Technology, Volume 74, 2022, https://doi.org/10.1016/j.yofte.2022.103078.

[4.2] Kanta, K.; Toumasis, P.; Tokas, K.; Stratakos, I.; Papatheofanous, et al., "Demonstration of a Hybrid Analog–Digital Transport System Architecture for 5G and Beyond Networks", Appl. Sci. 2022, 12, 2122. https://doi.org/10.3390/app12042122.

[4.3] C. Ranaweera, E. Wong, A. Nirmalathas, C. Jayasundara, and C. Lim, "5G C-RAN architectures: a comparison of multiple optical fronthaul networks," in International Conference on Optical Network Design and Modeling (ONDM), Budapest, Hungary, May 15–18, 2017.

[4.4] ZTE, "An optimal solution for 5G fronthaul based on 25G WDM-PON".

[4.5] T. Li, Y. Yang, M. Crisp, I. H. White and R. V. Penty, "Novel Digital and Analogue Hybrid Radio over Fibre System for Distributed Antenna System (DAS) Fronthaul Applications", Optical Fiber Communication (OFC) Conference, San Diego, 2019.

[4.6] D. Nesset, "PON roadmap," J. Opt. Commun. Netw. 9, A71–A76 (2017).

[4.7] J. Rendon Schneir and Y. Xiong, "Cost analysis of network sharing in FTTH/PONs," IEEE Commun. Mag. 52(8), 126–134 (2014).

[4.8] "40-gigabit-capable passive optical networks 2 (NG-PON2): physical media dependent (PMD) layer specification, Amendment 2," ITU-T Recommendation G.989.2, Feb. 2019.

[4.9] A. Di Giglio and A. Pagano, "Scenarios and economic analysis of fronthaul in 5G optical networks," J. Lightwave Technol. 37, 585–591 (2019).

[4.10] "Access, terminals, transmission and multiplexing (ATTM); sub-part 2: the use of lamp-posts for hosting sensing devices and 5G networking," ETSI Technical Specification TS 110 174-2-2 V1.1.1, June 2019.

[4.11] M. Gatzianas, G. Kalfas, C. Vagionas, and A. Mesodiakaki, "Downlink coordinated beamforming policies for 5G millimeter wave dense networks," in European Conference on Networks and Communications (EuCNC), Valencia, Spain (2019), pp. 342–346.

[4.12] M. Steeg, N. J. Gomes, A. Juarez, M. Kosciesza, M. Lange, Y. Leiba, H. Mano, H. Murata, and A. Stoehr, "Public field trial of a multi-RAT (60 GHz 5G/LTE/WiFi) mobile network," IEEE Wireless Commun. 25, 38–46 (2018).

[4.13] "Access networks—optical line systems for local and access networks, radio over fibre systems," ITU-T Recommendation G.9803, Nov. 2018.

[4.14] 3GPP, "Study on new radio access technology: radio access architecture and interfaces," 3GPP TR 38.801 V14.0.0, March 2017.

[4.15] Y. Tian, K. Lee, C. Lim, and A. Nirmalathas, "Performance evaluation of CoMP for downlink 60-GHz radio-over-fiber fronthaul," in International Topical Meeting on Microwave Photonics (MWP), Beijing, China (2017).

[4.16] L. Cheng, M. Usman, F. Lu, M. Zhu, J. Wang, M. Xu, X. Ma, and G.-K. Chang, "Coordinated multipoint transmissions in millimeterwave radio-over-fiber systems," J. Lightwave Technol. 34, 653–660 (2016)

[4.17] P. Torres-Ferrera, H. Wang, V. Ferrero, M. Valvo, and R. Gaudino, "Optimization of band-limited DSP-aided 25 and 50 Gbps PON using 10G-class DML and APD," J. Lightwave Technol. 38, 608–618 (2020).
[4.18] "Zynq UltraScale+ RFSoC," 2019, https://www.xilinx.com/publications/product-briefs/xilinx-rfsoc-product-brief.pdf.
[4.19] G. Kalfas, M. Agus, A. Pagano, L. A. Neto, A. Mesodiakaki, C. Vagionas, J. Vardakas, E. Datsika, C. Verikoukis, and N. Pleros, "Converged analog fiber wireless point-to-multipoint architecture for eCPRI 5G fronthaul networks," in IEEE GLOBECOM (2019).
[4.20] S. Bidkar, J. Galaro, and T. Pfeiffer, "First demonstration of an ultra-low-latency fronthaul transport over a commercial TDM-PON platform," in Optical Fiber Communication Conference (OFC), San Diego, California, USA (2018).
[4.21] Ericsson, "5G New Radio on FDD," https://www.ericsson.com/en/networks/offerings/5g/5g-radio-fdd.
[4.22] N. Argyris, G. Giannoulis, K. Kanta, N. Iliadis, and C. Vagionas, "A 5G mm wave fiber-wireless IFoF analog mobile fronthaul link with up to 24-Gb/s multiband wireless capacity," J. Lightwave Technol. 37, 2883–2891 (2019).
[4.23] W. Aziz, G. Abbas, E. Ahmed, S. Saleem, and Q. Islam, "Time offset estimation for OFDM using MATLAB," J. Expert Syst. 1, 56–61 (2012).
[4.24] M. K. Ozdemir and H. Arslan, "Channel estimation for wireless OFDM systems," IEEE Commun. Surv. Tutorials 9, 8–48 (2007).
[4.25] A. Singh and H. Kaur, "Non linearity analysis of high power amplifier in OFDM system," Int. J. Comput. Appl. 37, 37–41 (2012).
[4.26] "NR; Physical layer; General description," 3GPP specification TS 38.201 2017.

CHAPTER 5.

Live Demonstration of an SDN-reconfigurable, FPGA-based TxRx for Analog-IFoF/mmWave RAN, in MNO's infrastructure

As discussed in the previous sections, during recent years, the spotlight has been on the benefits of incorporating alternative transport systems like A-RoF into upcoming RANs. This is in spite of the notable hurdles that must be surmounted for these solutions to be implemented successfully and offer deployable solutions.

The efficiency of the scheme in densified deployments, stemming from the removal of Digital-to-Analog Conversion (DAC) and Analog-to-Digital Conversion (ADC) units from the Radio Units (RUs), the advanced bandwidth availability, and the possibility for the convergence of multiple optical and radio technologies have been highlighted and demonstrated through proof-of-concept experiments in both laboratories and field trials [5.1], [5.2], [5.3]. Still, its actual adoption in the standardized mobile networks is a major challenge and the implementation of proper interfaces that will allow for gradual integration in the access and edge domain infrastructures remains an open issue.

The integration of A-RoF interfaces with standard equipment, delivering real-world services, has been pursued in the past years by research groups working on these bandwidth-efficient fronthaul interfaces [5.3], [5.4], [5.5]. A first step for A-RoF systems to further penetrate into the market is the use of deployment-oriented A-RoF baseband processors that are based on state-of-the-art processor platforms, as well their interfacing with optoelectronics. In this direction, multiple A-IFoF fronthaul implementation ideas have been presented [5.6], [5.7]. Indicatively, an A-RoF fronthaul implementation, which is based on the development of a real-time A-IFoF signal processor, has been recently reported in [5.3] employing an Intel Arria 10 SoC development board that provides Cyclic Prefix (CP)-Orthogonal Frequency Division Multiplexing (OFDM) signals for external Baseband (BB)-to-Intermediate Frequency (IF) up-conversion through an analog mixing unit, while in [5.4], an FPGA-based transmission system showcases the transmission of 10GbE Ethernet frames over an A-IFoF/mmWave link, using the W-band for Over-the-Air (OTA) transmission.

The next step towards the full-scale integration of analog links in packet core infrastructure deployments, is the development of analog TxRx units being equipped with management and control functionalities for exposing these transceivers to the control/orchestration layers of the network, alongside the baseband processing ones for the physical infrastructure layer. By following this deployment path for the A-RoF transceivers, the Application Data transmission (physical and virtual) plane, and the management / control plane can be delivered in a unified, seamless and interoperable manner. Towards this goal, SDN-enabled RAN layouts have been discussed and experimentally presented, without involving though, physical layer testbeds [5.8],[5.9],[5.10]. Very recently, the demonstration of trial, real-time Ethernet services and

Ultra High Definition (UHD) video was presented over an analog FiWi link [5.11], paving the way for integrating the A-RoF deployments in mobile network infrastructures.

In the following paragraphs, which describe the final demonstrator of the European project 5GPHOS, the first demonstration of the integration of a custom, SDN-reconfigurable, real-time A-IFoF TxRx interface, over a real network infrastructure located in Athens is described. The implemented SDN controller offered active adjustment of the capacity provided by the TxRx for converged A-IFoF/mmWave RAN transport, based on constant traffic monitoring and automatic adaptation to the hosted applications' requirements. In a nutshell, in the physical layer of analog transport infrastructure, EVM measurements of 7.3% for QPSK-OFDM, converged FiWi transmission were achieved. The uninterrupted operation of the E2E deployment, was validated at application layer through the performance evaluation of various services such as AR/VR applications running on top of the infrastructure, as well as by throughput measurements, using traffic monitoring tools, showcasing peak data-rate per user up to 474Mbps. The reactive capacity optimization and network parameter reconfiguration capabilities provided by the SDN management and control layer of the presented solution were also successfully demonstrated. However, more details regarding the implementation of the analog TxRx, as well its integration in the mobile core infrastructure are provided in the following sections.

5.1. The envisioned Fronthaul Architecture relying on analog TxRx interfaces

The proposed SDN-compatible A-IFoF TxRx implementation comprised a Network Controller (NC), an FPGA-based Digital Signal Processing (DSP) engine, as well Analog-to-Digital (A/D) and electro-optic (e/o) interfaces that provide analog fiber connectivity towards the radio unit. The developed TxRx, was used in the experimental evaluation and demonstration of a converged A-IFoF/wireless layout, which was integrated as an alternative deployment option in the transport network segment of actual mobile network infrastructure, located in Athens. Figure 52 depicts the architectural view of this deployment, where mobile network transport connections of type Ethernet can be provisioned over both legacy transport technologies and A-IFoF links; the latter serving in cases where high-capacity transport network links are required, e.g. for the deployment of RAN nodes in crowded hot-spot places, or as PtP wireless extensions in places where fiber deployment is not feasible. The seamless operation of the application, network management and data layer of the presented implementation, is a key factor for the adaptability of A-RoF transceivers to the legacy core infrastructure.

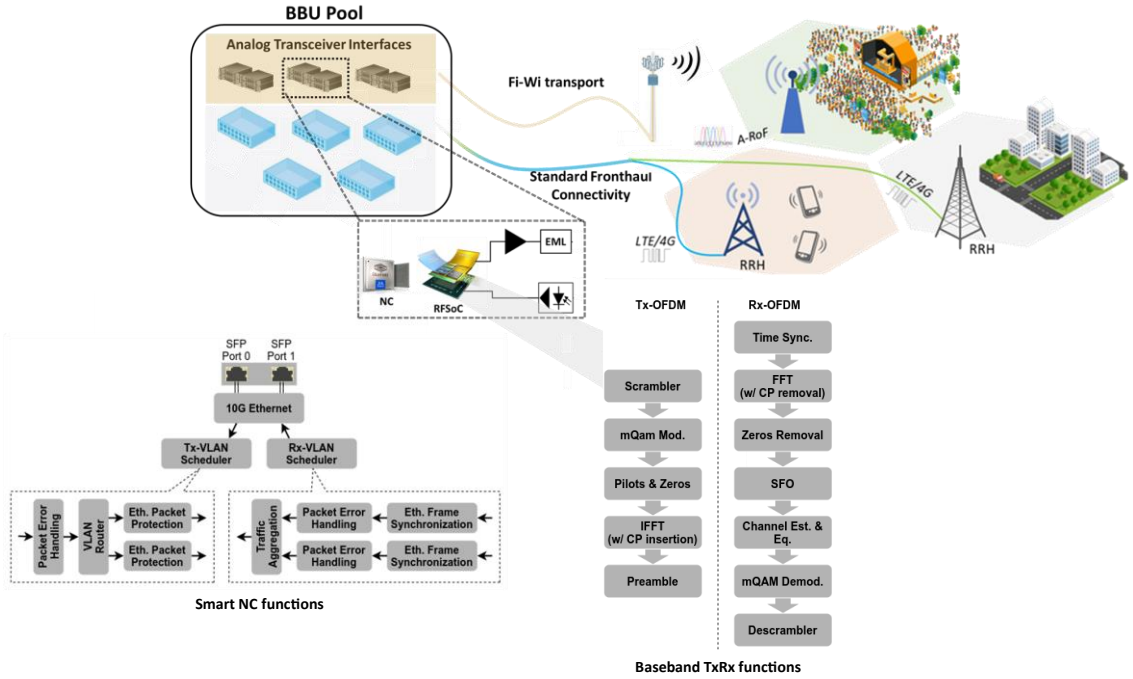

Figure 52. Schematic of the envisioned Fronthaul Architecture relying on the adoption of analog TxRx interfaces, for broadband FiWi connectivity.

5.1.1 RFSoC-based A-IFoF transceiver

The conversion of the Ethernet packets into complex native radio waveforms and vice-versa relied on the development of a real-time network adaptor, serving as a processing node that handled the Ethernet packets carrying real-time mobile services traffic. The full stack of DSP functions targeted efficient fiber/OTA transport through OFDM waveforms. The platform that was used for the development of this network adaptor was the single integrated Xilinx Zynq Ultrascale+ Radio Frequency System on Chip (RFSoC), and consisted of a 10G/25G Ethernet core, an FPGA board, and DAC/ADC. The reconfigurability properties of the FPGA processor offer great flexibility regarding the waveforms that can be generated and handled, as well compatibility with any-type SFP-based traffic. As such the employed baseband processor can be any time adapted to the requirements of the specific network segment and support varying signal formats, from complex up-converted OFDM waveforms to standard CPRI-compatible binary OOK traffic. The individual functionalities of the network adapter, depicted also in Figure 53 are the following:

- **Ethernet en/de-capsulation:**

The employed RFSoC has increased capabilities in terms of Gigabit Ethernet connectivity, as its Gigabit Transceivers can support up to 25G Ethernet with the (Media Access Control) MAC and Physical Coding Sublayer (PCS) implemented on the FPGA fabric. The Ethernet core performed data link layer functionalities to map the incoming Ethernet traffic to the DSP engine, as well to recover Ethernet frames from the demodulated waveforms. These

functionalities include basic error handling, flow control for access to the physical layer, and frame encapsulation into 802.1Q frames that enable Virtual Local area network (VLAN) tagging – the supporting mechanism of the management plane. Through implementation of the corresponding functionalities, the RFSoC platform also offers compatibility with a variety of standard protocols, including different options of the eCPRI interface.

- **Baseband processing:**

The signal processing functions of the implemented A-IFoF transceiver were executed within the FPGA fabric of the RFSoC platform. Multiple lane processing of up to 4 independent data streams were applied for low-latency implementation. Two independent and identical transmitter/receiver side DSP block chains were developed within the RFSoC for the establishment of full-duplex connectivity. At the transmitter side, the incoming bit-stream was initially mapped to QPSK symbols, while the OFDM signals were generated using a fixed 256-tap inverse Frequency Fourier Transform (iFFT) algorithm., which combined to the 200MHz analog bandwidth at the DACs' outputs correspond to a larger subcarrier spacing compared to the 3GPP specifications, approximating the value of 1MHz. The FPGA clock was 256MHz, corresponding to transmission of 204 MHz useful bandwidth, after zero-padding (52 out of 256 sub-carriers). A CP of 64 samples length was inserted to the signal before its Digital-to-Analog (D/A) conversion. It has to be mentioned that the parameters that were selected for the OFDM modulation are not based on the 3GPP specifications. Instead, signal robustness against distortive factors, such as ISI and phase noise, as well the resource utilization scaling of the employed FPGA platform were the main criteria for the determination of the OFDM parameters.

More specifically, based on the latest 3GPP specifications for extended symbol bandwidth values of up to 400MHz [5.12], the corresponding FFT size extends to 4096 taps, hence the subcarrier spacing can be as narrow as 98KHz for the specific parameters. In general, the 3GPP standards support subcarrier spacings in the range of 15KHz to 480KHz. The CP is in most cases calculated as a fraction of the FFT length. This fraction varies from 1/4 to 1/16, while longest CP ensures robustness to ISI [5.13]. It should be noted that the mentioned specifications target to meet the requirements of the access component in 5G mobile networks. More specifically, they are tailored for the connection between user equipment and radio units. These specifications have been designed considering transmission scenarios involving wireless frequencies of up to 28GHz [5.14].

The A-IFoF transceiver introduced aims to offer an alternative transport solution for connecting BBUs with their corresponding RUs, over analog-based fiber and converged fiber-Wireless paths. Aiming to benefit from the high bandwidth efficiency characteristics of A-IFoF scheme, the convergence of analog optical interfaces and high-frequency radio solutions, including mmWaves, sub-THz, and even THz, presents an opportunity to achieve extremely high capacities.

One of the main challenges towards adopting such high bandwidth technologies in analog transport layouts is their high susceptibility to distortion caused by the oscillators' phase noise [5.15]. The effect of phase noise gets even worse in OFDM-based transmission systems when narrow subcarrier spacing values are adopted [5.16]. In the custom analog transceiver that is being presented in the current work, the embraced 256-tap FFT size, combined to the 200MHz

analog bandwidth at the DACs' outputs correspond to a larger subcarrier spacing compared to the 3GPP specifications, approximating the value of 1MHz. As such, one of the criteria for the FFT size and subcarrier space selection was robustness to phase noise. At the same time, for the selection of the size of the FFT transformation the resource utilization scaling of the employed Xilinx IP core, especially the DSP and RAMB blocks was taken into consideration.

Furthermore, considering that employing an FPGA as a baseband processor allows for reconfigurability but may not achieve optimal performance, an extended CP of 64 points was utilized. This extended CP, which corresponds to a quarter of the FFT length, was chosen to ensure resilience against ISI and concurrently facilitate timing synchronization of the received OFDM symbols based on the CP, even in low-SNR reception cases.

At the receiver side, the timing synchronization of the signal was achieved through an auto-correlation function targeting to the identification of the CP, which indicates the start of the OFDM signals. After the CP elimination, a 256-tap FFT function was used for the demodulation of the OFDM symbols. Following, a Zero-Forcing (ZF) algorithm was implemented for the channel estimation and equalization of the received data. For this purpose, 21 pilot sub-carriers multiplexed with the data subcarriers were also transmitted. For the purposes of the current work, standard low-complexity processing algorithms were employed, to upgrade to higher-order modulation formats as in [5.17], would require advanced synchronization techniques and FEC coding.

- **RF data converter functions:**

The RFSoC device is equipped with 8 DACs and equal number of ADCs supporting sampling rates up to 4Gbps. Moreover, each converter has its own dedicated digital datapath implementing DSP blocks, such as interpolation, decimation filters and digital mixers to up-/down-convert from/to baseband. The programmability of the Analog Mixed Signal (AMS) blocks offers the ability to process real or complex signals and support multi-band operation.

- **Electro-optic interfaces:**

Highly linear optoelectronic units were used to realize an IM/DD communication strategy for the optical segment. In more detail, the use of an Electro-absorption Modulated Laser (EML)-based analog IFoF transmitter was selected as a cost effective, integrated solution that has been extensively proposed for the emerging densified 5G network topologies [5.18]. Commercial off-the-shelf photoreceivers were used to detect the analog optical signals, providing thereby the radio waveforms to the mixer stages of mmWave boards. As such, specific power consumption details of each stage of the transceiver are presented in Table 7. Apparently, the conversion of the digital streams to analog signals and vice-versa is the most power consuming process.

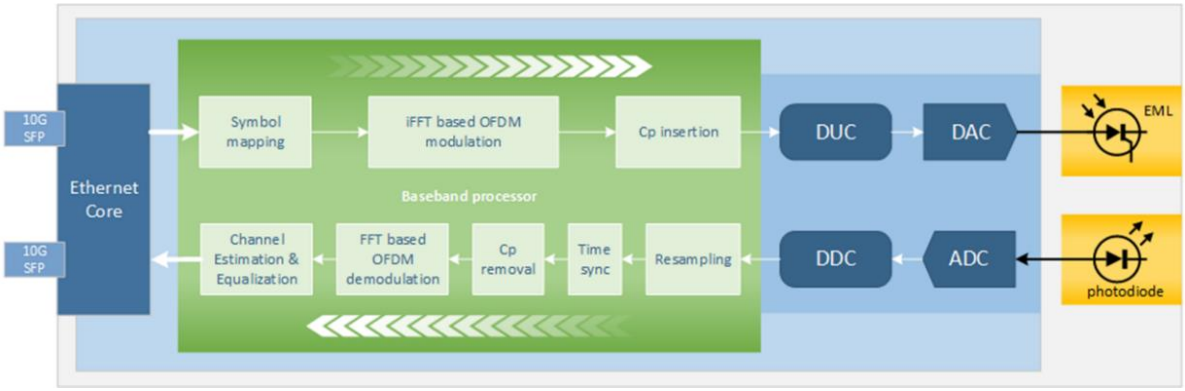

Figure 53. A-IFoF transceiver developed on state-of-the-art Xilinx RFSoC board, interconnected with 10GHz electro-optic units.

The evaluation of the presented A-IFoF transceiver design was initially per-formed through latency and power-consumption measurements (Table 7). The execution time for the accomplishment of the transmitter-side processing functions for each stream was measured to be 5usec, and the execution time for the receiver-side pro-cessing was found to be 9usec. Given that the wireless signal propagation delay is negligible, compared to the fiber transmission delay (5us/km for Standard Single Mode Fiber (SSMF)), the fiber transmission length is the main contributing factor to the total delay budget of the experiments. As a result, even for Ultra- Reliable and Low-Latency Communication (URLLC) applications with up to 100usec latency requirements for one way transmission delay [5.6], optical propagation distances up to 18 km can be sup-ported by our presented solution. Furthermore, the power consumption of the technology solutions involved in A-IFoF-based transport implementations is a key feature. As such, specific power consumption details of each stage of the transceiver are presented in Table 7. Apparently, the conversion of the digital streams to analog signals and vice-versa is the most power consuming process of the RFSoC, whilst the RF amplifications connected to the electro-optic components also contribute a fair share in the power consumption.

Table 7. Power consumption per TxRx unit

	Unit	Power Consumption (Watt)
RFSoC	FPGA fabric	2.3
	CPUs (used for signal performance monitoring)	2.7
	RFSoC clocks	1.2
	DAC/ADC units	3.3
Electro-optic modules	Optical modulation	2.07 (Driver) + 0.2 (EML)
	Photoreceiver	1.5

5.1.2 SDN-powered Management & Control Plane

The control plane of the developed TxRx unit, relies on a commercially available NC card [5.19], which was integrated into the setup via three different interfaces, the internet gateway (used for signaling with the open daylight controller), the Active Optical Cable (AOC) connection with the MNO components, and the AOC connection with the baseband processor's ports. The selected NC card features a number of capabilities that are of key essence to the selected experimental setup: a) multi-linux-Operating System (OS) support (to allow for easy installation in the master and slave flexbox nodes and b) hardware-accelerated Open Virtual Switch (OVS) implementation for very low latency execution of the OVSDB signaling commands and c) support for optical (SFP28) ethernet ports. The proprietary framework supported by the NC allowed to offload the datapath by programming the NC embedded switch and avoiding the need to pass every packet through the processor cores. The control plain remains the same as working with standard OVS. Two individual NC cards were employed, to host management and control layer operations, both at the BBU and the remote radio sites, thus enabling full-duplex connectivity.

For the implementation of management and control plane functionalities, the OVS L2 virtualization software was installed in a master and slave, desktop-grade pcs (using ubuntu 20.04 Server Lts) to allow for the generation of virtual L2 ports that will be used to manage the configuration of the uplink and downlink data flows of both the master and slave node. The physical (actual) ports of the nodes for the implementation of 802.1Q encapsulation and the control of the VLAN tagging mechanism, which was the method used for the routing of the legacy equipment's traffic over either one or two data lanes throughout the RFSoC platform. Essentially, the activation of a second data lane enabled the duplication of the traffic rate that could be supported by the analog TxRx.

The configuration of the OVS system was based on primitives such as the generation of a virtual switch for a virtual interface as well as management of queues and rules for the Downlink (DL) and Uplink (UL) direction. The original network input/output port is bridged in the OVS system using a virtual interface. There it is split into 2 different directions for the uplink and downlink traffic (different VLAN tags). Both flows are then connected to an actual port, i.e. the optical interfaces of the setup. The optical interfaces that are linked towards the physical layer, act as a "trunk" for both the uplink and downlink VLANs. After the deployments of virtual and physical network layers, an L2 data bridge was established between the two virtual network interfaces, to support the proprietary 3GPP-based L2/L3 protocols. This enabled E2E internet/TCP connectivity of all the showcased services and applications.

In order to provide remote, cloud-based management of automatic VLAN configuration, the OVS at both BBU and remote radio sites was operated under external remote management mode, connecting each OVS to an external OpenDaylight controller, hosted in external, over-the-internet infrastructure. The employed server used the OpenFlow protocol to exchange management and measurement messages with underlying OVS nodes using the OVS

Database Server (OVSDB-SB) extension. In particular, the solution relies on two core open-flow message types: i) Measurements of the virtual switch's ports (Tx/Rx Bytes) which map to the "controller-to-switch read-state" messages and ii) Messages that alter the open-flow rules of the virtual interfaces, Match-Rules for the manipulation of incoming traffic (downlink) and Action-rules for outgoing traffic (uplink), respectively – mapped in "Controller-to-switch Modify-State messages". The OpenDaylight controller acts as an abstraction on top of the open-flow layer (as well as the underlying south-bound protocol) and exposes a machine-friendly REST API mechanism (RESTConf) which allows for a programmatic manipulation of said parameters (read/write) via direct reference of their respective YANG model identifiers. For the purposes of this experimental setup, a preset mapping table between VLAN tags and functionalities allowed for different experimental scenarios to be tested. An example of such mapping that was used was VLAN tag 9 or 10 switching the downlink mode to single or dual lane. The same effect was also applied in the uplink virtual interface, using the VLAN tags 0 and 1. To be noted that, while for the sake of these demonstration activities, a preset (hard-coded) mapping table was used, a dynamic mapping table methodology has also been evaluated. After this connectivity had been established, the OpenDaylight controller exposed all the underlying component information via the RESTConf module, which provided a REST Application Programming Interface (API) that can be used for connection by external client software.

The Network, Planning and Orchestration (NPO) tool was the final component of the setup which used a Hypertext Transfer Protocol client to the RESTconf interface of OpenDaylight controller to provide a separate management and analytics plane for manual inspection/control, as well as a sandbox for developing closed management loops that employed analytics to perform management actions. The API provided full L2/L3 metric visibility of the underlying link to the NPO software, which was designed so as to allow users and applications access to the full operational context of the analog link. The developed setup could thus support intelligent algorithms and functionalities from commodity Ethernet infrastructure to be operated also on traffic stemming from A-IFoF/mmWave interfaces to (a) signaling traffic overhead analysis, (b) traffic profiling of the various applications hosted and (c) configuration and performance of the dynamic capacity de-/aggregation. As a monitoring solution, the NPO tool is applying the best practices with respect to the processing overhead of the actual data plane of the experimental setup. By utilizing the measurement values provided by RESTConf from the OpenDaylight Northbound interface, the NPO tool creates a 'digital twin' of each of the virtual network interfaces that can be accessed by client applications to acquire the latest measurement values. The visualization software (based on open-source typescript/javascript frameworks running on web browsers) as well as the intelligence algorithms (stand-alone java applications) are producing signaling load isolated to the NPO backend. Using this approach, horizontal scaling of these clients is not producing additional overhead propagated to the actual data plane nodes. For the enforcement of the management actions (i.e. the activation / de-activation of the additional bandwidth-providing lane, direct invocation of the "Modify-State" must be invoked. The selected NC cards, however, provide hardware accelerated SDN support (including the manipulation of the openflow parameters) which produced undetectable delays (due to the actual OS processing

delay of the network traffic itself) and also no packet loss during the configuration action. A final note on the "digital twin" approach is that the detected "state" of each of the virtual interfaces is directly related to the 'refresh interval' of the digital twin. To reduce the measurement frequency, we increase the sampling rate, introducing delay on the identification of various action-triggering states (i.e. states with throughput higher than the pre-selected threshold). This can increase the error rate of decision-making algorithms especially for traffic bursts that span over amounts of time that are smaller than the sampling interval period.

5.2. Experimental evaluation of the real-time analog Fronthaul topology and live demonstrator deployment

In the following paragraphs the experimental evaluation of the envisioned real-time analog TxRx-based topology will be reported, including the performance of preliminary testing involving different converged fiber-wireless transport scenarios, the preparation and execution of the large-scale demonstrator and finally the discussion of the acquired results.

5.2.1 Experimental investigation of FPGA-based A-IFoF/mmWave transceiver integration in mobile infrastructure

In this section, the successful integration of the real-time analog transceiver over an existing mobile infrastructure is presented. Three alternative optical/wireless converged network topologies were investigated and successfully demonstrated: (a) FiWi, (b) Wireless-Fiber (WiFi) and (c) Fiber-Wireless-Fiber (FiWiFi).

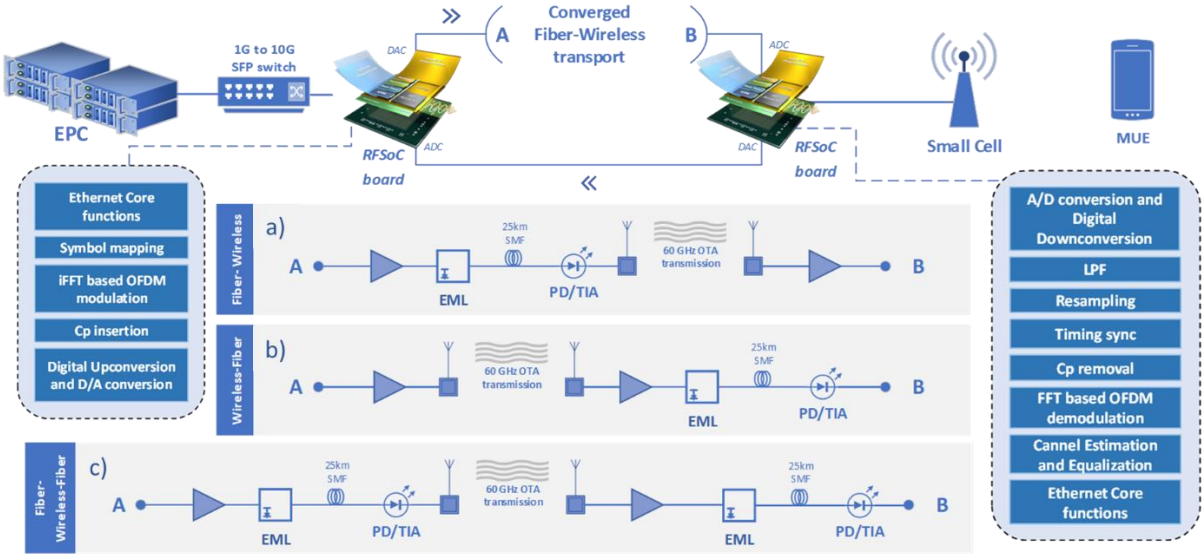

Figure 54. Experimental setup of (i) FiWi, (ii) WiFi and (iii) FiWiFi downlink segments of the FPGA-enabled EPC-to-Small cell interconnection.

Figure 54 shows the experimental set-up that was employed. The existing mobile infrastructure of Greece's largest Mobile Network Operator (MNO), (COSMOTE) was exploited, which among others included an Evolved Packet Core (EPC) and a Small Cell. Figure 55 depicts the fiber interconnection of the core equipment (located at the MNO's premises) and the access nodes (located at NTUA). Specifically, a pair of fibers stemming from COSMOTE premises is terminated at the NTUA's network operation center (NOC), which is located inside the NTUA campus. The length of each fiber was measured to be 22.65 Km and 17.5 Km, respectively. This link has also been characterized via OTDR measurements which indicated that the optical losses at 1550 nm were about 12.5 dB. Additionally, there is an extra fiber link that interconnects NTUA's NOC with the Photonics Communication Research Laboratory (PCRL) premises. This intra-campus link consists of six pairs of fiber. Each fiber length has been measured to be approximately 3 km with optical losses below 1 dB. This dark fiber deployment can be used to provide connectivity (also via switches at both sides) between the COSMOTE and the NTUA lab.

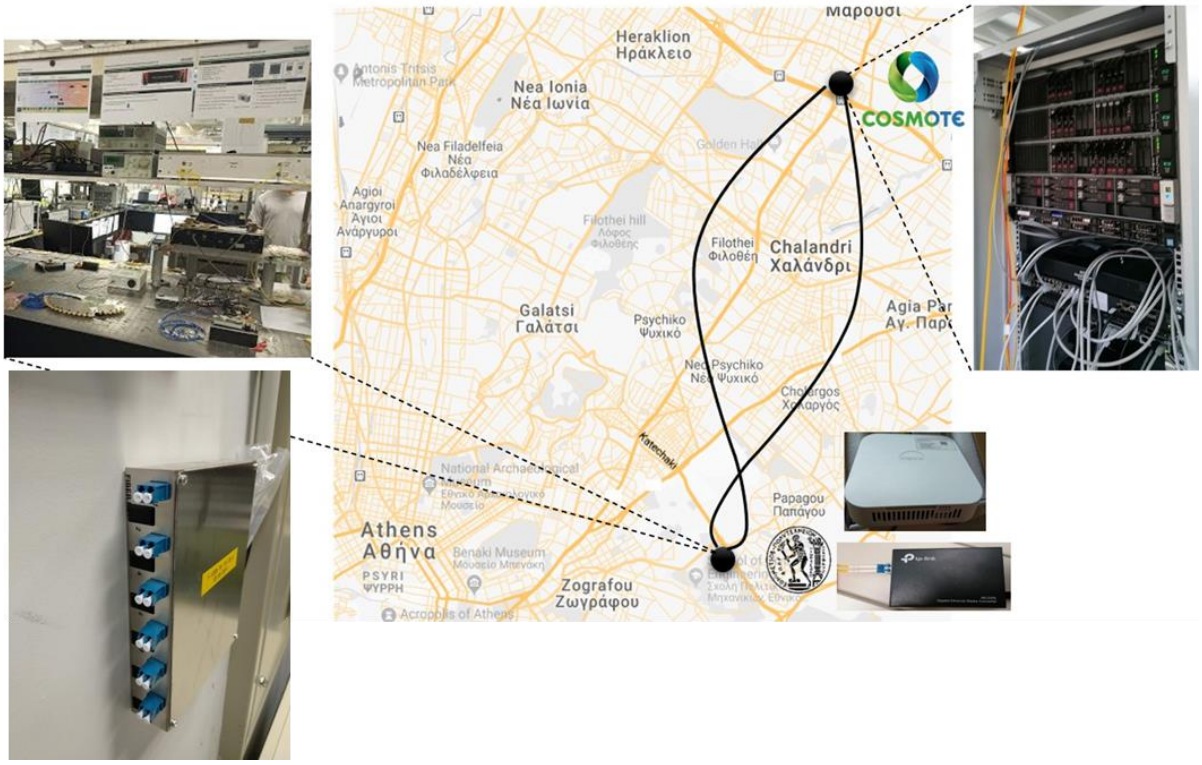

Figure 55. COSMOTE-NTUA premises interconnection – optical layer connectivity

Between these two network units, the FPGA-based analog TxRx unit emulated both Ethernet and signal processing functions of a Baseband Unit (BBU). In this experimental testing phase, the SDN capabilities of the TxRx were not utilized. More specifically, at this stage, the Ethernet core performed data link layer functionalities to map the incoming Ethernet traffic to the DSP engine, as well as, to recover Ethernet frames from the demodulated waveforms. These functionalities include basic error handling, flow control for access to the physical layer, frames encapsulation and Virtual Local Area Network (VLAN) taging. The RFSoC's FPGA engine generated and post-processed the OFDM waveforms that were propagated over the analog testbed. It has to be mentioned that the RFSoC implemented two independent and identical transmitter/receiver side DSP block chains and provided two pairs of DACs/ADCs, for the establishment of full-duplex connectivity. However, due to the lack of lab equipment, the investigated experimental layouts implemented only one signal direction (defined by A and B points in Figure 54), while in the other direction the IF signals were propagated over an electrical SMA cable.

The signals genereted in the RFSoC platform propagated in the fiber by exploiting highly linear Intensity Modulation/Direct Detection (IM/DD) opto-electronic units in three different optical-wireless network layouts. The FiWi and its symmetrical WiFi layout intended to emulate a bidirectional Fixed Wireless Access (FWA) scenario, while the extended FiWiFi layout served as a wireless bridge, interconnecting terminals of two spatially separated fiber transport segments [5.4], [5.20]. In the FiWi layout (Figure 54 (a)), the DAC output was amplified via a controllable gain amplifier and then used to drive the Electro Absorption Modulator (EAM) segment of an EML. The optical signal was transmitted over a 25 km fiber

spool of Standard Single Mode Fiber (SSMF) and detected by a 10G photoreceiver. The photoreceiver output was fed to an IF-to-V-band radio board. An identical Receiver-side antenna module located at 1 m horizontal distance was used to receive the mmWave radio waveforms and direct them to the ADC of the RFSoC after RF-to-IF down-conversion. Both commercial V-band radio boards operated at 60GHz

Regarding the WiFi layout, an inverted but symmetrical link to the FiWi layout was implemented, as depicted in Figure 54 (b). Finally, as shown in Figure 54Figure 56 (c), the FiWi layout was extended with an extra EML and a photoreceiver leading to the targeted FiWiFi layout. It should be also mentioned that the voltage input levels of all e/o and active RF components were carefully selected to ensure their linear operation.

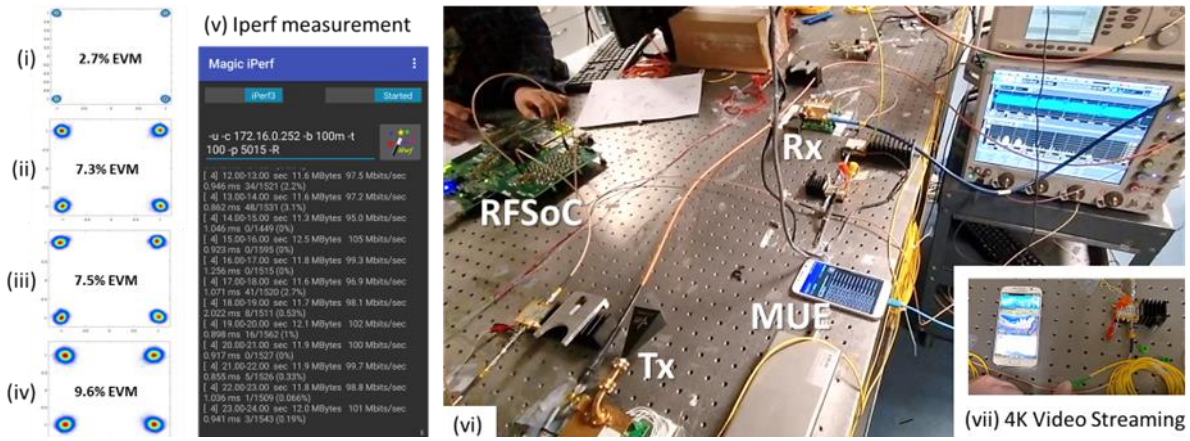

Figure 56. EVM measurements and constellation diagrams after (i) electrical back-to-back (ii) FiWi, (iii) WiFi and (iv) FiWiFi real-time transmission, (v) Iperf measurements of the FiWi segment, (vi) photo of the implemented testbed and (vii) screenshot of 4K video streaming

Figure 56 (i) - (iv) show the EVM results of the received IF signal after converged FiWi, WiFi and FiWiFi transmission, and the corresponding constellation diagrams after real-time processing. A photo of the actual setup is depicted in Figure 56 (vi). The initial signal generated by the RFSoC exhibited an EVM of 2.7% (Figure 56 (i)), while the use of the optical and RF modules through the FiWi setup introduced an EVM increase by 4.6%. As it was originally expected, the FiWi (Figure 56 - ii) and WiFi (Figure 56 - iii) transmission performance was similar, with an EVM offset of 0.2%. The identical EVM measurements in both links, is a strong indication that the active RF/optoelectronic units of the FiWi and WiFi testbeds were operating at their linear region. The extension of the FiWi link with an additional optoelectronic conversion stage, was responsible for an increase of the EVM value by 2.3% (Figure 56 - iv) compared to the FiWi case. Nevertheless, in all cases the transmission was well-bellow the 3GPP threshold of 17.5% EVM for successful demodulation of the QPSK modulation [5.21], indicating the robustness of the proposed analog IFoF/V-band/IFoF transport solution, thus its scale-up capabilities.

Aside from the physical layer performance metrics, the capability of the proposed solution to support real-world services over the MNO's infrastructure was assessed. To this end, for all previously described network layouts, a Mobile User Equipment (MUE) was used to perform

Iperf measurements, using Transmission Control Protocol (TCP) traffic, exhibiting 100Mbps stable connectivity (Figure 56 - v). Finally, 4K online video streaming (Figure 56 - vii), uninterrupted live IP-video teleconferences and web browsing were successfully demonstrated over the presented A-IFoF/mmWave network configurations.

5.2.2 Deployed Testbed of Live Demonstrator

The next step towards setting up the large-scale live demonstrator was to extend the testbed described in the previous section, by including the full capabilities of the analog TxRx, and especially the SDN reconfigurability functionality, and stress the capacity and real-time adaptability requirements of the unit, through integration with a highly demanding services/applications layer. The mobile services and applications on display could be reached by seamlessly combining the deployed analog transport layout with the MNO's mobile core equipment described in the previous paragraph.

More specifically, a plethora of advanced mobile services were (concurrently) demonstrated (e.g. Voice over LTE (VoLTE) and data services such as HD/4K real-time streaming, AR/VR applications, web-browsing and Internet of Things (IoT) applications), reflecting not only the needs of individual end-users but also entire vertical domains (e.g. physical security based on surveillance cameras, energy management/monitoring and any IoT domain). In brief:

- The establishment of full duplex e2e connectivity (access-analog transport-core) was verified
- The network performance (incl. handovers) was evaluated using various Apps (such as OOKLA Speedtest, nPERF, Magic-iPerf and COSMOtools) utilizing both public and private (iperf) servers
- The user’s experience (QoE) was assessed through the demonstration of single and concurrent (bandwidth hungry and low-latency) mobile apps/services
- The management and control layer of the SDN infrastructure was assessed, including: (a) setup configuration parametrization, (b) signalling traffic overhead analysis for the experiment and projections, (c) traffic profiling of the various applications hosted and (d) configuration and performance of the dynamic sub-band allocation SoN.
- The low energy consumption of the elements/nodes was measured and demonstrated.

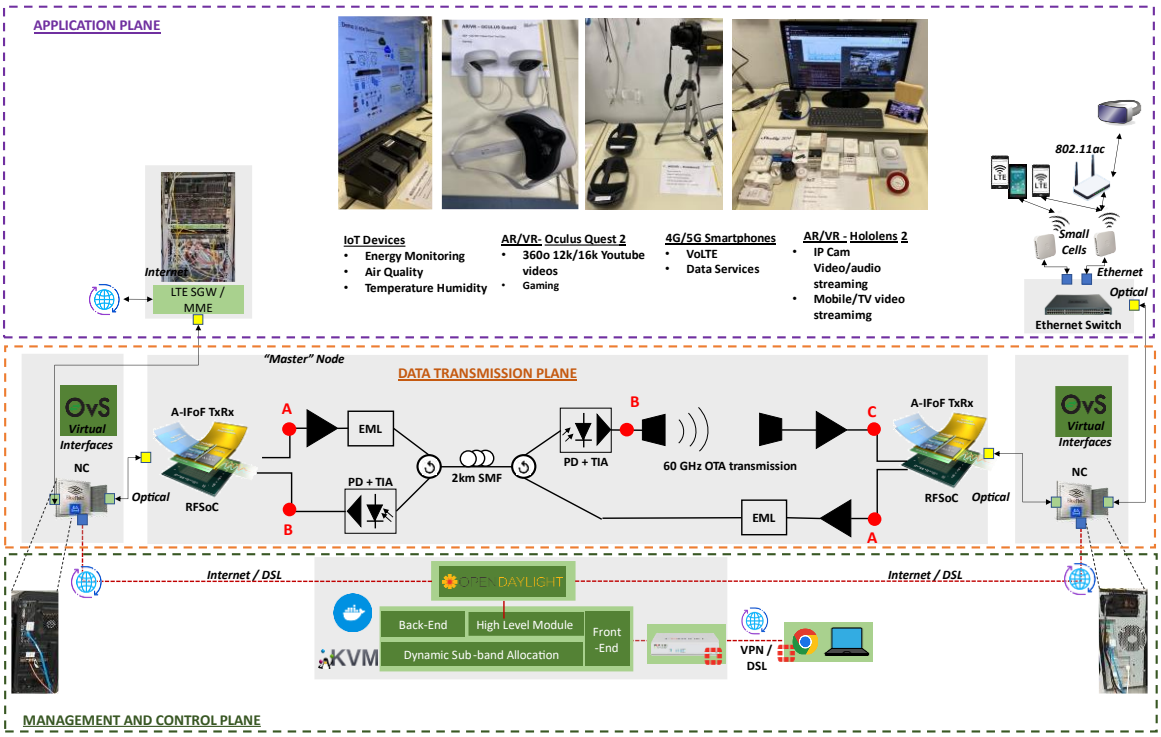

Figure 57. Experimental Demonstrator layout, involving the Data, Control and Services layers.

The mobile network infrastructure of the trial setup consisted of a fully-fledged Long Term Evolution (LTE) Core network and NOKIA's Flexi Zone Multiband Indoor 4G small cells (RAN part). The infrastructure was complemented with an Openstack multi-cloud infrastructure where applications were hosted. To validate the performance of the deployed A-IFoF transceivers-assisted transport network segment in the E2E deployment through performance evaluation of commercial applications running on top, the testbed also included: a COSMOTE TV Set-Top-Box (STB) for live video content provisioning, High Definition (HD) / 4K Internet Protocol (IP) and High Definition Multimedia Interface (HDMI) cameras to provide live footage, AR/VR Glasses (OCULUS Quest-2, HOLOLENS-2), as well as Internet-of-Things (IoT) devices including sensors, and Android/iOS smartphones/tablets. Carrier aggregation was also supported, so as to boost the RAN node capacity and as a result also to evaluate the active capacity reconfiguration capabilities of the TxRx and the maximum achievable throughput.

Figure 57 illustrates the E2E deployed setup including the physical-, the data management- and the application layers respectively. Considering the DL path, connectivity between the EPC (located at COSMOTE premises) and the Small Cell (located at National Technical University of Athens (NTUA) premises) was provisioned as follows: the EPC traffic towards the Small Cell was fed to the NC, via a dedicated dark fiber link, interconnecting the two remote locations, via standard Small Form-factor Pluggable (SFP) interfaces and then was carried forward to the FPGA fabric, as well the A/D and e/o interfaces. More specifically, the DAC output was amplified and fed to a (CANGLONG CEB510 series) Electro-absorption Modulated Laser (EML) emitting at 1560.42nm. The optical signal was transmitted over a 2 km fiber spool of Single Mode Fiber (SMF) and was detected by a (Discovery

Semiconductors DSC-R402) 10G linear InGaAs photoreceiver. The photoreceiver output was connected to the IF-to-V-band upconverter board (Gotmic gTCS020B). The upconverter output was interfaced with a directional Tx- pyramidal gain horn V-band antenna, featuring 23 dBi gain and 10° beamwidth, through a WR15 waveguide. An identical Rx-side radio unit (Gotmic gRCS016B) located at 1 m horizontal distance received the mmWave radio waveforms, and the down-converted radio waveforms were then directed to the ADC unit. The limitation on the transmission distance of the mmWave link was due to several factors, including space constraints, the length of RF cables, and the presence of a complex indoor environment with surrounding objects. However, it was demonstrated that the same mmWave link could effectively operate at a distance of 7 meters [5.11], while other mmWave deployments have showcased wireless transmission distances of up to 200 meters [5.22], in line-of-sight (LOS) condition.

The received IF upconverted waveforms were processed through the receiver-side DSP chain developed on the FPGA-based A-IFoF TxRx. The bitstreams were then converted to Ethernet traffic and forwarded to the NC and finally to a Small Cell, which offered access to mobile user equipment. For the establishment of bidirectional connectivity, a symmetrical Wireless-Fiber link should be employed, providing backwards communication of the Small Cell with the EPC. Due to limitations related to equipment availability, a symmetrical optical link was used for the implementation of the UL path of this setup. The experimental evaluation of the corresponding Wireless-Fiber link is provided in [5.23], indicating similar EVM performance of the Fi-Wi and Wi-Fi paths. The EML that was employed for the implementation of the UL direction was emitting at 1540nm, allowing the co-transmission of both directions in a single fiber. The multiplexing of the DL and UL optical paths in the same fiber core was achieved by using two low-loss optical circulators, as depicted in Figure 57.

To showcase the network's adaptation to traffic demands overcoming the capacity limits of small cell connectivity, two additional pairs of the A-IFoF TxRx's DAC and ADC units were employed, for the parallel implementation of a second bidirectional link. This identical analog RoF link was used to provide traffic to a second Small Cell and was dynamically activated, via the SDN controller, when the traffic demand exceeded the capacity of a single Small Cell, and accordingly deactivated when the demand was reduced. As a next step, the employment of external analog mixing modules, or electro-optical units emitting at slightly different lamdas, can enable the co-transmission of the parallel traffic lanes, over shared fiber or fiWi infrastructure.

Figure 58 depicts pictures of the deployed setup for the performed live demonstrator.

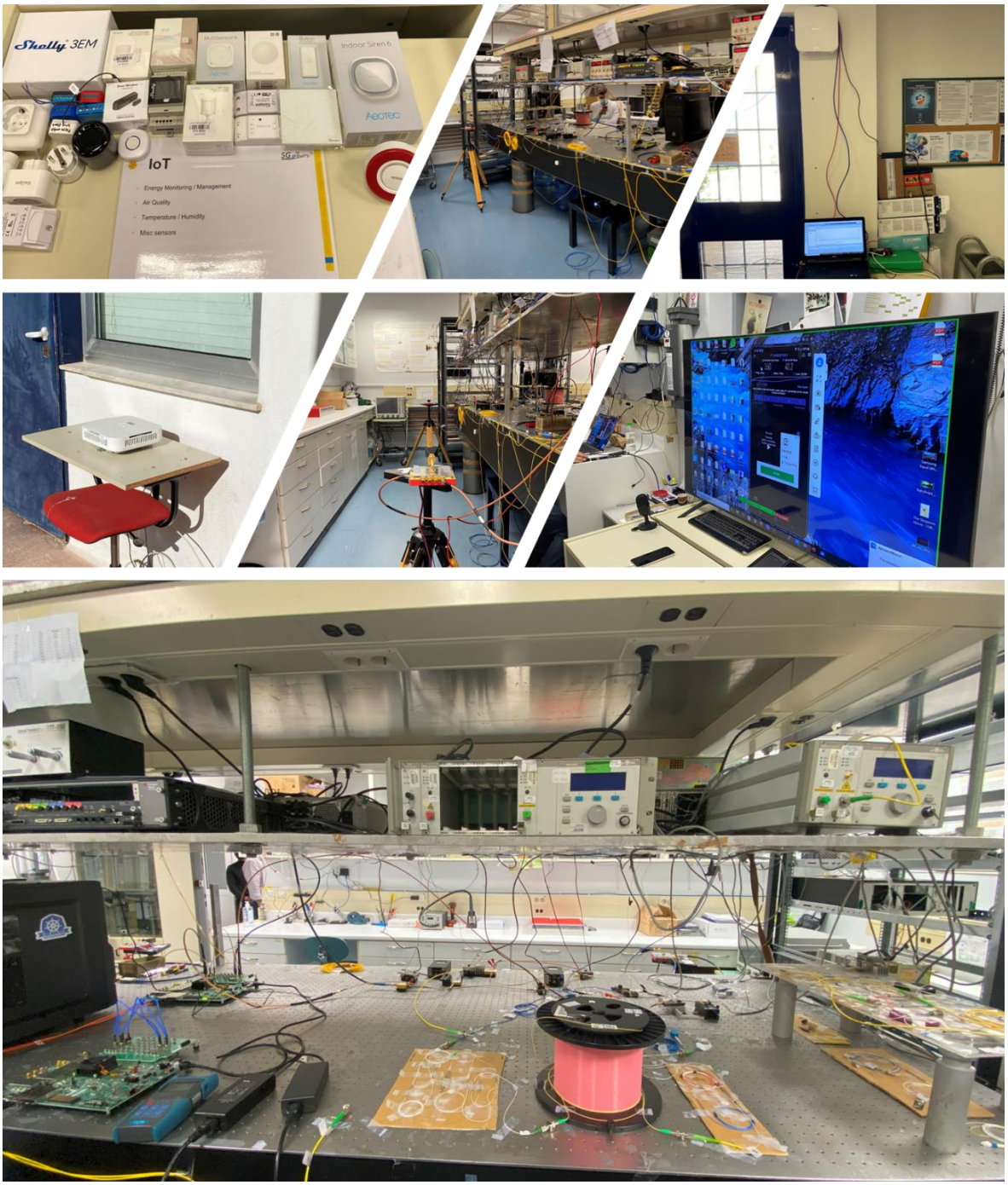

Figure 58. Pictures of the live demonstrator testbed.

5.2.3 Experimental Results and Real-Time Demonstration of Mobile Services

The first step towards examining the performance and functionality of the deployed testbed was to evaluate the quality of the analog waveforms that were propagated over the A-IFoF/mmWave transport deployment, after processing through the employed TxRx unit. The physical layer evaluation results are presented in Figure 59. The EVM measurements and the constellation diagrams were derived after real-time processing of the signals detected at the DACs' outputs (point A), after fiber (point B), corresponding to the UL and FiWi, transmission (point C) corresponding to the DL direction and indicate successful signals' retrieval (EVMs of 2.7%, 5.7% and 7.3% respectively). The measured EVM values are in all cases well below the requirement of 17.5% set by 3GPP for QPSK signals [5.21], validating the preservation of signal's integrity over the Fiber and FiWi analog transport segment, as well the possible adoption of up to 64QAM (EVM<8%) modulated signals in the presented testbed. Figure 59 also presents the EVM measurements that were obtained after using a Variable Optical Attenuator (VOA), to reduce the optical power at the input of the photoreceiver. After extended measurements the received EVM performance indicates successful signal retrieval for optical power levels above -28 dBm.

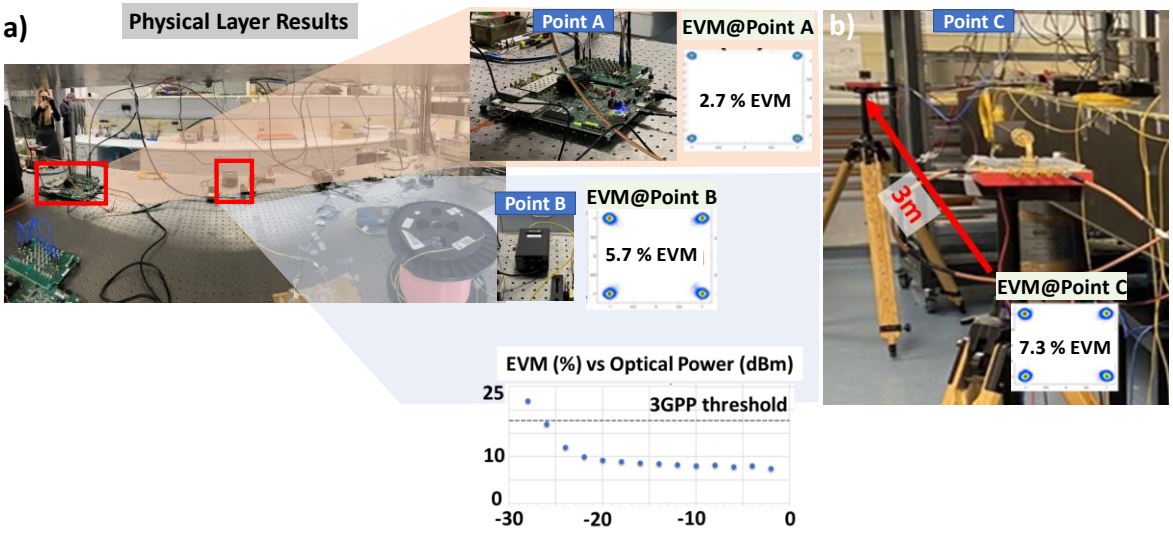

Figure 59. (a) Constellation diagrams and EVM measurements at the DACs' output (point A), Fiber (point B), and Downlink (point C) transmission, and (b) EVM measurements after FiWi transmission, after reducing the received optical power.

The next step was to assess the impact of the analog fiber-wireless link on the transport segment between a mobile network EPC and RAN node (Small Cell). The conducted demonstrator evaluated the proper operation and the multi-subband performance of the analog FiWi transport network through the use of a series of services and investigated whether there is any possible impact on the QoE after the integration/intervention of the A-IFoF-based link in an E2E mobile network. All services aim at:

- Verifying the establishment of full duplex E2E connectivity between commercial 4G Small Cells and the EPC/IMS testbed of COSMOTE over the employed analog network and correct establishment of voice and data calls from commercial smartphones.
- Demonstrating the proper operation of concurrent mobile services (VoLTE calls, HD/4K video streaming, AR/VR services, IoT services, etc.) over the deployed infrastructure.
- Verifying that the intervention of the alternative transport infrastructure (R-RRH, SL-RRH, analog TxRx units) does not have any negative impact on the mobile network performance and QoE.

At first, network performance-related tests were conducted (using various Apps such as OOKLA Speedtest, nPERF, Magic-iPerf and COSMOtools) utilizing both public and private (iperf3) servers, including handovers. The following performance-related measurements have been gathered at both test sites (MNO and NTUA premises), regarding:

- Max DL/UL bitrate (TCP/UDP) vs. distance from the Base Station (small cell)
- Max DL/UL bitrate (TCP/UDP) vs. Reference Signal Received Power
- Latency vs. distance from the Base Station (small cell)
- Latency vs. Reference Signal Received Power

Throughout the demonstrator, zero deterioration on the performance of the hosted services was noticed, indicating the flawless operation of the E2E deployment. On top of the user's experience, the performance assessment has been based on specific network performance tests, from which it can also be easily verified that the presented solution not only is capable of addressing the strict requirements of demanding real-time applications but also it can guarantee no impact on the QoE of the user. Figure 60 depicts the maximum achievable throughput (measured through Iperf and Ookla traffic monitoring tools) is limited by the Small Cell's capacity reaching 245Mbps DL and 190Mbps UL which was measure via live bandwidth measurements. In addition, these measurements were also performed during UE handover between two Small Cells, indicating smooth recovery of the achievable data rate, hence unimpacted operation of the E2E deployment, as well the correct operation of RAN's critical Control-Plane.

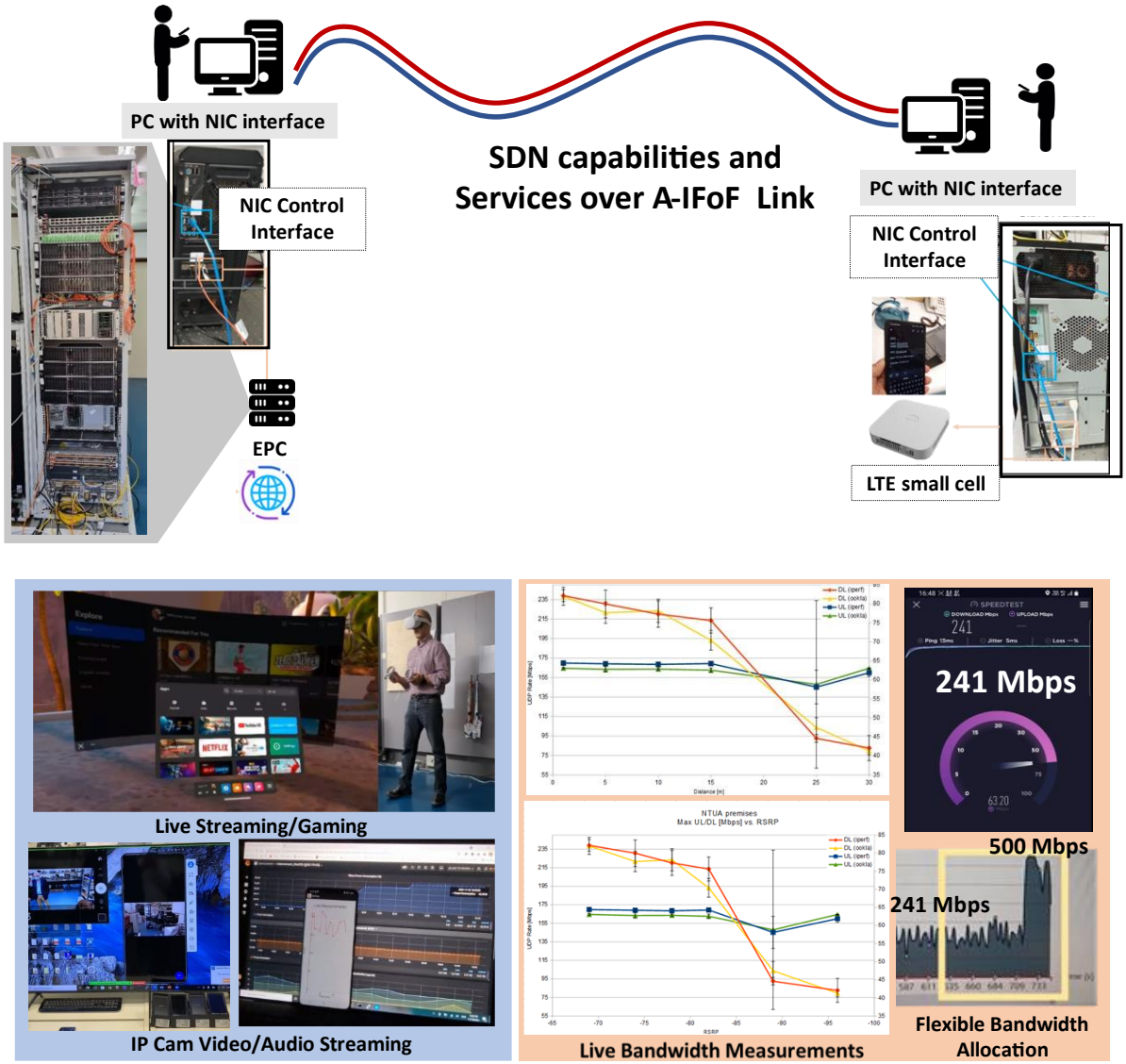

Figure 60. Service/Control layer evaluation of analog TxRx interface, including: Dynamic capacity reconfiguration, Live latency/bandwidth measurements, Live Bandwidth measurements, and Demonstration of the uninterrupted operation of AR/VR gaming, 4K video streaming, and IP videos, over the presented deployment.

Figure 61 shows some screenshots taken by the mobile UE that was used throughout the demonstrator to run the aforementioned traffic monitoring applications.

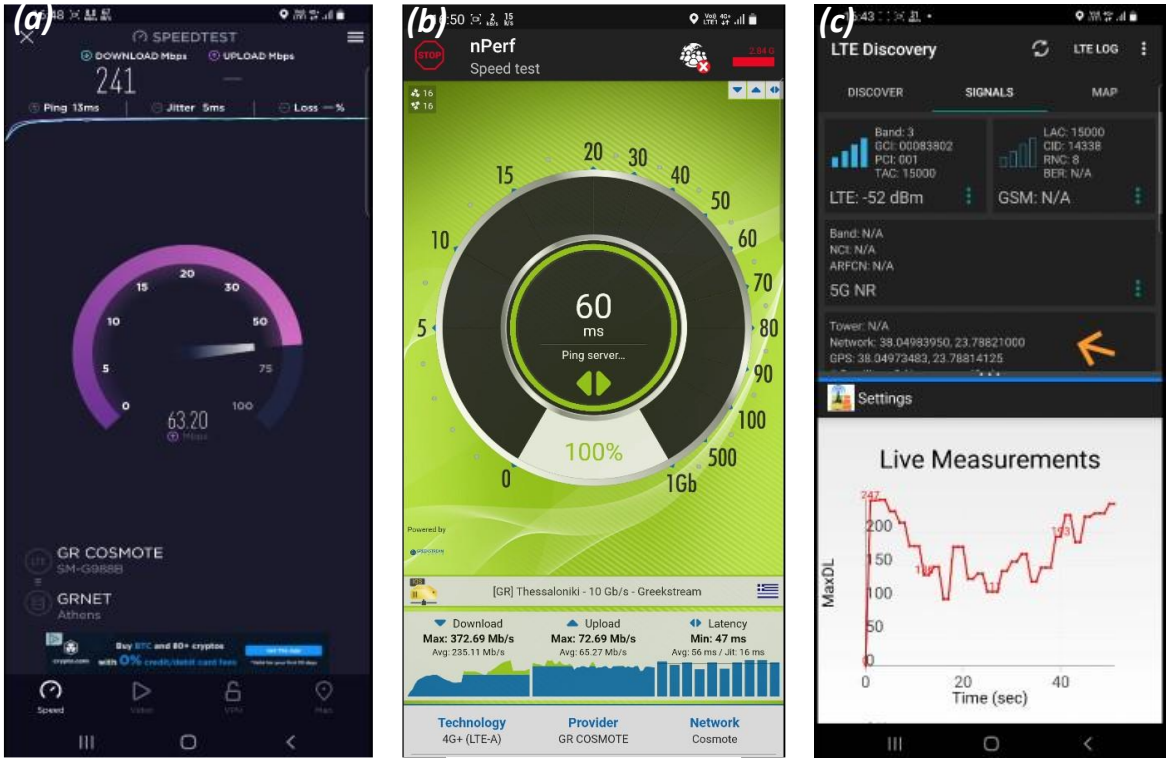

Figure 61. (a) Max UL/DL bitrate, (b) Latency and Jitter, and (c) Handover test between the 2 small cells installed at NTUA premises.

Finally, the SDN-controlled dynamic, capacity de-/aggregation of the A-IFoF TxRx was demonstrated. More specifically, through constant monitoring of the traffic profile via the NPO tool, the developed SDN controller activated a second transmission channel, supported by the implemented A-IFoF TxRx to adjust the available bandwidth, when requested. For demonstration purposes, the second deployed channel relied on a bidirectional RF link, interconnecting an independent pair of DACs and ADCs. The aggregated throughput supported by this solution reached 474Mbps, fully exploiting the capacity of two Small Cells, operating concurrently. Figure 60 represents the instant duplication of the transport layer capacity after maximization of the throughput request of both Small Cells, monitored by the NPO tool. During the dynamic capacity duplication, network traffic measurements were captured on the OpenDaylight controller to monitor the status of the link. Given that high delay values would cause out of context decision-making and make the network optimization ineffective, the data sampling parameter of the link capacity optimization function was closely related with the Round-Trip Time (RTT). After analysis of the logging derived from the operation of the algorithm, we noticed that for a preset interval of 5000ms (5s) we got delay values of 5050+-25 ms which resulted in actual RTT of ~ 68ms. This value is two orders of magnitude different than the sampling rate and therefore confirms that the RTT delay does not affect the dynamic subband allocation algorithm. Finally, The RTT delay inserted by the SDN monitoring/capacity de-/aggregation tool, in addition to the Tx and Rx baseband processing time, corresponding to 5usec and 9usec respectively correspond to minor delay insertion to the total delay budget of the data propagation, well explaining the uninterrupted operation of the E2E deployment and the successful delivery of the mobile services.

Figure 62 depicts indicative pictures of the varying applications and services that were employed either individually or concurrently throughout the demonstrator.

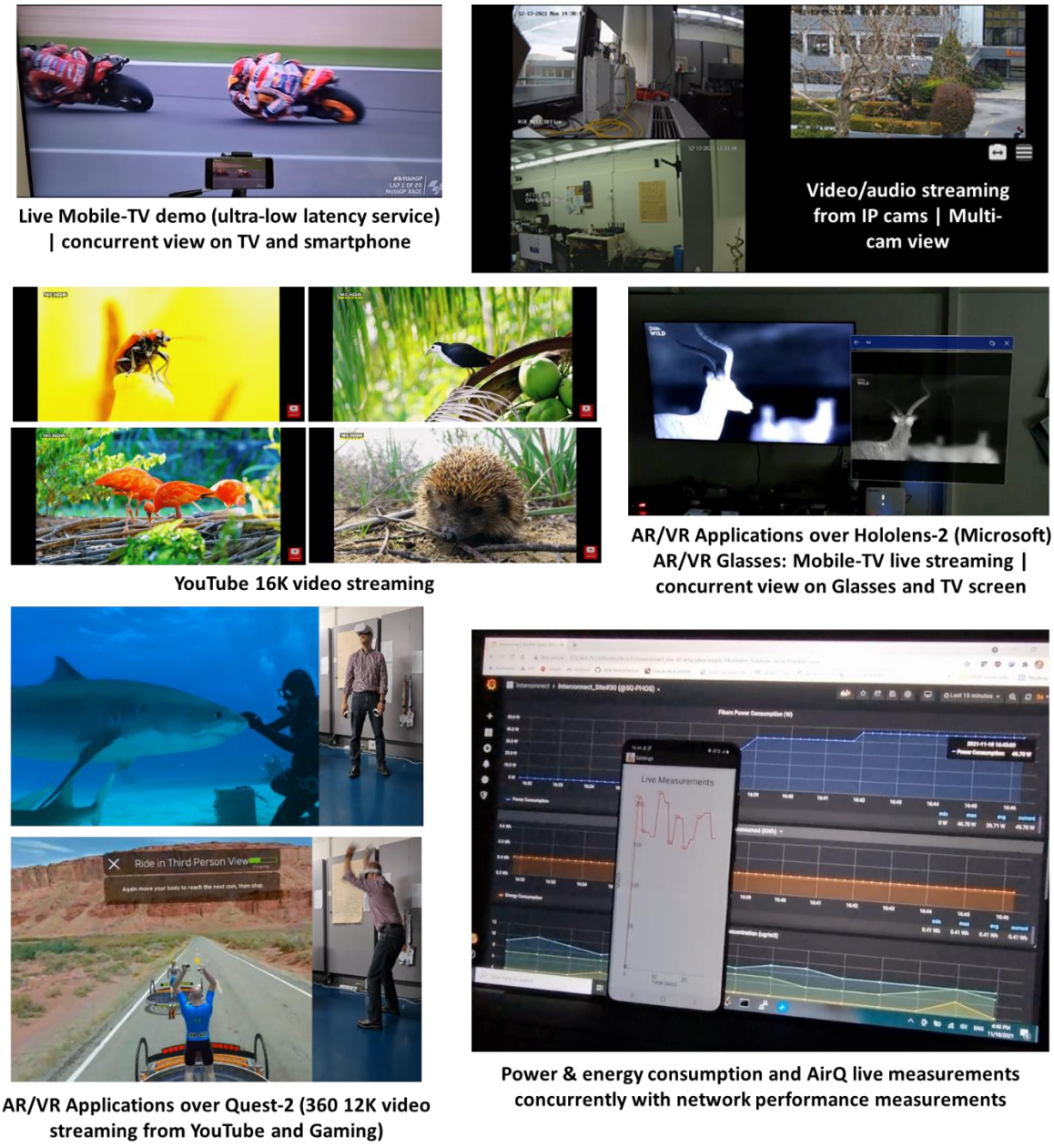

Figure 62. Indicative pictures and screenshots of the different hosted applications.

References

[5.1] Argyris, N., et al. “A 5G mmWave Fiber-Wireless IFoF Analog Mobile Fronthaul Link With up to 24-Gb/s Multiband Wireless Capacity.”, J. Light. Technol. 2019, 37, 2883–2891.

[5.2] M. Sung, J. Kim, S. Cho, H. S. Chung, J. K. Lee and J. H. Lee, "Experimental Demonstration of Bandwidth-Efficient Indoor Distributed Antenna System based on IFoF Technology supporting 4G LTE-A and 5G Mobile Services," 2018 Optical Fiber Communications Conference and Exposition (OFC), 2018, pp. 1-3.

[5.3] S. Rommel et al., "Real-Time Demonstration of ARoF Fronthaul for High-Bandwidth mm-Wave 5G NR Signal Transmission over Multi-Core Fiber," 2020 European Conference on Networks and Communications (EuCNC), 2020, pp. 205-208, doi: 10.1109/EuCNC48522.2020.920092.

[5.4] A. Bekkali, T. Kobayashi, K. Nishimura, N. Shibagaki, K. Kashima and Y. Sato, "Performance evaluation of real-time 10GbE data connectivity over a converged IF-over-Fiber links and millimeter-wave wireless bridge," 2017 IEEE International Conference on Communications (ICC), 2017, pp. 1-6, doi: 10.1109/ICC.2017.7996427.

[5.5] M. Sung, S. -H. Cho, J. Kim, J. K. Lee, J. H. Lee and H. S. Chung, "Demonstration of IFoF-Based Mobile Fronthaul in 5G Prototype With 28-GHz Millimeter wave," in Journal of Lightwave Technology, vol. 36, no. 2, pp. 601-609, 15 Jan.15, 2018, doi: 10.1109/JLT.2017.2763156.

[5.6] Kanta, K.; Pagano, A.; Ruggeri, E.; Agus, M.; Stratakos, I.; Mercinelli, R.; Vagionas, C.; Toumasis, P.; Kalfas, G.; Giannoulis, G.; et al. Analog fiber-wireless downlink transmission of IFoF/mmWave over in-field deployed legacy PON infrastructure for 5G fronthauling. IEEE/OSA J. Opt.

[5.7] Y. Alfadhli et al., "Real-Time FPGA Demonstration of Hybrid Bi-Directional MMW and FSO Fronthaul Architecture," 2019 Optical Fiber Communications Conference and Exhibition (OFC), San Diego, CA, USA, 2019, pp. 1-3.

[5.8] Muñoz, R., et.al, “Experimental demonstration of advanced service management in SDN/NFV Fronthaul Networks deploying ARoF and PoF.” ECOC 2019. https://doi.org/10.1049/cp.2019.1191.

[5.9] E. Datsika et al., "SDN-Enabled Resource Management for Converged Fi-Wi 5G Fronthaul," in IEEE Journal on Selected Areas in Communications, vol. 39, no. 9, pp. 2772-2788, Sept. 2021.

[5.10] A. Rostami, Kun Wang, Z. Ghebretensaé, P. öhlén and B. Skubic, "First experimental demonstration of orchestration of optical transport, RAN and cloud based on SDN," 2015 OFC, pp. 1-3.

[5.11] C. Vagionas et al., "End-to-End Real-Time Service Provisioning Over a SDN-Controllable Analog mmWave Fiber -Wireless 5G X-Haul Network," in Journal of Lightwave Technology, vol. 41, no. 4, pp. 1104-1113, 15 Feb.15, 2023, doi: 10.1109/JLT.2023.3234365.

[5.12] https://www.rfwireless-world.com/5G/5G-NR-FFT-Size-Sampling-Time-Subcarriers.html
[5.13] Al-jzari, Amar & Iviva, Kostanic, “Cyclic Prefix Length Determination for Orthogonal Frequency Division Multiplexing System over Different Wireless Channel Models Based on the Maximum Excess Delay Spread.” American Journal of Engineering and Applied Sciences. 8. 82-93, 2015. 10.3844/ajeassp.2015.82.93.
[5.14] https://portal.3gpp.org/desktopmodules/Specifications/SpecificationDetails.aspx?specificationId=3804
[5.15] Simon Bicaïs,Jean-BaptisteDoré,MajedSaad,MohammadAlawieh,FaouziBader,etal., “Wireless connectivityinthesub-THzspectrum:Apathto6G.”, [ResearchReport]CEA-Leti;CentraleSupélec; Siradel; ANFR.2021. hal-03525602.
[5.16] Mohseni, Saeed, "Study the Carrier Frequency Offset (CFO) for Wireless OFDM" (2013). Electronic Theses and Dissertations. 438. https://digitalcommons.du.edu/etd/438.
[5.17] Chen, Ming & Chen, Lin. (2015). Real-Time Demonstration of 1024-QAM OFDM Transmitter in Short-Reach IMDD Systems. Photonics Technology Letters, IEEE. 27. 824-827. 10.1109/LPT.2015.2392797.
[5.18] B. G. Kim, S. H. Bae, H. Kim and Y. C. Chung, "RoF-Based Mobile Fronthaul Networks Implemented by Using DML and EML for 5G Wireless Communication Systems," in Journal of Lightwave Technology, vol. 36, no. 14, pp. 2874-2881, 15 July15, 2018.
[5.19] NVIDIA® Mellanox® BlueField® SmartNIC for Ethernet https://network.nvidia.com/files/doc-2020/pb-bluefield-smart-nic.pdf
[5.20] S. Koenig et al., "20 Gbit/s wireless bridge at 220 GHz connecting two fiber-optic links," in IEEE/OSA Journal of Optical Communications and Networking, vol. 6, no. 1, pp. 54-61, Jan. 2014, doi: 10.1364/ JOCN.6.000054.
[5.21] 3GPP specification TS 38.201, NR; Physical layer; General description, April 2017.
[5.22] Tirdad Sowlati et. al. “A 60-GHz 144-Element Phased-Array Transceiver for Backhaul Application”, IEEE Journal of Solid-State Circuits, Vol. 53, Issue 12, Dec. 2018.
[5.23] Kanta, K.; Toumasis, P.; Tokas, K.; Stratakos, I.; Papatheofanous, et al., “Demonstration of a Hybrid Analog–Digital Transport System Architecture for 5G and Beyond Networks”, Appl. Sci. 2022, 12, 2122. https://doi.org/10.3390/app12042122.

CHAPTER 6.
Conclusions and discussion on potential future research extensions

This chapter wraps up the present thesis by highlighting the key points discussed in each section of this document. As a step forward, the document explores research extensions aimed at enhancing the presented concept and moving it closer to practical deployment in future mobile networks.

6.1. Summary of the presented work and conclusions

As presented in the **first chapter** of this document, over the past three decades, significant advancements have occurred in wireless communication, in the transition from 1G to 4G, to meet the demands for high bandwidth and extremely low latency. The advent of 5G is driven by the continuous tightening of mobile networks' requirements by offering extremely high data rates, enhanced Quality of Service (QoS), low latency, extensive coverage, high reliability, and economically feasible services. To this direction, the evolution of the optical RAN infrastructures, as well the available optical interfaces and technologies that can support the migration to future mobile networking plays a crucial role.

During the past years, the RAN equipment has adopted innovative designs to address these challenges. To alleviate the demands on these specifications, diverse functional splits of the RAN machine have been established. Additionally, novel network segments, namely fronthaul, midhaul, and backhaul, are now defined as X-Haul links connecting the radio equipment to the core network. The high cost or complexity of hosting fully updated RAN equipment at the antenna site led the transition to C-RAN network layouts. At the same time the migration to new interfaces, including CPRI enhancements as well the adoption of completely new transport technologies, including the A-RoF scheme serves as a potential solution to overcome the limitations of current RAN deployments. Benefiting from the legacy of PON networking, the reuse of the abundant transceiver and fiber installations in metropolitan areas, concurrently with WDM- And TDM-based traffic aggregation, in synergy with advancements in SDN networking can further increase the cost efficiency and capacity performance of X-Hauling and provide suitable network solutions, capable of efficiently supporting the services and applications envisioned in the beyond 5G era.

In **Chapter 2,** the concept of Digital Signal Processing (DSP)-assisted optical transmission capable to support analog MFH is discussed. This RoF concept aims to alleviate the bandwidth limitations of the 5G MFH through the use of analog optics, which can carry native wireless data signals via installed fibers. It introduces this ambitious analog concept within the 5G landscape emphasizing structural changes and challenges that analog MFH attempts

to address. In the next paragraphs, the architectural shift towards Centralized Radio Access Network (C-RAN) topologies is thoroughly discussed, which put the traditional digital MFH transport on the question**.** The DSP-enabled Analog architecture supporting the MFH is then presented, focusing on the digital functions undertaken from a powerful centralized DSP engine.

The next paragraphs focus on the Analog RoF-based optical transport alternatives, presenting the basic idea behind this scheme and then moving on to a more conceptual view of an indicative A-RoF architectural structure. The main benefits related to A-RoF and A-IFoF deployments are then discussed, while a more thorough description of the various optical methods that are available for generating and transmitting analog radio signals through fiber is provided. Moreover, RoF systems rely on the transmission of analog signals through optical fibers, thus their performance is often constrained by several impairments, including optical fiber chromatic dispersion, phase noise, and nonlinearity, which is the main constraint related to widely adopting these schemes in actual mobile networks. Following the discussion of analog-based fiber advancements towards future mobile RAN installations, the migration to mmWave technologies, as promising candidate access points, but also as possible fiber extensions for flexible and scalable X-haul implementations is introduced. More specifically, an architectural view of mmWave-based fiber-wireless bridges for mobile transport deployments, as well the main challenges and motivations associated with the employment of mmWave links are examined. Finally, initial results from preliminary experiments aiming at the verification of the proposed A-RoF solution for realistic fronthaul scenarios are also included.

Chapter 3 explores in depth the domain of modulation and signal processing techniques, crucial elements supporting analog fiber/fiber-wireless transport transmission. Within this chapter, an extensive exploration of modulation techniques in mobile communication systems is presented. This involves a detailed comprehension of digital modulation methods, including single carrier digital modulation and the OFDM scheme, unveiling the fundamental principles underpinning effective signal modulation in the context of mobile communication. The focus then transitions to multi-carrier candidates for 5G and beyond mobile communication, providing an overview of varying candidates that promise to evolve the landscape of mobile communication systems. A systemic comparison of these formats based on their applicability for indicative actual use case scenarios is also provided.

The next paragraphs focus on actual algorithmic implementation and for this purpose the focus is put on CP-OFDM waveform, which has been adopted for the investigation of an end-to-end A-IFoF transceiver implementation, experimental evaluation, and integration into varying analog transport segments, as it will be extensively presented in the following chapters. Finally, a set of initial experimental results, captured after fiber and converged A-IFoF/V-band air transmission, are presented. These experimental studies aim to evaluate the DSP assisted A-IFoF concept for efficient accommodation of both single and multiple radio signals, using commercial off-the shelf electronic/photonic components, employing the CP-OFDM modulation format. Prior to the description of the experimental layouts that were deployed for analog fiber and FiWi transmission performance evaluation, the key components

of these layouts, used for electro-optical conversion and vice-versa, as well the radio boards and antenna units that served the IF-to-RF conversion and wireless propagation are described.

Chapter 4 focuses on the demonstration of a seamless analog FiWi transport link, employing A-IFoF signals over an FMC topology deployment of TIM's PON legacy infrastructure, directly connected to a mmWave wireless link, recirculating traffic between Ethernet-compliant analog IF-transmit interfaces of an FPGA at the network nodes. The Downlink operation of the presented FMC topology was experimentally demonstrated. The real-time IF transmitter was implemented with a Xilinx Zynq Ultrascale+ RFSoC platform, carrying the transmitter side DSP functions and generating digitally upconverted OFDM signals with bandwidths up to 400MHz. The A-IFoF signal was transmitted through the field, simultaneously with residential traffic and redirected to the mmWave wireless link, resulting to EVM values well below the 3GPP specifications, paving the way towards true FMC convergence in emerging future PON architectures.

More specifically, the proposed FMC architecture enabling the reuse of the legacy optical (access) networks for A-IFoF/wireless transmission and its benefits are presented, taking into account the TIM's PON legacy infrastructure existing in Turin to bring the proposed concept one step closer to reality. Afterwards, the experimental setup used for the performance evaluation of the above A-IFoF over converged PON/wireless transmission is described and the corresponding captured results are demonstrated.

Finally, **Chapter 5** describes the final demonstrator of the European project 5GPHOS, in which the first demonstration of the integration of a custom, SDN-reconfigurable, real-time A-IFoF TxRx interface, over a real network infrastructure located in Athens is described was performed. The implemented SDN controller offered active adjustment of the capacity provided by the TxRx for converged A-IFoF/mmWave RAN transport, based on constant traffic monitoring and automatic adaptation to the hosted applications' requirements. Towards the description of the demonstrator, the envisioned fronthaul architecture which inspired the actual deployment is initially presented. Afterwards, a detailed description of the different parts of the implemented analog transceiver unit is provided, including latency and power consumption measurements.

Moreover, initial experimental results targeting the evaluation of the analog transceiver's integration into a mobile infrastructure, supporting three alternative optical/wireless converged network topologies (FiWi, WiFi and FiWiFi) are discussed, prior to the description of the final demonstrator's layout. Finally, the deployed testbed and results of the large-scale demonstrator are discussed. In a nutshell, in the physical layer of analog transport infrastructure, EVM measurements of 7.3% for QPSK- OFDM, converged FiWi transmission were achieved. The uninterrupted operation of the E2E deployment, was validated at application layer through the performance evaluation of various services such as AR/VR applications running on top of the infrastructure, as well as by throughput measurements, using traffic monitoring tools, showcasing peak data-rate per user up to 474Mbps. The reactive capacity optimization and network parameter reconfiguration capabilities provided by the SDN management and control layer of the presented solution were also successfully demonstrated. However, more details regarding the implementation of the analog TxRx, as well its integration in the mobile core infrastructure are provided in the following sections.

6.2. Potential future research extensions

The potential of employing novel A-RoF-based transceivers within the 5G and beyond era has been detailly addressed within the current thesis, providing also an architectural approach towards actual deployment, as well the demonstration of actual integration solutions with legacy mobile equipment and proof-of-concept experimental activities that show the validity of this concept. Still, the co-existence of both digital and analog mobile data streams in a unified, heterogenous optical network layout remains a challenge. The idea of employing reconfigurable WDM optical nodes for the co-integration of standard Fronthaul streams with futuristic analog solutions is being elaborated on, in the following paragraphs. The rest of the current chapter focuses on the possible advancements that can be achieved through the integration of analog RoF-based transport links with optical wireless technologies, being currently in the spotlight for the enhancement of the efficiency, flexibility and scalability of beyond 5G mobile deployments.

6.2.1 WDM-based Hybrid Analog/Digital Transport Layouts for 5G and Beyond RAN

As discussed in the previous chapters, within the already mature, digitized Fronthauling environment, it is inevitable that CPRI-based links will remain the most common interface for the interconnection between the Baseband Units and the RRHs, despite the inherently limited bandwidth efficiency of CPRI protocol and the flexibility limitations that have been widely presented throughout literature [6.1]. Nonetheless, a series of brand-new technological enablers have arisen, promising large bandwidth availability, flexibility, and easy deployment, hence increased scalability. More specifically, the adoption of large unlicensed bands at high radio frequencies (i.e. V-band, D-band), combined to advanced radio techniques (such as cooperative beamforming and massive MIMO transmission), and the embracement of photonic processing/networking solutions seems to be a promising path, towards surpassing the capacity and scalability bottleneck of current deployments. On top of that, innovative beyond-CPRI fronthaul alternatives, such as the Analog Radio-over-Fiber (A-RoF) and Sigma Delta-over-Fiber (SDoF) schemes have been widely visited as possible candidates to host these technological blocks, showcasing Gbps-scale connectivity over fiber and converged wired-wireless topologies [6.2],[6.3]. As such, it is essential to migrate to a network infrastructure that can efficiently integrate various heterogenous technologies and enable internetworking of existing small cells and future deployment extensions.

For the implementation of such densified and versatile network deployments, Cloud Radio Access Networks (C-RAN) are highly attractive, as they offer greater network scalability, efficient transport and increased Network Function Virtualization (NFV) [6.1]. The cloud-based virtual BBUs (vBBUs) can support dynamic allocation of baseband processor platform resources based on the traffic demand. Within this centralized, reconfigurable universe, the

vBBUs can concurrently and interoperably accommodate heterogeneous, remotely located radio units equipped with different interfaces, reached via the already existing optical paths or beyond-legacy, currently emerging optical transport schemes. The adaptation of the optical transport architectures, interconnecting Central Units (CUs), Distributed Units (DUs) and RUs in this everchanging multi-technology ecosystem has been widely discussed during the past years [6.4]. Specifically, the transition to hybrid topologies co-hosting inhomogeneous transceivers and protocols in a transparent manner while interconnecting BBUs and RUs in a versatile and reconfigurable way is necessary [6.4][6.5]. For this purpose, current static Point-to-Point (PtP) optical interconnection of a single BBU with an RRH should evolve and be replaced with scalable, ptMp layouts, offering wavelength aggregation and reconfigurable routing of variable types of waveforms and protocols.

The concept of evolving optical transport networks to support multiple traffic streams addressed for varying radio terminals has been explored in [6.6]. More specifically, the use of optical networking segments to setup and orchestrate the BBU/DU/RU inter-connection has been recently discussed through literature as a practical solution for the support of active functionalities across the optical edge of mobile networks [6.7], [6.8], [6.9], [6.10]. At the same time, the exploitation of optical switching-enabled hybrid transport layouts, handling standardized legacy traffic has been showcased in [6.10], [6.11], including, the concurrent transmission of multiple CPRI lanes in or the co-existence of 5G, Passive Optical Network (PON) and Datacenter (DC) traffic. Inspired from these works, similar architectures could accommodate reconfigurable fiber and Fiber-Wireless (FiWi) transport architectures, relying on flexible Point-to-Multi-Point (PtMP) connectivity of both analog and digital centralized transceivers with variable radio units, located anywhere in the field.

The migration to flexible, dynamically reconfigurable transport network segments, enabled by Wavelength Division Multiplexing programable optical nodes is a necessary step for the flexible interconnection of centralized BBU pools and multiple radio units distributed in the field. More specifically, standard interconnection between each single BBU with its corresponding RU has reached a bottleneck in terms of capacity growth, adoptability of emerging technologies and efficient utilization of centralized resources [6.12], [6.13]. The above limitations are inseparably connected to the static nature of PtP fronthaul connectivity. As such, PtMP architectures have been recently investigated throughout literature, promising flexible bandwidth steering and dynamic management of resources allocation among edge and radio sites, based on traffic demand [6.14], [6.15].

Inspired by the legacy of WDM-PON networking [6.16], the use of optical switching and wavelength aggregation units can host the evolving heterogeneous PtMP fronthauling. Benefiting from the low-loss, protocol agnostic and SDN-compatibility characteristics they offer, WDM nodes can transparently aggregate disparate optical transmission schemes (D-/A-/SDoF) and modulation formats, enabling heterogeneous deployments that comprise both fiber and converged FiWi lanes. Therefore, such architectures are capable of co-hosting of heterogeneous fronthaul segments, and radio terminals in a cooperative manner, enabling the synergy of multiple BBUs to concurrently provide enhanced capacity to selected radio sites (i.e. for hot-spot use cases) or the exploitation of advanced newly deployed RRHs operating at the mmWaves by varying MNOs' baseband equipment. In a few words, WDM-based

transport deployment enables adaptive transformation of the baseband-to-radio hardware internetworking, based on the occurrence of a plethora of services with varying requirements.

During the past years the adoption of new fiber transmission schemes along the standard D-RoF solution has been explored mostly in lab-scale experiments targeting the demonstration of mixed analog and digital formats propagation over shared fiber infrastructure [6.6], aiming to show the benefits of hybrid A/D-RoF fronthauling. In this direction, [6.9] discusses the employment of an AWGR-enabled ptMp transport topology, aggregating and steering A-RoF traffic to the radio units. Such nodes can provide efficient coexistence and even internetworking between heterogeneous data streams, supporting WDM and Space Division Multiplexing (SDM) functionalities for the dynamic distribution of the traffic to the radio sites. In detail, the proposed approach (depicted in Figure 63) relies on the coexistence of fiber and FiWi fronthaul implementations, such as the following ones:

- legacy CPRI connectivity in which the data transmission is done by fragmenting and encapsulating the radio data using well established standards such as IP or Ethernet. The resulting data stream can then be multiplexed with other network traffic, switched in Ethernet switches and routed in IP routers (Long-Term Evolution (LTE)/4G),
- broadband binary streams for digital optical links for B5G connectivity scenarios as in 5G-oriented RAN. Intensity Modulation/Direct Detection (IM/DD) systems with digital modulation formats such as Non-Return-to-Zero (NRZ) and 4-level Pulse Amplitude Modulation (PAM-4) are promising candidates.
- B5G A-IFoF/A-RoF/SDoF implementations which are spectrally efficient transport schemes and can support extremely high capacities.

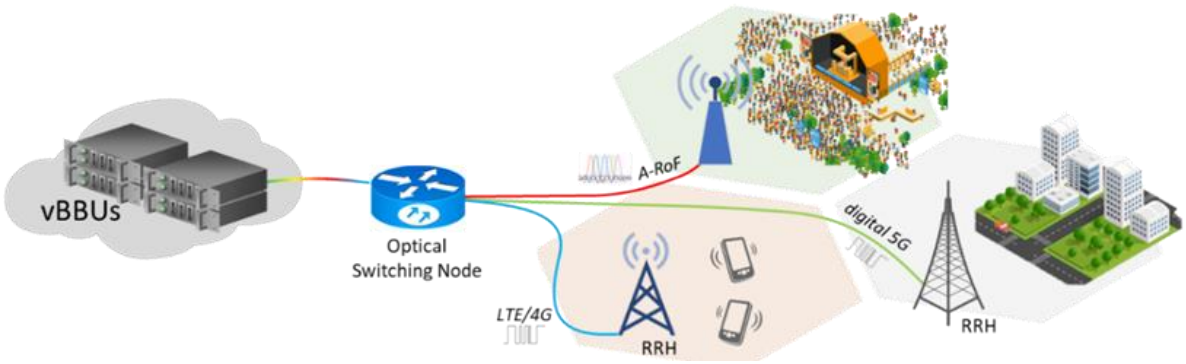

Figure 63. A WSS-based hybrid optical transport architecture [6.17].

6.2.2 Analog Radio over Fiber Links over Converged Fiber/FSO Infrastructures

Despite the progress in mm-Wave Radio Frequency (RF) communications [6.18] and the emerging sub-THz bands which can efficiently integrated with fiber X-haul scenarios [6.19], [6.20] a radio-based X-haul might not suit the capacity requirements since its capability to

haul tens of GHz-scale wideband signals is limited by the system bandwidth and propagation effects.

As a natural evolution step for replacing the mm-Waves and sub-THz bands in the analog X-hauling, Free-Space Optical (FSO) communications, can act as an enabler for the flexible deployment of such links – provided that the associated optical sub-systems are very cost-efficient, they are compatible with the fiber-optics transceiver equipment, and they can be easily deployed in a seamless way with the existing fiber-based networks. Through the literature, analog Radio-over-Air experimental links have been demonstrated showing robust operation for local C-RAN applications [6.21]. In [6.22] the use of optical wireless links as a robust outdoor backhaul solution for small radio cells, such as WiFi, Long Term Evolution (LTE) and 5G has been conducted, focusing on the link availability, and the achieved network metrics such as data rate and latency. FSO links have also been successfully demonstrated as fronthaul network extensions being compatible with 4G/5G systems while they can support hybrid fiber-wireless scenarios [6.23] .In [6.24] a flexible bidirectional fiber-FSO-5G wireless convergent system with sub-6 GHz and mm-Wave 5G hybrid data signals was successfully demonstrated. Very recently, 5G New Radio (NR) Fiber-Wireless systems including FSO systems have been demonstrated showing high and flexible transmission capacity [6.25].

In this direction, Figure 64 showcases a cutting-edge multi-technology converged Fiber/FSO architecture, which utilizes flexible optical interconnections between various Mobile Network Operators, Distributed Units (DUs) and Centralized Units (CUs). The proposed architecture draws inspiration from the proven principles of Wavelength Division Multiplexing-Passive Optical Networks (WDM-PON) networking and strategically harnesses the potential of optical switching and wavelength aggregation units to optimize the transport segments of the RAN.

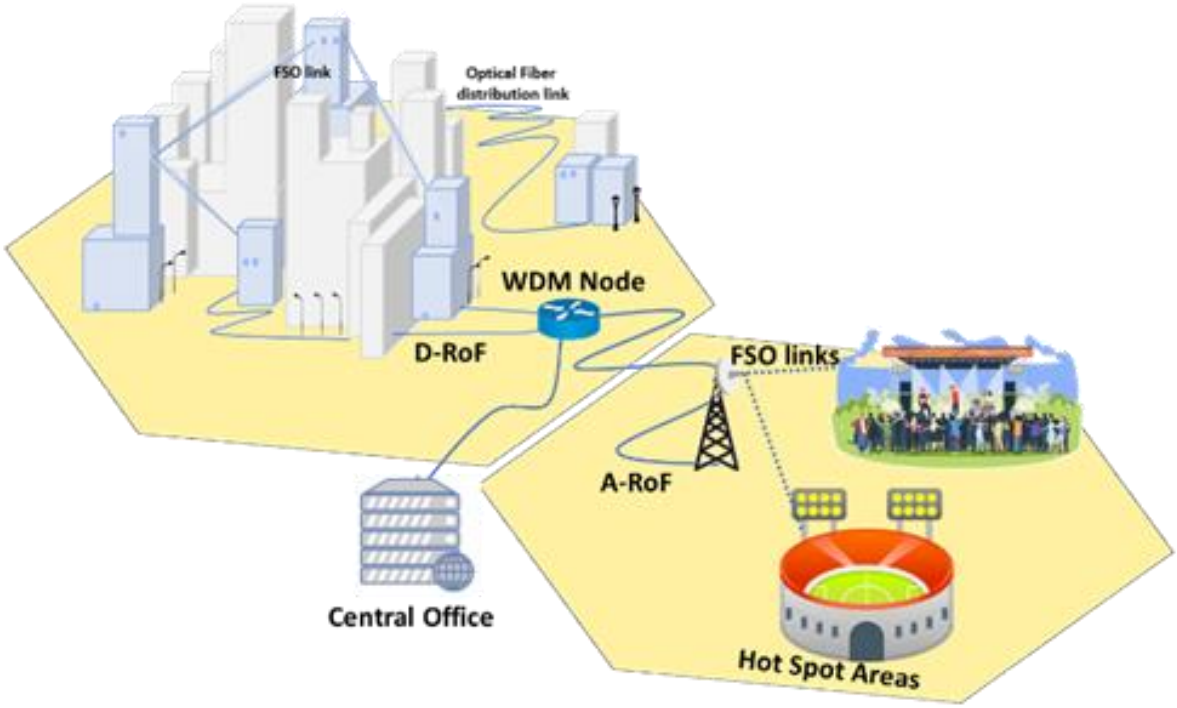

Figure 64. Architecture of a converged Fiber/FSO infrastructure where D-RoF/A-RoF streams are multiplexed.

This approach capitalizes on the remarkable advantages of WDM nodes, including low-loss, protocol agnosticism, and SDN compatibility, to seamlessly aggregate disparate optical transmission schemes such as D-/ARoF and various modulation formats. As a result, the architecture enables heterogeneous deployments, incorporating both fiber and converged Fiber/FSO lanes. This co-hosting capability facilitates the cooperative interaction of heterogeneous fronthaul segments and radio terminals. As a result, the envisioned RAN ensures robust support for access connectivity requests with diverse KPIs. Moreover, it achieves enhanced capacity through the utilization of analog wired-wireless directional lanes, capitalizing on the exceptional bandwidth potential of FSO technology while simultaneously accommodating the legacy traffic. To realize this concept, the proposed hybrid optical RAN architecture facilitates dynamic interconnections between central offices and RRHs via both digital and analog paths. An optical node employing SDN-compatible WSS serves as a foundation for WDM and SDM functionalities, dynamically distributing the traffic. In particular, the architecture embraces the coexistence of two fronthaul implementations:

- Legacy DROF connectivity, where data transmission occurs through SFPs. The resulting data stream can be multiplexed with other network traffic, switched in Ethernet switches, and routed in IP routers, supporting technologies like LTE/4G and 5G.
- B5G A-IFoF implementations, which offer spectrally efficient transport schemes capable of supporting extremely high capacities, catering to the demands of next-generation wireless services.

References

[6.1] Alimi, I.A.; Patel, R.K.; Muga, N.J.; Pinto, A.N.; Teixeira, A.L.; Monteiro, P.P. Towards Enhanced Mobile Broadband Communications: A Tutorial on Enabling Technologies, Design Considerations, and Prospects of 5G and beyond Fixed Wireless Access Networks. Appl. Sci. 2021, 11, 10427. https://doi.org/10.3390/app112110427.

[6.2] N. Argyris et al., "A 5G mmWave Fiber-Wireless IFoF Analog Mobile Fronthaul Link With up to 24-Gb/s Multiband Wireless Capacity," in Journal of Lightwave Technology, vol. 37, no. 12, pp. 2883-2891, 15 June15, 2019, doi: 10.1109/JLT.2019.2897109.

[6.3] H. Li et al., "A 21-GS/s Single-Bit Second-Order Delta–Sigma Modulator for FPGAs," in IEEE Transactions on Circuits and Systems II: Express Briefs, vol. 66, no. 3, pp. 482-486, March 2019.

[6.4] J. Zou et al., "Demonstration of X-Haul Architecture for 5G over Converged SDN Fiber Network," 2018 Optical Fiber Communications Conference and Exposition (OFC), 2018, pp. 1-3.

[6.5] V. Agarwal, C. Sharma, R. Shetty, A. Jangam and R. Asati, "A Journey Towards a Converged 5G Architecture & Beyond," 2021 IEEE 4th 5G World Forum (5GWF), 2021, pp. 18-23, doi: 10.1109/5GWF52925.2021.00011.

[6.6] S. Yao et al., "Non-Orthogonal Uplink Services Through Co-Transport of D-RoF/A-RoF in Mobile Fronthaul," in Journal of Lightwave Technology, vol. 38, no. 14, pp. 3637-3643, 15 July15, 2020, doi: 10.1109/JLT.2020.2980208.

[6.7] Giannoulis G, Tokas K, Poulopoulos G et al. Integrated Photonic Filters in Support of Converged 5G Mobile Fronthaul & Midhaul Transport Layers. Fiber and Integrated Optics. 2019;38(6):333-348. doi:10.1080/01468030.2019.1697908.

[6.8] S. Koenig et al., "20 Gbit/s wireless bridge at 220 GHz connecting two fiber-optic links," in Journal of Optical Communications and Networking, vol. 6, no. 1, pp. 54-61, Jan. 2014, doi: 10.1364/JOCN.6.000054.

[6.9] Ronis Maximidis et al., “A Centralized and Reconfigurable 4x2.5Gb/s Fiber-Wireless mmWave Fronthaul for Network Sharing Applications”, ECOC 2021, Bordeaux, France (2021).

[6.10] Jiawei Zhang, et al., "Experimental demonstration of fronthaul flexibility for enhanced CoMP service in 5G radio and optical access networks," Opt. Express 25, 21247-21258 (2017).

[6.11] C. Browning et al., "A Silicon Photonic Switching Platform for Flexible Converged Centralized-Radio Access Networking," in Journal of Lightwave Technology, vol. 38, no. 19, pp. 5386-5392, 1 Oct.1, 2020, doi: 10.1109/JLT.2020.2984379.

[6.12] R. Li, “Network 2030: Market drivers and prospects,” ITU Workshop on Network 2030, New York, Oct. 2018.

[6.13] C. Lim, Y. Tian, C. Ranaweera, N. Ampalavanapillai, E. Wong, K.L. Lee, "Evolution of Radio-over-Fiber Technology" IEEE J. Lightwave Technology, vol. 37, no. 6, pp. 1647-1656, Mar. 2019.

[6.14] T. S. Rappaport et al., "Millimeter Wave Mobile Communications for 5G Cellular: It Will Work!," in IEEE Access, vol. 1, pp. 335-349, 2013 W. Hong et al., "Multibeam Antenna Technologies for 5G Wireless Communications," in IEEE Transactions on Antennas and Propag., vol. 65, no. 12, pp. 6231- 6249, Dec. 2017.

[6.15] M. Sung, J. Kim, S. Cho, H. S. Chung, J. K. Lee and J. H. Lee, "Experimental Demonstration of Bandwidth-Efficient Indoor Distributed Antenna System based on IFoF Technology supporting 4G LTE-A and 5G Mobile Services," 2018 Optical Fiber Communications Conference and Exposition (OFC), 2018.

[6.16] Alimi, I.A.; Teixeira, A.L.; Monteiro, P.P. Toward an Effcient C-RAN Optical Fronthaul for the Future Networks: A Tutorial on Technologies, Requirements, Challenges, and Solutions. IEEE Comm. Surv. Tut. 2018, 20, 708–769.

[6.17] Kanta, K.; Toumasis, P.; Tokas, K.; Stratakos, I.; Papatheofanous, E.A.; Giannoulis, G.; Mesogiti, I.; Theodoropoulou, E.; Lyberopoulos, G.; Lentaris, G.; et al. Demonstration of a Hybrid Analog–Digital Transport System Architecture for 5G and Beyond Networks. Appl. Sci. 2022, 12, 2122. https://doi.org/10.3390/app12042122.

[6.18] Sakaguchi, K., Haustein, T., Barbarossa, S., et al.: 'Where, When, and How mmWave is Used in 5G and Beyond', IEICE Trans. Electron., 2017, E100-C, (10), pp. 790–808.

[6.19] R. Maximidis et al., "Demonstration of Low-Complexity D-band Extension of Fiber X-haul for 5G and Beyond Infrastructure," 2023 17th European Conference on Antennas and Propagation (EuCAP), Florence, Italy, 2023, pp. 1-4, doi: 10.23919/EuCAP57121.2023.10133343.

[6.20] E. Andrianopoulos et al., "Real-Time Sub-THz Link Enabled Purely by Optoelectronics: 90–310 GHz Seamless Operation," in IEEE Photonics Technology Letters, vol. 35, no. 5, pp. 237-240, 1 March1, 2023, doi: 10.1109/LPT.2023.3235932.

[6.21] B. Schrenk, D. Milovančev, N. Vokić, H. Hübel and F. Karinou, "Face-to-Face EML Transceiver Tandem for Full-Duplex Analogue Radio-Over-Air," in Journal of Lightwave Technology, vol. 38, no. 11, pp. 2976-2983, 1 June1, 2020, doi: 10.1109/JLT.2020.2982175.

[6.22] D. Schulz et al., "Robust Optical Wireless Link for the Backhaul and Fronthaul of Small Radio Cells," in Journal of Lightwave Technology, vol. 34, no. 6, pp. 1523-1532, 15 March15, 2016, doi: 10.1109/JLT.2016.2523801.

[6.23] Akeem O. Mufutau, Fernando P. Guiomar, Marco A. Fernandes, Abel Lorences-Riesgo, Arnaldo Oliveira, and Paulo P. Monteiro, "Demonstration of a hybrid optical fiber–wireless 5G fronthaul coexisting with end-to-end 4G networks," J. Opt. Commun. Netw. 12, 72-78 (2020).

[6.24] C. -Y. Li et al., "A Flexible Bidirectional Fiber-FSO-5G Wireless Convergent System," in Journal of Lightwave Technology, vol. 39, no. 5, pp. 1296-1305, 1 March1, 2021, doi: 10.1109/JLT.2020.3037943.

[6.25] H.-H. Huang et al., “5G NR Fiber-Wireless Systems with Dual-Polarization Scheme and Single-Carrier Optical Modulation”, in Proc. of CLEO 2023, paper No. JTh2A.101, 07-12 May 2023, San Jose, CA, USA.

List of publications

1. N. Argyris, **K. Kanta**, N. Iliadis, G. Giannoulis, D. Apostolopoulos and H. Avramopoulos, School of Electrical and Computer Engineering, National Technical University of Athens, S. Papaioannou, C. Vagionas, G. Kalfas, and N. Pleros, Department of Informatics, Aristotle University of Thessaloniki, “DSP enabled Fiber-Wireless IFoF/mmWave link for 5G Analog Mobile Fronthaul”, in IEEE 5G Word Forum, 2018 (WF5G).
2. D. Apostolopoulos, G. Giannoulis, N. Argyris, N. Iliadis, **K. Kanta** and H. Avramopoulos, School of Electrical and Computer Engineering, National Technical University of Athens, “Analog Radio-over-Fiber Solutions in Support of 5G”, in 22nd Conference on Optical Network Design and Modelling, 2018 (ONDM).
3. G. Giannoulis, N. Argyris, N. Iliadis, G. Poulopoulos, **K. Kanta**, D. Apostolopoulos, and H. Avramopoulos, School of Electrical and Computer Engineering, National Technical University of Athens, “Analog Radio-over-Fiber Solutions for 5G Communications in the beyond-CPRI era”, in 20th international conference on transparent optical networks 2018 (ICTON).
4. C. Vagionas, S. Papaioannou, Department of Informatics, Aristotle University of Athens, N. Argyris, **K. Kanta**, N. Iliadis, G. Giannoulis, D. Apostolopoulos, H. Avramopoulos, School of Electrical and Computer Engineering, National Technical University of Athens, C. Caillaud, H. Debregeas, III-V Lab, France, G. Kalfas, N. Pleros, Department of Informatics, Aristotle University of Athens, “A 6-band 12Gb/s IFoF/V-band Fiber-Wireless Fronthaul link using an InP Externally Modulated Laser”, in 44th European Conference on Optical Communication 2018 (ECOC).
5. **K. Kanta** et al.,"SOI-ring based analog phase processing for chromatic dispersion compensation in A-IFoF Fronthaul," in Optical Fiber Communication Conference (OFC) 2019, OSA Technical Digest (Optical Society of America, 2019), paper W3I.4.
6. N. Argyris, **K. Kanta** et al., "A 5G mmWave Fiber-Wireless IFoF Analog Mobile Fronthaul Link With up to 24-Gb/s Multiband Wireless Capacity," in Journal of Lightwave Technology, vol. 37, no. 12, pp. 2883-2891, 15 June15, 2019.
7. C. Vagionas, **K. Kanta** et al., "A six-channel mmWave/IFoF link with 24Gb/s Capacity for 5G Fronthaul Networks," 2018 International Topical Meeting on Microwave Photonics (MWP), Toulouse, 2018, pp. 1-4.
8. V. Kitsakis, **K. Kanta** et al., "Design of a Real-Time DSP Engine on RF-SoC FPGA for 5G Networks", 23rd Conference on Optical Network Design And Modeling (ONDM), Athens, 13-16 May 2019.
9. N. Argyris, **K, Kanta** et al., "12 Gb/s Multiband Fiber-Wireless Link Using Coherent IFoF and V-band mmWave Radio", 23rd Conference on Optical Network Design And Modeling (ONDM), Athens, 13-16 May 2019.
10. **K. Kanta**, et al., “Analog fiber-wireless downlink transmission of IFoF/mmWave over in-field deployed legacy PON infrastructure for 5G fronthauling”, in IEEE/OSA

Journal of Optical Communications and Networking, vol. 12, no. 10, pp. D57-D65, October 2020, doi: 10.1364/JOCN.391803.

11. G. Giannoulis, P. Toumasis, **K. Kanta**, G. Poulopoulos, K. Tokas, D. Apostolopoulos, H. Avramopoulos, "Integrated Photonic Filters for Flexible Analog-based Mobile Fronthauling," 2019 International Workshop on Fiber Optics in Access Networks (FOAN), Sarajevo, Bosnia and Herzegovina, 2019, pp. 11-15, doi: 10.1109/FOAN.2019.8933752.
12. G. Giannoulis, K. Tokas, G. Poulopoulos, P. Toumasis, **K. Kanta**, D. Apostolopoulos, H. Avramopoulos, "Integrated Photonic Filters in Support of Converged 5G Mobile Fronthaul & Midhaul Transport Layers", in Fiber and Integrated Optics, vol. 38, no. 6, pp. 333-348, December 2019, doi: 10.1080/01468030.2019.1697908.
13. P. Toumasis, G. Giannoulis, G. Poulopoulos, **K. Kanta**, D. Apostolopoulos, H. Avramopoulos, "On the Ring Resonator-Based Dispersion Compensation Method for Analog 5G/B5G Mobile Fronthauling", Journal of Lightwave Technology, 1109/jlt.2020.3042056.
14. G. Giannoulis, D. Zavitsanos, P. Toumasis, **K. Kanta**, and H. Avramopoulos, "Modeling Filtering Impairments towards Enhanced Monitoring via QKD Performance Metrics," in Asia Communications and Photonics Conference/International Conference on Information Photonics and Optical Communications 2020 (ACP/IPOC).
15. C. Vagionas, E, Ruggeri, G. Kalfas, B. Sirbu, Y. Leiba, **K. Kanta,** G. Giannoulis, C. Caillaud, G. Cerulo, F. Mallecot, T. Raddo, A. Mesodiakaki, M. Gatzianas, D. Apostolopoulos, H. Avramopoulos, I. M. Tafur T. Tekin, A. Miliou, N. Pleros, (2020), An end-to-end 5G fiber wireless A-RoF/IFoF link based on a 60 GHz beamsteering antenna and an InP EML. 9. 10.1117/12.2544866.
16. D. Zavitsanos, A. Ntanos, P. Toumasis, A. Raptakis, K. Tokas, **K. Kanta**, C. Kouloumentas, G. Giannoulis, & H. Avramopoulos, "On the Impact of Center Frequency Drifts on QKD Performance in WDM-based Nodes", In 2021 Conference on Lasers and Electro-Optics Europe and European Quantum Electronics Conference, OSA Technical Digest (Optical Society of America), paper EB-P.4.
17. D. Klonidis, D. Apostolopoulos, G. P. Katsikas, G. Giannoulis, **K. Kanta,** K. Tokas, T. Xirofotos, R. Munoz, F. Moscatelli, G. Torfs, C. Vagionas, D. L. Lopez, Z. S. He, J. Sterle, D. Levi, G. Lyberopoulos, V. L. Alvarez, E. Trouva, Y. Leiba, X. Vilajosanna, J. C. T. Casals, H. Avramopoulos, "Int5Gent: An integrated end-to-end system platform for verticals and data plane solutions beyond 5G," 2021 Joint European Conference on Networks and Communications & 6G Summit (EuCNC/6G Summit), Porto, Portugal, 2021, pp. 604-609, doi: 10.1109/EuCNC/6GSummit51104.2021.9482436.
18. P. Toumasis, **K. Kanta** et al, "Demonstration of FPGA-based A-IFoF/mmWave transceiver integration in mobile infrastructure for beyond 5G transport", 2021 European Conference on Optical Communications (ECOC).
19. P. Toumasis, **K. Kanta**, K. Tokas, G. Giannoulis, D. Apostolopoulos, and H. Avramopoulos, "A Dynamically Reconfigurable Optical Switching Node for Hybrid

Analog/Digital RoF Transport," in Optical Fiber Communication Conference (OFC) 2022.

20. **Kanta K**, Toumasis P, et al., “Demonstration of a Hybrid Analog–Digital Transport System Architecture for 5G and Beyond Networks.”, Applied Sciences. 2022; 12(4):2122.
21. C. Vagionas, R. Maximidis, I. Stratakos, A. Margaris, A. Mesodiakaki, M. Gatzianas, **K. Kanta**, et al, "End-to-End Real-Time Service Provisioning over a SDN-controllable 60 GHz analog FiWi X-haul for 5G Hot-Spot Networks," in Optical Fiber Communication Conference (OFC) 2022, San Diego.
22. J. Sterle, I. Mesogiti, L. Korsic, E. Theodoropoulou, F. Setaki, G. Lyberopoulos, F. Moscateli, **K. Kanta,** G. Giannoulis, P. Toumasis, D. Apostolopoulos, H. Avramopoulos, J. Avramidis, Y. Leiba, D. Klonidis, “A Framework to Support the Deployment of PPDR Services Across Edge and Cloud Domains.” In Artificial Intelligence Applications and Innovations 2022., IFIP Advances in Information and Communication Technology, vol 652. Springer, Cham.
23. I. Mesogiti, E. Theodoropoulou, F. Setaki, G. Lyberopoulos, F. Moscateli, **K. Kanta**, G. Giannoulis, P. Toumasis, D. Apostolopoulos, H. Avramopoulos, L. Lopacinski, J. G. Teran, A. Nanos, Y. Leiba, M. Anastasopoulos, A. Tzanakaki, “Advancements in Edge Computing and Service Orchestration in Support of Advanced Surveillance Services.” In Artificial Intelligence Applications and Innovations 2022., IFIP Advances in Information and Communication Technology, vol 652. Springer, Cham.
24. **K. Kanta**, P. Toumasis, et al., “End-to-End Demonstration of an SDN-reconfigurable, FPGA-based TxRx Interface for Analog-IFoF/mmWave X-haul”, in European Conference on Optical Communication (ECOC) 2022, Basel.
25. P. Toumasis, **K. Kanta**, C. Vagionas, G. Giannoulis, Z. S. He, G. Torfs, E. Kyriazi, G. Brestas, R. Maximidis, C. Meysmans, W. Wasko, D. Apostolopoulos, A. Miliou, N. Pleros, H. Avramopoulos, “First Real-Time Demonstration of a Flexible multi-λ DRoF/ARoF/SDoF Transport for fiber/mmWave RAN”, European Conference on Optical Communications (ECOC), Glasgow, Oct 2023.
26. C. Vagionas, R. Maximidis, I. Stratakos, A. Margaris, A. Mesodiakaki, M. Gatzianas, **K. Kanta**, P. Toumasis, G. Giannoulis, D. Apostolopoulos, E. A. Papatheofanous, G. Lentaris, D. Reisis, D. Soudris, K. Tsagkaris, N. Argyris, D. Syrivelis, P. Bakopoulos, R. Oldenbeuving, G. Kalfas (2023). (2023). End-to-End Real-Time Service Provisioning over a SDN-controllable analog mmWave Fiber-Wireless 5G X-haul Network. Journal of Lightwave Technology. PP. 1-10. 10.1109/JLT.2023.3234365.
27. **K. Kanta**, P. Toumasis, G. Giannoulis, I. Stratakos, G. Lentaris, E. A. Papatheofanous, I. Mesogiti, E. Theodoropoulou, A. Margaris, D. Syrivelis, E. Kyriazi, G. Brestas, K. Tokas, N. Argyris, C. Vagionas, R. Maximidis, P. Bakopoulos, A. Mesodiakaki, M. Gatzianas, G. Kalfas, K. Tsagkaris, N. Pleros, D. Reisis, G. Lyberopoulos, D. Apostolopoulos, D. Soudris, and H. Avramopoulos, "Live demonstration of an SDN- reconfigurable, FPGA-based TxRx for an analog-IFoF/mmWave radio access network in an MNO’s infrastructure," J. Opt. Commun. Netw. 15, C299-C306 (2023).

28. M. Vargemidou, P. Toumasis, **K. Kanta**, R. Maximidis, G. Giannoulis, Z. S. He, Y. Leiba, D. Apostolopoulos, H. Avramopoulos, A. Miliou, N. Pleros, C. Vagionas, “Sub-THz Fiber Wireless Multi-IFoF fronthaul of a V-band massive MIMO antenna for multi-user 6G networks”, European Conference on Optical Communications (ECOC), Glasgow, Oct 2023.
29. **K. Kanta**, N. K. Lyras, A. Ntanos, A. Stathis, P. Toumasis, E. Andrianopoulos, C. Tsokos, G. Giannoulis, D. Apostolopoulos, H. Avramopoulos, “Multiplexing Multi Gbps Analog Radio over Fiber Links over a Converged Fiber/FSO Intra Campus Infrastructure”, 15th International Congress on Ultra-Modern Telecommunications and Control Systems (ICUMT), Ghent, Oct 2023.
30. R. Maximidis, C. Vagionas, S. Soukaras, Z. S. He, **K. Kanta**, P. Toumasis, G. Giannoulis, D. Apostolopoulos, G. Kalfas, A. Mesodiakaki, M. Gatzianas, H. Avramopoulos, A. Miliou, N. Pleros, "Demonstration of Low-Complexity D-band Extension of Fiber X-haul for 5G and Beyond Infrastructure," 2023 17th European Conference on Antennas and Propagation (EuCAP), Florence, Italy, 2023, pp. 1-4, doi: 10.23919/EuCAP57121.2023.10133343.
31. G. Giannoulis, A. Ntanos, A. Stathis, **K. Kanta**, P. Toumasis, D. Zavitsanos, NN. Lyras, D. Apostolopoulos, H. Avramopoulos, (2023). Practical decoy-state sender implemented over analog RoF transmitters for secure 5G and beyond x-haul connections. 48. 10.1117/12.2649707.
32. C. Vagionas, R. Maximidis, **K. Kanta**, P. Toumasis, G. Giannoulis, D. Apostolopoulos, G. Kalfas, M. Gatzianas, A. Mesodiakaki, H. Avramopoulos, A. Miliou, NN. Pleros, "Multi-RAT Fiber-Wireless Technologies towards 6G Networks," 2023 23rd International Conference on Transparent Optical Networks (ICTON), Bucharest, Romania, 2023, pp. 1-4, doi: 10.1109/ICTON59386.2023.10207366.

List of Figures

List of Tables